Report
P-17-06
August 2023

Modelling heterogeneous hydration behaviour of bentonite by a FracMan-Thames coupling method for the Bentonite Rock Interaction Experiment (BRIE) at Äspö HRL

Task 8 of SKB Task Forces EBS and GWFTS

Atsushi Sawada
Kazuhiko Sakamoto
Takanori Watahiki
Hisashi Imai

SVENSK KÄRNBRÄNSLEHANTERING AB

SWEDISH NUCLEAR FUEL
AND WASTE MANAGEMENT CO

Box 3091, SE-169 03 Solna
Phone +46 8 459 84 00
skb.se

SVENSK KÄRNBRÄNSLEHANTERING

ISSN 1651-4416
SKB P-17-06
ID 2017785
August 2023

Modelling heterogeneous hydration behaviour of bentonite by a FracMan-Thames coupling method for the Bentonite Rock Interaction Experiment (BRIE) at Äspö HRL

Task 8 of SKB Task Forces EBS and GWFTS

Atsushi Sawada, Japan Atomic Energy Agency

Kazuhiko Sakamoto, Inspection Development Company Ltd.

Takanori Watahiki, NESI Inc.

Hisashi Imai, HAZAMA ANDO CORPORATION

Abstract

One aim of Task 8 was to improve the knowledge of the bedrock-bentonite interface with regard to groundwater flow, mainly based on a set of data obtained by Bentonite Rock Interaction Experiment (BRIE) at Äspö HRL. JAEA developed an approach for Task 8 assuming that the discrete features dominate the delivery of groundwater to the bentonite columns emplaced into the vertically drilled boreholes from TASO tunnel floor, resulting in heterogeneous bentonite wetting behaviour. This assumption was implemented as a FracMan Discrete Fracture Network (DFN) model for groundwater flow. Due to this approach, no permeable rock matrix was modelled in the resulting HydroDFN model.

Groundwater transported from the HydroDFN to the bentonite columns, was modelled using the code Thames including a developed specific feature for the interface between the fractured rock mass and the bentonite. Thames models water movement in the bentonite using Richards' equation for each finite element mesh which is modelled as homogeneous and isotropic porous media.

The results of bentonite wetting calculation were compared with measured data, the "Bentograph" picture of surface of the dismantled bentonite column from Hole 18, the evolution of relative humidity data measured by six sensors installed in each bentonite column (Hole 17 and 18), and the spatial distribution of water content measured by sampling of dismantled bentonite columns. In general, the FracMan-Thames DFN/Bentonite wetting simulation approach and the assumption of fractures dominated bentonite wetting appears to be able to provide a reasonable approximation to the observed heterogeneous bentonite wetting behaviour of BRIE.

Sammanfattning

Ett syfte med Task 8 var att förbättra kunskapen om gränssnittet berg-bentonit med avseende på grundvattenflöde, huvudsakligen baserat på en uppsättning data som erhållits från försöket Bentonite Rock Interaction Experiment (BRIE) som utfördes i Äspölaboratoriet. JAEA utvecklade ett tillvägagångssätt för Task 8 som antar att bergets diskreta egenskaper dominerar leveransen av grundvatten till bentonitpelarna som placerats in i de vertikalt borrade borrhålen från TASO-tunnelgolvet, vilket resulterar i heterogena bentonitvätningsbeteenden. Detta antagande implementerades som en FracMan Discrete Fracture Network (DFN) modell för grundvattenflöde. På grund av detta tillvägagångssätt modellerades ingen permeabel bergmatris i den resulterande HydroDFN-modellen.

Grundvatten som transporterades från HydroDFN till bentonitpelarna modellerades med koden Thames som hade utvecklats för att inkludera gränssnittet mellan den sprickiga bergmassan och bentoniten. Thames modellerar vattenrörelser i bentoniten med hjälp av Richards ekvation för varje finita elementnät som modelleras som homogena och isotropa porösa medier.

Resultaten av bentonitvätningsberäkningar jämfördes med uppmätta data, ”Bentograph”-bilden av ytan på den demonterade bentonitkolonnen från hål 18, utvecklingen av relativ fuktighetsdata uppmätt av sex sensorer installerade i varje bentonitpelare (hål 17 och 18), och den rumsliga fördelningen av vatteninnehåll mätt genom provtagning av demonterade bentonitkolonner. I allmänhet verkar FracMan-Thames DFN/Bentonite-vätningssimuleringsmetoden och antagandet om sprickdominerade bentonitvätning kunna ge en rimlig approximation till det observerade heterogena bentonitvätningsbeteendet i BRIE.

Executive Summary

An aim of Task 8 was to improve the knowledge of the bedrock-bentonite interface with regard to groundwater flow, mainly based on a set of data obtained by Bentonite Rock Interaction Experiment (BRIE) at Äspö HRL. JAEA had developed an approach for Task 8 assuming that the discrete features dominate the delivery of groundwater to the bentonite columns emplaced into the vertically drilled boreholes from TASO tunnel floor, resulting in heterogeneous bentonite wetting behaviour. This assumption was implemented as a FracMan Discrete Fracture Network (DFN) model for groundwater flow. Due to this assumption, no permeable rock matrix was modelled. The variability and uncertainty of this stochastic "HydroDFN" model was constrained by conditioning the model to match measured fracture location and orientation, and specific capacity (transmissivity) data observed at five probe boreholes. Groundwater from the HydroDFN being delivered to the bentonite columns, was modelled using Thames code with developing a specific feature at the interface between the fractured rock mass and the bentonite. Thames models water movement in the bentonite using Richards' equation for each finite element mesh which is modelled by homogeneous and isotropic porous media. This application of Thames code was verified by the laboratory test data of water uptake using the same bentonite block and conditions as used in BRIE.

One of JAEA's goals for Task 8 was to quantify the uncertainty of the stochastic HydroDFN. To achieve this, one thousand realisations of the stochastic HydroDFN model were examined by Darcy flow calculations, and the calculated groundwater flow rate and pressure at the five probe boreholes were compared with BRIE measurements. The simulated flow rate and pressure from the one thousand realisations does cover the measured values, but distributes over a wide range due to the relatively wider range of transmissivity distribution for HydroDFN model. Six realisations which reproduce reasonable range of pressure and flow rate to the probe boreholes were screened out from 1 000 realisations of the stochastic HydroDFN model, and they were used for applied to the bentonite wetting simulations with Thames code. The results of bentonite wetting calculation were compared with measured data, the "Bentograph" picture of surface of the dismantled bentonite column from Hole 18, the evolution of relative humidity data measured by six sensors installed in each bentonite column (Hole 17 and 18), and the spatial distribution of water content measured by sampling of dismantled bentonite columns. In general, FracMan-Thames DFN/Bentonite wetting simulation approach and the assumption of fracture dominated bentonite wetting appears to be able to provide a reasonable approximation to the observed heterogeneous bentonite wetting behaviour of BRIE. The geologically mapped fracture data along the boreholes was shown to be useful to constrain the stochastic HydroDFN model to reproduce the locations of bentonite wetting. However, a lack of data for the hydraulic connectivity and permeability of these mapped fractures caused an uncertainty of the model evaluation results, and the data was not enough to reproduce the local scale heterogeneous bentonite wetting behaviour as shown by the data of relative humidity sensors and water content. Based on the findings as described above, we would suggest that a systematic investigation at pilot holes, including both geological mapping of the fractures and also testing of the hydraulic properties of the low permeable fractures and their extent, by conducting the transient pressure tomography and directional ground penetration radar investigation of each intersecting fracture, might be required to get more practical prediction of heterogeneous wetting behaviour in bentonite, as observed in BRIE.

Contents

1 Introduction

1.1 Background

The hydraulic interaction between the system components of compacted bentonite and the near-field host rock composed of hard and fractured bedrock rock is one of the key issues to understand hydraulic behaviour for evaluating the safety of high-level radioactive waste disposal programs. The bentonite sacks groundwater from the fractured rock through the various void spaces that are typically conceptualised by a porous media of rock matrix and a network of rock fractures, under the multiple phases of groundwater, liquid and vaper. Consequently, at the initial stage of the bentonite hydration, groundwater penetrates heterogeneously into the bentonite. Bentonite Rock Interaction Experiment (BRIE) was conducted in deep underground tunnel at Äspö Hard Rock Laboratory, in order to characterise the bentonite wetting behaviour in hydraulically heterogeneous groundwater flow condition of fractured rock, under isothermal condition (Fransson et al. 2017). The experiment was subdivided into two main parts: Part I describing the selection and characterisation of a test site and two central boreholes (Hole 17 and 18) and Part II handling the installation, hydration and dismantling of the bentonite parcels in two central borehores. In addition to the field experiment, a laboratory water uptake test was performed.

The main objective of BRIE was an increase scientific understanding of the exchange of water across the bentonite-rock interface. It also tried to provide the scientific bases for the better predictions of the wetting of the bentonite buffer and for the better characterisation methods of the deposition holes. BRIE was set as a task (named “Task 8”) of Äspö modelling task force which is a forum for the international organisations supporting the Äspö Hard Rock Laboratory to interact in the area of conceptual and numerical modelling of groundwater flow and solute transport in fractured rock as well as of engineered barrier systems. Task 8 was a joint effort of the SKB Task Force on Modelling Groundwater Flow and Transport of Solutes (GWFTS) and that on Engineered Barrier Systems (EBS). The overall objective of the task is to obtain a better understanding (through modelling and analyses) of the hydraulic interaction between the near-field host rock and backfill materials in the repository, specifically the bentonite buffer in a deposition hole.

JAEA (Japan Atomic Energy Agency) had been joining the SKB Task Force on Modelling GWFTS and carried out the modelling and calculations of heterogeneous groundwater transport behaviour in fractured rock and bentonite to evaluate BRIE, according to the Task 8 descriptions (Vidstrand et al. 2017).

1.2 Objectives

The main objective of JAEA’s Task 8 modelling was to study an effect of heterogeneous groundwater flow and head distribution caused by the network of fractures onto bentonite hydration behaviour, under the assumption that the network of fracture might dominate groundwater supply to the bentonite columns emplaced in the fractured rock although low permeable rock matrix might have large volume to contact to the bentonite columns and have connected void space. To archive this, the simulation codes for groundwater flow through the fracture network in rock and bentonite hydration were applied by implementing interface tools to run them alternately at each short time step for simulating coupling groundwater transport between fractured rock and bentonite. The uncertainty of hydrogeological model by the stochastic discrete fracture network modelling procedure on calculating hydraulic measures such as head and flow rate to the specific local points (boreholes) was also examined as a part of JAEA’s main objective. The capabilities of the implemented simulation tools were demonstrated by comparing the simulation results with the BRIE results. The sensitivity of the hydraulic connectivity intersecting of the fractures intersecting to the bentonite columns on to the heterogeneous hydration behaviour in the bentonite was also examined. Then, the requirement to the further investigation methodology was suggested.

1.3 Scope

Task 8 was subdivided into six subtasks as listed below:

- Task 8A: Initial scoping calculation for simplified two-dimensional axisymmetric condition.
- Task 8B: Scoping calculation for the 40 m × 40 m × 40 m cubic block around BRIE site, with hypothetical single fracture intersecting a vertical borehole where the bentonite block is emplaced.
- Task 8C: Prediction of hydraulic conditions at the bentonite emplacing two boreholes in the 40 m × 40 m × 40 m cubic block around BRIE site and bentonite wetting.
- Task 8D: Update the predicting calculation by newly obtained data and actual specifications of bentonite emplacing boreholes.
- Task 8E: Additional application of numerical models used for Task 8 to Prototype Repository experiments, which is the real scale in-situ emplacement of bentonite and over pack with thermal heating into six deposition holes at Äspö HRL.
- Task 8F: Back analysis and evaluation of the simulation using resulting data of BRIE.

JAEA had conducted mainly Task 8C, Task 8D and Task 8F. In addition, using Task 8B specification, a capability of the newly developed simulation tools for coupling two numerical codes was demonstrated. The numerical code for bentonite wetting behaviour was verified by comparing with the laboratory water uptake, which is reported in Appendix A1. Task 8E is an extension of Task 8 to apply the simulation method developed for Task 8 to the real scale of deposition holes with considering an effect thermal loading and wetting process of backfilling material in tunnel above the deposition holes. JAEA had also tried to apply the newly developed simulation tools to this subtask (Task 8E) and the results are summarised in an Appendix A2.

In this study, we developed an approach to Task 8 which could consider the assumption that the discrete features dominate the delivery of groundwater to the bentonite columns emplaced into the vertically drilled boreholes from TASO tunnel floor, resulting in heterogeneous bentonite wetting behaviour. More detailed assumptions and conditions adopted in this study are listed in Table 1-1, comparing with the realistically conceptualised model.

One of the goals of this modelling study was to improve understanding of the effect of the natural fractures network on the heterogeneous hydration behaviour in the bentonite columns. The model did try to improve the understanding of the interface between natural fractures and bentonite. Specifically, modelling focused on understanding the effects of location and properties of fractures potentially providing water to the bentonite, considering permeability, flow rate (time varying) and pressure (time varying) of the fractures connecting to the bentonite.

- Location and permeability of deterministically defined (relatively larger) fractures which constrain pressure distribution in the modelling region.
- Distribution and hydraulic behaviour of the background fractures (by the stochastic DFN process, uncertainty of the stochastic parameter values and potential range of the stochastic modelling) in the modelling region which provide pressure distribution around the test holes.
- Local connectivity to the test holes and permeability of the local features which provide groundwater flow (or pressure) to the bentonite.
- The outer boundary conditions of the modelling region which provide pressure distribution of the model.

On the other hand, for the bentonite, the uncertainty of the conceptual model and parameter values were not addressed. A constant model parameter values were used for the bentonite and the interface, without taking account for the uncertainty relevant to the bentonite.

Table 1-1. The comparison model used in this study with the realistic model.

	Realistic conceptual model	Model in this study
Rock	**Features:** The network of fractures (heterogeneously distributed) dominates groundwater flow in a fractured crystalline rock. The roughness of fracture surfaces and in-filling materials cause variable aperture in a fracture, which influences the hydraulic and transport behaviour in the fracture. The porosity (heterogeneous void space: minor fractures, mineral grain boundaries, cleavages) in the rock matrix also has potential to influence groundwater and air transport. **Processes:** Two phase (saturated and unsaturated) flow of groundwater and air (including gas phase water) are transported in both of the network of fractures and in the rock matrix. An unsaturated zone in fractures and rock matrix might occur near the open tunnel and boreholes. Hydraulic and transport characteristics might be influenced by the change of water content and the mechanical condition (stress, pressure, mechanical properties changes caused by the openings and swelling pressure of the bentonite) **Conditions:** Groundwater pressure distribution and chemical composition at surrounding area in Äspö HRL also control groundwater pressure distributions in the project area.	**Features:** The network of discrete fractures provides porosity for groundwater flow. The fractures larger radius than 0.25 m (fracture model suggested by the task descriptions) are assumed to have a potential to interconnect each other and provide groundwater to bentonite. The porosity in the rock matrix including small fractures radius less than 0.25 m is assumed to be small enough that it can be included in the porosity and permeability of those fractures that are implemented explicitly. Fractures are implemented as polygons tessellated to triangular finite elements. Each fracture is specified by a single value of size (area), orientation, and spatial coordinates. The single fracture has a single (representative) value for transmissivity, storativity and aperture (The in-plane heterogeneity caused by the variable aperture in a fracture is ignored). Fracture tessellation is designed to preserve fracture shapes and intersections. **Processes:** Single phase groundwater flow based on Darcy's law is assumed in the discrete fracture network model, and is solved by a Conjugate gradient Galerkin finite element solver. **Conditions:** The parameter values of fracture radius, orientation, transmissivity, storativity and aperture are stochastically generated, according to specified correlations and probability density functions (PDFs). It is assumed that a single set of stochastic parametres describing the distribution of the fractures (PDFs) could reproduce the potential discrete fracture network model of rock. The specific correlations among fracture radius, transmissivity and storativity are considered.
Interface	**Features:** The gap (1 mm) between rock and bentonite and the pouring water into the gap might causes heterogeneous re-saturation behaviour at the surface of the bentonite column, heterogeneous swelling in the bentonite, and subsequent hetero-geneous porosity, density and pressure distribution in the bentonite.	**Features:** The gap (1 mm) between rock and bentonite was ignored. No specific feature was considered between rock and bentonite. **Processes:** N/A **Conditions:** The groundwater flow rate through the fracture network to the interface, calculated by using fracture network model is transferred as the bentonite surface boundary condition for unsaturated condition at the bentonite surface boundary. The pressure distribution in the bentonite column is calculated using the specified flow rate at the bentonite column surface during each time step, and the calculated pressure at the bentonite column surface is trans-ferred to the boundary condition for calculating using fracture network model. After saturated at each the bentonite surface point, a constant head (z coordinate +5 m) is assumed as the boundary condition for both rock and bentonite calculation.
Bentonite	**Features:** The bentonite blocks might behave as an inhomogeneous, channelised, and anisotropic porous media due to the heterogeneous re-saturation process in the bentonite column. **Processes:** Two phase isothermal groundwater and air (including gas phase water) movement might cause swelling pressures that couple hydraulic properties. Heterogeneous swell causes deformation of bentonite blocks and affects the mechanical and hydraulic properties of the bentonite. Chemical composition of groundwater also potentially effects these properties **Conditions:** Heterogeneous re-saturation might causes the heterogeneous capillary pressure and permeability in the bentonite column.	**Features:** The homogeneous and isotropic porous media which has 0.15 m outer radius and 0.02 m inner radius, about 3 m (2.87 m at Hole 18 and 3.378 m at Hole 17) hollow cylinder shaped column is modelled as the bentonite. The hollow cylinder is discretised by hexahedron elements, by height about 30 division (10 cm), 8 division along radius direction and 16 division along radial direction. **Processes:** The Richards' equation is assumed to control groundwater movement in the bentonite and is solved by the finite element (hexahedral element) solver. **Conditions:** The relative permeability is assumed to be correlated to the cubic of saturation. The capillary pressure is assumed to be correlated to the saturation, based on van Genuchten model of water retention curve.

2 Task 8B – Simulation codes setup and demonstration

2.1 Objectives

The overall aim of Task 8 was to improve the knowledge of the bedrock-bentonite interface with regard to groundwater flow. Task 8B was a scoping calculation exercise that was contained within the simulation of a simplified fracture and sub-local site-specific three-dimensional groundwater flow specification. A hypothetical simplified fracture was assigned as a circular feature of a diameter of 10 metres (m) with its centre axis of the 30 centimetre (cm) diameter borehole, which was modelled as a 3 m depth starting coordinate, x = 1551588, y = 6367795, z = –416.7.

Among the multiple objectives for Task 8B described in the Task 8 descriptions (Vidstrand et al. 2017), we decided to examine the newly developed simulation system that is an implicitly coupling of two distinct simulation codes: saturated groundwater flow simulation code through discrete fracture network in rock and a thermo-hydro-mechanical coupling simulation code in bentonite. The effect of the preferential pathway of groundwater by a single fracture with no permeable rock matrix was demonstrated.

2.2 Approach

A simulation system implicitly coupling two codes, FracMan/MAFIC (Dershowitz et al. 2007, Miller et al. 2001) and Thames (Chijimatsu et al. 2000) was implemented for Task 8 studies (Figure 2-1). In rock, a discrete fracture network (DFN) structure of the potentially water flowing fractures was modelled by FracMan and saturated fluid flow based on Darcy law through the fracture network calculated by MAFIC. Groundwater movement in rock matrix was neglected in this study. Thames is a thermo-hydro-mechanical coupling simulation code for continuous porous media. In this study, re-saturation and fluid movement behaviour in the bentonite based on Richards' equation assumption (Bear 1972) was solved by Thames. Two utility programs, MTOT (Mafic to Thames) and TTOM (Thames to Mafic), were developed to provide an interface between these two codes. The heterogeneous groundwater flow rate to the 30 cm boreholes where bentonite columns were installed, calculated from MAFIC, is transferred to Thames by the utility program MTOT. MTOT also identifies elements and nodes at the surface of the bentonite column models corresponding to the location of fracture traces which are intersected by bentonite installing boreholes, and groundwater flow rate flowing through the bentonite surface along the fracture traces. The flow rate, Q, calculated from MAFIC is reallocated to the surface nodes of bentonite model which are regularly gridded of bentonite column model (Figure 2-2). The value of Q is redistributed to adjacent nodes weighted by the distance between the nodes. It is the flow rate boundary condition which is set on the surface node of the bentonite column model as infiltration rate from fracture during unsaturated condition. If the infiltration rate is relatively larger than the maximum suction of bentonite, pressure at bentonite surface increases artificially. The dumping factor to moderate high flow rate from fracture to each node of bentonite surface is defined by MTOT. The maximum allowable flow rate was assumed as 1×10^{-7} Litre/sec at a Finite Element Mesh (FEM) node of bentonite surface. This flow rate is derived by the result of sensitivity analysis to prevent the artificial pressure increases at the bentonite/rock interface as a result of the flowboundary condition. The representative cross-sectional area of each node at bentonite surface is 5.85×10^{-2} square metres (m^2). Once the surface node has made to be saturated, the flow boundary condition is replaced with head boundary condition (z coordinate + 5 m). The head value of z + 5 m was assumed to account for the influence of the water pressure table at the base of the tunnels above the emplacement boreholes. TTOM transfers head values at surface nodes of bentonite model calculated by Thames to the adjacent fracture node for MAFIC calculations. If pressure value calculated from Thames is negative (caused by suction), atmospheric pressure is set at borehole wall boundary of MAFIC model. The dumping factor to moderate high pressure from bentonite surface nodes to fracture nodes is defined by TTOM. The maximum allowable head value was assumed z coordinate + 5 m, which is same value for identifying whether the surface node is saturated or not, as described above.

Figure 2-3 shows a conceptual illustration of the calculation sequence for coupling two codes. Firstly, a steady state groundwater flow field with atmospheric pressure condition at 30 cm boreholes, which simulate the condition before installing the bentonite to the boreholes, is simulated. Groundwater flow rate to the boreholes are transferred to Thames as boundary condition, and the coupling simulation is started. After Thames runs, pressure conditions at bentonite surface is transferred to MAFIC as boundary condition at 30 m borehole walls and MAFIC runs with same time step as Thames. The time step for terminating calculation for switching two codes is optimised empirically with taking account of convergence of the codes and computational time.

This simulation system was examined by using a simplified geological condition specified as Task 8B.

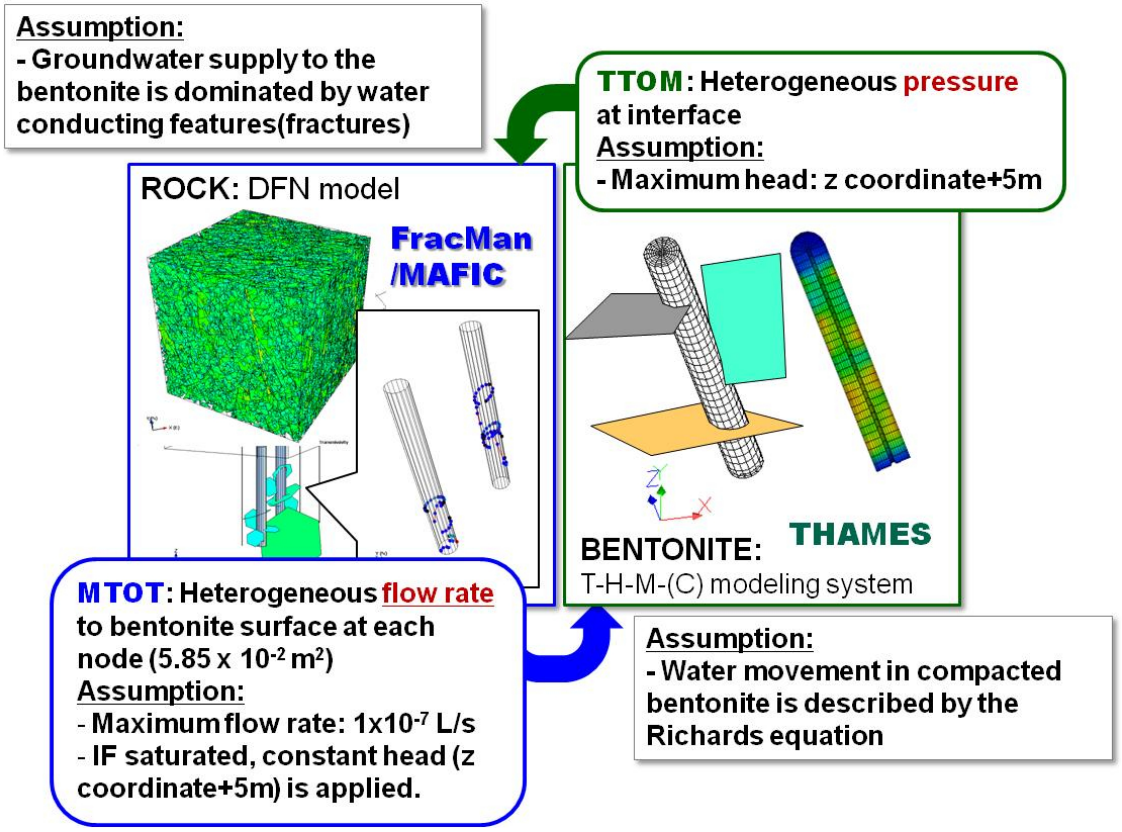

Figure 2-1. *Conceptual illustration of a simulation system coupling FracMan/MAFIC and Thames with two interface utility programs, MTOT and TTOM.*

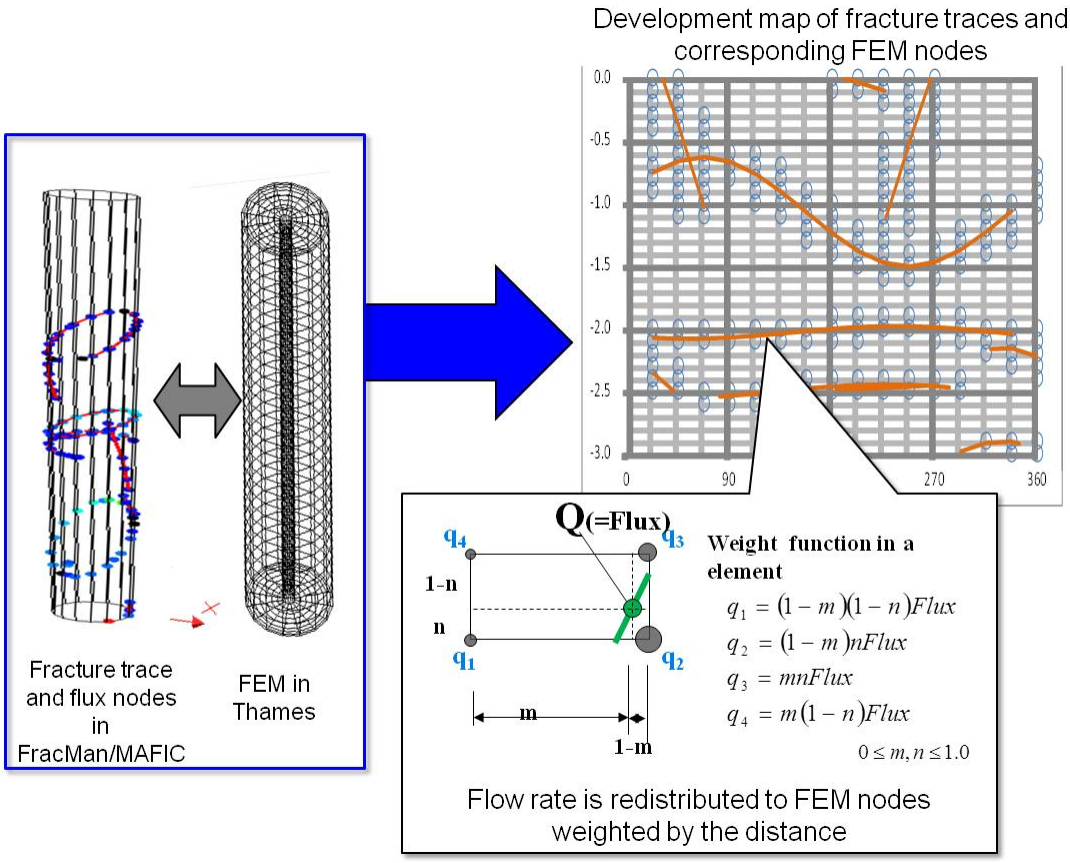

Figure 2-2. *Conceptual illustration of MTOT functions, nodes identification of bentonite column FEM corresponding to the fracture traces, and flow rate reallocation of MAFIC results to nodes of bentonite FEM.*

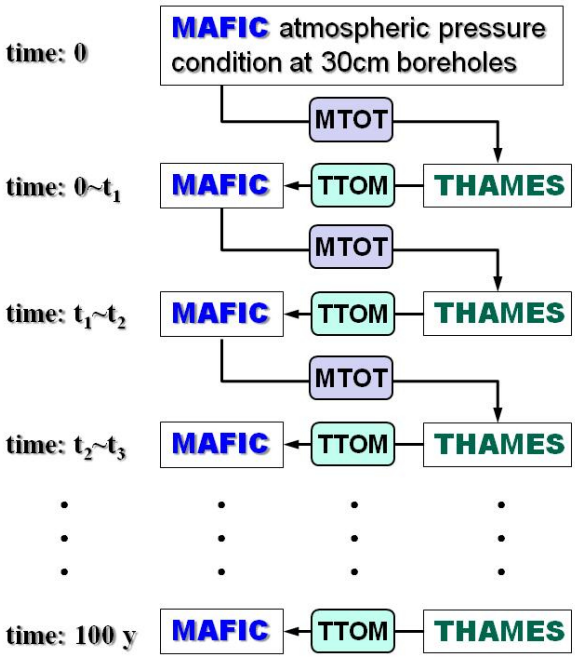

Figure 2-3. *Conceptual illustration of iterative calculation sequence for an implicitly coupling MAFIC and Thames codes.*

2.3 Model Setup

A hypothetical simplified fracture was assigned as a circular (modelled by a hexagon plan) fracture of a diameter of 10 metres. The centre of a fracture is located at half depth of the 30 cm diameter borehole, which is modelled as 3 m depth starting coordinate, x = 1551588, y = 6367795, z = –416.7. Figure 2-4 shows the fracture and fault model in specified 40 m × 40 m × 40 m box region. Task 8B specification (Vidstrand et al. 2017) suggests seven large fractures for the deterministically defined larger fractures. However, in order to keep model consistency among Task 8B, 8C and 8D in this study, it was decided to add only three faults, NNW-4, wfracture01 and wfracture02 specified in Task 8D as a reference model. It was confirmed that a hypothetical fracture could connect to these faults model, which provide head values from the specified constant head at outer boundary of modelling region. Figure 2-5 shows head distribution estimated from DarcyTool's simulation of the full regional Äspö HRL model, provided by the Task 8 descriptions (Vidstrand et al. 2017). The location and orientation of wfracture01 had been varied through Task 8B to 8D specification. The effect of the variability of wfracture01 was examined in Task 8C (see Chapter 3), and wfracture01 model specified in Task 8D (see Chapter 4) was defined as a reference model. Table 2-1 summarises the material properties of a hypothetical single fracture specified in Task 8B and deterministically defined faults specified in Task 8D.

Bentonite column was hypothetically installed in a 30 cm diameter borehole. The material properties of the bentonite are listed in Table 2-2.

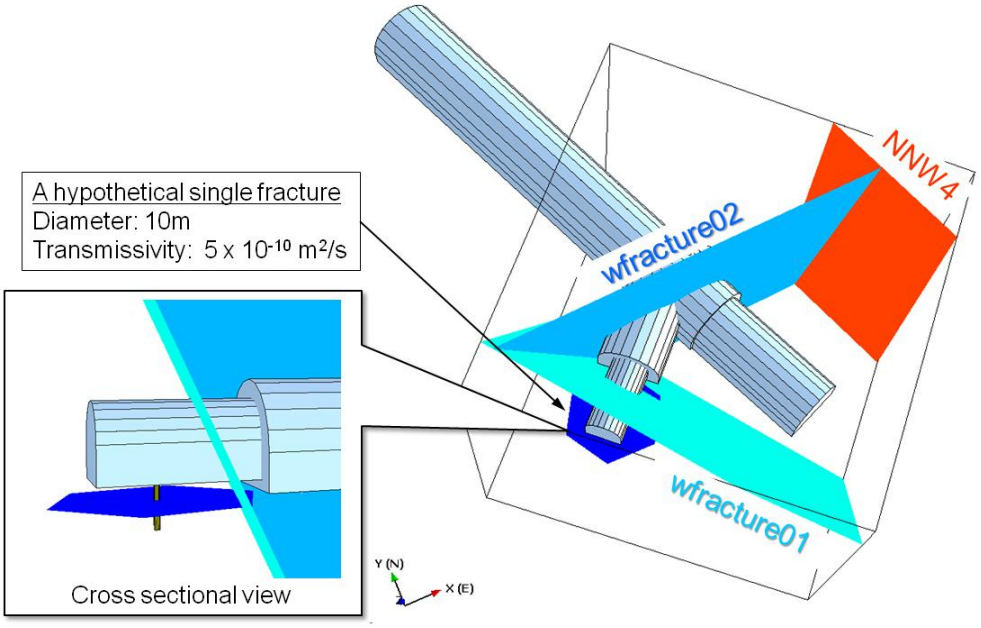

Figure 2-4. *A hypothetical single fracture model and deterministically defined fault zones, NNW4, wfracture01 and wfracture02.*

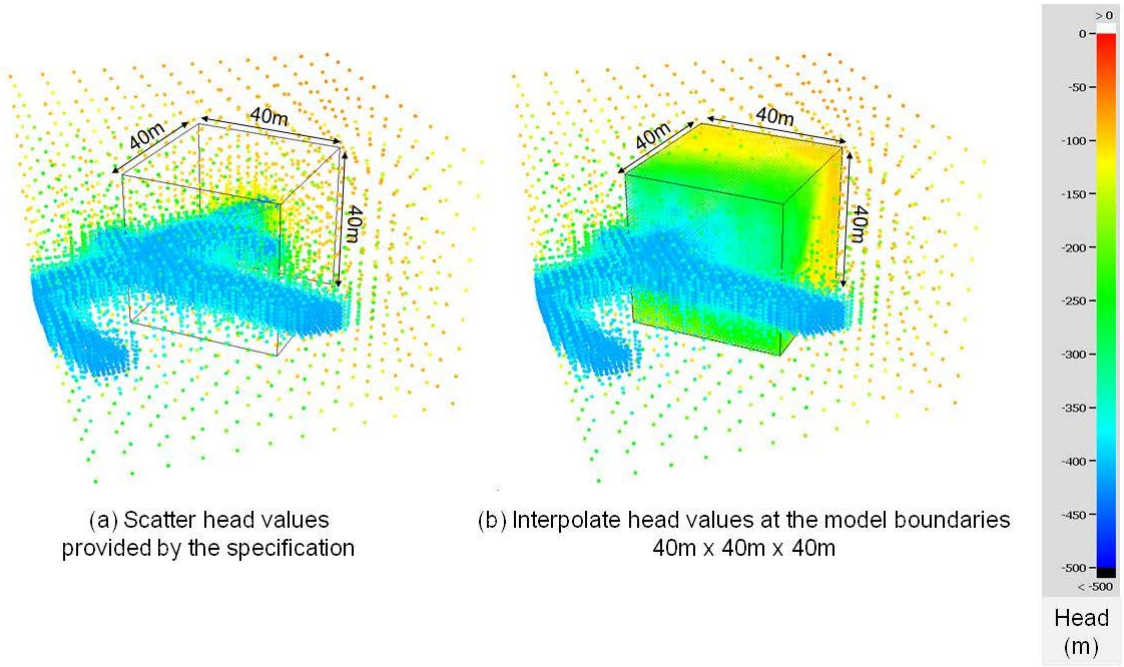

(a) Scatter head values provided by the specification

(b) Interpolate head values at the model boundaries 40m x 40m x 40m

Figure 2-5. *Heterogeneous head distribution estimated from DarcyTool's simulation results provided by Task 8 descriptions (Vidstrand et al. 2017).*

Table 2-1 Material properties of a hypothetical single fracture specified in Task 8B and deterministically defined faults specified in Task 8D.

	Tansmissivity (m^2/s)	**Aperture (m)**	**Storativity (-)**
A hypothetical single fracture	5×10^{-10}	1×10^{-6}	1×10^{-9}
wfracture01	4×10^{-9}	1×10^{-5}	1×10^{-8}
wfracture02	2×10^{-9}	1×10^{-5}	1×10^{-8}
NNW4	6.5×10^{-7}	1×10^{-5}	1×10^{-7}

Table 2-2. Material properties and initial conditions of bentonite.

Parameter	**unit**	**value**
Porosity	-	0.438
Intrinsic permeability	m^2	6.4×10^{-21}
Dry density	Mg/m^3	1.56
Relative permeability, k_r	-	$k_r = S_l^3$ S_l: water saturation
Water retention curve		van Genuchten's equation $S_l(P_l) = \left\{1 + \left(\frac{P_g - P_l}{P_0}\right)^{\frac{1}{1-\lambda}}\right\}^{-\lambda}$ P_l: water pressure P_g: Gas pressure: 0.1MPa P_0: empirical constant: 9.23MPa λ: empirical constant: 0.3
Water density	Mg/m^3	1
Water viscosity	Pa s	0.001
Temperature	°C	25

2.4 Results

Figure 2-6 shows a head distribution around a hypothetical single fracture, under the steady state condition with atmospheric pressure condition at 30 cm diameter borehole. This head distribution was used for an initial condition (time=0 as described in Figure 2-3), before installing bentonite into 30 cm diameter borehole. Figure 2-7 and Figure 2-8 shows pressure and saturation evolution in bentonite column, respectively. The limited groundwater supply from a fracture controls groundwater re-saturation behaviour, and whole bentonite column would not be saturated under this simulation condition even the 100 years would be elapsed. At each time step, both of MAFIC and Thames were designed to calculate transient flow behaviour. However, under the saturated condition in rock fractures which is one of basic assumptions in this study, the storativity effect in rock fractures is relatively smaller than bentonite. The steady state MAFIC calculation which does not take account of storativity, has an advantage of simpler and faster calculation than transient runs. The comparison of bentonite re-saturation behaviour between the transient MAFIC calculation and steady state shows no significant differences. It was decided to apply steady state MAFIC calculation for a series of Task 8 simulation study for simplicity.

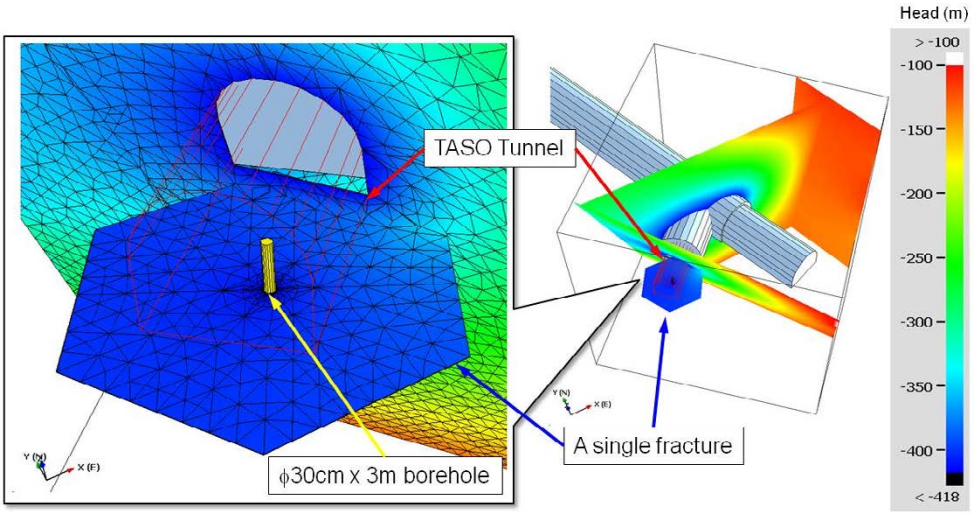

Figure 2-6. *Simulated head distribution around a hypothetical single fracture, steady state condition with atmospheric pressure condition at 30 cm diameter borehole.*

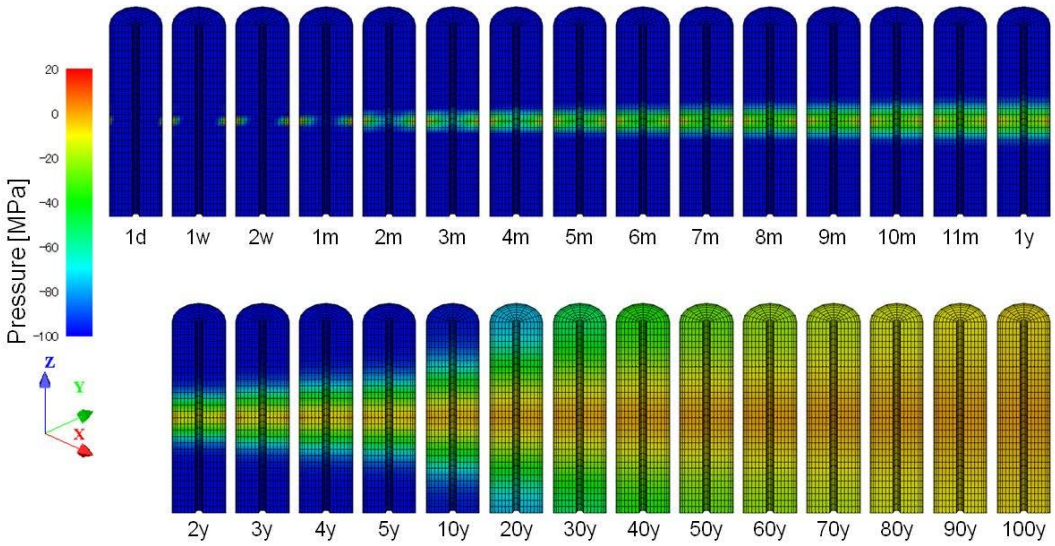

Figure 2-7. *Pressure distribution after installing bentonite into 30 cm diameter borehole.*

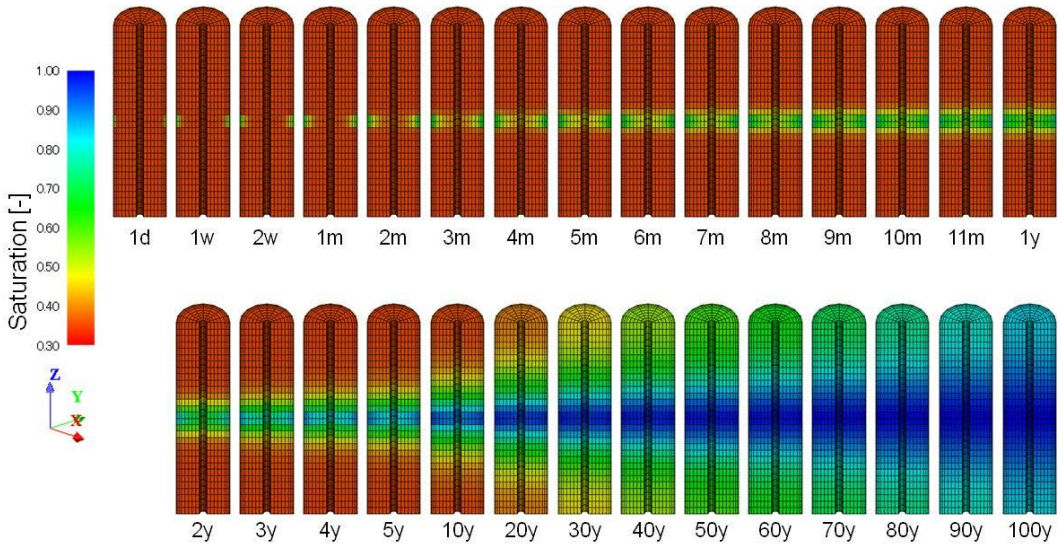

Figure 2-8. *Saturation distribution after installing bentonite into 30 cm diameter borehole.*

Flow rate and pressure evolution at the interface between rock (fracture in this study) and bentonite were examined. The interface, Node A, shown in Figure 2-9 was selected as one of the representative points, because there are no significant head differences around 30 cm diameter borehole at a single fracture. Figure 2-10 shows the flow and pressure change at Node A. Before being saturated at the bentonite surface, Thames runs under the condition of constant groundwater flow rate, 1×10^{-7} Litre/sec, at bentonite surface, because the groundwater flow rate calculated by MAFIC under the atmospheric pressure boundary condition (BC) at 30 cm diameter borehole wall exceeds upper limit, which is 1×10^{-7} Litre/sec specified by MTOT. When bentonite surface is close to be saturated, the constant flow rate boundary condition to the bentonite surface yields sudden pressure increase. Identification of the saturated condition at the interface is a key to avoid numerical oscillations in the iterative sequential coupling system. A pulse increase of pressure shown in Figure 2-10 is caused by numerical error. However, there is no significant oscillation shown in the figure, using Task 8B simplified model. TTOM identifies being saturated at the interface by pressure value exceeding 5 m at bentonite surface calculated by Thames. It was assumed that bentonite suction might not significantly affect on groundwater flow behaviour in rock fractures. Before being saturated, it was assumed that negative pressure value caused by suction of bentonite might not be transferred to the boundary condition of MAFIC, and MAFIC continues to use atmospheric pressure at the wall of 30 cm diameter borehole as the boundary condition. After being saturated at the bentonite surface, the pressure value is reset to 5 m and the atmospheric pressure boundary condition at 30 cm borehole wall for MAFIC is replaced with constant head boundary z coordinates + 5 m. MTOT also replaces constant flow boundary condition at the interface with z coordinates + 5 m constant pressure boundary. After being saturated at the bentonite surface, the flow rate through this node is decreasing as propagating saturation into bentonite column by decreasing suction at the saturated bentonite.

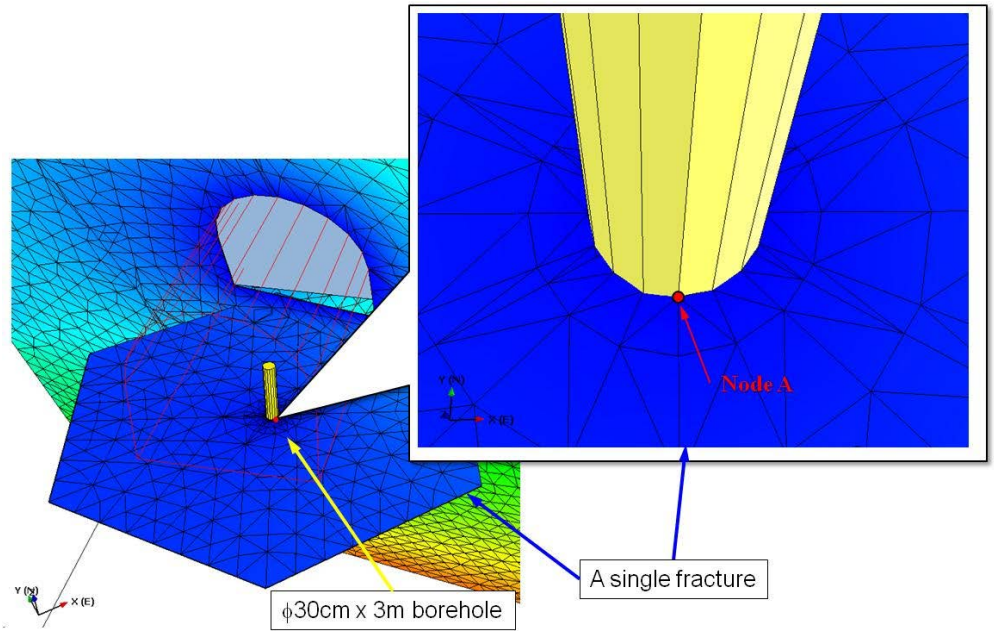

Figure 2-9. *Location of arbitrary selected node, "Node A", at the interface between fracture and bentonite.*

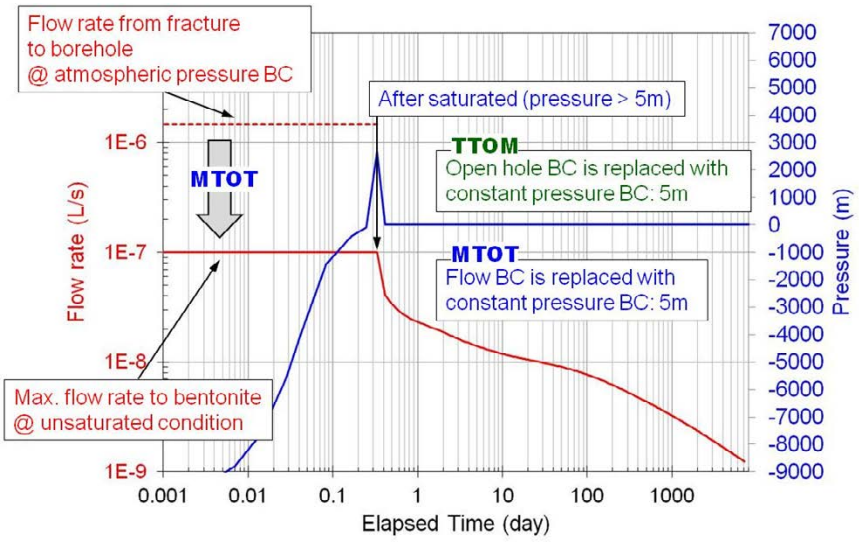

Figure 2-10. *Flow rate and pressure history at the interface between fracture and bentonite, at Node A.*

2.5 Discussion

In order to demonstrate a capability of the coupling simulation system, several sensitivity cases as listed below were conducted.

1. Increase dumping factor of flow rate in MTOT from 1×10^{-7} to 1×10^{-6} Litre/sec.
2. Decrease transmissivity of a single fracture (original $T = 5 \times 10^{-10}$ m^2/sec).
   a. original $T \times 0.12$ (6×10^{-11} m^2/sec)
   b. original $T \times 0.05$ (2.5×10^{-11} m^2/sec)
   c. original $T \times 0.005$ (2.5×10^{-12} m^2/sec)
   d. original $T \times 0.001$ (5×10^{-13} m^2/sec)

The sensitivity calculation results of flow rate evolutions and pressure evolutions at the interface (Node A) are shown in Figure 2-11 and Figure 2-12, respectively. Case 1) is a sensitivity case of how the dumping factor of flow rate affects water movement behaviour through the interface. When increasing the dumping factor (flow rate), the larger initial flow rate being in unsaturated condition causes the faster saturation time at bentonite surface and larger pulse of pressure increase at the time of saturation. Although initial flow rate through the interface is larger, it converges to the same trend of the reference case of Task 8B model before elapsing 1 day, and the cumulative flow to bentonite column also converges to the same curve to the reference case (see Figure 2-13). The flow rate through the interface is controlled primarily by the permeability of saturated bentonite, the depth of the saturated zone from the interface and the suction in the inner unsaturated bentonite. As the depth of saturation in the bentonite increases, the flow rate through the interface decreases.

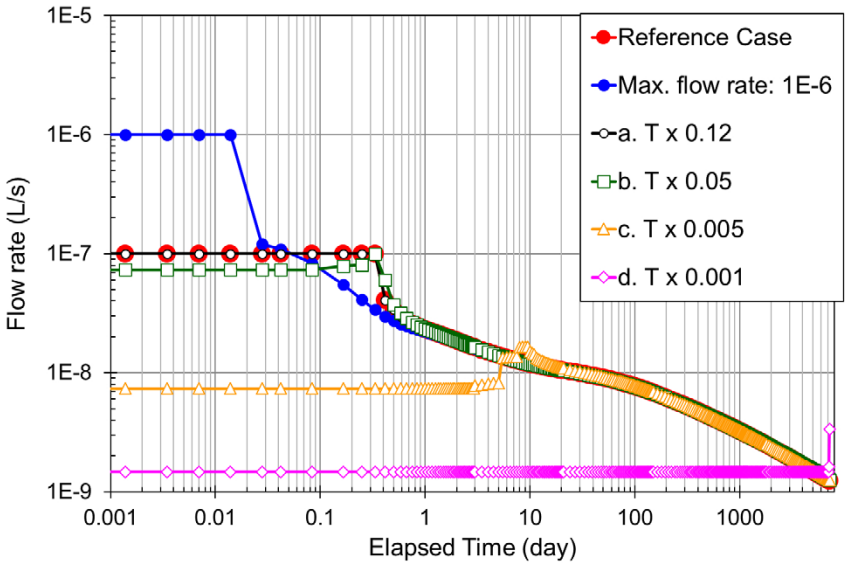

Figure 2-11. *Sensitivity calculation results, flow rate evolutions at the interface between fracture and bentonite, at Node A.*

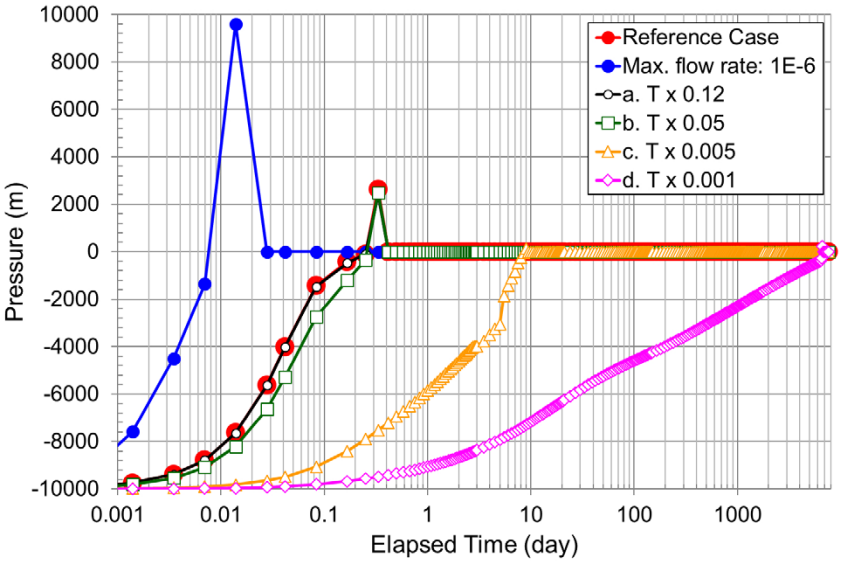

Figure 2-12. *Sensitivity calculation results, pressure evolutions at the interface between fracture and bentonite, at Node A.*

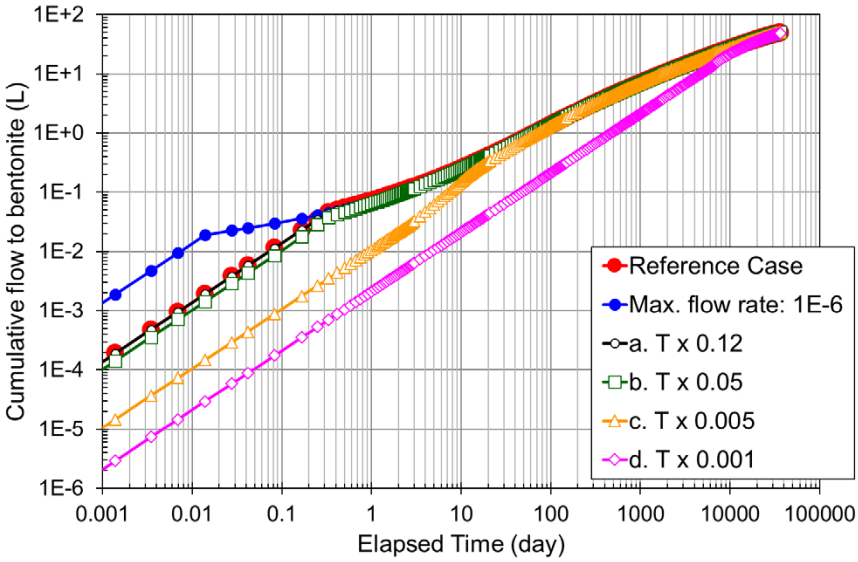

Figure 2-13. *Sensitivity calculation results, cumulative flow to bentonite column.*

A series of Case 2) is a sensitivity case of how the transmissivity of a single fracture affects water flow rate to the bentonite. Case a. and Case b. are adjusted to get ground water flow rate just over and below the dumping factor, respectively. These two cases have similar flow rate and pressure at the interface. Case c. and Case d. are cases of reducing availability of groundwater supply to the bentonite column. Lower flow rate at initial duration causes delay of saturation time at the bentonite surface. The flow rate through the fractures calculated by MAFIC is controlled by fracture transmissivity and hydraulic gradient. The flow rate and cumulative flow converges to the same values as the reference case after being saturated at the surface of bentonite. During bentonite resaturation, groundwater is distributed to the inside of the bentonite column. This causes decreases suction in unsaturated bentonite. This might be one of the main reasons why the evaluation of flow rate at the interface converges to the same value for the different fracture transmissivity sensitivity cases studied.

2.6 Conclusions and Recommendations

In this section, the simulation system newly developed for a series of Task 8 studies is described. The feasibility of the newly developed simulation system was demonstrated using the simplified model specification, Task 8B. In addition, the capability of the system was examined by the sensitivity studies. From the examination using simplified Task 8B model specification, the followings could be concluded:

- The newly developed simulation system implicitly coupling two codes, groundwater flow simulation code through DFN model (FracMan/MAFIC) and a thermo-hydro-mechanical coupling code for continuous porous media (Thames), could simulate the effects both of heterogeneous flow through the rock fractures and groundwater movement in bentonite without any significant numerical oscillations, although pulse type pressure increase might be generated at the time of saturation at the bentonite surface.
- It was confirmed that the system could simulate two major fundamental processes: the saturation time at the bentonite surface is controlled by availability of groundwater flow of fractures connecting to the bentonite, and groundwater flow rate through the interface is controlled by the groundwater diffusion behaviour in bentonite after being saturated at the bentonite surface.

The pulse type pressure increase at the time of bentonite surface saturation, might have a potential for causing numerical error in the heterogeneous DFN model cases, although there were no significant errors in a simplified homogeneous Task 8B model case. In order to avoid this artefactual errors, a modification in TTOM was made for Task 8C and 8D examinations. If the pressure at the bentonite surfaces calculated by Thames is higher than z+5 m, TTOM demands Thames to re-calculate the previous time step again by changing flow boundary condition at each high pressure bentonite surface point.

3 Task 8C – BRIE prediction for central holes

3.1 Objectives

Task 8C was divided into two parts, Task 8C1 and Task 8C2. Figure 3-1 summarises the structures of Task 8C. In order to establish "BRIE" prediction, Task 8C constitutes two aspects for the modelling scale; 40 m block scale around the tunnels to provide heterogeneous head distribution around the tunnels, and more detailed scale around the boreholes (simulating disposal holes). The Task 8C1 exercise was to predict groundwater flow distribution to the 30 cm diameter holes. Incorporation of bentonite was not considered in the Task 8C1 exercise. Instead, the inflow to open boreholes was addressed to test the modelling tool's ability to predict inflow to deposition holes based on limited information. Task 8C2 addressed the wetting of bentonite based on the flow field and flow distribution established in Task 8C1. The scope of this calculation exercise is contained within the simulation of a sub-local site-specific three-dimensional groundwater flow specification. This modelling examination has an advantage for the methodology development of site investigation and model evaluation for the disposal holes at underground tunnel excavation phase of the disposal project.

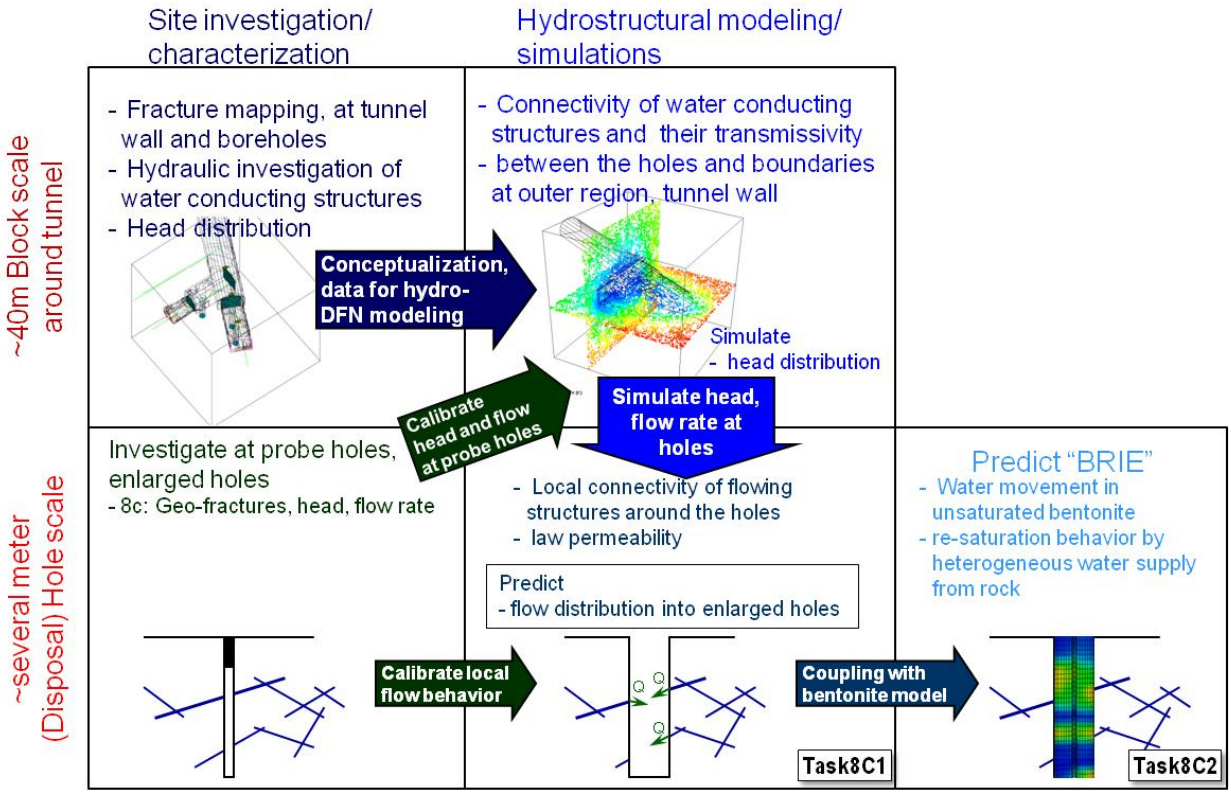

Figure 3-1. *Task 8C model exercise structures.*

3.2 Approach

The DFN model, FracMan/MAFIC, assuming that the fracture network structure dominates groundwater flow and the rock matrix surrounded by the fracture network has no permeability was used for Task 8C1 modelling in the 40 m × 40 m × 40 m cubic region. The base case of the DFN model was constructed according to the Task 8 descriptions (Vidstrand et al. 2017). The alternative cases defined by considering the uncertainties of the model definitions and parameter values were compared with a limited number of measured data which includes head and flow rate at five probe boreholes drilled at TASO tunnel flow to examine how to modify the base case groundwater flow model at the target volume. The base case model was devoted to the coupling simulation system described in Chapter 2, to simulate "BRIE" re-saturation behaviour in bentonite emplaced in 30 cm enlarged boreholes along KO00017G01 and KO00018G01, respectively. Some selected cases of the alternative model were also adopted to simulate bentonite re-saturation behaviour of BRIE.

3.3 Model Setup

The DFN model contains deterministically defined larger faults; NNW4, wfracture01 and wfracture02, and stochastically defined fractures. Figure 3-2 and Table 3-1 show the location and extent, and transmissivity of the deterministically defined faults, respectively. The specification for the location and transmissivity of wfracture01 had been varied through the Task 8 modelling taskforce project as shown in Figure 3-2 and Table 3-1. In order to keep the consistency of model conceptualisations among the subtasks, Task 8C and 8D, wfracture01 specified in Task 8D was selected as reference case and the other cases are examined as the alternative model cases.

Table 3-1. Transmissivity of the deterministically defined faults.

Faults name		Transmissivity (m^2/s)
NNW4		6.5×10^{-7}
wfracture01	Task 8C specification	2×10^{-8}
	Task 8C modified specification	5×10^{-9}
	Task 8d specification	4×10^{-9}
wfracture02		2×10^{-9}

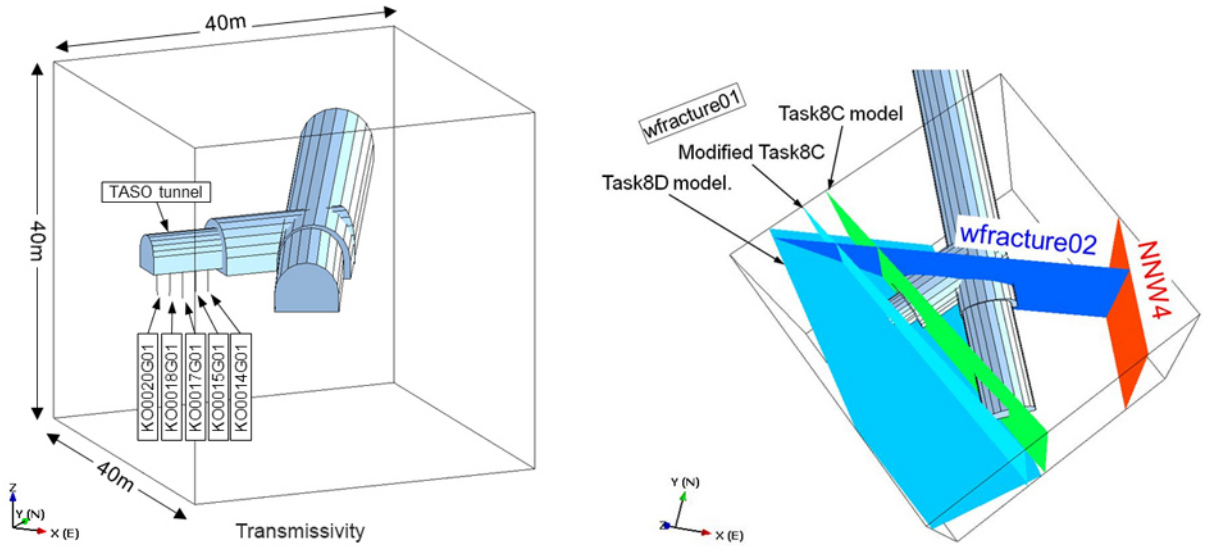

(a) Modeling region and five probe boreholes.

(b) Deterministically defined faults; NNW4, wfracture01 and wfracture02.

Figure 3-2. *Model region and deterministically defined faults.*

The three stochastic background fracture sets were defined as listed in Table 3-2, which specifies a DFN model for geological fractures. The hydraulic properties of the geological DFN model were not provided by the Task 8 descriptions (Vidstrand et al. 2017). As is widely alleged, the number of hydraulically active fractures are smaller than one of the geological fractures. Judging from the observation of tunnel walls, it is said that 1/5 or 1/10 of geological fractures might be the water conducting fractures. In this case, the observation quantity of "wetting", "dipping" "flowing" might be helpful for identifying the water conducting fractures. However, there is no clear quantitative definition such as detection limit of water conducting fractures of tunnel wall investigation. There is no universal method to identity the water conducting fractures and to estimate the transmissivity of the water conducting fracture. For the hydraulically active DFN modelling in this task, it was not adopted to decrease the number of fractures. Instead, transmissivity was estimated from a correlation with fracture size. Figure 3-3 shows the distribution of fracture size and transmissivity, indicating a correlation. The base case model employs the size correlation as described in the following equation:

$$\text{Transmissivity} = 7 \times 10^{-11}\ \text{Length}^{1.7}$$

Figure 3-3 also indicates a wider uncertainty for the correlation. The alternative cases were considered by changing an equation of the correlation.

Table 3-2. Stochastic fracture sets.

Set#	Orientation			Size (power law)		Spatial distribution	Intensity $P_{32}(r_0,\infty)$ m^2/m^3
	Trend	Plunge	Fisher K	r_0	k_r		
Set1	280	20	10			Poison process	1.1
Set2	20	10	15	0.25	2.6		2.0
Set3	180	50	10				0.75

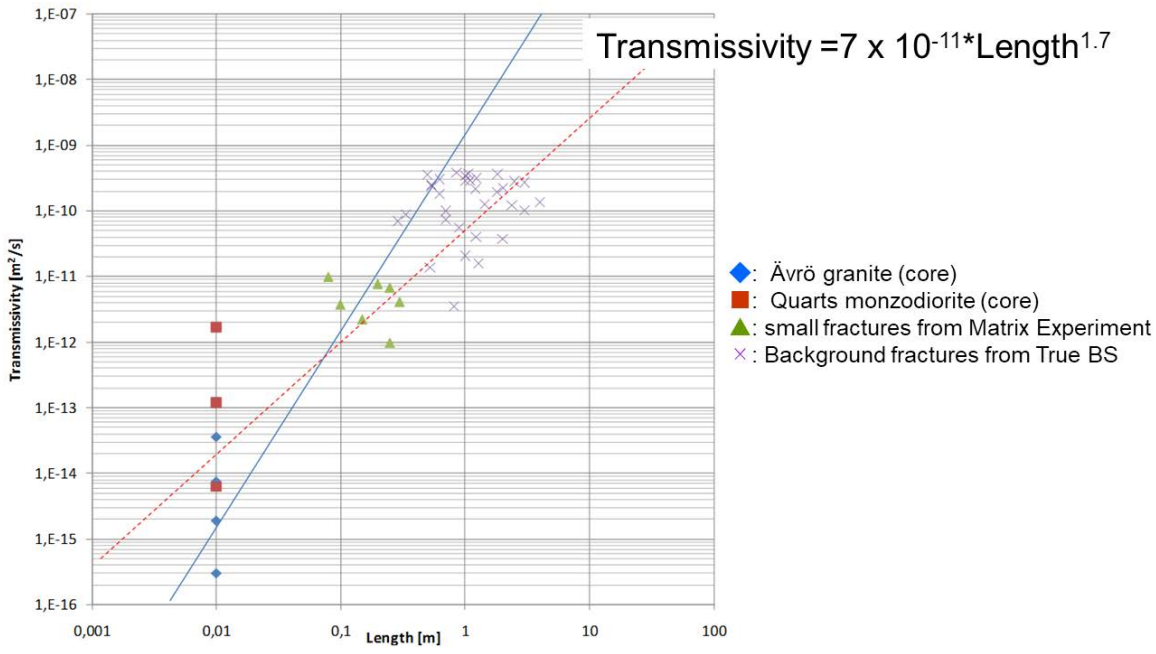

Figure 3-3. *The correlation between fracture transmissivity and fracture length.*

Figure 3-4 shows an example of background fractures for a base case model, generated by FracMan. In order to reduce computational size of the model, the fractures smaller radius of 0.6 m was removed at the outer region of the model as shown in Figure 3-4. Because, the smaller fractures have lesser transmissivity and smaller potential of forming network of fractures (lesser potential of connecting other fractures). The cut off size for the removal was judged from the analysis of sensitivity to the equivalent hydraulic conductivity in a 10 m scale of block. Figure 3-5 shows the sensitivity calculation results of the size for removing fractures to hydraulic conductivity at a 10 m × 10 m × 10 m block region, by five realisations of DFN model. The three orthogonal directions (EW: East to West, NS: North to South, UD: Up to Down) of hydraulic conductivity were examined. The cases of radius cut off larger than 0.6 m show slightly reducing of hydraulic conductivity of 10 m block scale of DFN model.

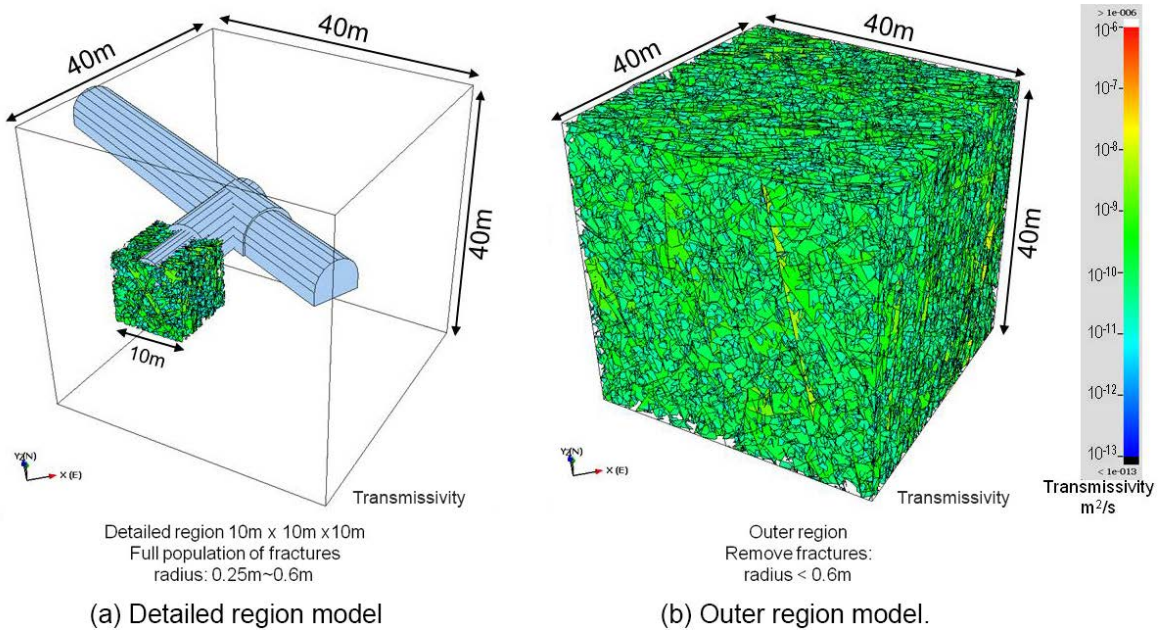

Figure 3-4. *Example of the stochastic background fractures for a base case model, generated by FracMan.*

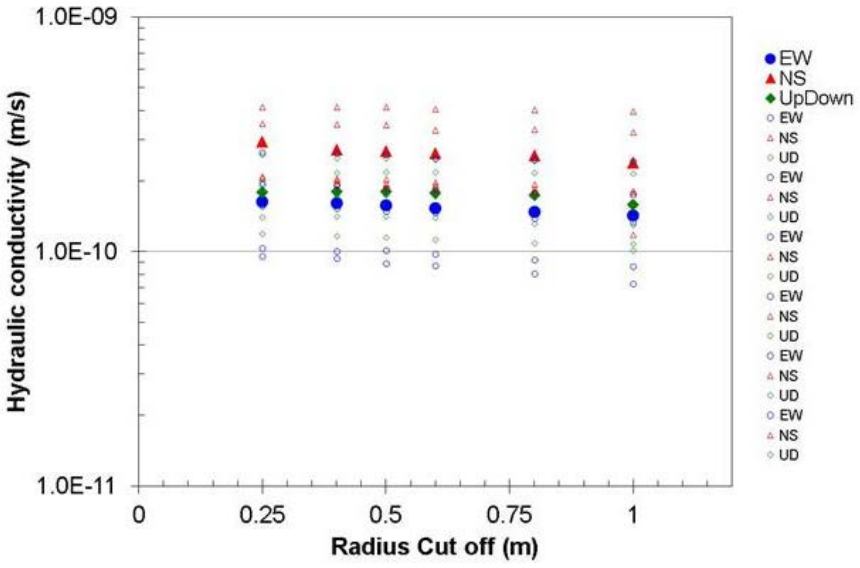

Figure 3-5. *Sensitivity of a cut off size removing fractures from DFN smaller radius than the cut off size, to hydraulic conductivity of 10 m × 10 m × 10 m block. Solid symbol: average of five realisations at each three orthogonal direction. Open symbol: result of each realisation at each three orthogonal direction.*

The same outer boundary condition as used for Task 8B was applied for base case model. The scatter values of head shown in Figure 2-5 (a) was provided from the Task 8 descriptions (Vidstrand et al. 2017), and the head distribution at surfaces of 40 m × 40 m × 40 m block shown in Figure 2-5 (b) was estimated by a kriging (Remy et al. 2009).

Tunnels and open boreholes were specified as constant head that equals elevation, to simulate atmospheric pressure conditions. The five probe boreholes drilled from the TASO tunnel floor as shown in Figure 3-2(a) were also included in the model. For simulating packed off condition at the boreholes, the modelled packed off section was specified as a zero "group flux," which assumes zero resistance to flow within a packer section of the borehole that heads are the same. While, for simulating flows to the boreholes, constant head equals to −417 m assuming average TASO tunnel floor was set to calculate overflow to the borehole collar which was drilled from TASO floor vertically.

The steady state groundwater flow calculation using a base case model was compared with the measured data provided by the Task 8C specification. Table 3-3 shows the measured flow and head values during initial pressure build-up tests at the five probe boreholes.

For the Task 8C2 examination, 30 cm diameter by 3 m length bentonite columns for installing an enlarged borehole along KO00017G01 and KO00018G01 were modelled by homogeneous continuum media (Figure 3-6), discretised by hexahedron elements, height about 30 divisions (10 cm), 8 divisions along radius direction, and 16 divisions (22.5°) along radial direction. Re-saturation and fluid movement behaviour in the bentonite, was modelled by Richards' equation assumption. Table 3-4 summarises the parameter values used for Task 8C2 examination defined by the specification, which are the same values as Task 8B specification (Table 2-2).

Table 3-3. Measured flow rate and head during initial pressure built-up in packed off at five probe holes.

	KO0020G01	KO0018G01	KO0017G01	KO0015G01	KO0014G01
inflow	(√)	"no"	√ Q ≈ 0.5 ml/min p ≈ 6 bar ≈ 2–3 m	"no"	√ Q ≈ 1 ml/min p ≈ 3 bar ≈ 0.5–1 m

Table 3-4. Material properties and initial conditions of bentonite.

Parameter	Unit	Value
Porosity	-	0.438
Intrinsic permeability	m^2	6.4×10^{-21}
Dry density	Mg/m^3	1.56
Relative permeability, k_r	-	$k_r = S_l^3$ S_l: water saturation
Water retention curve		van Genuchten's equation $S_l(P_l) = \left\{1 + \left(\frac{P_g - P_l}{P_0}\right)^{\frac{1}{1-\lambda}}\right\}^{-\lambda}$ P_l: water pressure P_g: Gas pressure: 0.1MPa P_0: empirical constant: 9.23MPa λ: empirical constant: 0.3
Water density	Mg/m^3	1
Water viscosity	Pa s	0.001
Initial Saturation	%	36
Temperature	°C	25

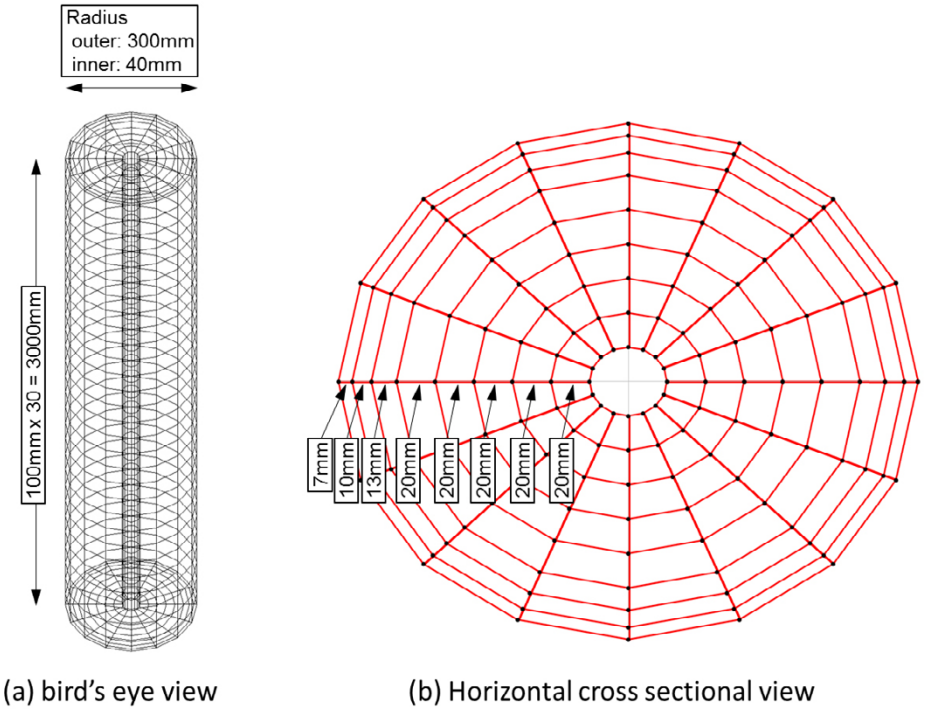

Figure 3-6. *Finite elements for modelling bentonite columns.*

3.4 Results

Groundwater flow rate and head values at five probe holes were evaluated using the five realisations of the base case model, described in Section 3.3. Figure 3-7 shows the calculated flow rate and head compared with the measured value (Table 3-3). A limited number of measured data was compared. In these figures, a base case model has 1) relatively high permeable behaviour to the probe hole, KO0017G01 and KO0014G01 compared with the measured values, and 2) wider variation among the five realisations. It was required to modify a base case model to, 1) reduce average permeability of the model, and 2) constrain a wider variability among the stochastic realisations.

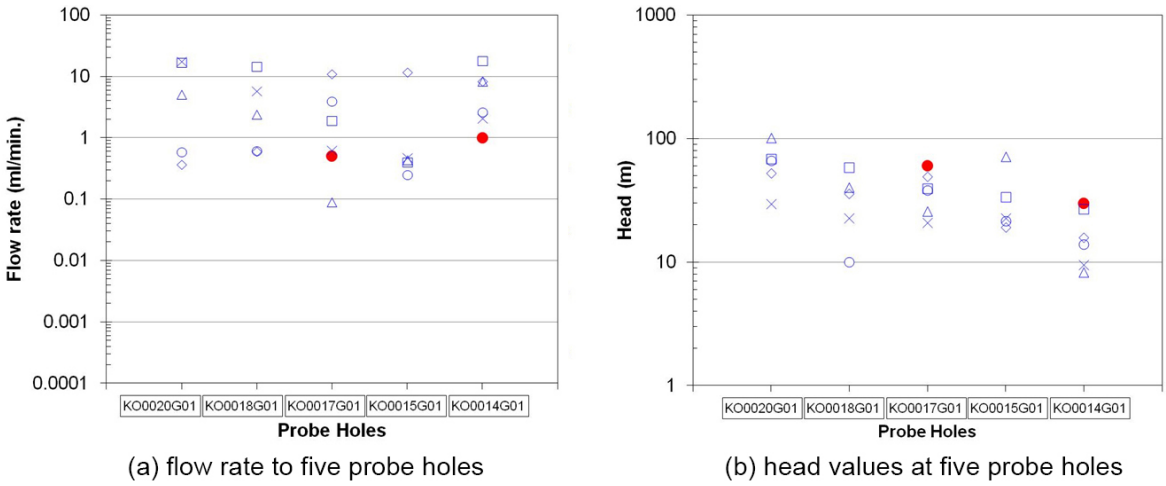

Figure 3-7. *Groundwater flow rate and head values simulated by base case model. Open symbol (Blue): simulation results of five realisations. Solid circle (Red): measured data.*

The base case model was devoted to the coupling simulation system described in Chapter 2, to simulate "BRIE" re-saturation behaviour in bentonite emplaced in 30 cm diameter boreholes enlarged along KO00017G01 and KO00018G01, respectively, as the Task 8C2 examination. A single realisation (realisation number 01), among five realisations that examined Task 8C1, was applied for the bentonite re-saturation simulation, in order to demonstrate the heterogeneous resaturation behaviour by means of sparsely distributing water conducting fractures intersecting bentonite. Figure 3-8 through Figure 3-11 show pressure distribution, saturation distribution for each KO00017G01 and KO00018G01 borehole, respectively. Heterogeneous pressure and saturation distribution caused by a limited groundwater supply from the rock fractures were reproduced by coupling FracMan/MAFIC code in rock and Thames code in bentonite.

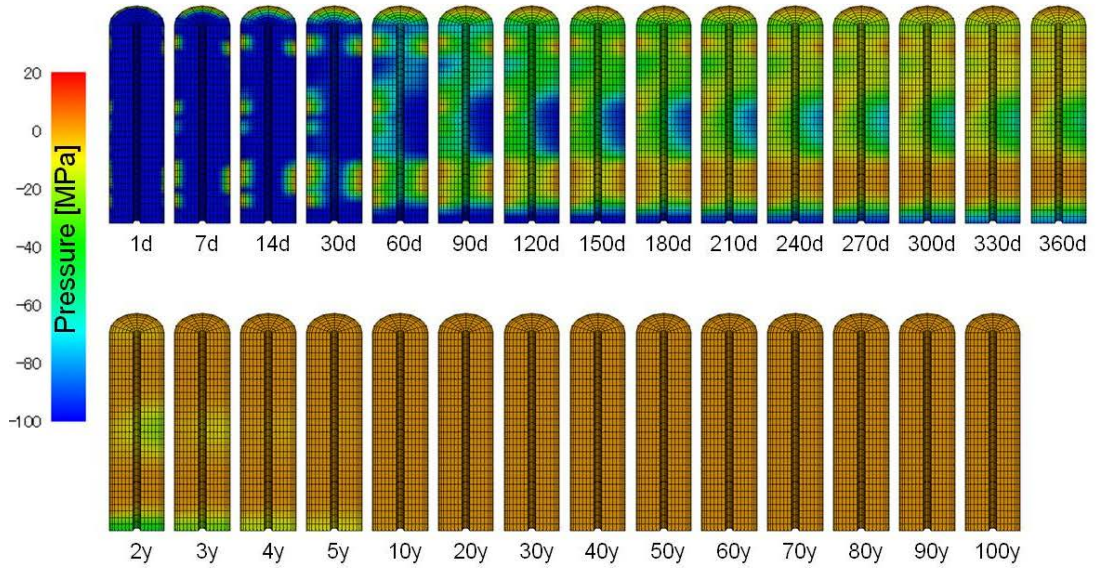

(a) vertical cross sectional view, N45E direction close to TASO tunnel axis.

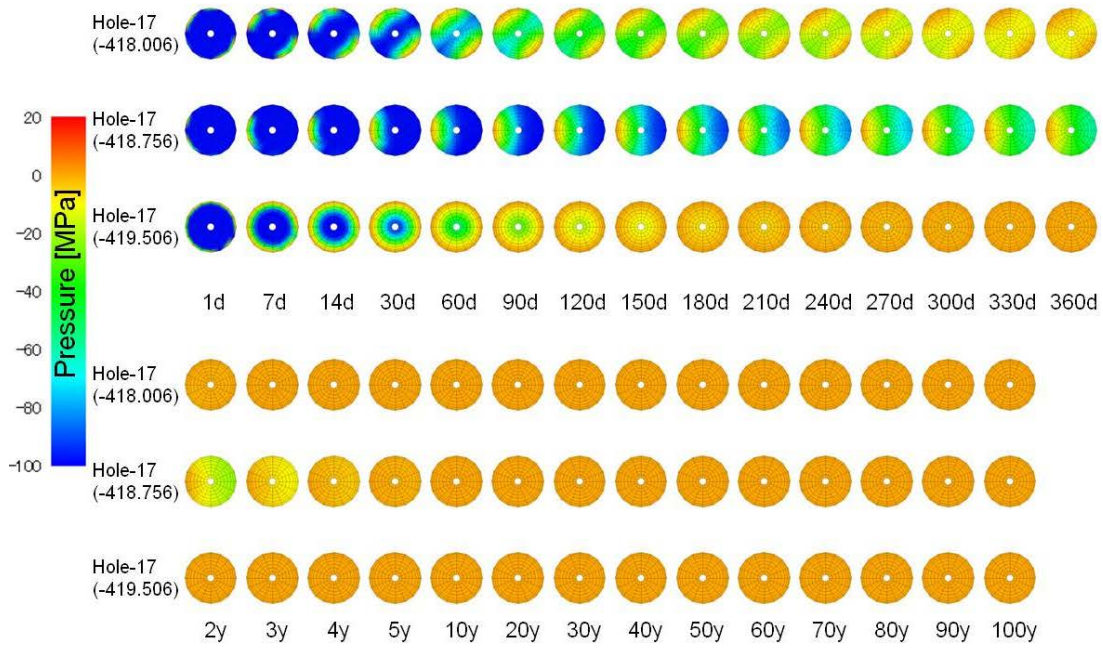

(b) horizontal cross sectional view at specified depth, top: north, right: east.

Figure 3-8. *Pressure distribution in bentonite column at KO00017G01, base case model.*

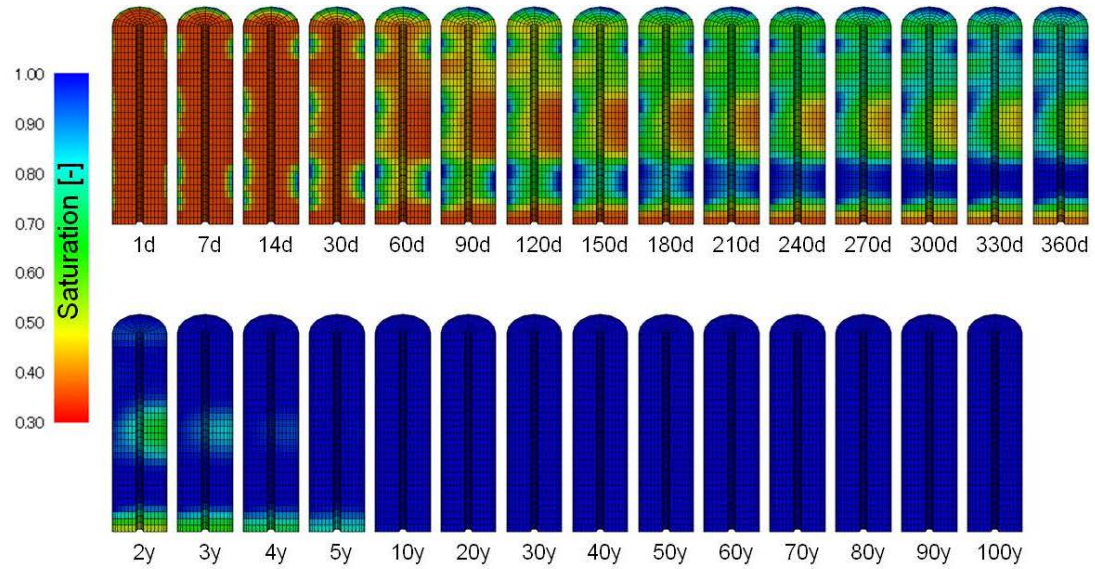

(a) vertical cross sectional view, N45E direction close to TASO tunnel axis.

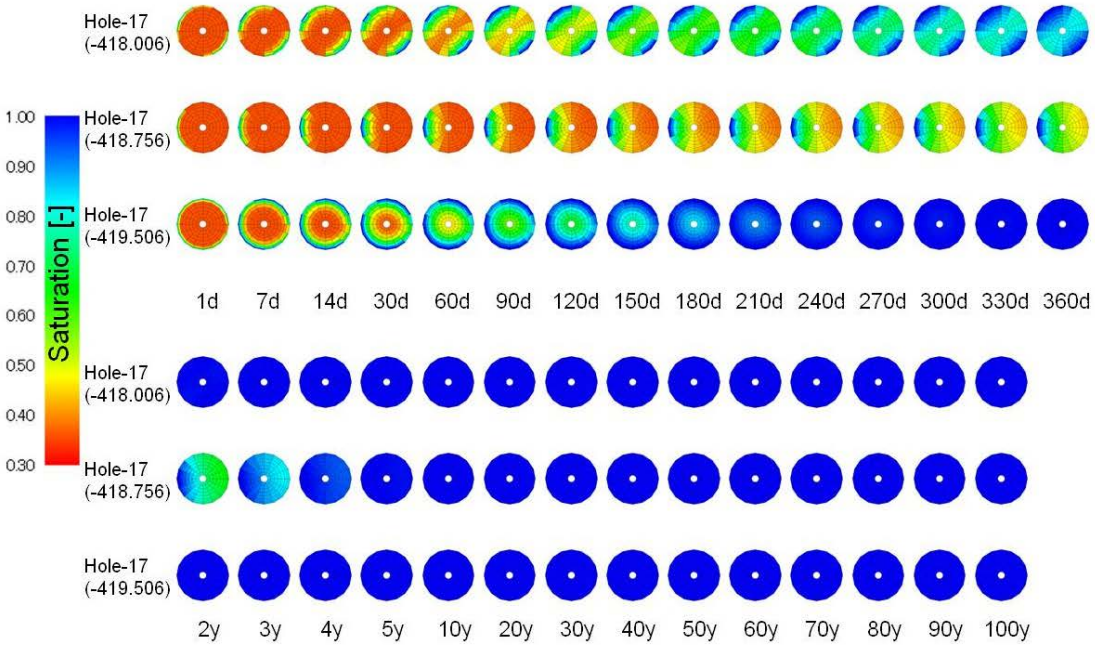

(b) horizontal cross sectional view at specified depth, top: north, right: east.

Figure 3-9. *Saturation distribution in bentonite column at KO00017G01, base case model.*

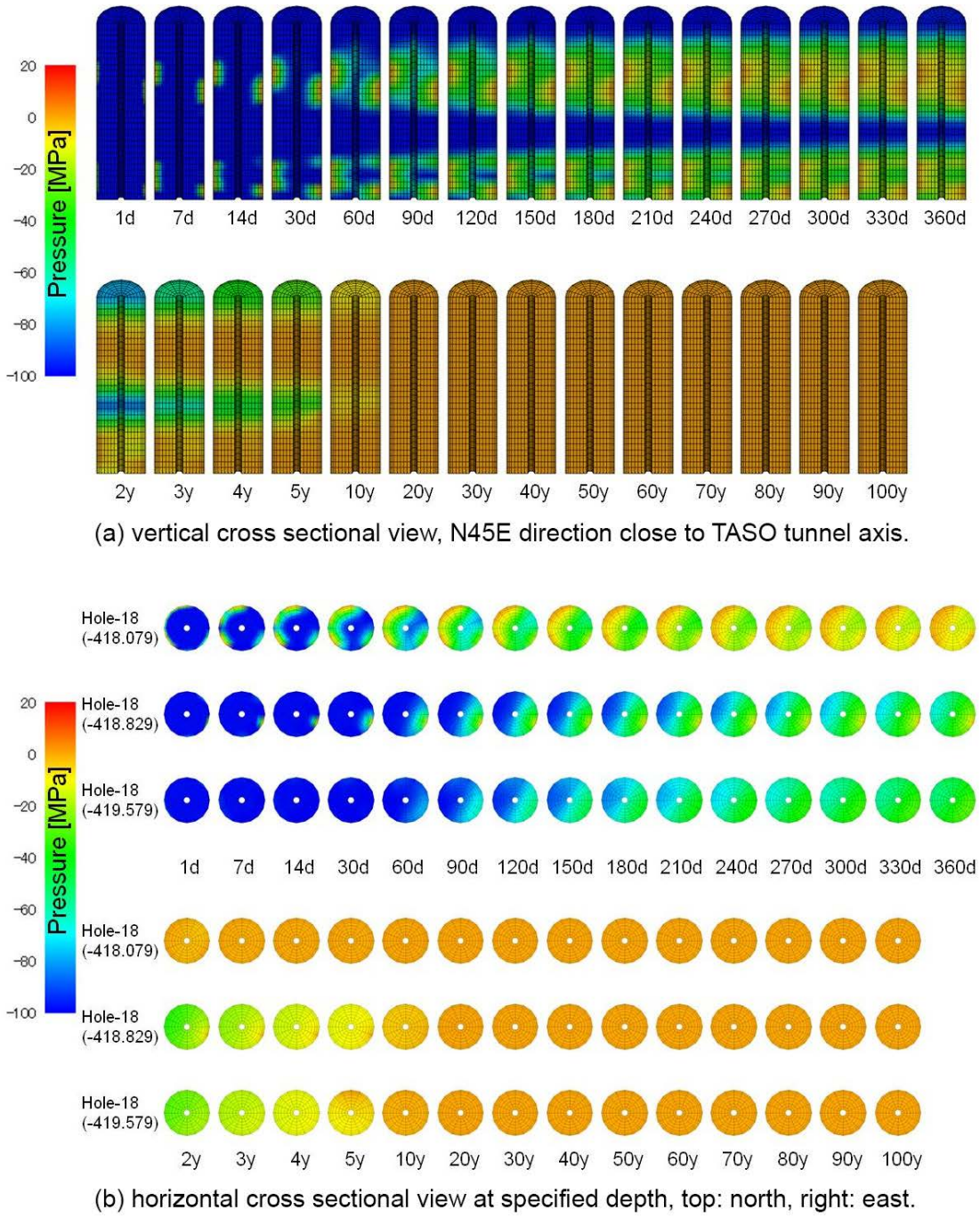

Figure 3-10. *Pressure distribution in bentonite column at KO00018G01, base case model.*

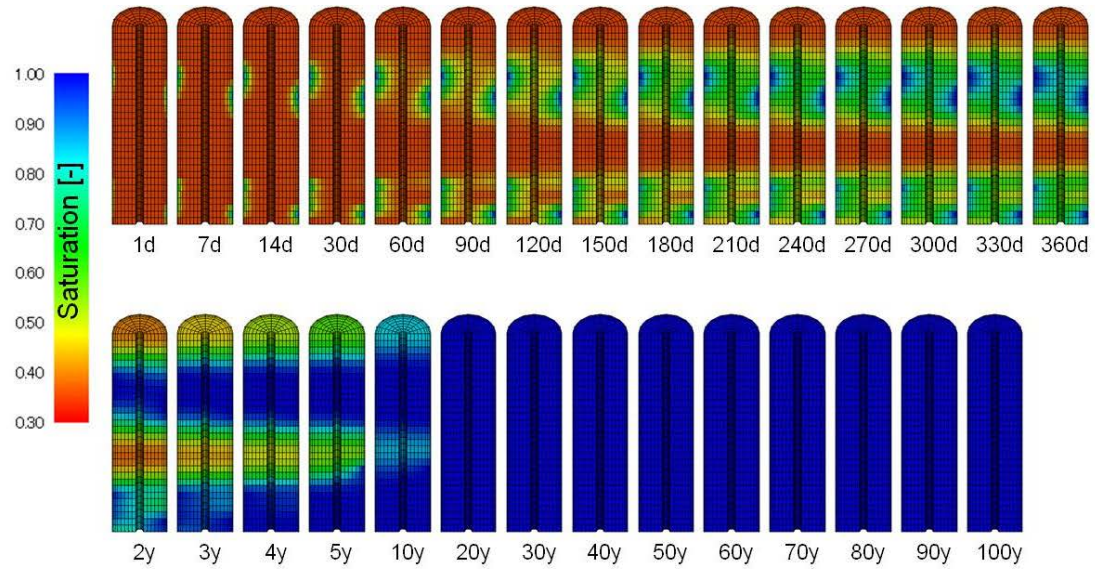

(a) vertical cross sectional view, N45E direction close to TASO tunnel axis.

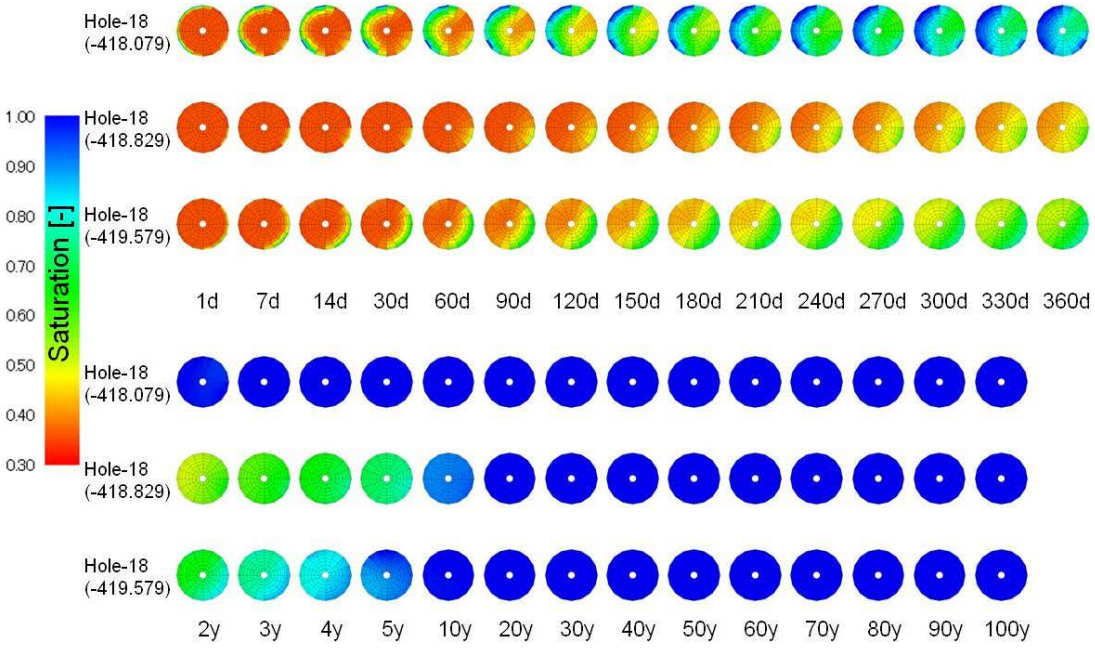

(b) horizontal cross sectional view at specified depth, top: north, right: east.

Figure 3-11. *Saturation distribution in bentonite column at KO00018G01, base case model.*

3.5 Discussion

The alternative conditions and parameter values of the DFN model for Task 8C1 were examined as one of the potential scenarios to modify or calibrate the base case model. The following is a list for the alternative conditions and parameter values.

- Transmissivity
- Boundary condition
- Location of wfracture01
- Constrain fracture location along five probe holes

1) Transmissivity

Transmissivity of stochastic background fractures of the base case was defined by using an empirical correlation to the fracture size, which has a wider range of uncertainty as discussed in Section 3.3. In order to reduce DFN model permeability with considering an uncertainty range of the transmissivity correlation shown in Figure 3-3, three cases, a) 1/10 times of transmissivity, b) 1/50 times of transmissivity and c) 1/100 times of transmissivity of all base case model fracture were set as an alternative case. The sensitivity analysis was made using a single realisation among five realisations used for the base case model, by changing transmissivity by 1/10, 1/50 and 1/100. Figure 3-12 shows the sensitivity calculation results by an arbitrary selected single realisation (circle case). Decreasing transmissivity of whole model region significantly affects the flow rate to probe holes, except for KO0014G1, but does not affect heads at the five probe holes. The reason of the exception is that flow condition around KO0014G1 might be strongly affected by the deterministically defined fracture, "wfracture01" which is located to be close to KO0014G1 (see also "3) Location of wfracture01", below). For this single realisation, a case of 1/10 transmissivity might be closer to the measured flow rate at KO0014G01 and KO0017G01.

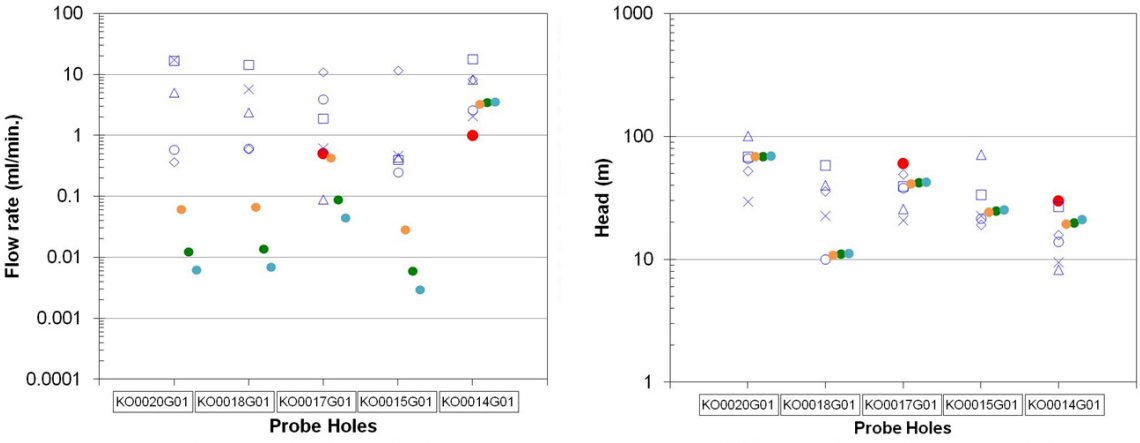

(a) flow rate to five probe holes (b) head values at five probe holes

Figure 3-12. *Sensitivity analysis results for alternative transmissivity distribution. Open symbol (Blue): base case simulation results of five realisations. Solid circle (Red): measured data. Solid circle (Yellow): a) 1/10 transmissivity case. Solid circle (Green): b) 1/50 Transmissivity case. Solid circle (Light blue): c) 1/100 Transmissivity case.*

2) Boundary condition

Outer boundary condition at the 40 m × 40 m × 40 m block region was specified by the heterogeneously distributed head (constant in time at each specified value) as shown in Figure 2-5. Constant head boundary constrains only the head value at specified planes or points, and could therefore produce an unreasonably a high flow rate into the model, since there is not limitation on hydraulic conductivity outside of the model region. This would not be a concern if the boundary condition were defined sufficiently far away. However, for the current study, the model region was a 40 m scale block extracted from deep underground at Äspö URL tunnel. In order to moderate the effect of constant head model boundaries, a low permeability skin was added to the model to represent hydraulic resistance of rock outside of the modelling region. This was modelled by decreasing transmissivity by one order of magnitude within 1 m width from the outer surface of the model was added to the DFN model as one of the alternative outer boundary conditions. Three cases, a) low permeable skin, b) homogeneous constant head (−50 m) without low permeable skin, and c) homogeneous constant head (−50 m) with low permeable skin were made for the sensitivity calculations. The sensitivity of the alternative boundary condition to the flow rate and head values at five probe holes calculated by a single realisation (realisation number 01) is shown in Figure 3-13. All cases of alternative boundary conditions have a certain level of effects on the flow rate and head values at the five boreholes. The low permeable skin decreases flow rate and head values at the five probe holes. In contrast, homogeneous head boundary increases them. This might be caused by a relatively high head of −50 m compared with the specified heterogeneous head distribution in which the northwest side has lower head caused by tunnel excavation as shown in Figure 2-5. The effect of changing boundary conditions considered in this study seems to be minor compared to the other alternative cases.

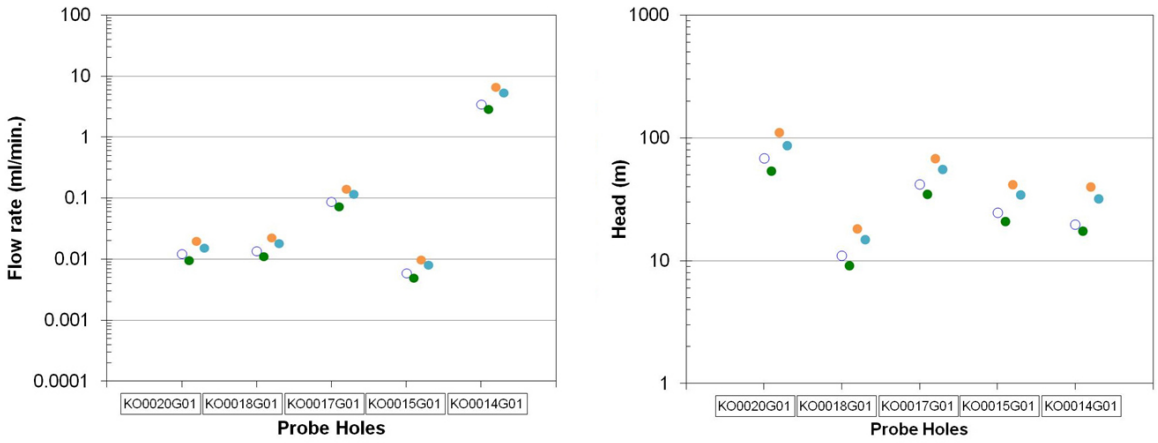

(a) flow rate to five probe holes (b) head values at five prove holes

Figure 3-13. *Sensitivity analysis results for alternative transmissivity distribution. Open circle (Blue): 1/50 trasmissivity of base case result. Solid circle (Green): a) low permeable skin case. Solid circle (Yellow): b) homogeneous constant head (−50 m). Solid circle (Light blue): c) homogeneous constant head (−50 m) with low permeable skin.*

3) Location of wfracture01

As described in Section 3.3 and Figure 3-2, the characteristics of "wfracture01" had been uncertain. The characteristic of wfracture01 defined in Task 8D is used as base case model in this report, in order to keep consistency of base case model through the subtasks. The sensitivity of these alternatives suggested from SKB through the task force activities was examined. Two cases, a) original Task 8C model, and b) modified Task 8C model with a single realisation of stochastic DFN model (realisation number 01) were compared with 1/50 trasmissivity of base case result (Figure 3-12, green circle). The location of wfracture01 was moved to the southwest along the TASO tunnel and transmissivity was also changed to 5×10^{-9} m^2/s for the modified Task 8C model (case b). Both cases have minor effect on flow rate and head at four probe holes KO0015G01 to KO0020G01, as shown in Figure 3-14. However, the flow rate and head values at KO0014G01 are strongly affected by the location and transmissivity of wfracture01. And, the base case model (Task 8D model for wfracture01) indicates a closer flow rate and head values at KO0014G01 probe hole.

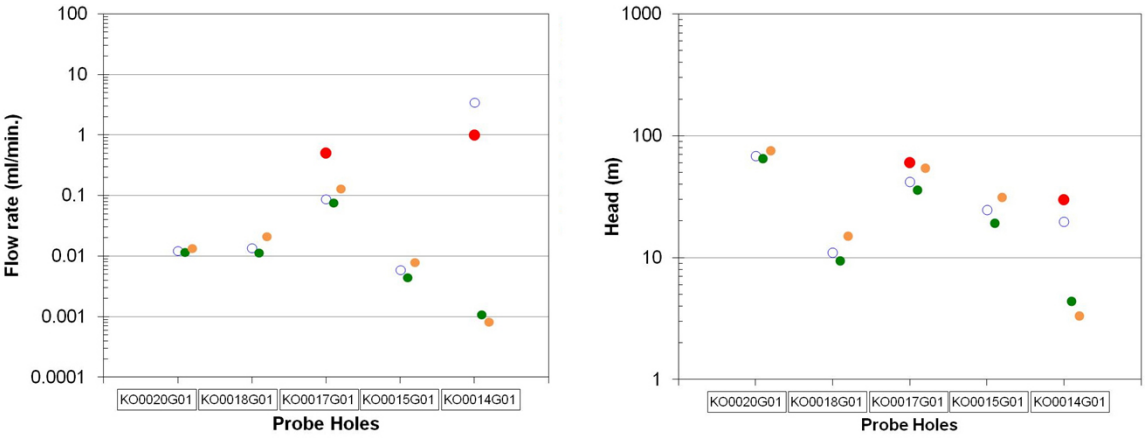

(a) flow rate to five probe holes

(b) head values at five prove holes

Figure 3-14. *Sensitivity analysis results for alternative wfracture01 model. Open circle (Blue): 1/50 trasmissivity of base case result (with Task 8D wfracture01 model). Solid circle (Red): measured data. Solid circle (Green): a) original Task 8C model case. Solid circle (Yellow): b) modified Task 8C model.*

4) Constrain fracture location along five probe holes

There was no hydraulic data for indicating the water conducting fractures around TASO tunnel, especially along the five probe holes. However, geological fracture mapping data by BTV and core along the five boreholes was provided in Task 8C specification. In this modelling challenge, by assuming that fractures described by "Broken/Open" and "Calcite" might indicate a water conducting fracture, fracture locations and orientations were picked up from the fracture mapping data, as shown in Figure 3-15. The fracture radius of these fractures was assumed to be smaller than the average half interval between five probe holes, to avoid direct intersection of two boreholes by a single water conducting fracture. Because, no evidence of direct connection between the boreholes was shown in the geological mapping data. It was also assumed that transmissivity could be estimated by the same correlation to fracture radius applied to the background fractures. Figure 3-16 shows the conceptual illustration of the procedure for constraining fracture location, and other characteristics to data mapped (selected) fracture data. Firstly, all fractures intersecting the boreholes for constraining (Red line) were removed. Then, fractures to be constrained (Blue line) were added. By conditioning location and other properties of the assumed water conducting fractures, the connection of fractures providing head propagating from the outer boundary to the five probe holes seems to be constrained as shown in Figure 3-17. Although the data set of water conducting fractures was assumed by geological characteristics, "Broken/Open" and "Calcite," the conditioning to a specific data set around a target area might improve local connectivity as discussed in Section 3.1 and Figure 3-1. The calculated flow and head distribution for the five stochastic realisations are shown in Figure 3-18, with comparisons of measured data, base case model results, and 1/50 transmissivity case results. Conditioning fracture location at the five probe holes decreases flow rate by constraining the connectivity to fracture network. In contrast, head values are not significantly affected by the conditioning. This "conditioning" method for modelling local connectivity along the holes might not be enough to constrain the wider variability of flow rate and head values around five holes among the stochastic realisations.

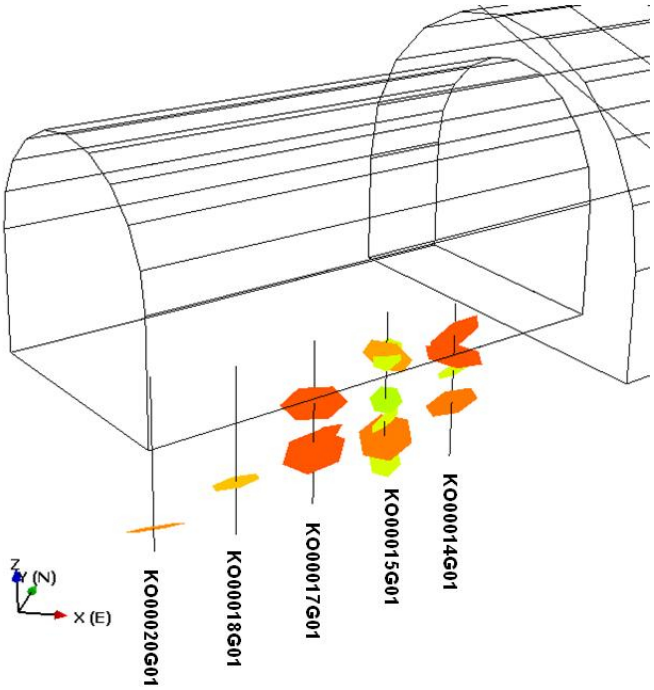

Figure 3-15. *Locations and orientation of modelled water conducting fractures picked up from fracture mapping by assuming that "Broken/Open" and "Calcite" indicates water flowing fractures.*

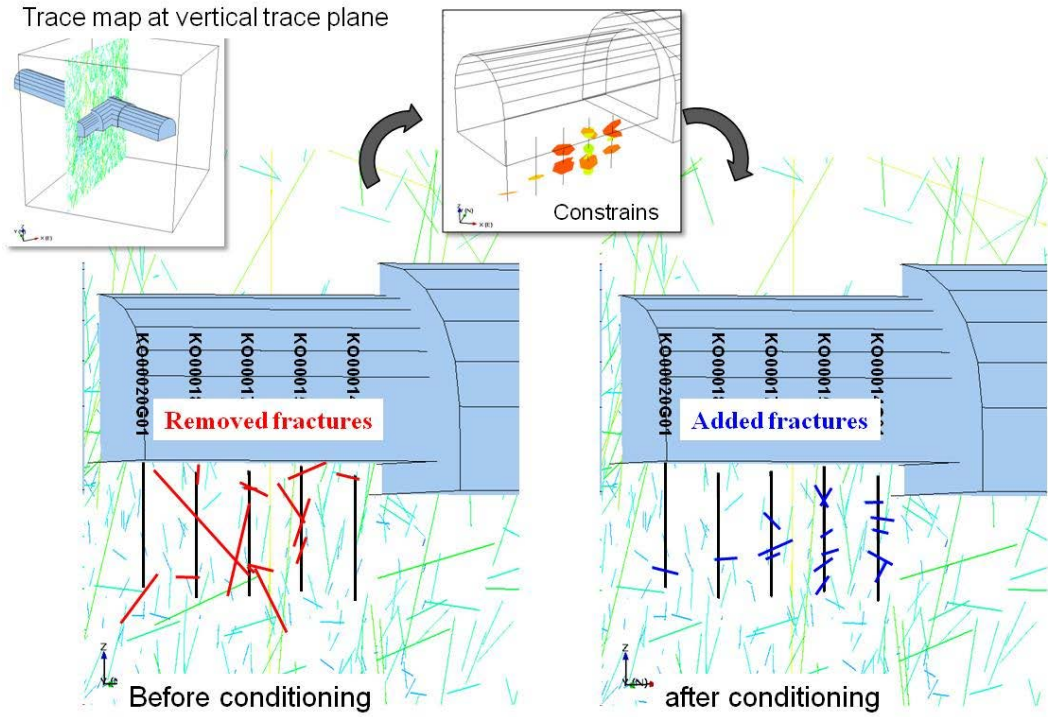

Figure 3-16. *Conceptual illustration of method of the fracture conditioning to specified fracture mapping data.*

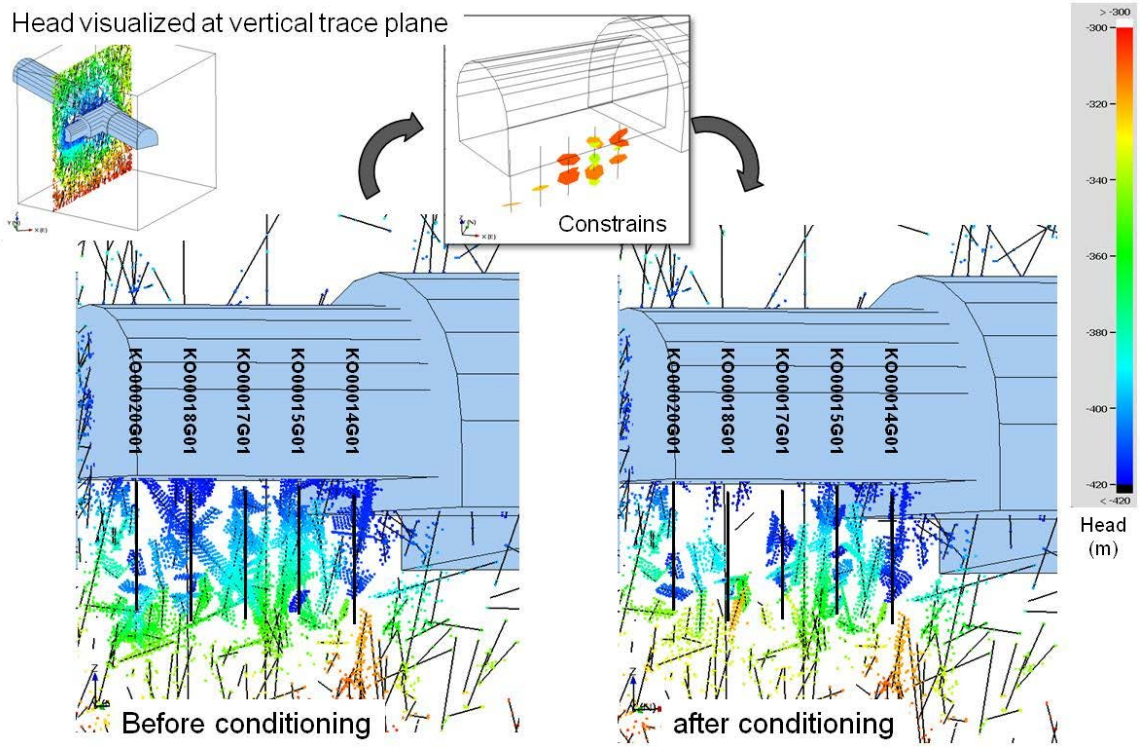

Figure 3-17. *Example of calculated head distribution around five probe holes, before and after condition fractures.*

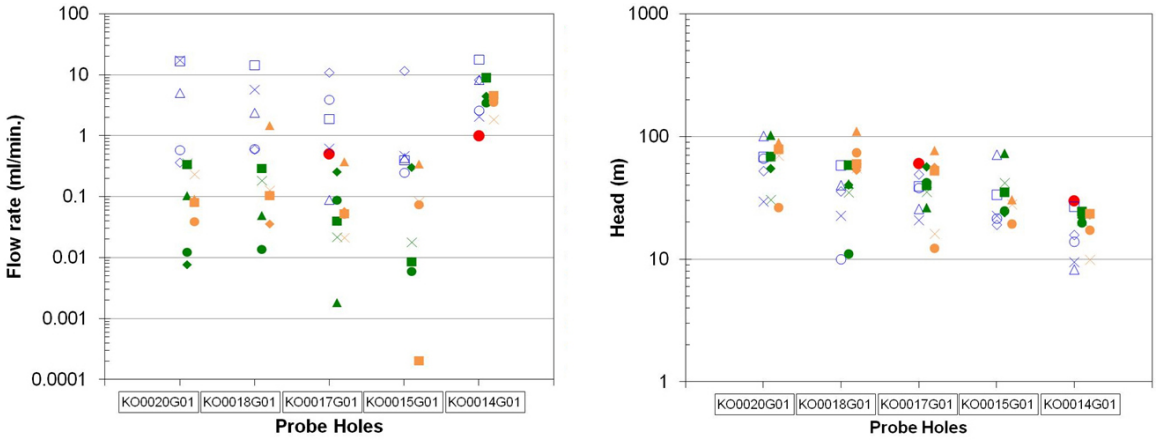

Figure 3-18. *Effect of fracture conditioning compared with other cases. Open symbol (Blue): base case simulation results of five realisations. Solid circle (Red): measured data. Solid symbol (Green): 1/50 transmissivity of base case simulation results of five realisations. Solid circle (Yellow): Fracture conditioning case of five realisations.*

Based on the sensitivity analyses by considering alternative parameter values, conditions, and models; the three cases; base case, 1/50 transmissivity case, and fracture conditioning case, were selected as the potential reference cases for demonstrating performance measures defined by the Task 8C specification and simulation of bentonite re-saturation calculation.

Figure 3-19 shows the comparison of head distribution at vertical and horizontal cross-sectional planes. An arbitrary selected single realisation case is presented. No significant differences among the three cases are shown, but minor differences around the BRIE local region for fracture conditioning case are recognised. Figure 3-20 shows fractures intersecting 30 cm diameter boreholes and groundwater flow rate along the fracture traces at the borehole walls, which is an example of a single realisation of fracture conditioning case. In whole model region, the head distribution is smoothly decreased toward a tunnel that is caused by an effect of averaging out heterogeneously distributed DFN as shown in Figure 3-19. However, in a local scale around 30 cm boreholes, heterogeneously distributed groundwater flow due to a local connectivity of fractures to the boreholes is reproduced. The cumulative flow distribution to 30 cm boreholes (from bottom to top) of five realisations are summarised in Figures 3-21 through 3-23 for each case. The cumulative flow rate distributes widely among the realisations at each case. If high permeable fracture would be intersected to the 30 cm borehole, flow rate might increase. The probability of the hydraulic connectivity of the fractures intersecting the 30 cm boreholes might control the flow distribution.

The localised groundwater flow discussed above provides the heterogeneous re-saturation behaviour in bentonite columns installed in 30 cm boreholes by the coupling simulation. The examples of the bentonite re-saturation simulation results for each case are visualised in Figure 3-24 through Figure 3-31, which shows the time-dependent change of pressure and saturation distribution at vertical and horizontal cross sections, for each case of 1/50 transmissivity case and fracture conditioning case. In both 30 cm enlarged boreholes, the saturated areas are initiated by the points intersecting groundwater flowing fractures and are propagated to column centre and both upward and downward of the bentonite columns.

Each case produces heterogeneous re-saturation behaviour (pressure and saturation) for both KO00017G01 and KO00018G01, by both vertical and horizontal cross-sectional views. The heterogeneous unsaturated parts are sustained for at least 10 years. In case of 1/50 transmissivity, similar pressure and saturation pattern to the base case results are re-presented, but the propagation seems to be slower than the base case results, by reducing transmissivity of fractures to provide groundwater to the bentonite. The case of fracture conditioning has different pressure and saturation propagation patterns than the other cases, because fractures intersecting 30 cm diameter enlarged boreholes are changed to constrain to fractures observed at the boreholes drilled at the centre of enlarged boreholes. The number of locations to provide groundwater to the bentonite is also more limited than the other cases. Due to lower transmissivity and a limited number of fractures intersecting the boreholes, the propagation rate of pressure and saturation seems to be slower than base case results.

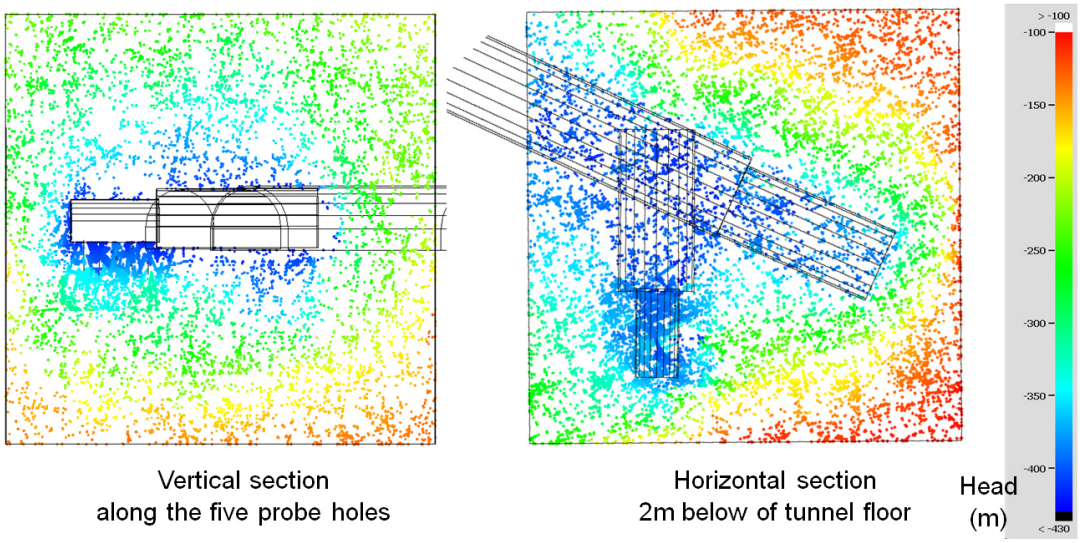

(a) Base case (realization 01)

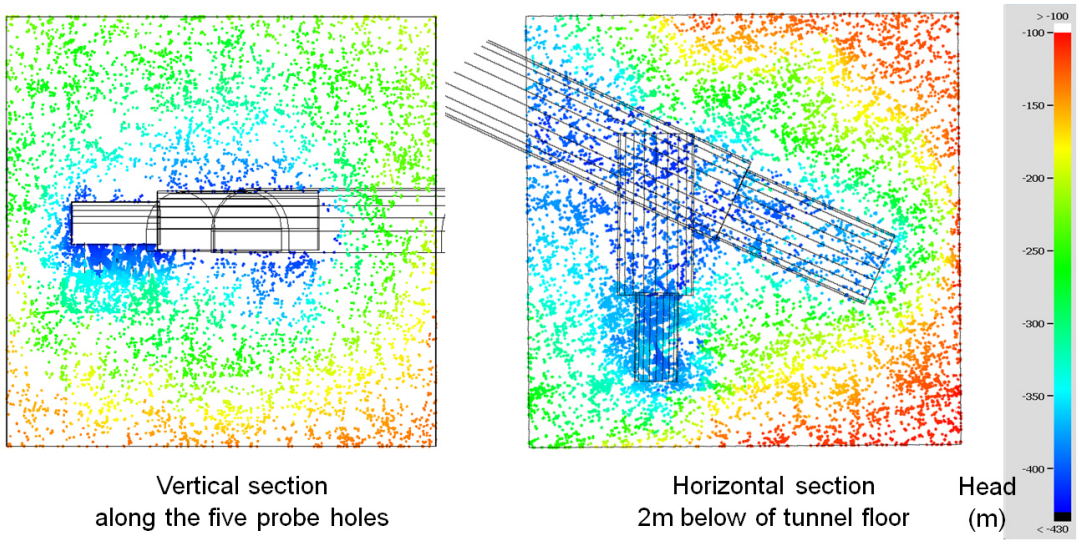

(b) 1/50 Transmissivity case (realization 01)

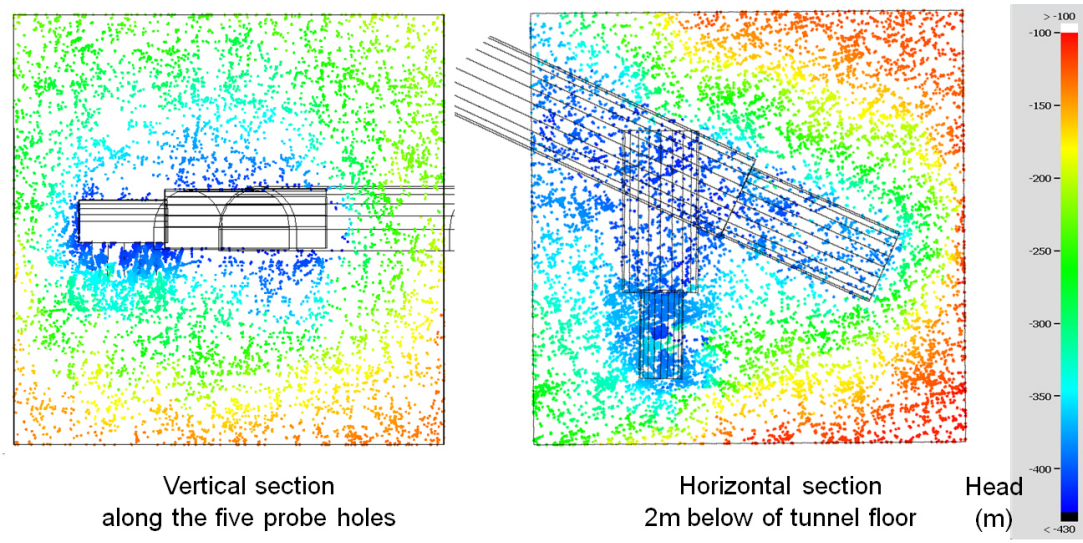

(c) Fracture conditioning case (realization 01)

Figure 3-19. *Comparison of head distribution at vertical and horizontal cross sectional planes. . . .*

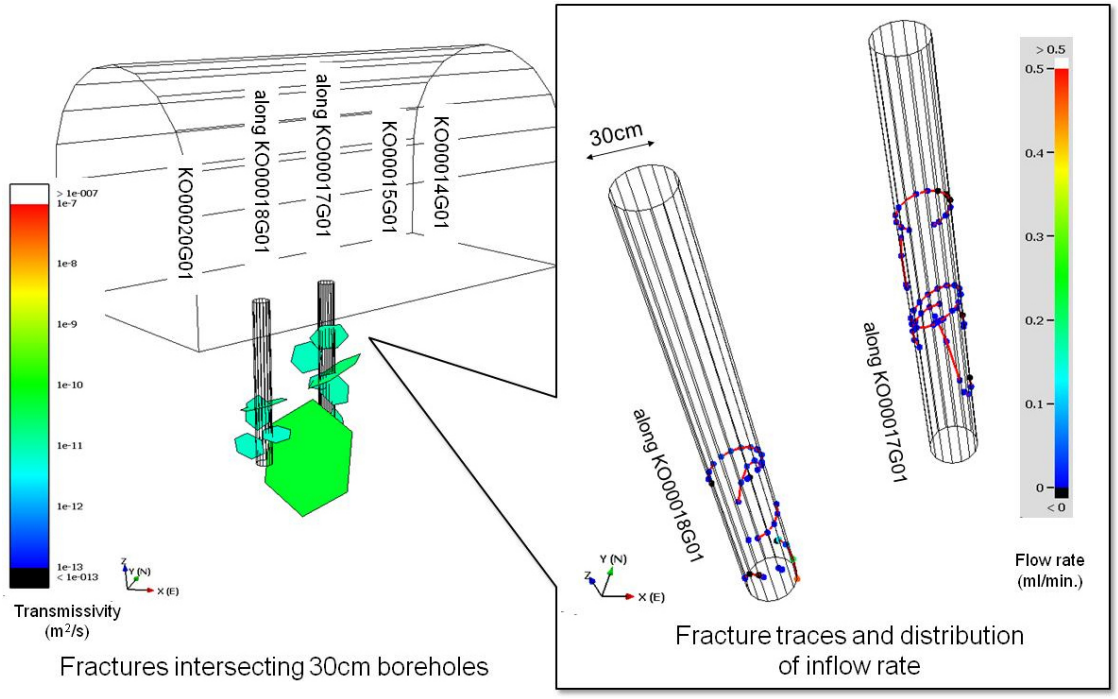

Figure 3-20. *Groundwater flow distribution at enlarged borehole wall. Example of fracture conditioning case model (realisation 01).*

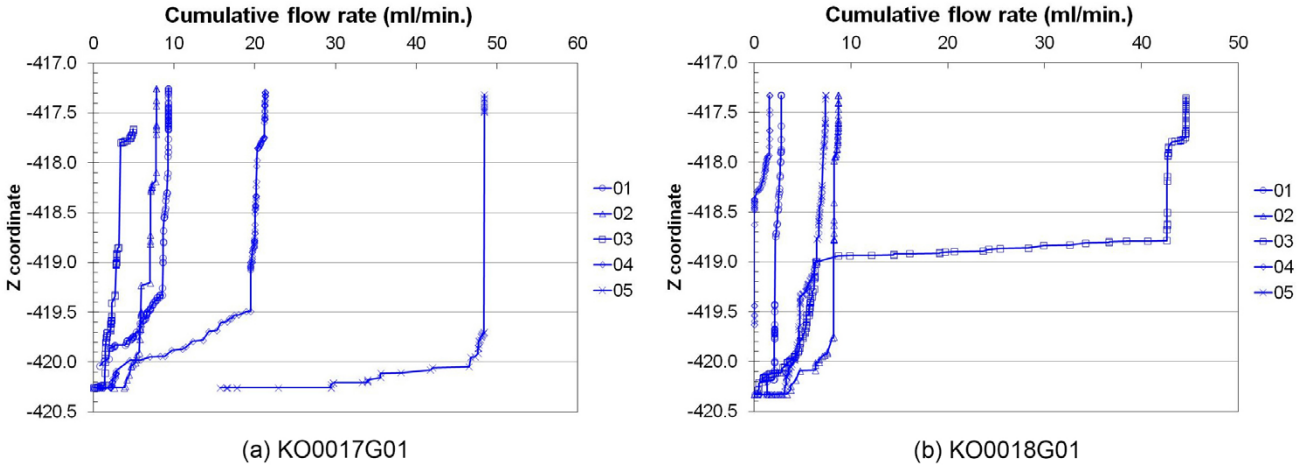

Figure 3-21. *Cumulative flow distribution at enlarged borehole wall, Base case (five realisations).*

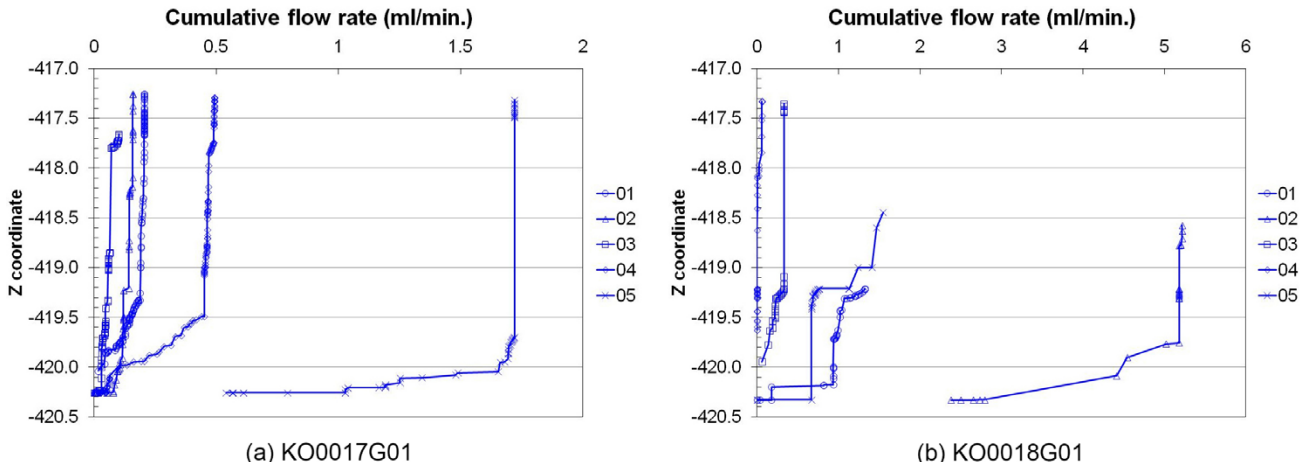

Figure 3-22. *Cumulative flow distribution at enlarged borehole wall, 1/50 Transmissivity case (five realisations).*

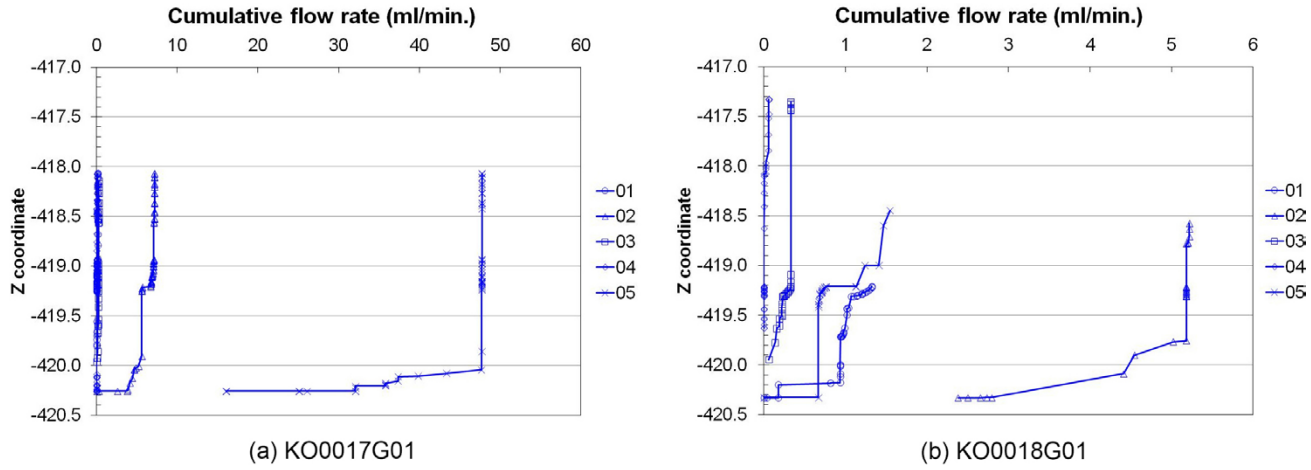

Figure 3-23. *Cumulative flow distribution at enlarged borehole wall, Fracture conditioning case (five realisations).*

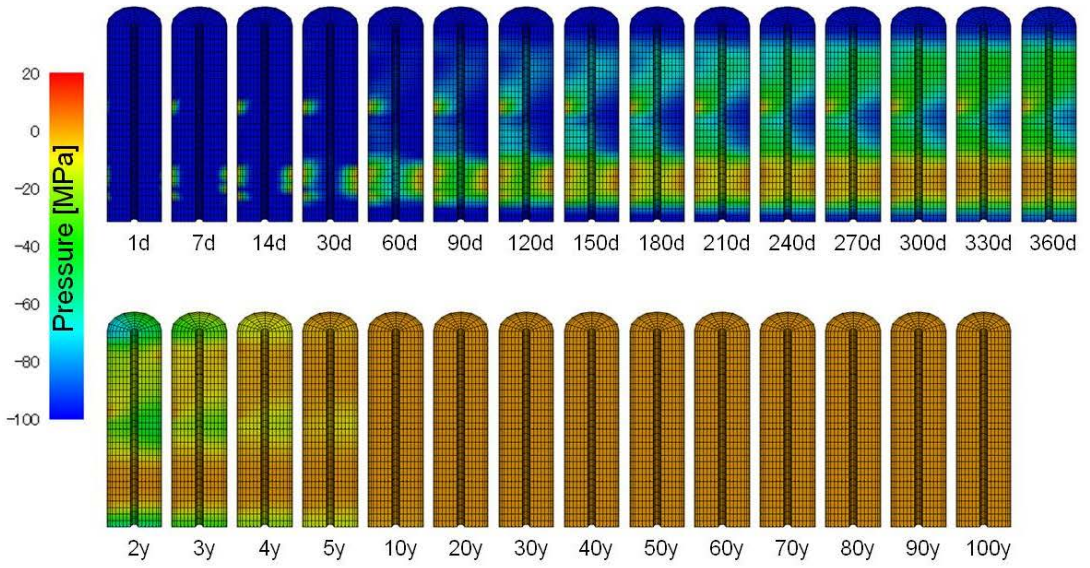

(a) vertical cross sectional view, N45E direction close to TASO tunnel axis.

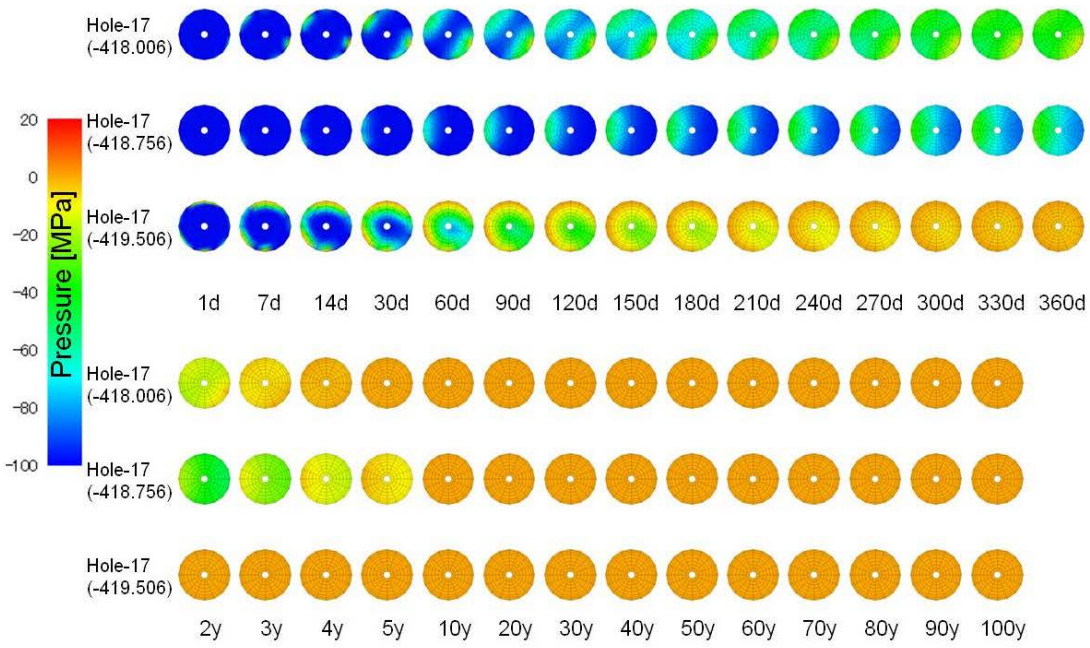

(b) horizontal cross sectional view at specified depth, top: north, right: east.

Figure 3-24. *Pressure distribution in bentonite column at KO00017G01, 1/50 transmissivity case model.*

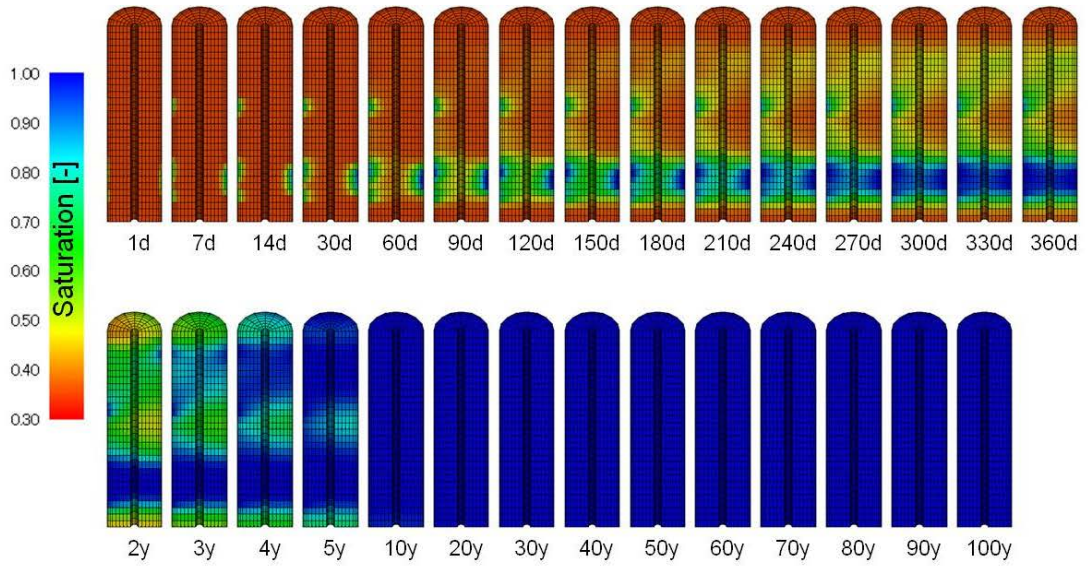

(a) vertical cross sectional view, N45E direction close to TASO tunnel axis.

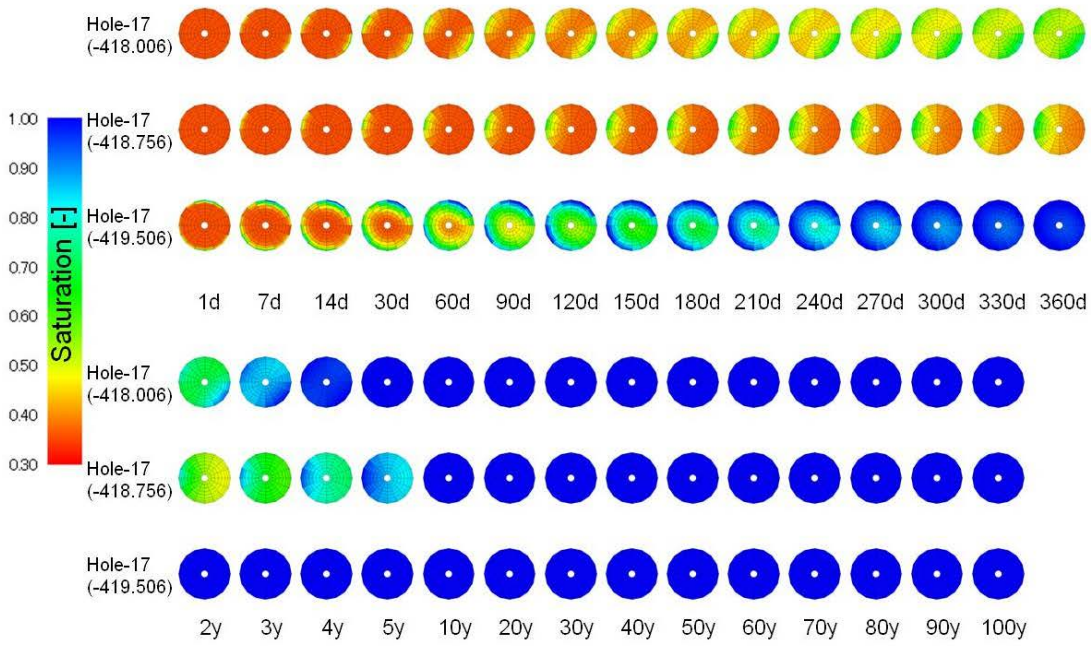

(b) horizontal cross sectional view at specified depth, top: north, right: east.

Figure 3-25. *Saturation distribution in bentonite column at KO00017G01, 1/50 transmissivity case model.*

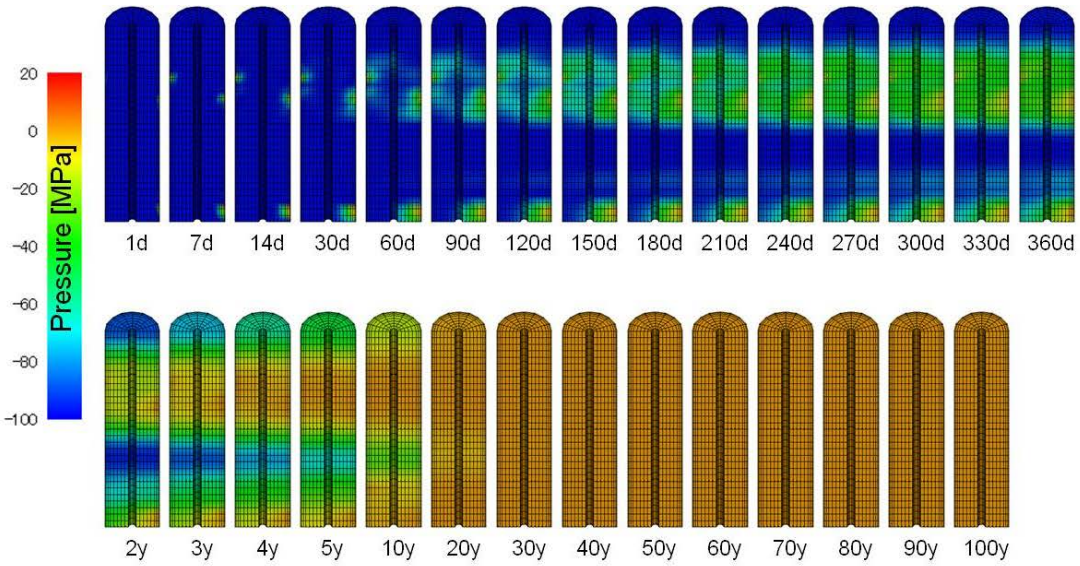

(a) vertical cross sectional view, N45E direction close to TASO tunnel axis.

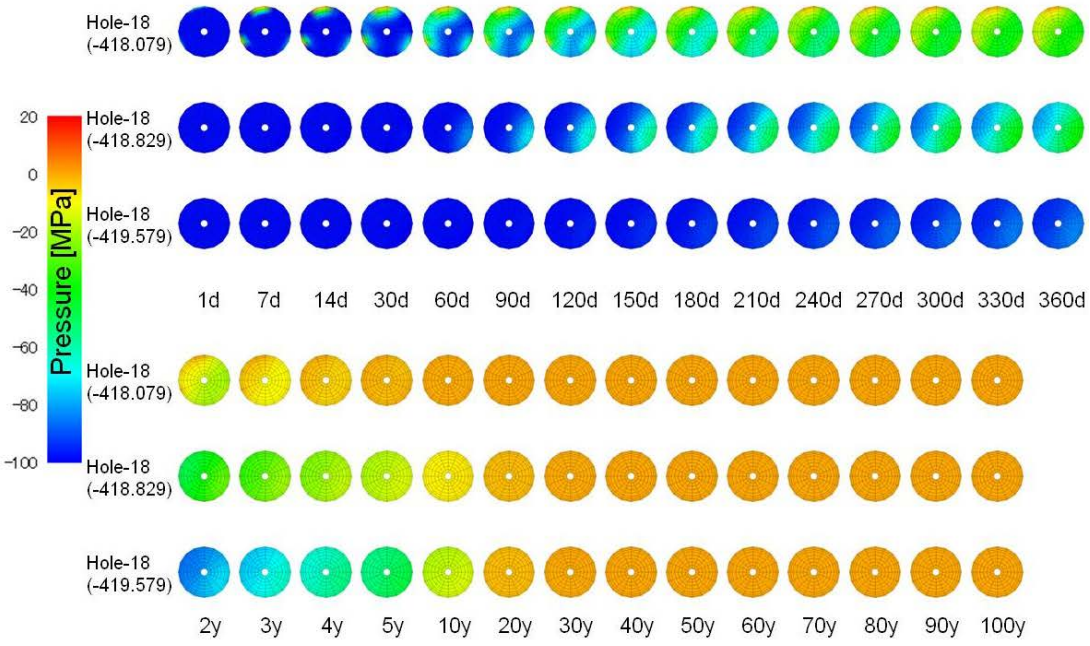

(b) horizontal cross sectional view at specified depth, top: north, right: east.

Figure 3-26. *Pressure distribution in bentonite column at KO00018G01, 1/50 transmissivity case model.*

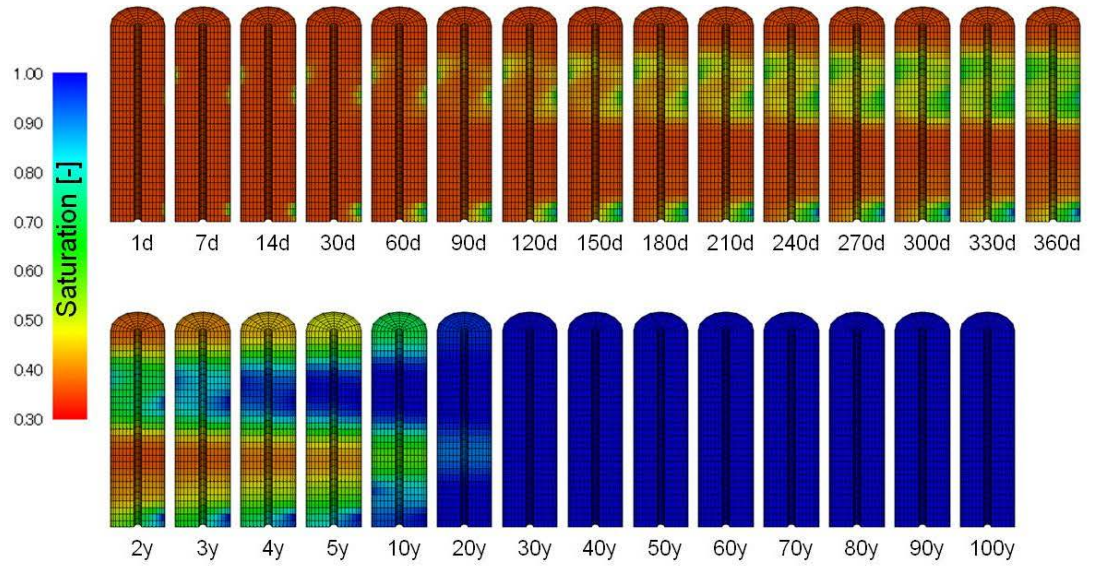

(a) vertical cross sectional view, N45E direction close to TASO tunnel axis.

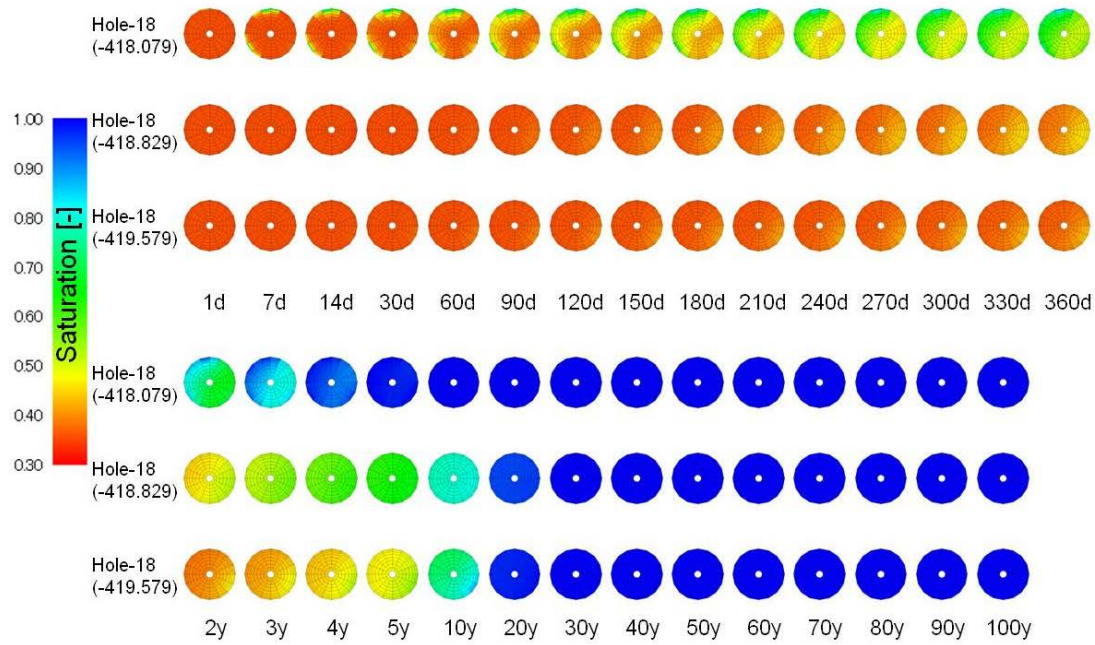

(b) horizontal cross sectional view at specified depth, top: north, right: east.

Figure 3-27. *Saturation distribution in bentonite column at KO00018G01, 1/50 transmissivity case model.*

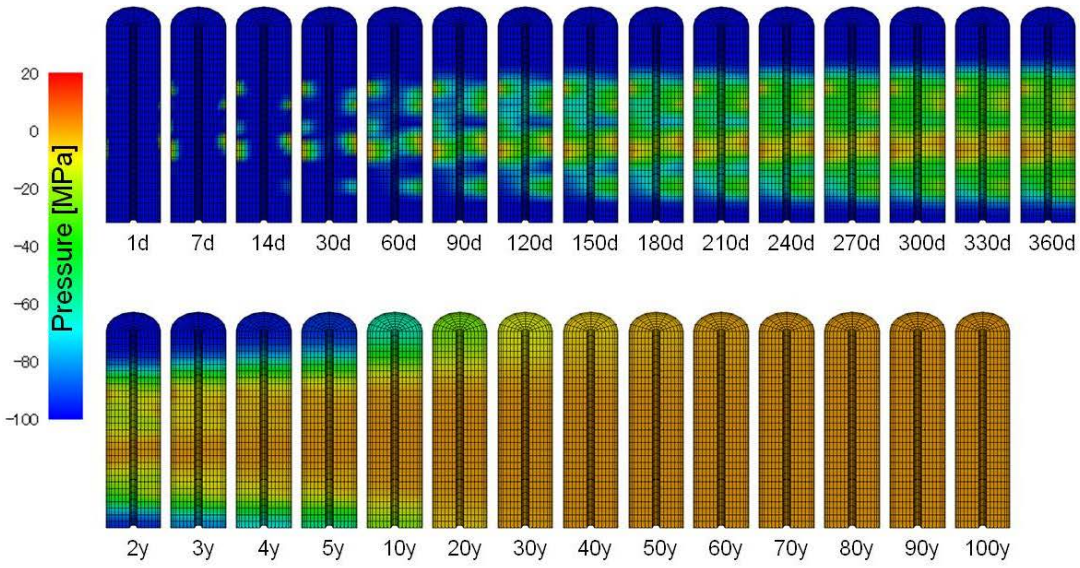

(a) vertical cross sectional view, N45E direction close to TASO tunnel axis.

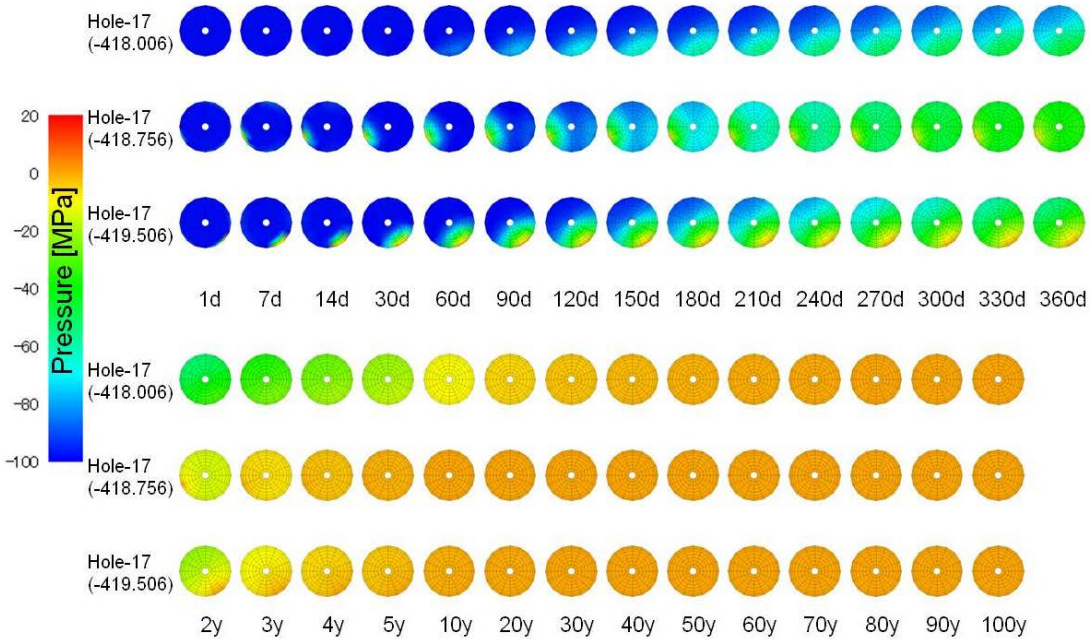

(b) horizontal cross sectional view at specified depth, top: north, right: east.

Figure 3-28. *Pressure distribution in bentonite column at KO00017G01, Fracture conditioning case model.*

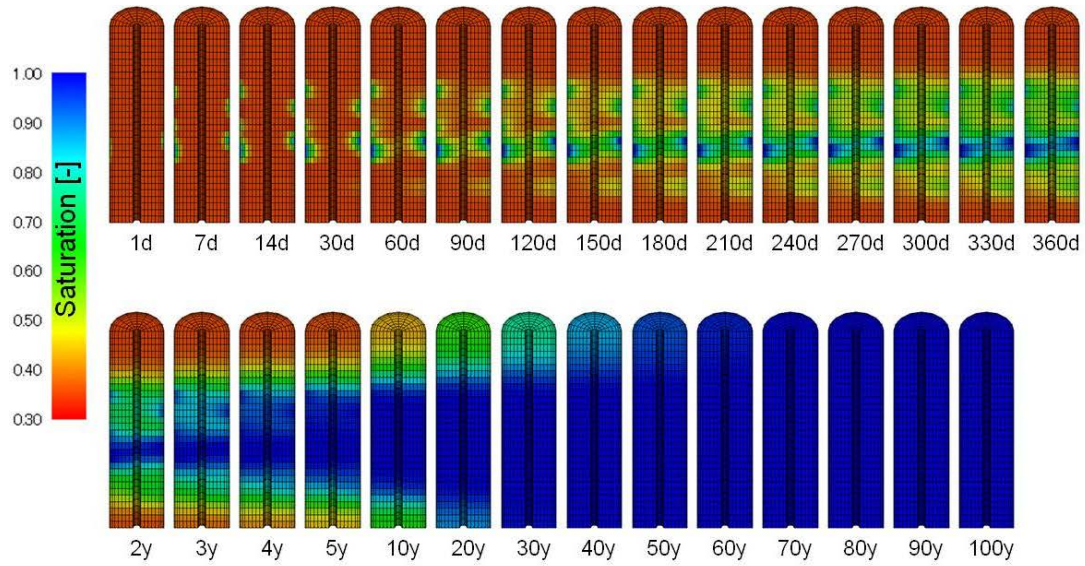

(a) vertical cross sectional view, N45E direction close to TASO tunnel axis.

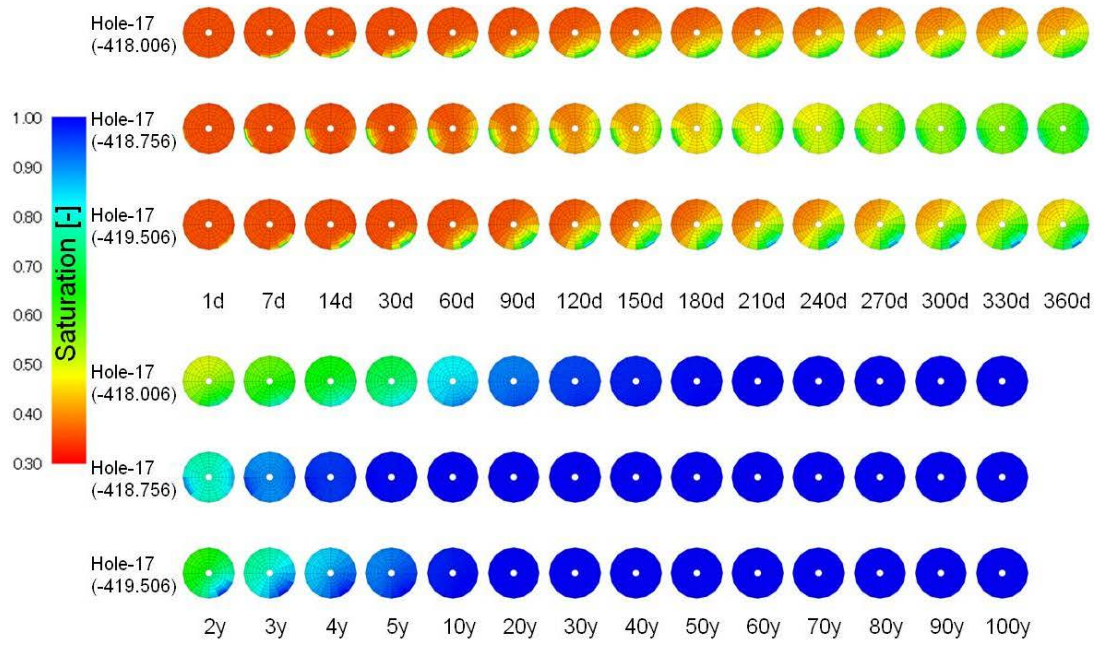

(b) horizontal cross sectional view at specified depth, top: north, right: east.

Figure 3-29. *Saturation distribution in bentonite column at KO00017G01, Fracture conditioning case model.*

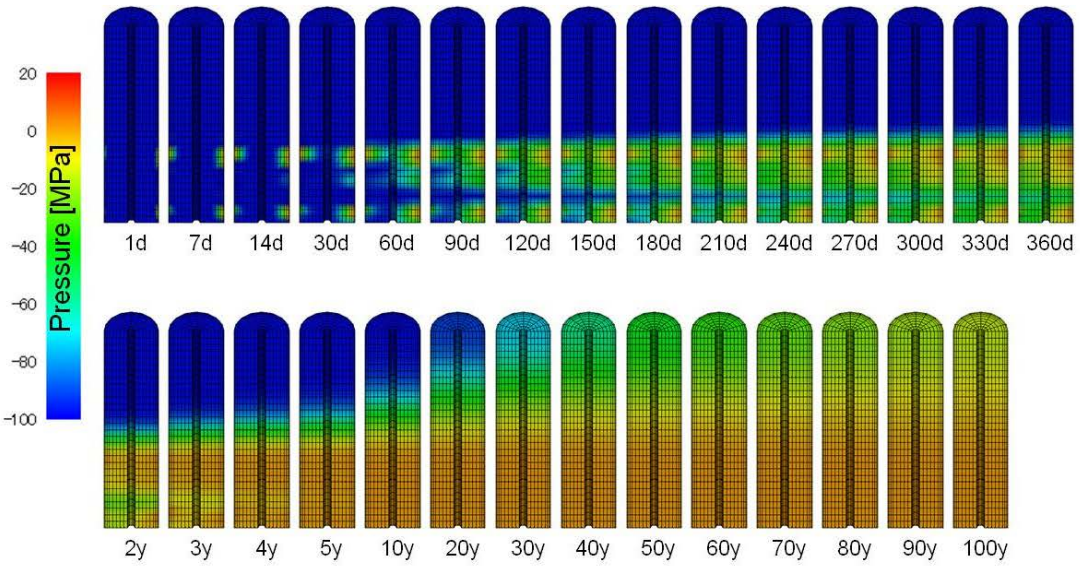

(a) vertical cross sectional view, N45E direction close to TASO tunnel axis.

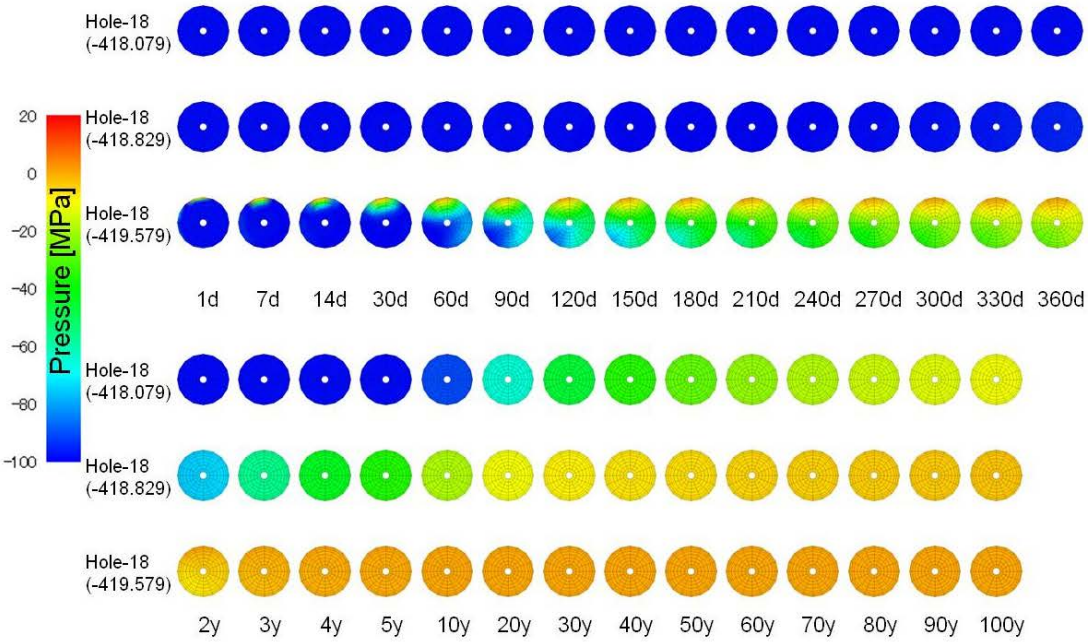

(b) horizontal cross sectional view at specified depth, top: north, right: east.

Figure 3-30. *Pressure distribution in bentonite column at KO00018G01, Fracture conditioning case model.*

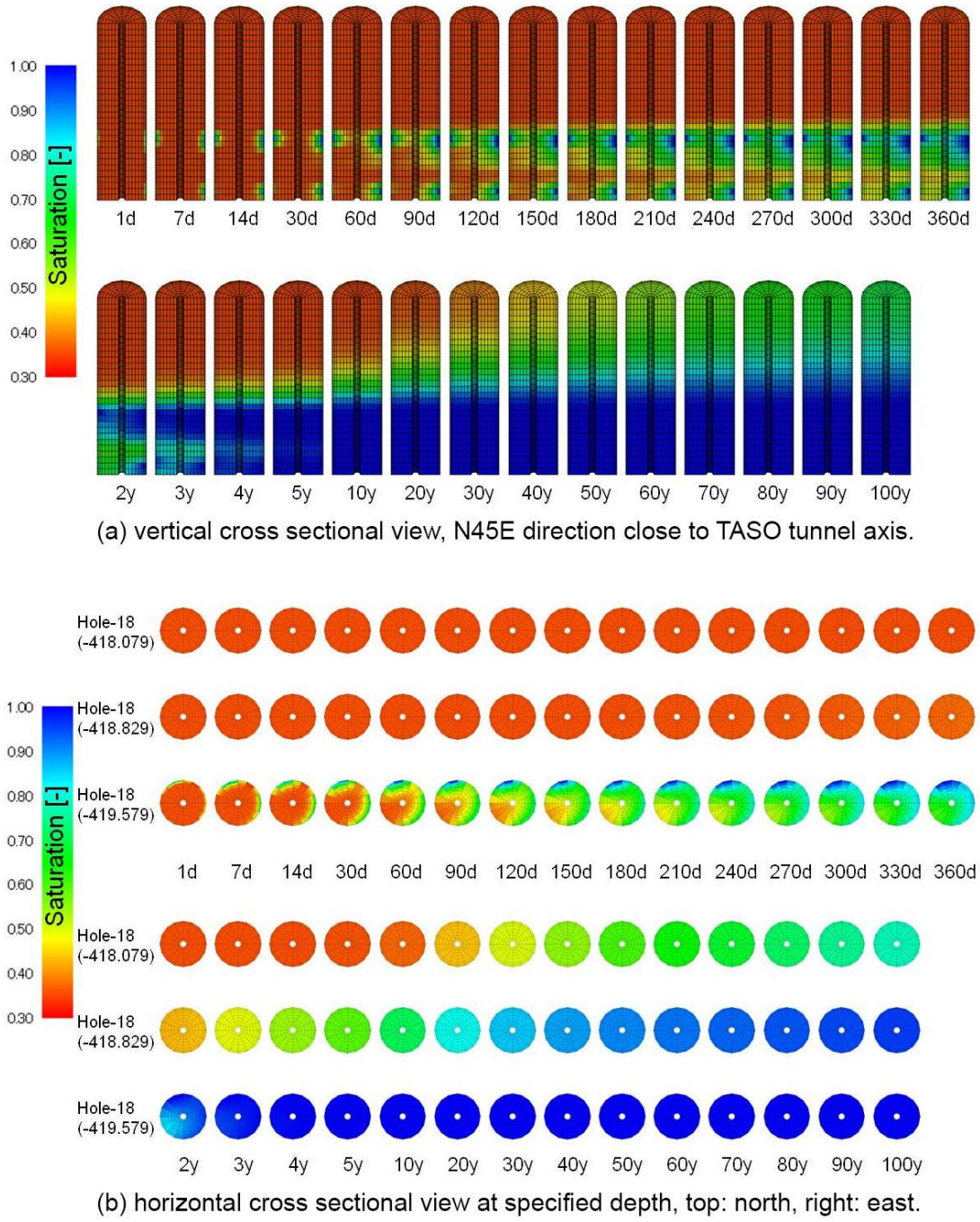

Figure 3-31. *Saturation distribution in bentonite column at KO00018G01, Fracture conditioning case model.*

3.6 Conclusions and Recommendations

In this section, a hydrogeological structure in the 40 m × 40 m × 40 m block region around TASO tunnel was modelled by discrete fracture networks, as followed by the Task 8C1 specifications. The five stochastic realisations were examined to compare with the limited number of measurement data including head and flow rate measured at five probe boreholes. The model calibrations were examined by conducting a sensitivity analysis for the alternative models and parameter values. Consequently, the three cases, (a) the base case specified by Task 8C1, (b) a case of reducing the transmissivity by 1/50 times, and (c) a case of conditioning fractures to match five measured borehole were defined as the potential reference case for simulating bentonite re-saturation (Task 8C2). The newly developed simulation system for coupling groundwater flow in rock and bentonite was applied for each case.

From Task 8C examination, the following could be concluded:

- The simulated values such as flow rate and head value at a specific point varies widely, more than one order of magnitude, among the stochastic realisations of the DFN model although no parameter values are changed, from the base case simulation results.
- Both cases of reducing transmissivity for all fractures in the model and conditioning local connectivity to boreholes could reproduce similar flow rate and head values to measured data.
- By coupling these DFN models with groundwater movement simulation in the bentonite columns, the heterogeneous pressure and saturation propagation from limited number of flow points (fractures) could be reproduced.
- The heterogeneous unsaturated parts are sustained at least 10 years.
- The number of locations to provide groundwater to the bentonite and transmissivity of the fractures control propagation rate of pressure and saturation in bentonite column.

4 Task 8D – Prediction of inflow and wetting of KO0017G01 and KO0018G01 based on detailed characterisation data

4.1 Objectives

Task 8D was divided into two parts, Task 8D1 and Task 8D2. Figure 4-1 shows the conceptual illustration of Task 8D structure, in which Task 8D specific information is added to Figure 3-1. Incorporation of bentonite was not considered in the Task 8D1 exercise. Instead the inflow to the open 30 cm boreholes was addressed and was intended to be compared with field data from the BRIE experiment. Task 8D2 addresses the wetting of the bentonite based on the flow model established in Task 8D1. The wetting results were planned to be used as predictions of the field results of the on-going field experiment of BRIE. The scope of this calculation exercise was contained within the simulation of a sub-local site-specific three-dimensional groundwater flow specifications, similar to Task 8C. However, Task 8D was specified with additional detailed hydraulic data.

The main objectives with this exercise are:

Task 8D1

- To calculate inflows and inflow characteristics to two 76 millimetre (mm) diameter probing boreholes.
- To calculate inflows and inflow characteristics to two 30 cm diameter open boreholes.
- To compare inflows calculated for probing boreholes with inflows calculated for enlarged 30 cm boreholes.
- To supply boundary conditions and initial conditions to the field experiment on the emplaced bentonite packs within the two 30 cm boreholes.

Task 8D2

- To evaluate the resulting wetting of the bentonite installed in the borehole characteristics established in Task 8D1.
- To evaluate effects of heterogeneous fracture flow on the wetting.
- To evaluate effects of heterogeneous matrix properties on the wetting.
- To serve as a base case for comparison with earlier results based on less elaborated hydrogeological models.

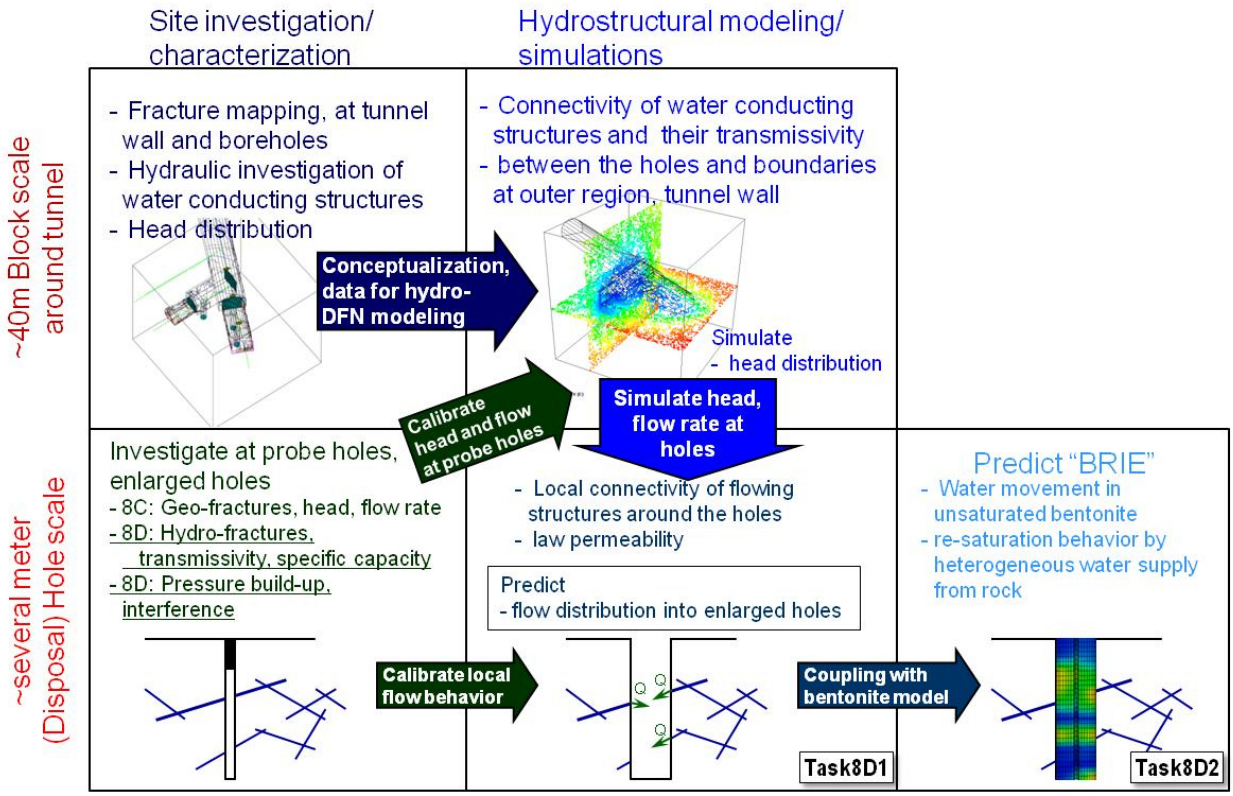

Figure 4-1. *Task 8D model exercise structures, incremented to Figure 3-1.*

4.2 Approach

The models demonstrated in Task 8C ware modified by the new data provided by Task 8D specification. The three cases, hydrogeological model, base case; 1/50 transmissivity case; and fracture conditioning case, were applied to be updated and examined. The model modification was made by using the following two data, in order to constrain hydraulic characteristics at the target area, around KO0017G01 and KO0018G01.

- Water conducting fractures observed at the walls of 30 cm diameter holes.
- Specific flow capacity data observed at the five probe holes.

The applicability of the modified models was checked by using flow rate and head values measured at five probe holes and head values measured at long boreholes horizontally drilled from the tunnel wall short of TASO tunnel.

The models of three cases were also applied to the coupling simulation system described in Chapter 2 to simulate "BRIE" re-saturation behaviour in bentonite emplaced in 30 cm enlarged boreholes along KO00017G01 and KO00018G01, respectively.

4.3 Model Setup

Figure 4-2 shows the water conducting fractures observed at the walls of 30 cm diameter holes along KO0017G01 and KO0018G01, respectively. Locations and orientations are defined by the Task 8D specification. The radius of these fractures was assumed to be 1 m for KO0017G01 and 0.5 m for KO0018G01, respectively, to avoid direct intersection to the other boreholes. Transmissivity of the KO0017G01 fracture was defined as 5×10^{-11} m^2/sec, but the KO0018G01 fracture was not specified. Instead, the specific capacity was reported ranging from 1×10^{-12} to 5×10^{-12} m^2/sec. In this study, 5×10^{-12} m^2/sec was set as the transmissivity of the KO0018G01 fracture.

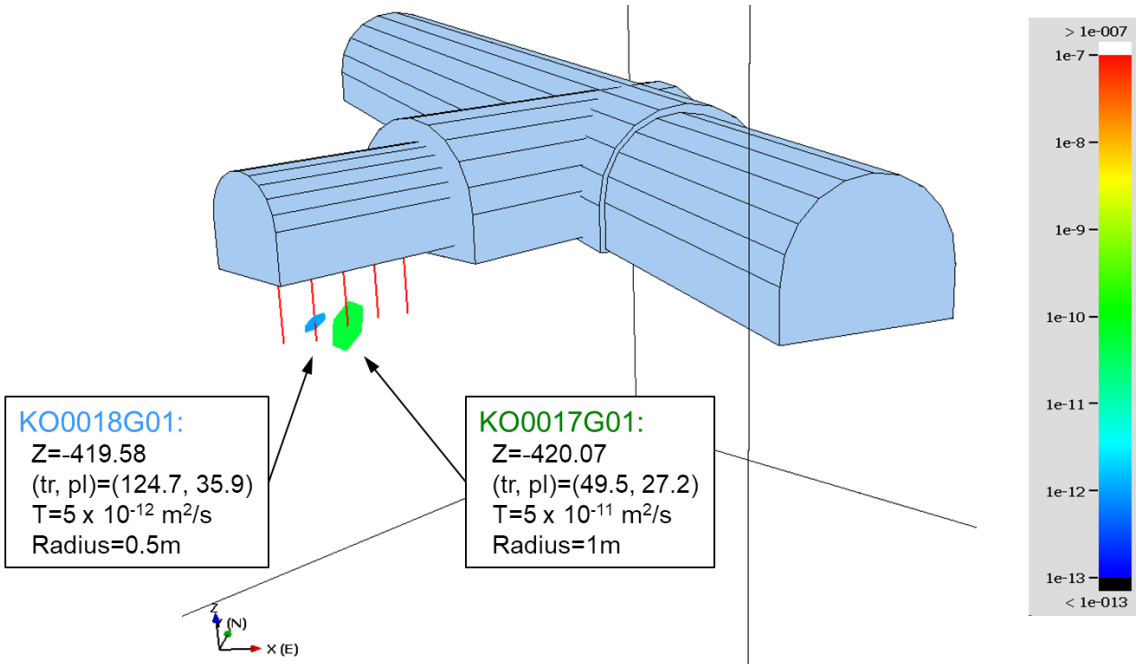

Figure 4-2. *Water conducting fractures observed at the walls of 30 cm diameter holes.*

The borehole specific capacity measured at the five probe holes by the injection test was reported in Task 8D specification.

- KO0014G01: 0.5–3.0 m, Q/dh 6.0×10^{-10} m^2/s
- KO0015G01: 0.75–3.03 m, Q/dh 1.7×10^{-7} m^2/s
- KO0017G01: 0.5–2.97 m, Q/dh 8.0×10^{-11} m^2/s including −420.07 m fracture (3.0×10^{-11} m^2/s excluding −420.07 m fracture)
- KO0018G01: 0.55–3.06 m, Q/dh 4.5×10^{-7} m^2/s, but 1×10^{-12} m^2/s at 2.1–3.1 m
- KO0020G01: 0.82–3.1 m, Q/dh 4.2×10^{-10} m^2/s

These specific capacity data was used to calibrate hydraulic conditions around the BRIE area. The model calibration was conducted by three steps as illustrated in Figure 4-3. Firstly, the specific capacity, Q/dh_{sim}, at each probe hole was calculated by steady state simulations with constant head drawdown, dh, conditions at each probe hole, and simulated Q/dh_{sim} at each probe hole was compared with the measured value. Secondary, transmissivity of fractures intersecting at each probe hole was changed by multiplying the ratio measured Q/dh to simulated Q/dh_{sim}, to calibrated hydraulic property around the probe holes. Both measured and simulated Q/dh_{sim} was dominated not only by the fractures intersecting the probe holes, but also by continuously connecting fractures of DFN to the probe holes. However, the extent of the drawdown is usually uncertain for the measured data. In this calibration, it was assumed that the fractures intersecting to the probe holes might dominate the borehole capacity. Then, transmissivity for only the fractures intersecting the probe holes were changed. In order to check the effectiveness of this modification, the constant head drawdown simulations were repeated and Q/dh_{sim} was compared with the measured Q/dh in third step. Ideally, the second step and the third step should be iteratively repeated until getting Q/dh_{sim} provides an acceptable match to measured data. However, due to time constraints, only a single iteration was carried out. Table 4-1 shows the changes for Q/dh_{sim} values compared with measured data, for each case of five realisations of DFN models. For base case and 1/50 transmissivity case, “no flow” to KO0018G01 borehole was calculated by realisation #02 because the fractures intersecting KO0018G01 borehole might not connect to head boundary to provide groundwater (but, it has the flowing connections to 30 cm diameter enlarged borehole along KO0018G01). Whereas, the local network of flowing fractures was modified by conditioning fractures to the boreholes, and a certain value of flow rate to KO0018G01 borehole was calculated shown in and is shown in Table 4-1 (c). The calculation for realisation #04 model for fracture conditioning case was not numerically converged.

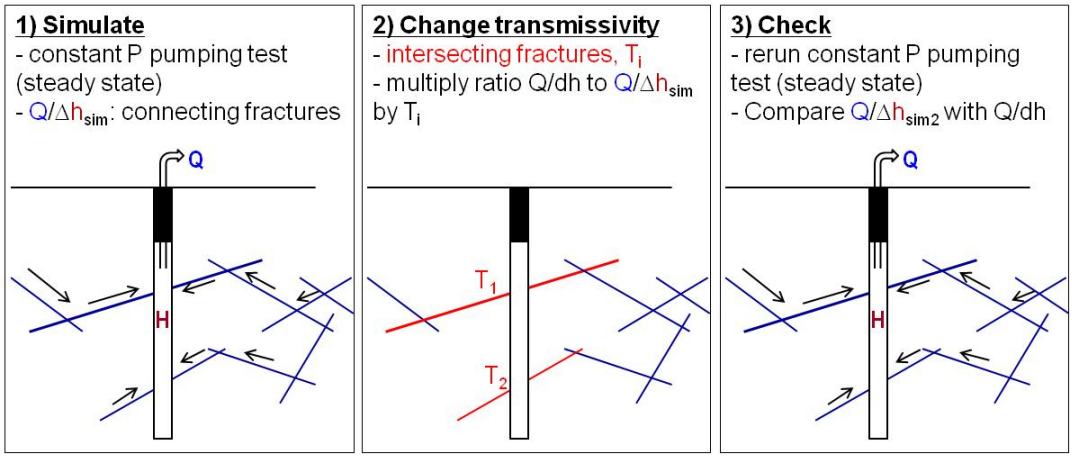

Figure 4-3. *Conceptual illustration for calibrating specific capacity around the five probe holes.*

Table 4-1. An example of Q/dh changes during model calibration by the specific capacity, (a) base case, five realisations (#01~#05).

holes	Measured Q/dh m^2/s		Simulated Q/dh m^2/s	Ratio for Transmissivity calibration	Q/dh of calibrated model m^2/s
KO0014G01	6.0×10^{-10}	#01	2.9×10^{-10}	2.08	3.9×10^{-11}
		#02	7.0×10^{-10}	0.86	5.8×10^{-11}
		#03	1.0×10^{-9}	0.58	5.0×10^{-11}
		#04	8.9×10^{-10}	0.68	4.0×10^{-9}
		#05	3.5×10^{-10}	1.70	6.2×10^{-11}
KO0015G01	1.7×10^{-7}	#01	2.1×10^{-10}	819.8	6.6×10^{-8}
		#02	6.3×10^{-11}	2712.0	1.2×10^{-9}
		#03	2.2×10^{-10}	764.0	2.0×10^{-9}
		#04	1.1×10^{-8}	16.0	9.3×10^{-8}
		#05	3.5×10^{-10}	481.8	3.2×10^{-8}
KO0017G01	3.0×10^{-11}	#01	1.5×10^{-9}	0.02	3.3×10^{-11}
		#02	2.8×10^{-11}	1.08	3.0×10^{-11}
		#03	1.5×10^{-10}	0.20	3.2×10^{-11}
		#04	3.3×10^{-9}	0.01	2.7×10^{-11}
		#05	3.7×10^{-10}	0.08	1.3×10^{-7}
KO0018G01	4.5×10^{-7}	#01	1.5×10^{-9}	294.7	3.0×10^{-7}
		#02	not flow	-	-
		#03	6.4×10^{-9}	70.2	6.2×10^{-9}
		#04	3.8×10^{-10}	1196.5	6.9×10^{-8}
		#05	5.4×10^{-10}	833.2	2.0×10^{-7}
KO0020G01	4.2×10^{-10}	#01	1.6×10^{-10}	2.68	3.1×10^{-10}
		#02	8.7×10^{-10}	0.48	4.4×10^{-10}
		#03	4.4×10^{-9}	0.10	3.6×10^{-10}
		#04	1.0×10^{-10}	4.08	2.6×10^{-10}
		#05	9.5×10^{-9}	0.04	5.3×10^{-6}

(b) 1/50 transmissivity case, five realisations (#01~#05).

Holes	Measured Q/dh m^2/s		Simulated Q/dh m^2/s	Ratio for Transmissivity calibration	Q/dh of calibrated model m^2/s
KO0014G01	6.0×10^{-10}	#01	2.8×10^{-10}	2.18	3.9×10^{-11}
		#02	5.6×10^{-10}	1.07	4.1×10^{-11}
		#03	5.8×10^{-10}	1.04	4.2×10^{-11}
		#04	3.3×10^{-10}	1.84	3.0×10^{-9}
		#05	2.8×10^{-10}	2.12	3.8×10^{-11}
KO0015G01	1.7×10^{-7}	#01	4.2×10^{-12}	40 984	5.7×10^{-8}
		#02	1.3×10^{-12}	135 117	2.5×10^{-11}
		#03	4.5×10^{-12}	38 027	5.0×10^{-11}
		#04	2.2×10^{-10}	784.6	7.1×10^{-8}
		#05	7.1×10^{-12}	24 077	1.0×10^{-9}
KO0017G01	3.0×10^{-11}	#01	2.4×10^{-11}	1.25	2.2×10^{-11}
		#02	3.3×10^{-13}	91.61	2.5×10^{-12}
		#03	2.2×10^{-12}	13.79	2.1×10^{-11}
		#04	5.8×10^{-11}	0.51	7.8×10^{-12}
		#05	6.2×10^{-12}	4.81	8.7×10^{-10}
KO0018G01	4.5×10^{-7}	#01	3.0×10^{-11}	14 882	2.9×10^{-7}
		#02	not flow	-	-
		#03	1.3×10^{-10}	3 507	1.1×10^{-9}
		#04	7.5×10^{-12}	59 757	4.5×10^{-8}
		#05	1.0×10^{-11}	44 164	1.4×10^{-9}
KO0020G01	4.2×10^{-10}	#01	3.1×10^{-12}	134.1	3.5×10^{-11}
		#02	1.7×10^{-11}	24.11	2.0×10^{-10}
		#03	8.7×10^{-11}	4.82	5.2×10^{-10}
		#04	2.1×10^{-12}	202.28	2.8×10^{-11}
		#05	1.9×10^{-10}	2.20	4.14×10^{-10}

(c) Fracture conditioning case, five realisations (#01~#05).

Holes	Measured Q/dh m^2/s		Simulated Q/dh m^2/s	Ratio for Transmissivity calibration	Q/dh of calibrated model m^2/s
KO0014G01	6.0×10^{-10}	#01	3.2×10^{-10}	1.87	4.2×10^{-10}
		#02	3.1×10^{-10}	1.93	5.9×10^{-10}
		#03	3.2×10^{-10}	1.90	5.8×10^{-10}
		#04	NA	-	-
		#05	3.1×10^{-10}	1.96	6.1×10^{-10}
KO0015G01	1.7×10^{-7}	#01	6.3×10^{-11}	2695	5.4×10^{-9}
		#02	1.9×10^{-10}	910.9	5.3×10^{-8}
		#03	1.6×10^{-11}	10 515	2.8×10^{-11}
		#04	NA	-	-
		#05	5.0×10^{-11}	3 426.7	7.2×10^{-10}
KO0017G01	3.0×10^{-11}	#01	6.9×10^{-11}	0.43	3.5×10^{-11}
		#02	1.0×10^{-10}	0.29	3.2×10^{-11}
		#03	1.8×10^{-11}	1.72	2.9×10^{-11}
		#04	NA	-	-
		#05	1.5×10^{-11}	2.04	3.1×10^{-11}
KO0018G01	4.5×10^{-7}	#01	1.3×10^{-11}	34 842	4.6×10^{-10}
		#02	3.8×10^{-20}	1.194×10^{13}	1.6×10^{-14}
		#03	1.1×10^{-11}	41 377	7.3×10^{-11}
		#04	NA	-	-
		#05	3.9×10^{-11}	11 696	7.7×10^{-10}
KO0020G01	4.2×10^{-10}	#01	2.5×10^{-11}	16.9	9.4×10^{-11}
		#02	1.6×10^{-11}	26.24	4.5×10^{-11}
		#03	1.8×10^{-11}	23.04	2.7×10^{-10}
		#04	NA	-	-
		#05	5.5×10^{-11}	7.61	2.0×10^{-10}

Most of the cases seem to reproduce similar ranges of Q/dh, except for the KO0018G01 of fracture conditioning case. However, relatively high Q/dh boreholes, KO0015G01 and KO18G01, tend to show insufficient calibration. Several orders of magnitude changed transmissivity would be necessary to match Q/dh when calibrating only the transmissivity of the fractures connecting the boreholes. For the case in why the KO0017G01 boreholes were calibrated, all cases except #05 shows similar range to measured Q/dh, 6×10^{-10} m^2/s. For borehole KO0018G01, some cases such as #01 and #05 of base case and #01 of 1/50 transmissivity case could reproduce similar Q/dh, however other cases could not establish it. Especially, fracture conditioning case did not improve Q/dh. It is expected that this is due to the weak connectivity around KO0018G01 borehole, which was caused by only a single fracture (see Figures 3-16 and 3-17) allowed intersecting by fracture conditioning (Figure 3-15) might make it difficult to calibrate Q/dh. This result indicates that the calibration procedure examined in this study might not partially enough to measured Q/dh distribution, due to a simple assumption of only fractures intersecting to the probe holes might dominate the borehole capacity. In addition, repeating of the calibration process might reproduce better results.

The modified models were applied to calculate the groundwater flow rate to 30 cm diameter boreholes, and to the coupling simulation for predicting "BRIE" re-saturation behaviour in bentonite. The geometry of 30 cm diameter boreholes was slightly adjusted to BRIE conditions. Location and diameter for both boreholes were the same as Task 8C specification, but length of each borehole was changed. At KO0017G01, 30 cm diameter borehole was started from the elevation −417.29 m and was ended at elevation −420.788 m, and bentonite column was emplaced between elevation −417.34 m and −420.718 m (length 3.378 m). At KO0018G01, the enlarged borehole was started from the elevation −417.365 m and was ended at elevation −420.375 m, and bentonite column was emplaced between elevation −417.415 m and −420.285 m (length 2.87 m). The finite element used for Task 8D is shown in Figure 4-4. The excavated lengths for each enlarged borehole were represented in the model for calculating groundwater flow rate to the boreholes under atmospheric pressure condition, but for calculating bentonite re-saturation, the lengths of installing bentonite columns were allocated to be an interface between rock and bentonite. The remaining zones at the top and bottom of each borehole were sealed in the model, although the bottom of the boreholes were filled by sand in BRIE.

The property values for the bentonite were the same as Task 8C (Table 3-4) except for the initial saturation applied to the Task 8D2 simulations. The initial saturation of 41.3 % corresponding to the initial water content of 11.6 % is used (Table 4-2).

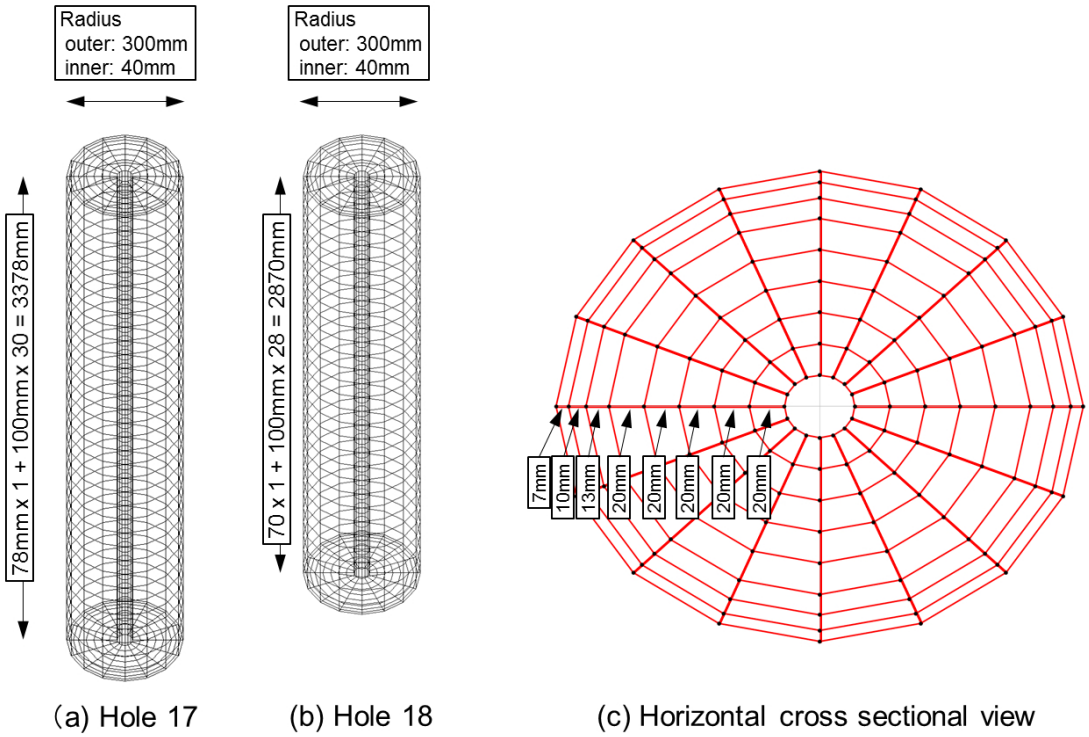

Figure 4-4. *Finite elements for modelling bentonite columns used for Task 8D.*

Table 4-2 Material properties and initial conditions of bentonite.

Parameter	Unit	Value
Porosity	-	0.44
Intrinsic permeability	m^2	6.4×10^{-21}
Dry density	Mg/m^3	1.56
Relative permeability, k_r	-	$k_r = S_l^3$ S_l: water saturation
Water retention curve		van Genuchten's equation $S_l(P_l) = \left\{1 + \left(\frac{P_g - P_l}{P_0}\right)^{\frac{1}{1-\lambda}}\right\}^{-\lambda}$ P_l: water pressure P_g: Gas pressure: 0.1MPa P_0: empirical constant: 9.23MPa λ: empirical constant: 0.3
Water density	Mg/m^3	1
Water viscosity	Pa s	0.001
Initial Saturation	%	41.3
Temperature	°C	20

4.4 Results

Steady state flow simulations assuming same boundary conditions as used for Task 8C reference condition for modified models were examined. For each case, a) base case, b) 1/50 transmissivity case, c) fracture conditioning case, the five stochastic realisation models were modified as described in Section 4.3. Simulated flow rates and head values at the five probe holes were compared with the measurements as shown in Figure 4-5. Task 8D specification provides additional data to Task 8C, which are emphasised by a pink solid circle in Figure 4-5. The base case model tends to have larger flow rate than that measured at KO0014G01~KO0017G01, especially at KO0020G01 which has more than two order of magnitude larger flow rate than measured. The case of 1/50 transmissivity seems have smaller flow rate at KO0015G01 and KO0017G01, closer values at KO0014G01 and larger flow rate to KO0020G01. Head values do not show wider sensitivity among the three cases compared with the sensitivity to flow rate. In addition, the wider variability among the stochastic realisations remains regardless of constraining specific capacity around five probe holes.

Head values measured at horizontally drilled boreholes from the tunnels, as shown in Figure 4-6 were also compared with the simulation results (see Figure 4-7). The simulated head values at these boreholes also have wider variation among the stochastic realisations. At the southeast side of the tunnel, simulated head values tend to show lower than measured, which might require higher conductive structure to provide high head from outer boundaries or lower connectivity to the tunnel to prevent head drawdown. The northwest side has similar or higher head values as measured, which are dominated by low head boundary condition at the northwest side as shown in Figure2-5.

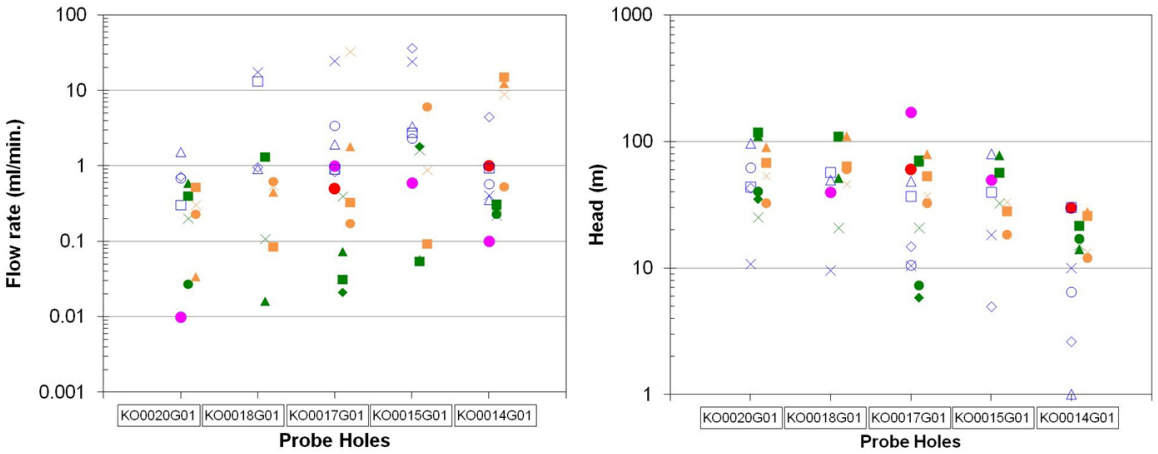

(a) Flow rate to five probe holes. (b) head values at five prove holes.

Figure 4-5. *Simulated flow rate to and head values at the five probe holes. Solid circle (Red): measured data provided in Task 8C. Solid circle (Pink): measured data provided in Task 8D. Open symbol (Blue): a) base case simulation results of five realisations. Solid symbol (Green): b) 1/50 transmissivity case simulation results of five realisations. Solid symbol (Yellow): c) fracture conditioning case simulation results of five realisations.*

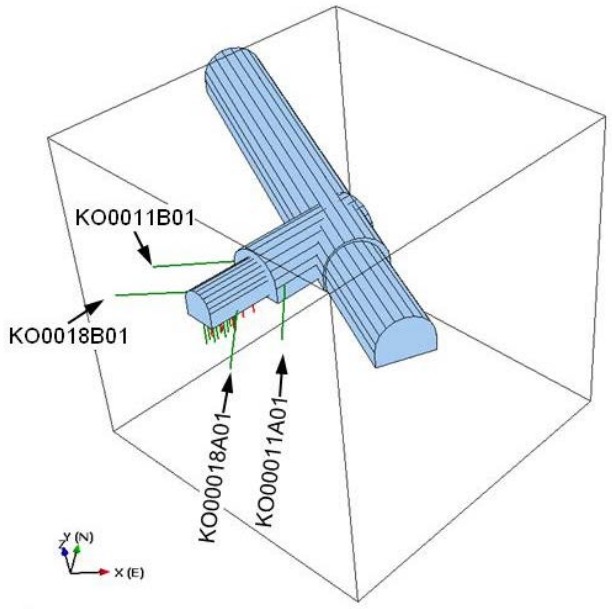

Figure 4-6. *Boreholes horizontally drilled from the tunnel providing additional measured head values.*

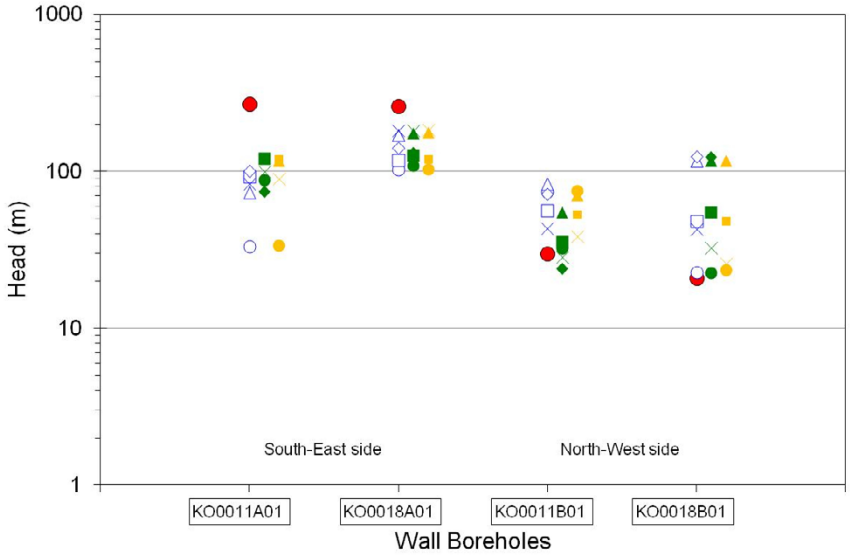

Figure 4-7. *Simulated head values at horizontally drilled boreholes. Solid circle (Red): measured data provided in Task 8D. Open symbol (Blue): a) base case simulation results of five realisations. Solid symbol (Green): b) 1/50 transmissivity case simulation results of five realisations. Solid symbol (Yellow): c) fracture conditioning case simulation results of five realisations.*

The examples of the simulated head distribution at vertical and horizontal cross sections for each case is shown in Figure 4-8. No significant differences among the three cases are shown, but minor differences around the BRIE local region for the fracture conditioning case are recognised. Figure 4-9 shows fractures intersecting 30 cm diameter boreholes and groundwater flow rate along the fracture traces at the borehole walls, which is an example of a single realisation of the fracture conditioning case. In whole model region, the head distribution is smoothly decreased toward a tunnel that is caused by an effect of averaging out of heterogeneously distributed DFN as shown in Figure 4-8. However, in a local scale around 30 cm boreholes, heterogeneously distributed groundwater flow due to a local connectivity of fractures to the boreholes is reproduced. The cumulative flow distribution from the bottom of the 30 cm boreholes are summarised in Figures 4-10 through 4-12 for each case with the five stochastic realisations for DFN model. Because the measured groundwater flow rate to the 30 cm diameter boreholes are suggested as range of 0.12~0.25 ml/min at KO0017G01 (depth 2.1~3.5 m) and 0.01~0.03 ml/min at KO0018G01 (depth 2.1~3.1 m), the maximum value of flow rate for each figure is set as 10 ml/min to compare with the suggested values. Although specific capacity around the probe holes were constrained, flow rate to the 30 cm boreholes was not well matched to measured data, some realisations have extremely large flow rate to the 30 cm boreholes than measured flow rate.

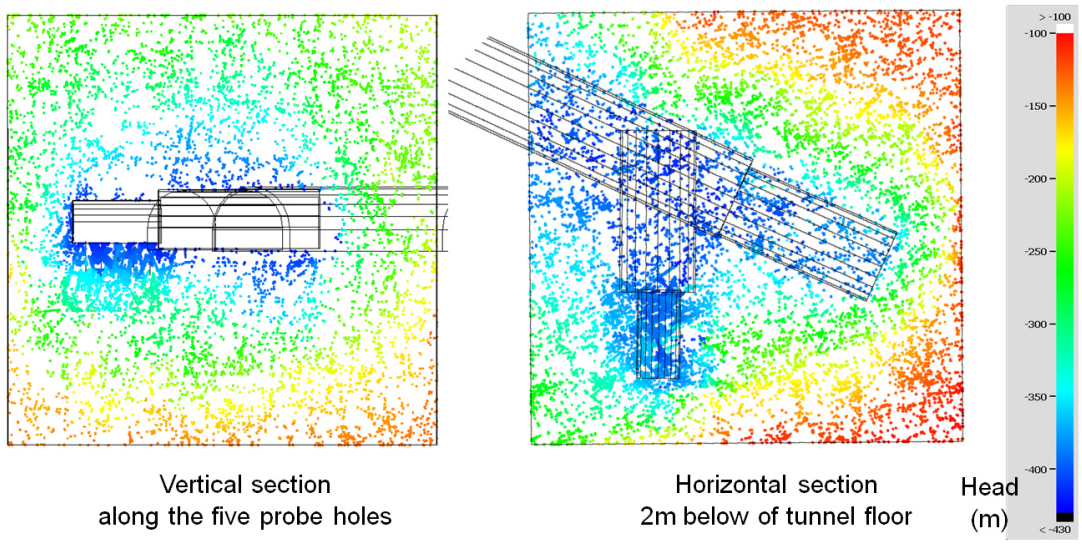

(a) Base case

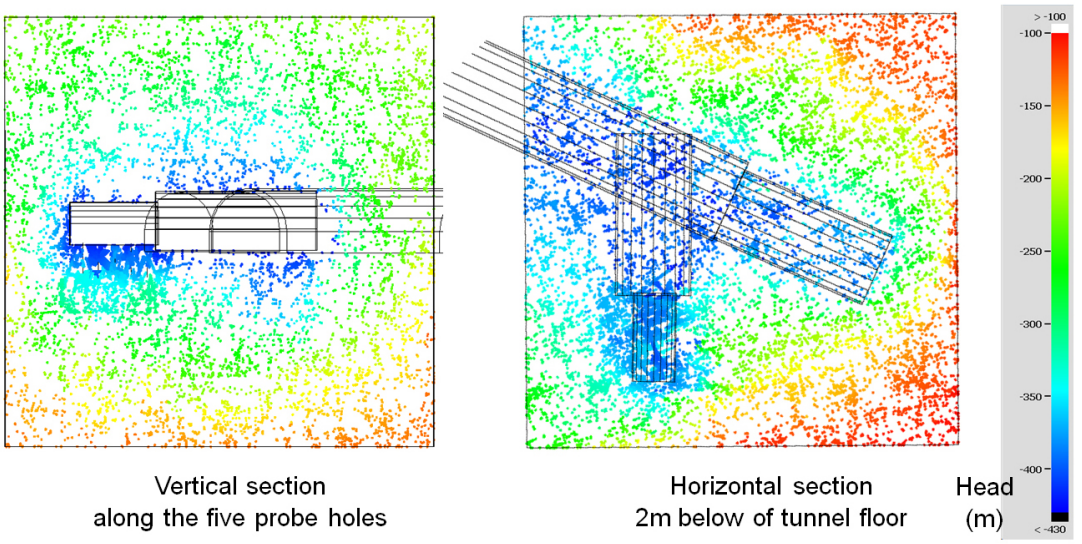

(b) 1/50 Transmissivity case

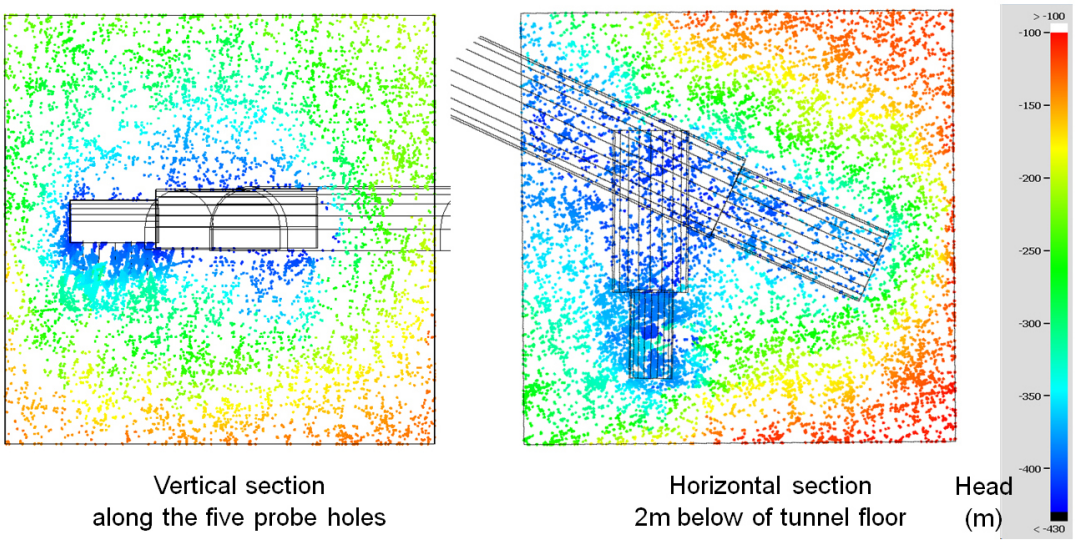

(c) Fracture conditioning case

Figure 4-8. *Comparison of head distribution at vertical and horizontal cross sectional planes.*

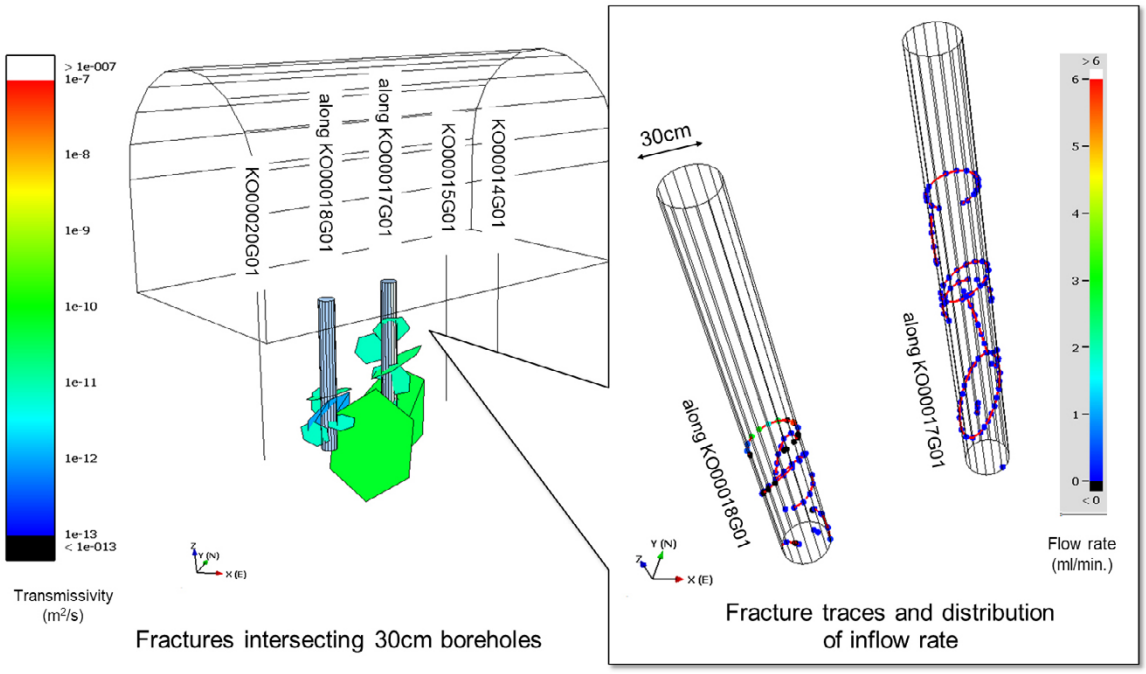

Figure 4-9. *Groundwater flow distribution at enlarged borehole wall. Example of fracture conditioning case (realisation 01).*

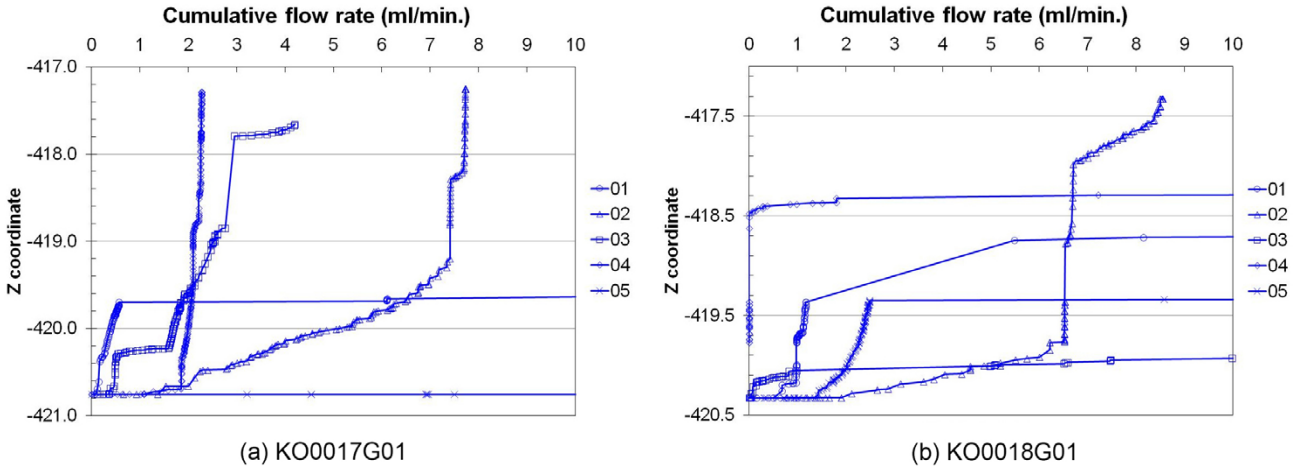

Figure 4-10. *Cumulative flow distribution at enlarged borehole wall, Base case (five realisations).*

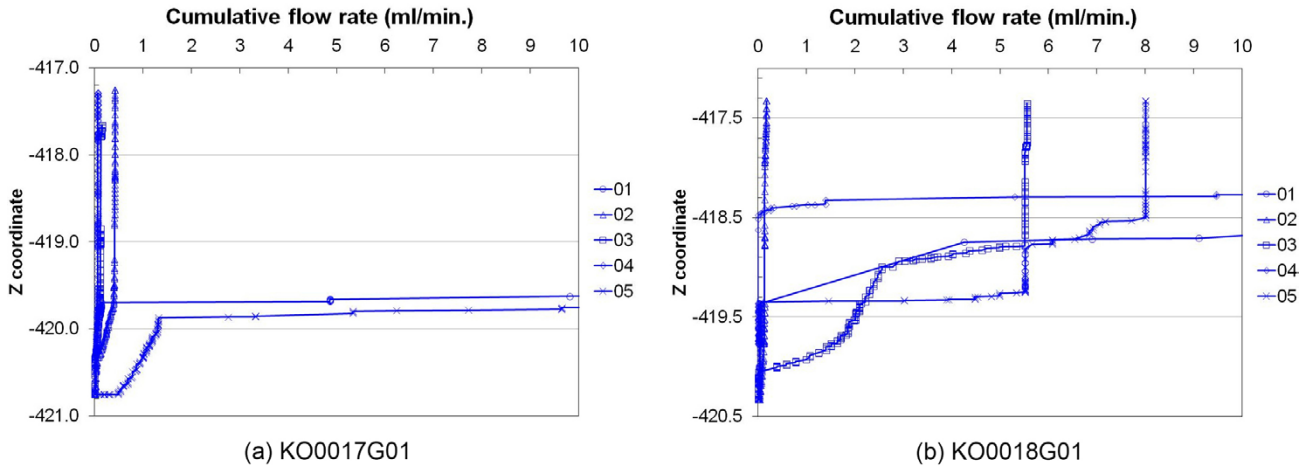

Figure 4-11. *Cumulative flow distribution at enlarged borehole wall, 1/50 Transmissivity case (five realisations).*

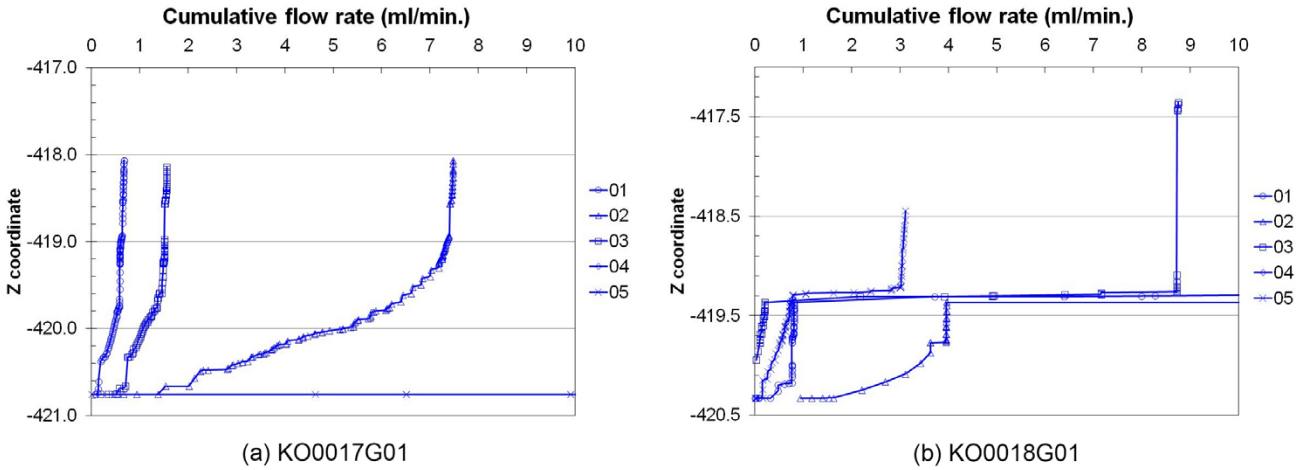

Figure 4-12. *Cumulative flow distribution at enlarged borehole wall, Fracture conditioning case (five realisations).*

Consequently, the localised groundwater flow provides the heterogeneous re-saturation behaviour in bentonite columns installed in 30 cm boreholes by the coupling simulation. The bentonite wetting simulation results for each case with five stochastic realisation model are visualised in Figures 4-13 through 4-40, which shows the time-dependent change of pressure and saturation distribution at vertical and horizontal cross sections. The realisation #04 of fracture conditioning case was not applied to the bentonite wetting simulation because of convergent failure for the steady state groundwater flow calculation in the DFN model. In both 30 cm boreholes, the saturated areas were initiated by the points intersecting groundwater flowing fractures and were propagated to column centre and both upward and downward of the bentonite columns.

The distribution and propagation of both pressure and saturation behaves in a similar pattern for all cases. Basically, wetting pattern is controlled by the intersecting location and resistances (such as transmissivity) of fractures potentially providing groundwater to the bentonite columns. The fracture distribution intersecting 30 cm enlarged boreholes is different among five realisation models, for base case and 1/50 transmissivity case. Bentonite wetting location and propagation pattern is controlled by the different patterns of fracture trace at the surface of bentonite column for base case and 1/50 transmissivity case. 1/50 transmissivity case shows a bit slower wetting propagation than base case when the same realisation model is compared. This delay is caused by only the transmissivity differences. The realisations of #01~#03 and #05 have similar Q/dh along KO0017G01 for base case (see Table 4-1 (a)), but the saturation rate is different among them. #04 model seems to be the fastest and #03 model is the slowest. The average interval of fractures intersecting 30 cm enlarged boreholes along the borehole axis might also affect the saturation rate of the bentonite. For example, relatively sparse fractures are intersecting KO0017G01 for realisation #3 model, and it tends to remain unsaturated zone 10 years after the emplacement. On the other hand, the fastest model, realisation #04 has more fracture intersecting points than the others. For the realisation #5 of base case, Q/dh at KO0017G01 is four orders of magnitude larger than the other realisations (not well conditioned by the measured specific capacity). But, due to a long interval not intersecting fractures at the upper part, the unsaturated zone remains more than 50 years after emplacing the bentonite.

By calibrating hydraulic properties around the BRIE area for reproducing measured specific capacity, the bentonite wetting behaviour was slightly changed. For example, in case of comparing the base case realisation #01 model between Task 8C (Figure 3-9) and Task 8D (Figure 4-14(a)) results for KO0017G01, the saturation rate of Task 8D model seems to become slower than Task 8C model. Because, the Task 8D calibrated model has about 1/45 times smaller specific capacity at this borehole. In contrast, at KO0018G01, the calibrated Task 8D model result (Figure 4-14(b)) seems to have a faster saturation rate than Task 8C model (Figure 3-11). This is caused by increasing specific capacity around KO0018G01 by ca. 350 times.

The fracture condition case has similar wetting pattern among the realisations for both KO0017G01 and KO0018G01 (Figures 4-33 through 4-40), except for KO0018G01 of realisation #05 model. For these models, fractures intersecting five probe boreholes were constrained by measured data (Figure 3-15). And, two fractures observed at 30 cm enlarged boreholes shown in Figure 4-2 were deterministically added. It is possible to reproduce same fracture patterns intersecting 30 cm enlarged boreholes. Exceptions can be made by potentially intersecting minor fractures to 30 cm enlarged boreholes but not intersecting probe boreholes. An additional minor fracture seems to intersect at the top of enlarged borehole along KO0018G01 in the realisation #03 model, and some minor fractures are intersecting to the lower part of KO0018G01 in the realisation #04 model. These minor fractures affect the wetting pattern in the bentonite. Calibrating the specific capacity to measured values also enforces the saturation rate. For all realisation models, Q/dh was well calibrated for KO0017G01 as shown in Table 4-1(c). The similar saturation rate could be reproduced. For KO0018G01 borehole, it was not well constrained by measured specific capacity. Especially, Q/dh of the realisation #02 is extremely smaller than the other case. It causes the delay of saturation rate of the bentonite column.

The time-dependent change of humidity at specified points in bentonite columns are summarised in Figures 4-41 through 4-43, for each case. The specified points were selected for placing and relative humidity sensors of BRIE. The location of these sensors were defined to set as close as possible to the fracture of interest in each borehole, depth of 2.3 m and 2.6 m at KO0017G01 and 2.3 m and 2.7 m at KO0018G01. Base case and 1/50 transmissivity case measures behave similar in trend for each realisation, but 1/50 transmissivity has a relatively slower increase of relative humidity than the base case model. For the fracture conditioning case, similar pressure and relative humidity profiles among the realisations are expected especially at KO0017G01because pressure and saturation patterns are similar as shown in Figures 4-33 through 4-40. However, some points seem to have a different profile among the realisations, when they are comparing the specific point values at initial 500 days, quantitatively. Figure 4-44 shows the comparison of relative humidity for KO0017G01 among the different realisations. At WBR0001, all realisations have a similar increase of the relative humidity. Realisation #03 model is a slower increase at WBR0002 and a faster increase WBR0003 than the others. At WBR0004, WBR0005, and WBR0006 the profiles for increasing relative humidity are a bit spread.

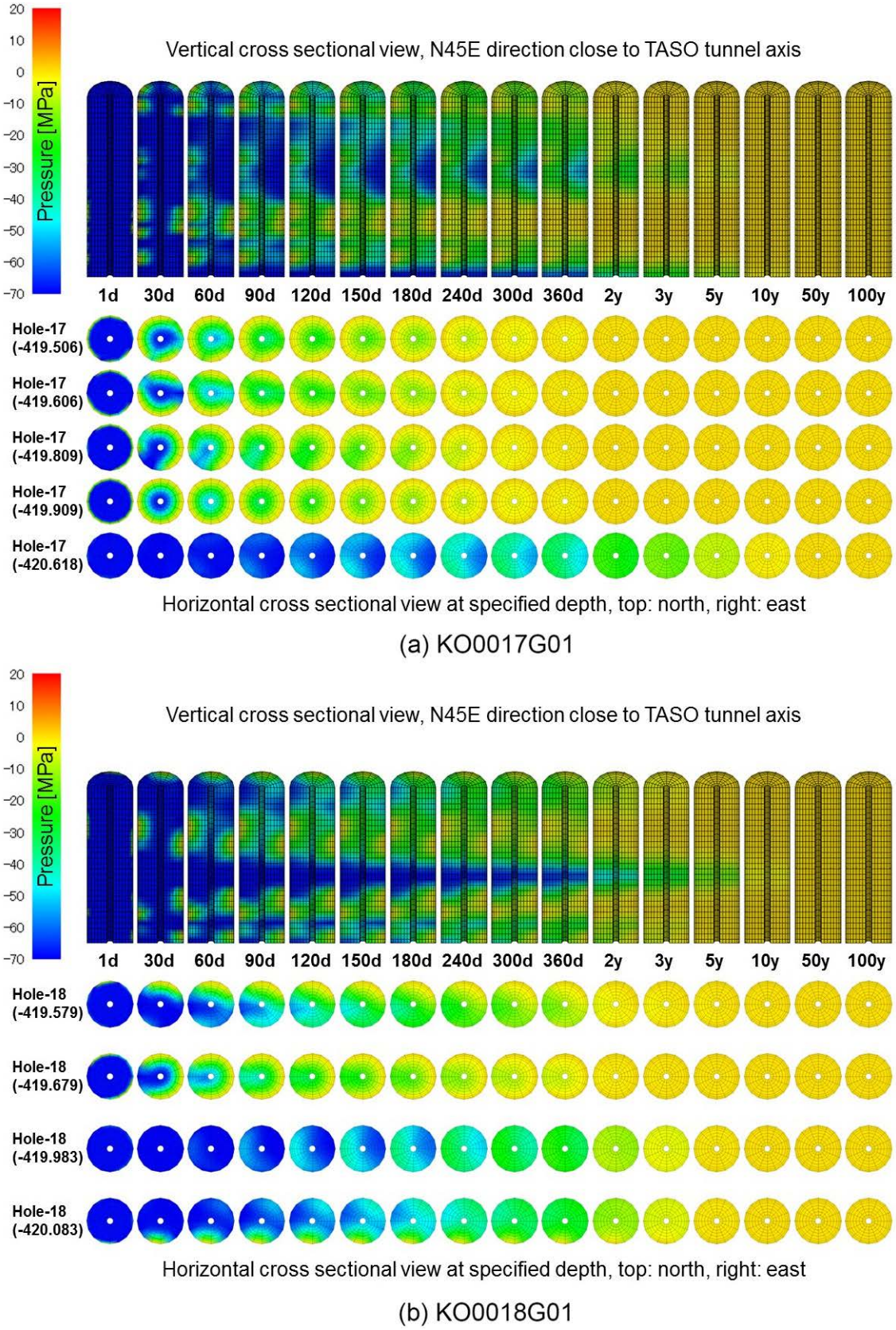

Figure 4-13. *Pressure distribution in bentonite column at KO0017G01 and KO0018G01, base case model, realisation #01.*

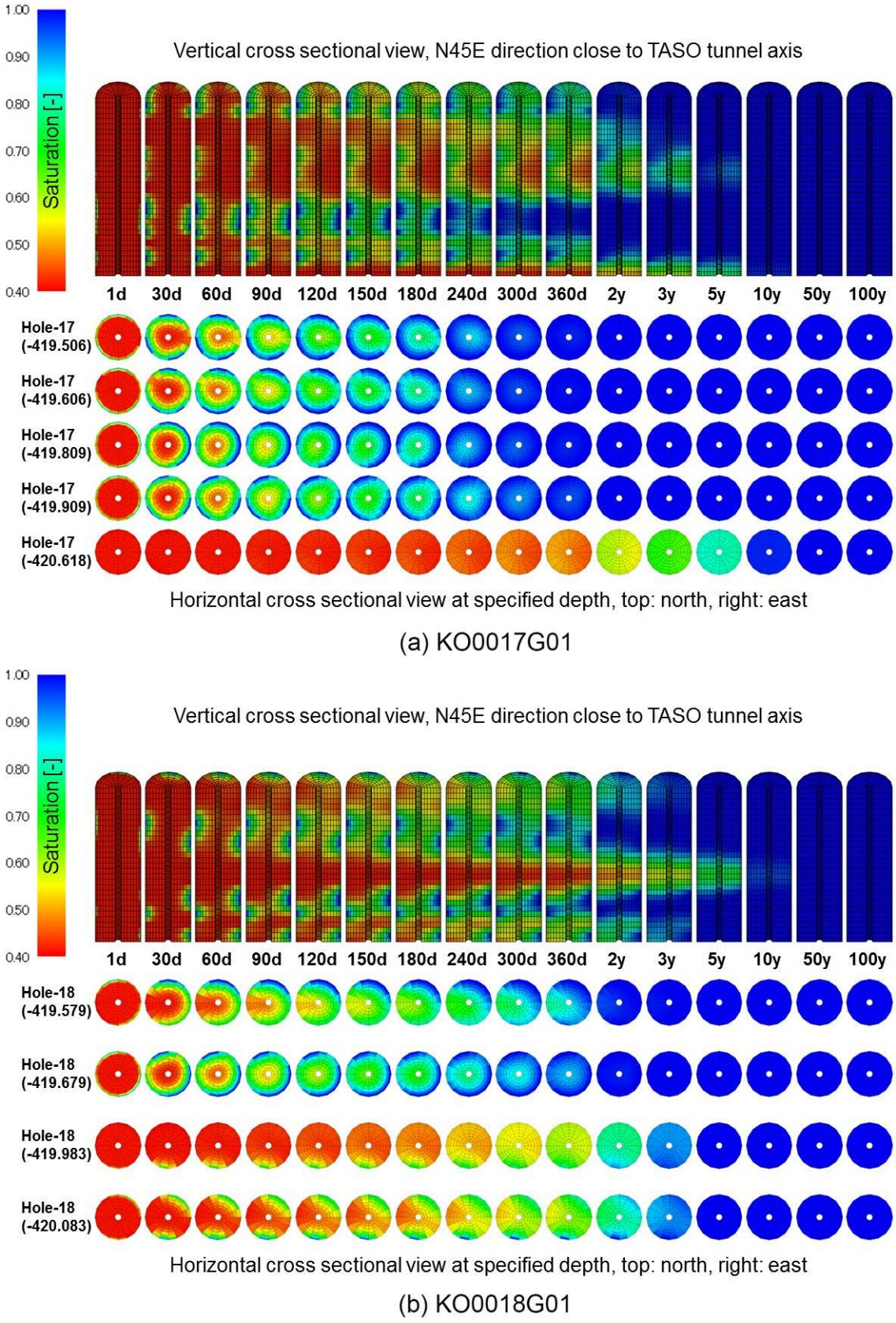

Figure 4-14. *Saturation distribution in bentonite column at KO0017G01 and KO0018G01, base case model, realisation #01.*

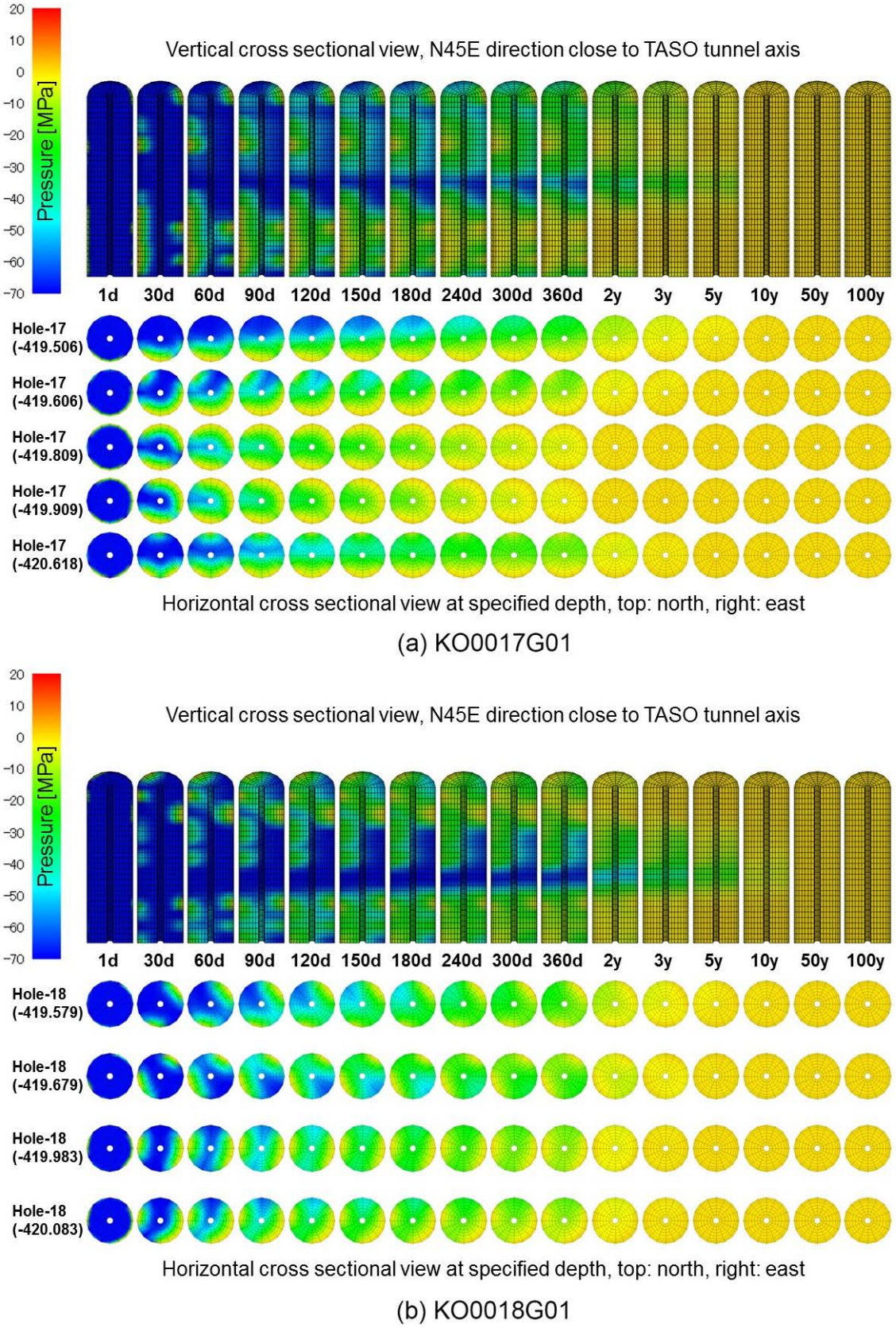

Figure 4-15. *Pressure distribution in bentonite column at KO0017G01 and KO0018G01, base case model, realisation #02.*

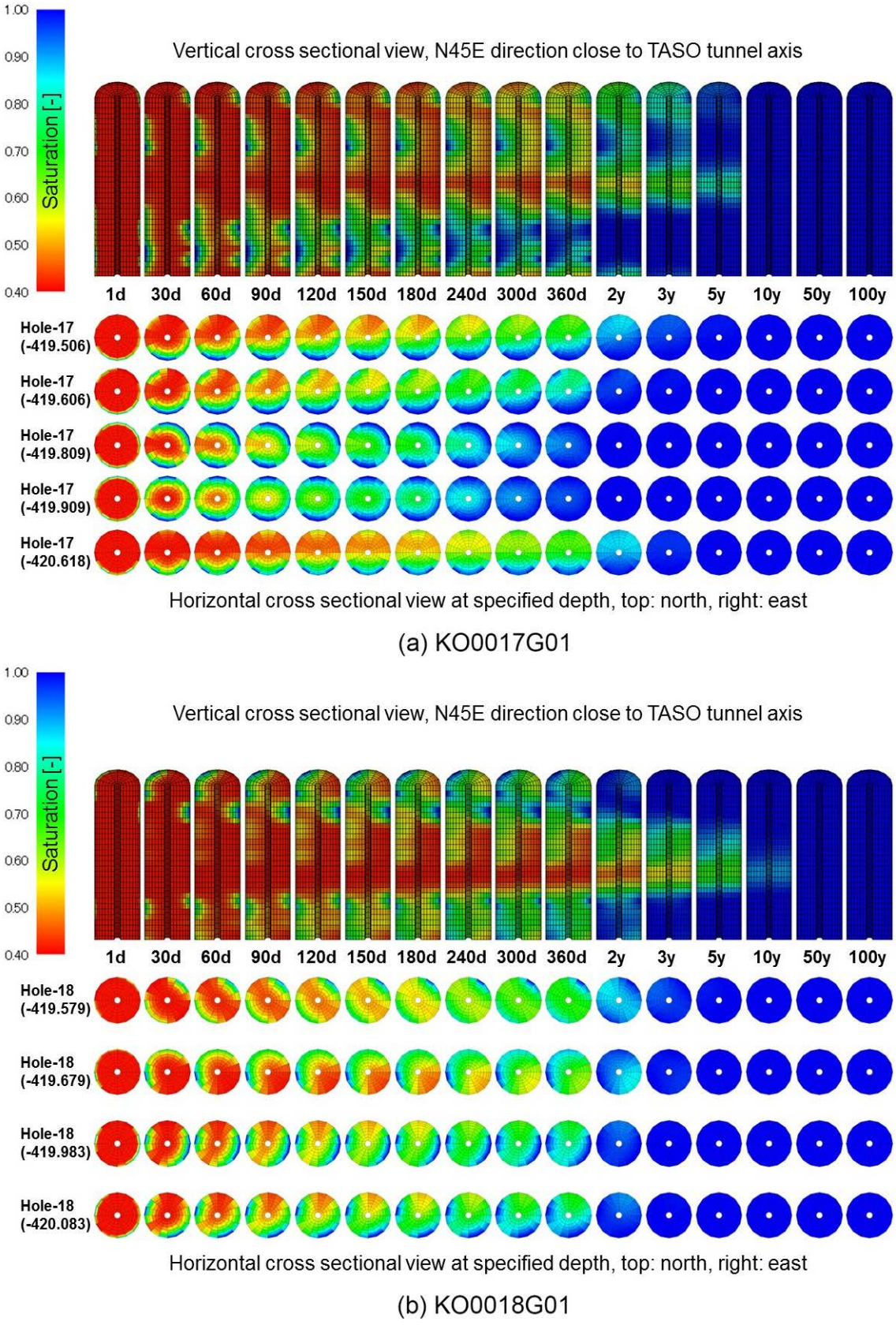

Figure 4-16. *Saturation distribution in bentonite column at KO0017G01 and KO0018G01, base case model, realisation #02.*

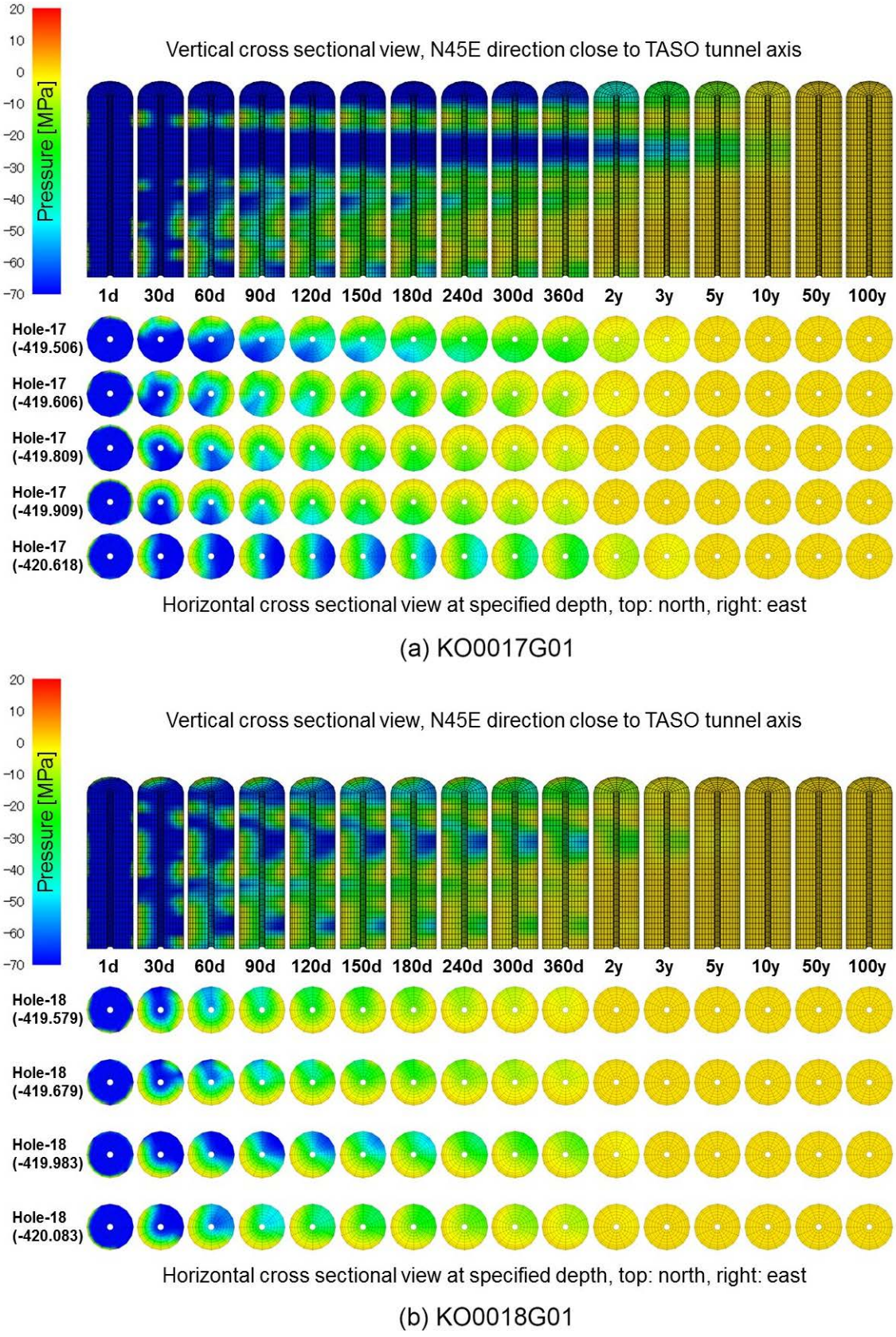

Figure 4-17. *Pressure distribution in bentonite column at KO0017G01 and KO0018G01, base case model, realisation #03.*

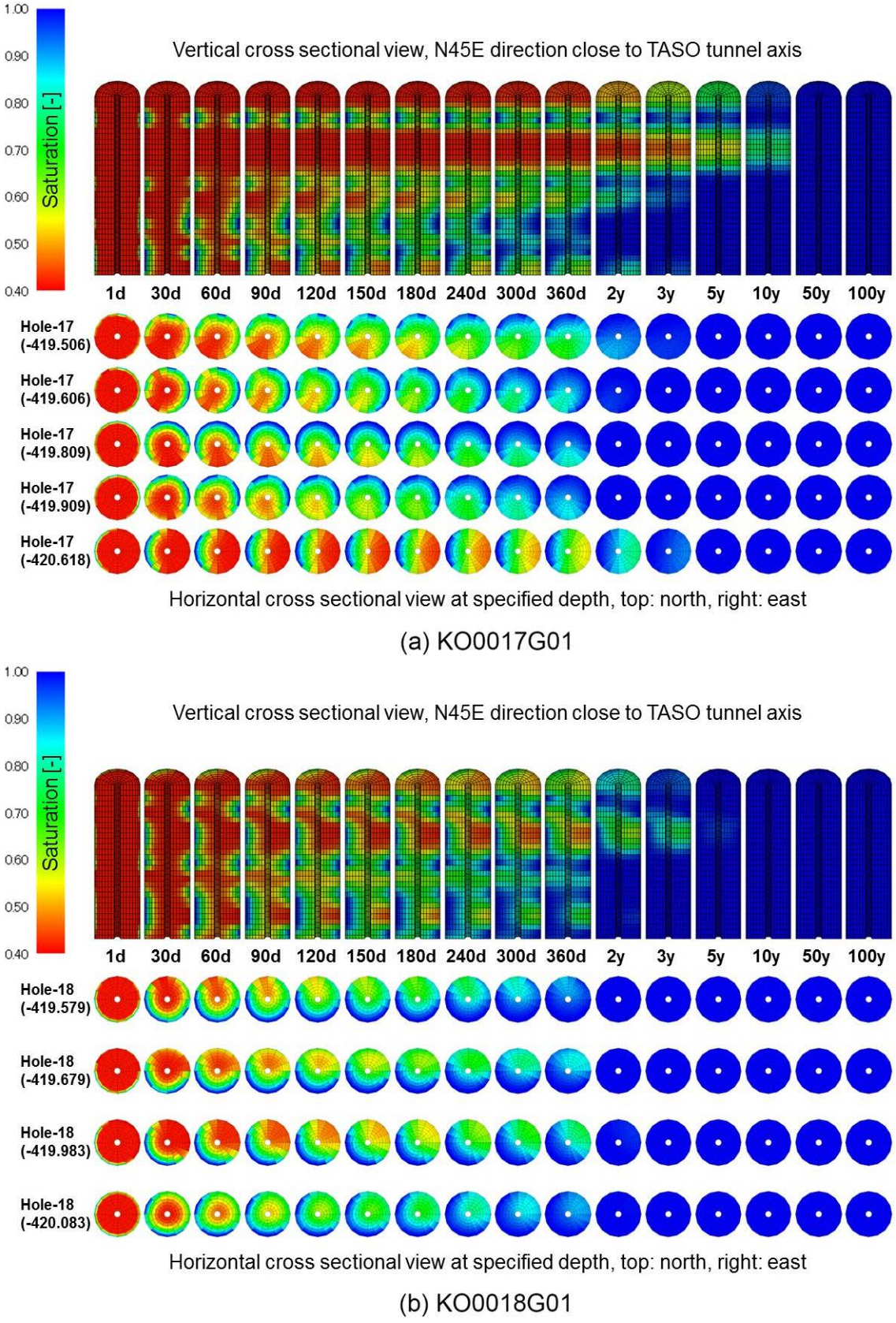

Figure 4-18. *Saturation distribution in bentonite column at KO0017G01 and KO0018G01, base case model, realisation #03.*

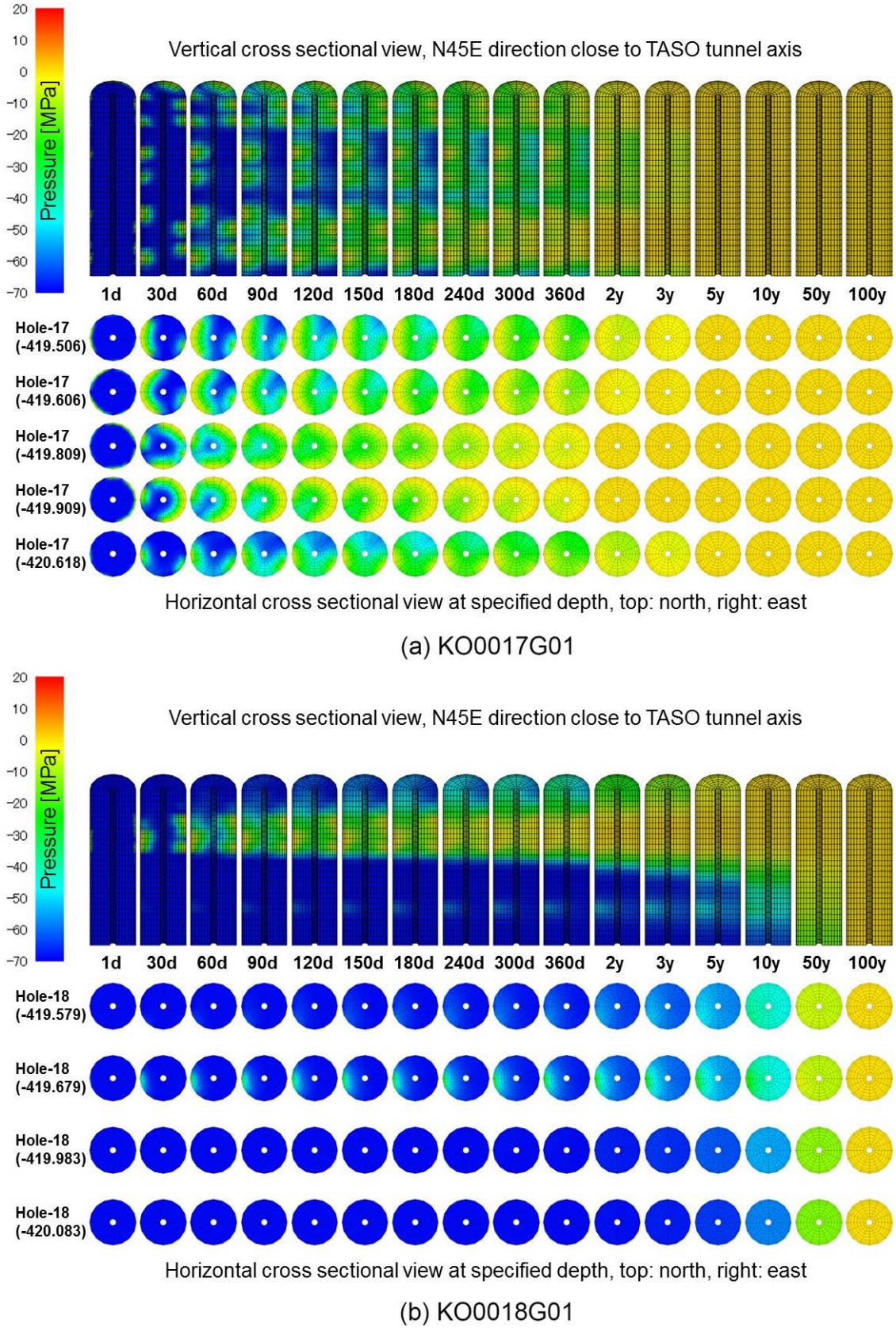

Figure 4-19. *Pressure distribution in bentonite column at KO0017G01 and KO0018G01, base case model, realisation #04.*

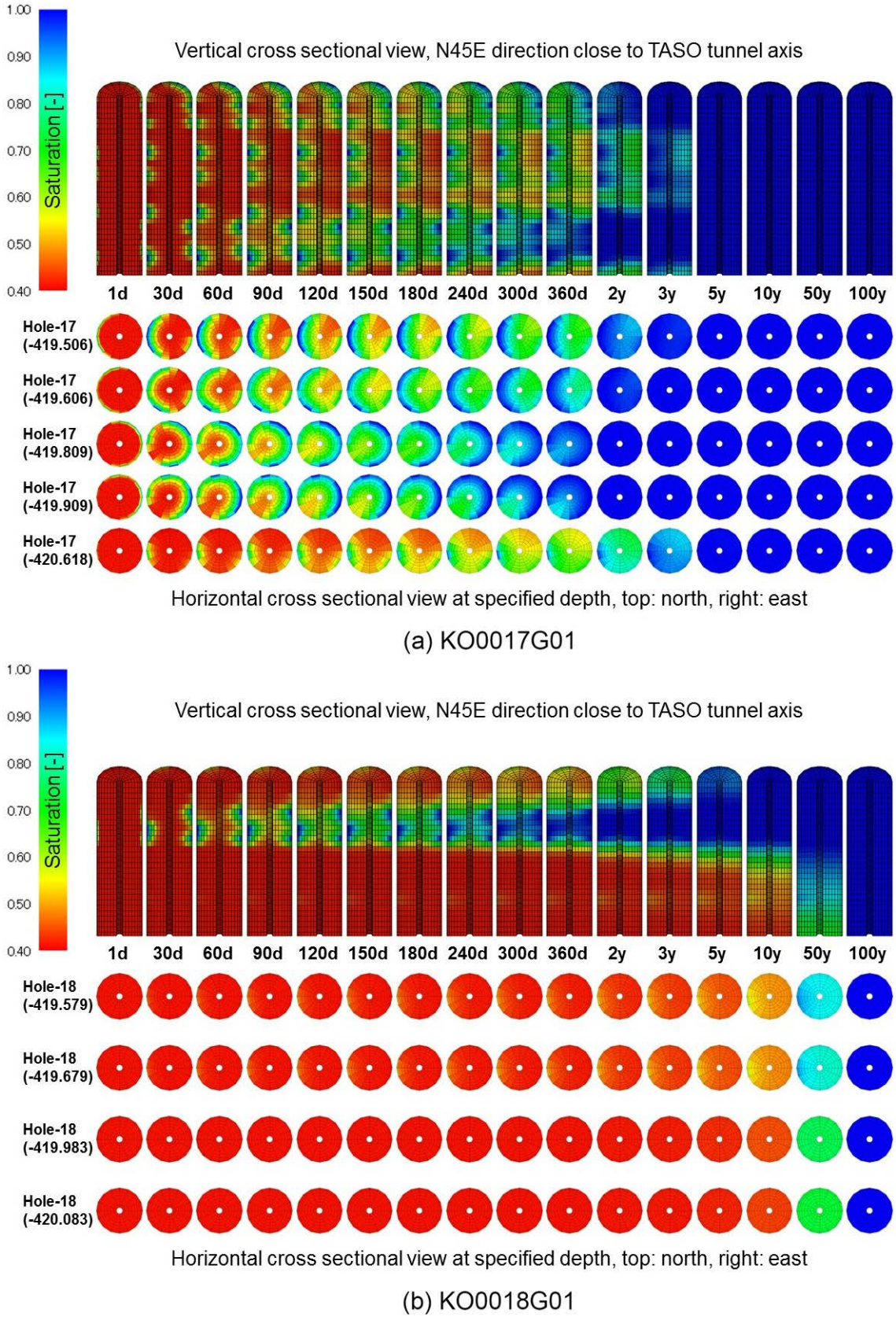

Figure 4-20. *Saturation distribution in bentonite column at KO0017G01 and KO0018G01, base case model, realisation #04.*

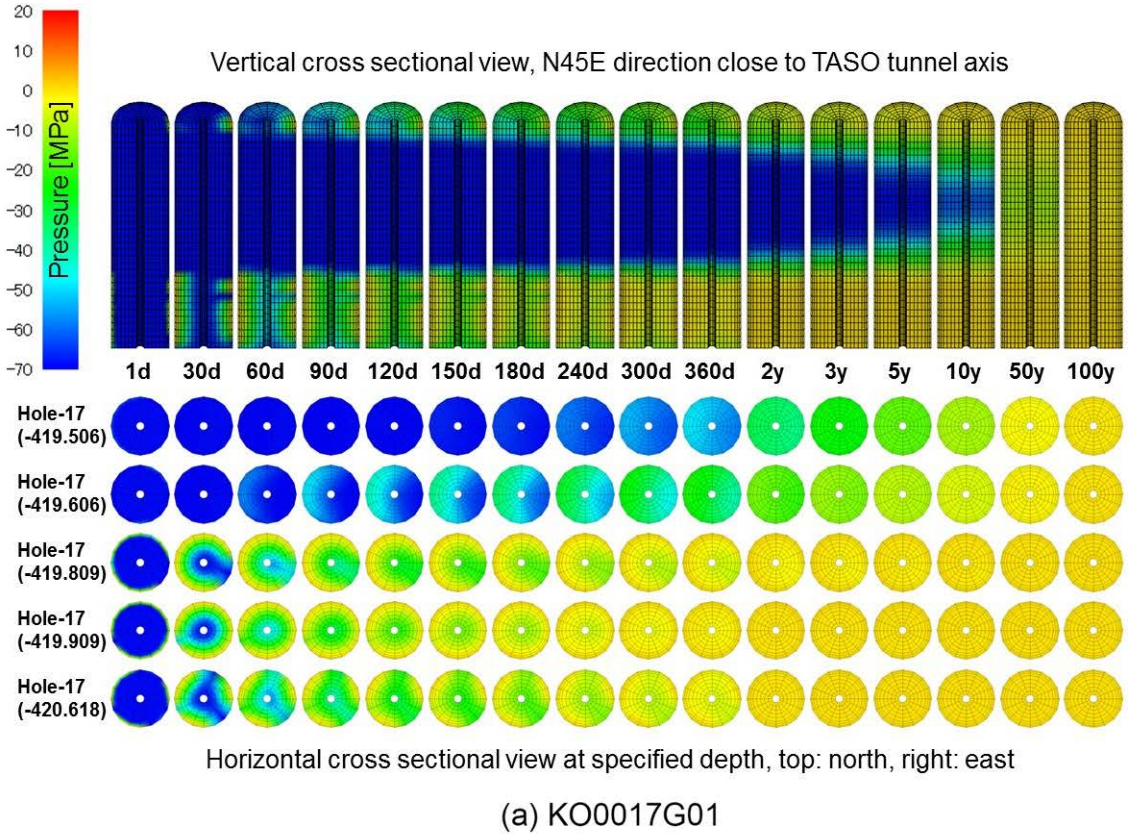

(a) KO0017G01

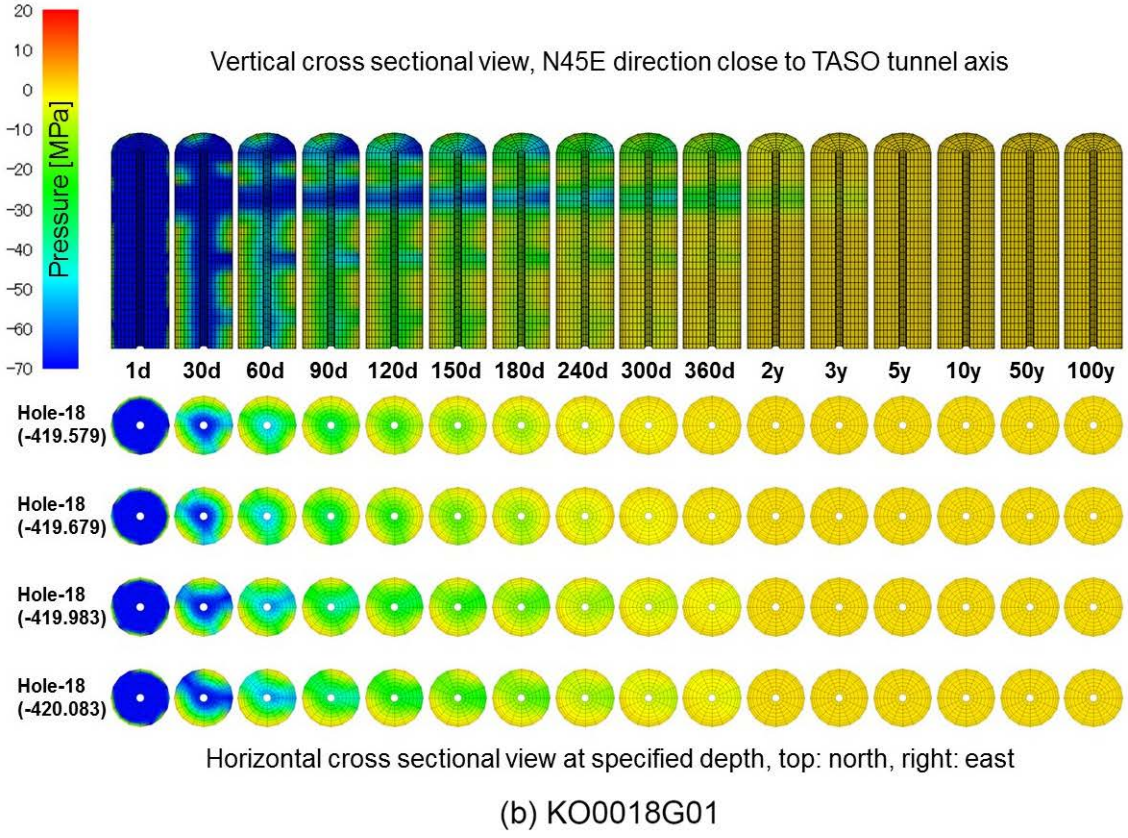

(b) KO0018G01

Figure 4-21. *Pressure distribution in bentonite column at KO0017G01 and KO0018G01, base case model, realisation #05.*

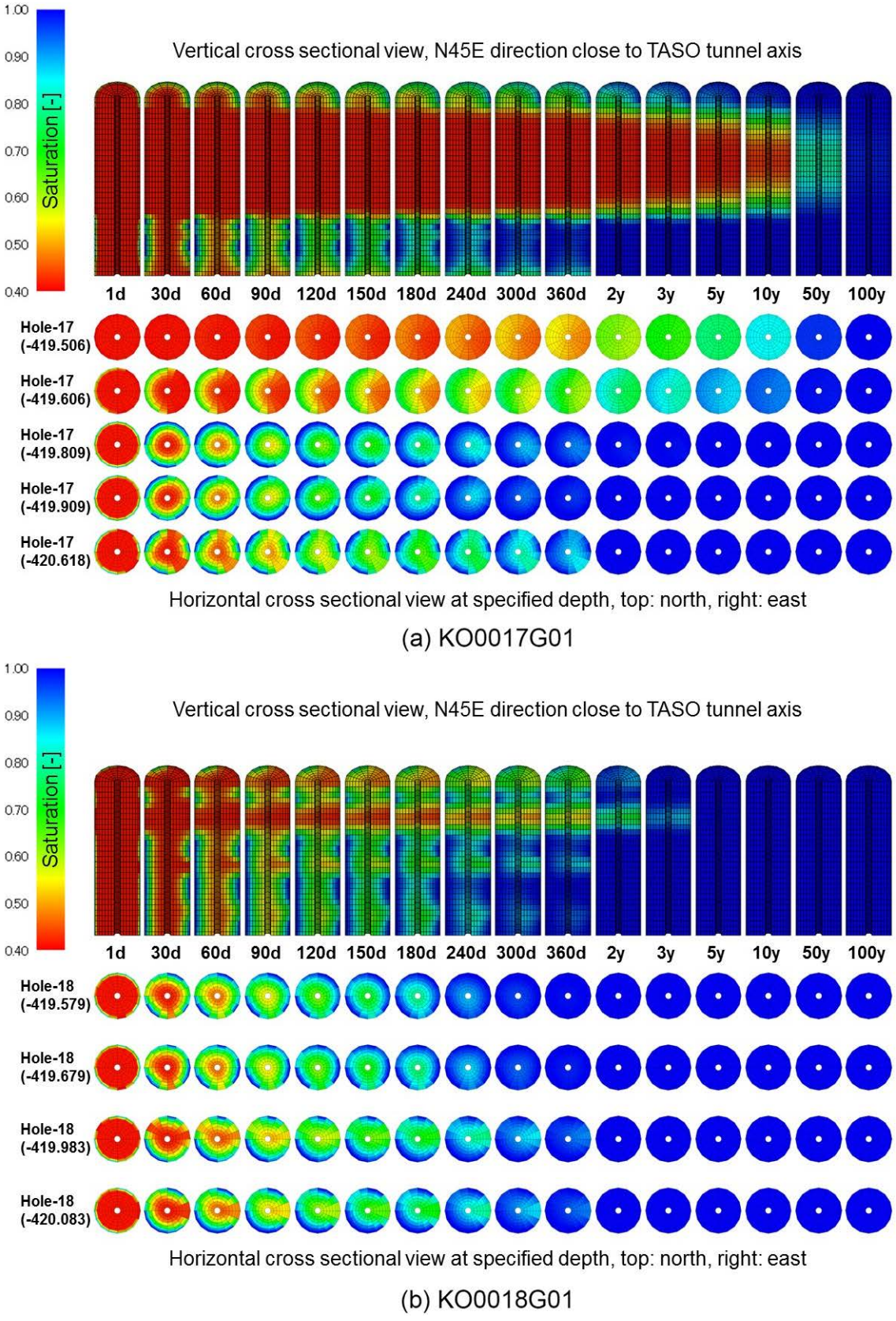

Figure 4-22. *Saturation distribution in bentonite column at KO0017G01 and KO0018G01, base case model, realisation #05.*

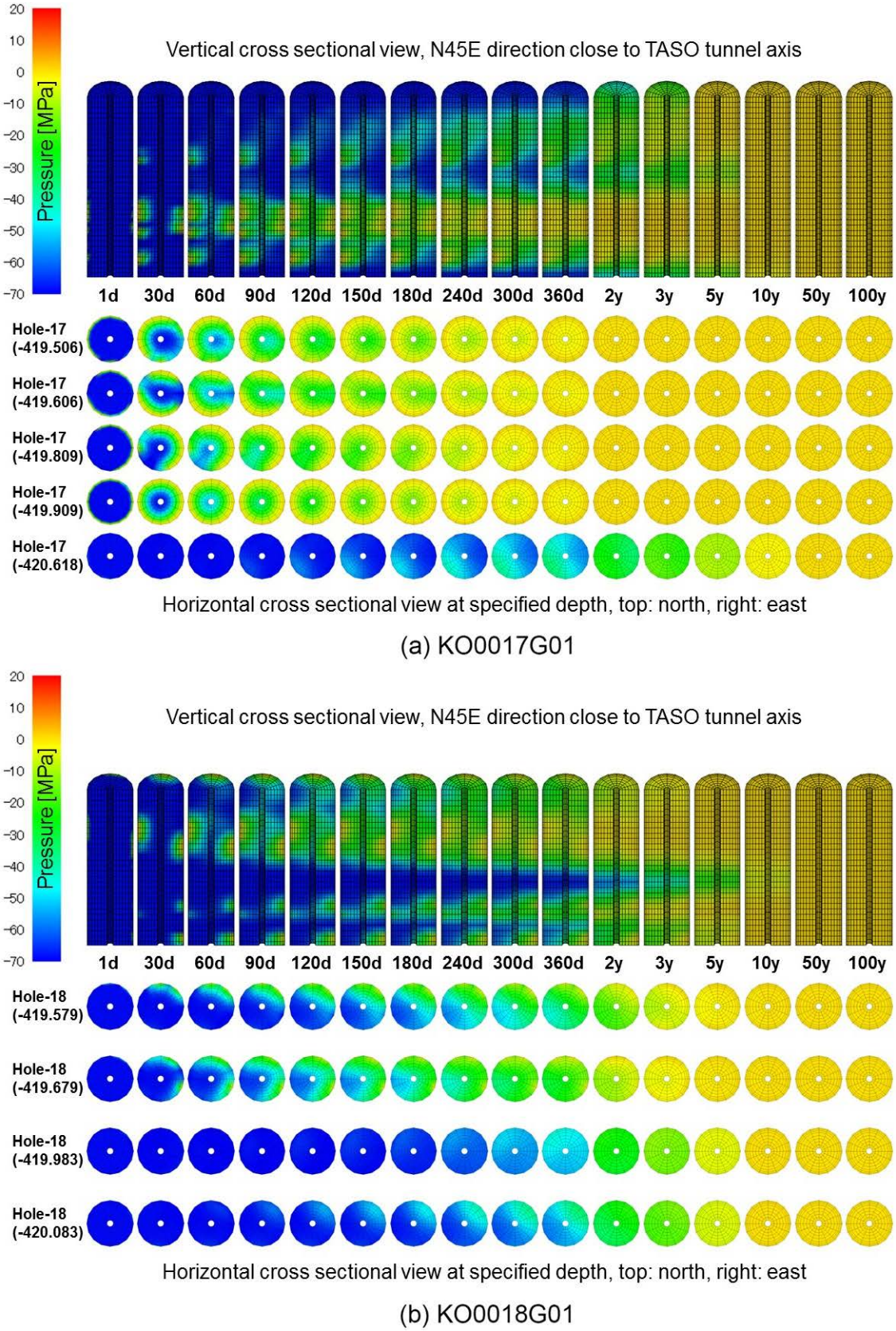

Figure 4-23. *Pressure distribution in bentonite column at KO0017G01 and KO0018G01, 1/50 transmissivity case model, realisation #01.*

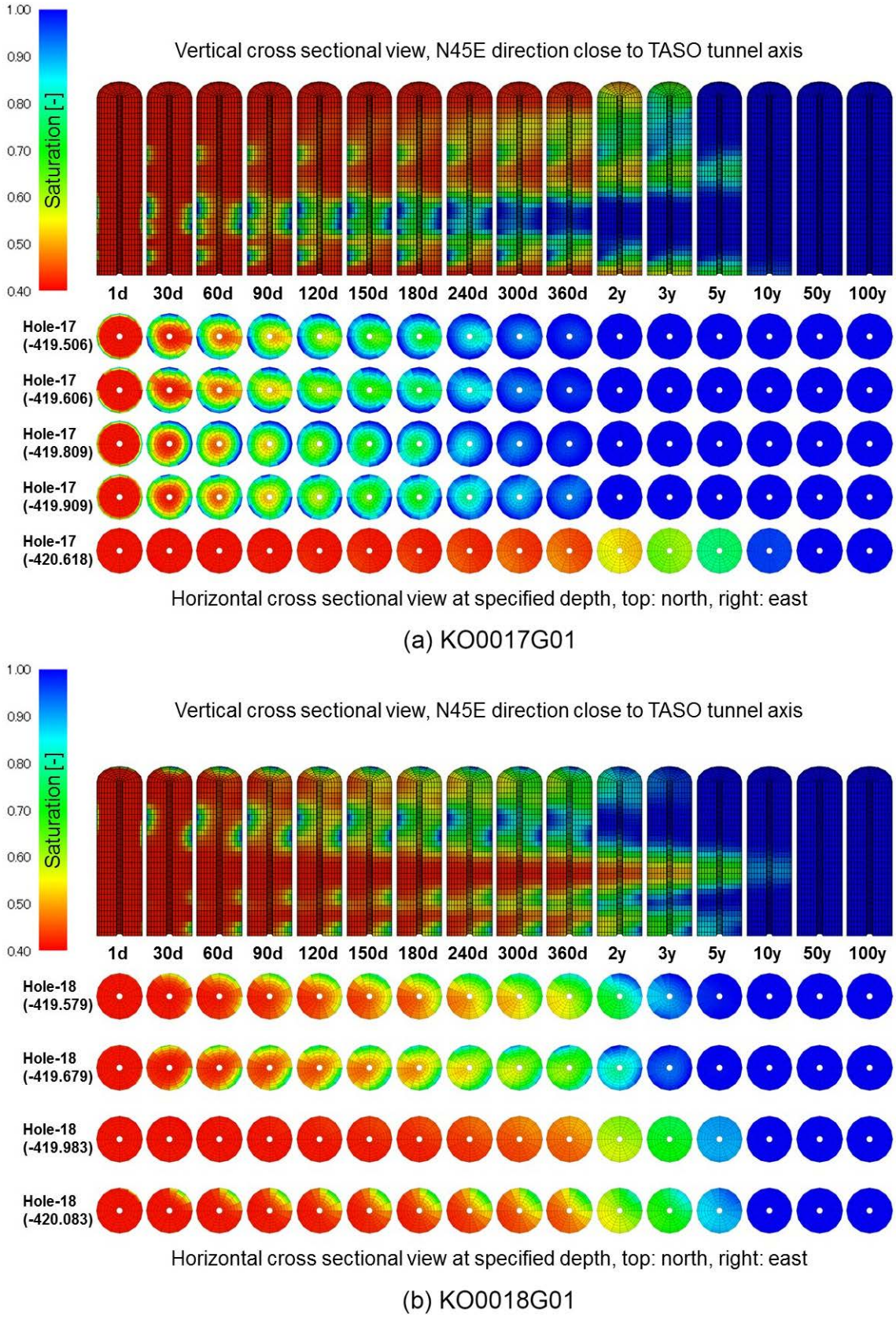

Figure 4-24. *Saturation distribution in bentonite column at KO0017G01 and KO0018G01, 1/50 transmissivity case model, realisation #01.*

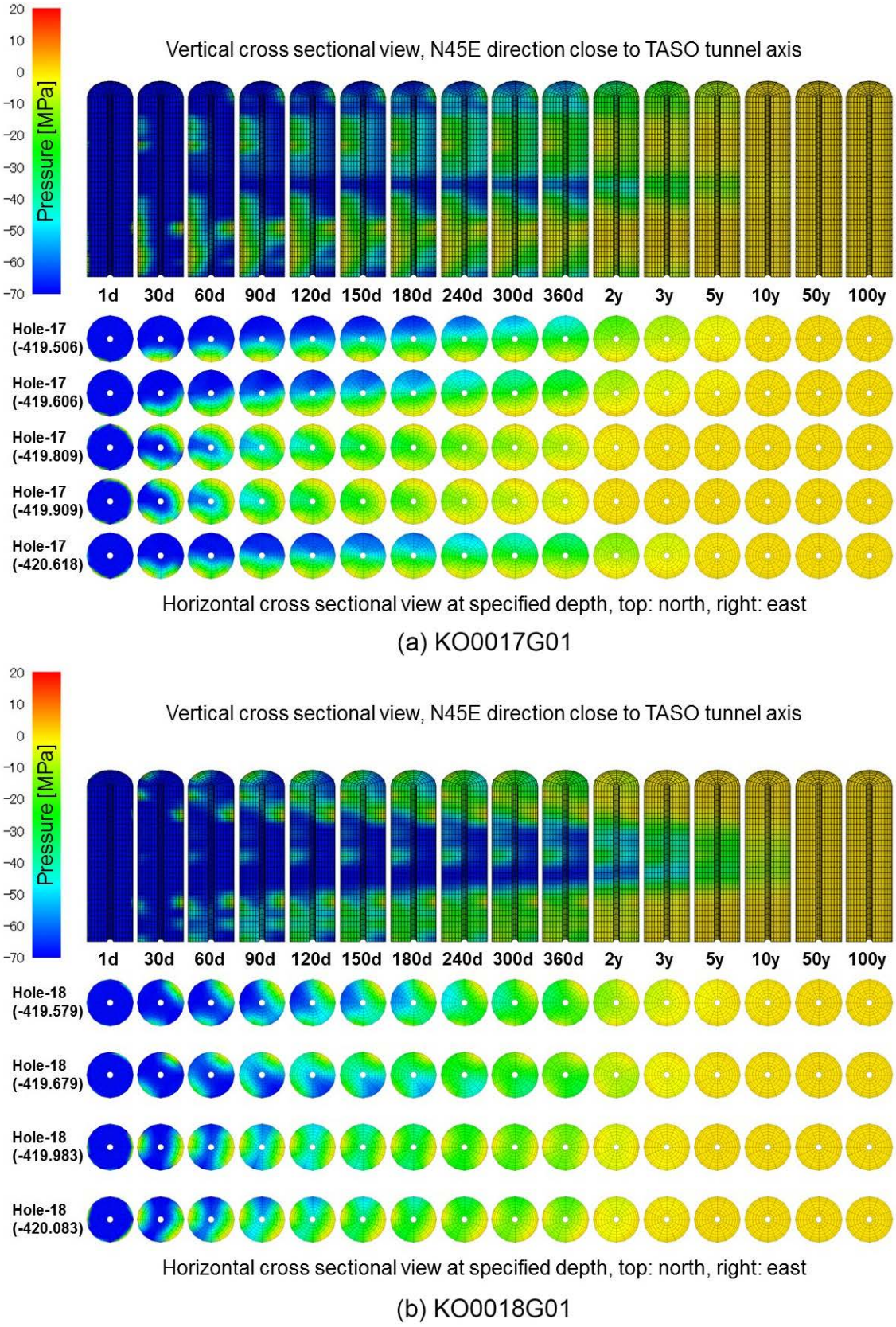

Figure 4-25. *Pressure distribution in bentonite column at KO0017G01 and KO0018G01, 1/50 transmissivity case model, realisation #02.*

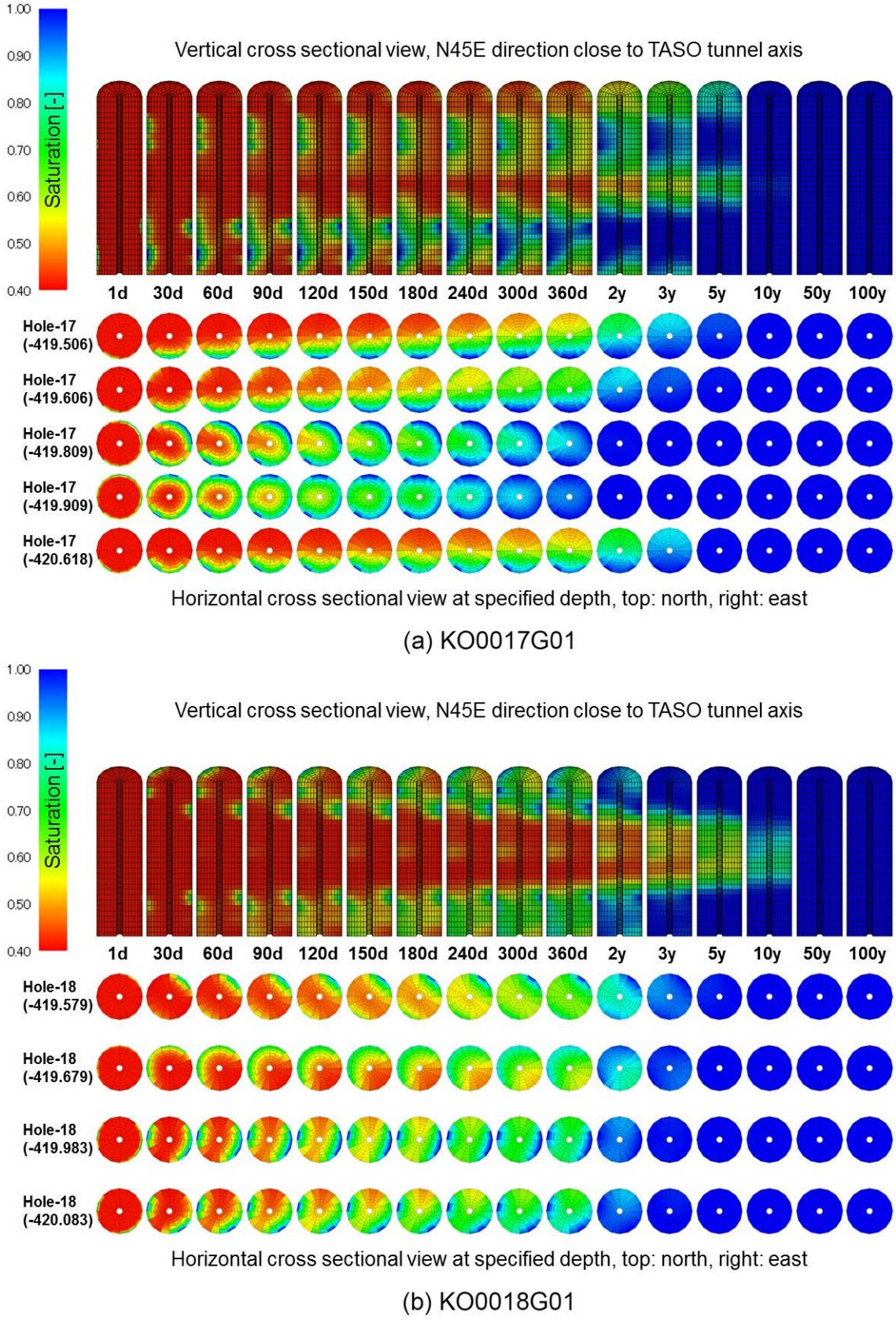

Figure 4-26. *Saturation distribution in bentonite column at KO0017G01 and KO0018G01, 1/50 transmissivity case model, realisation #02.*

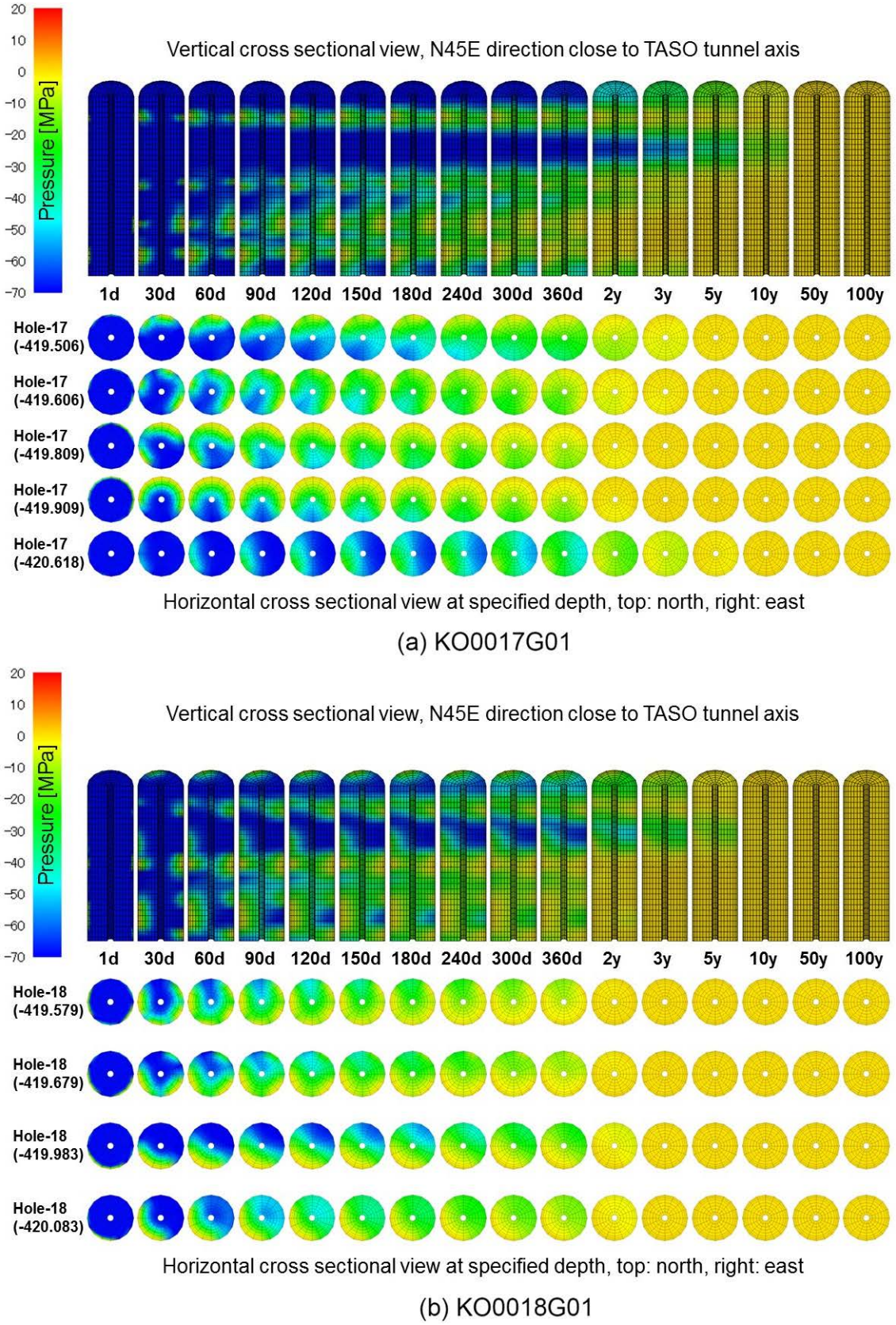

Figure 4-27. *Pressure distribution in bentonite column at KO0017G01 and KO0018G01, 1/50 transmissivity case model, realisation #03.*

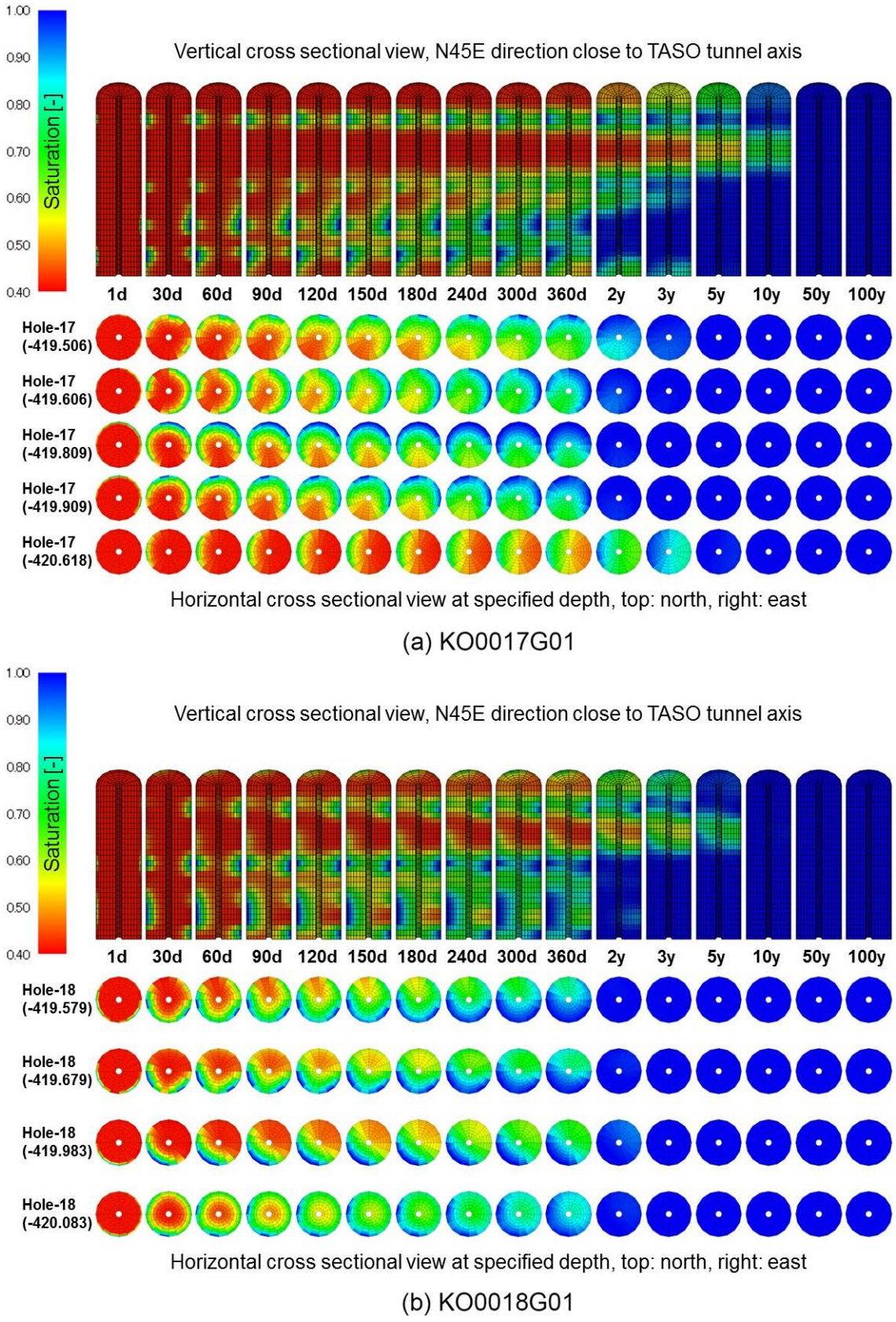

Figure 4-28. *Saturation distribution in bentonite column at KO0017G01 and KO0018G01, 1/50 transmissivity case model, realisation #03.*

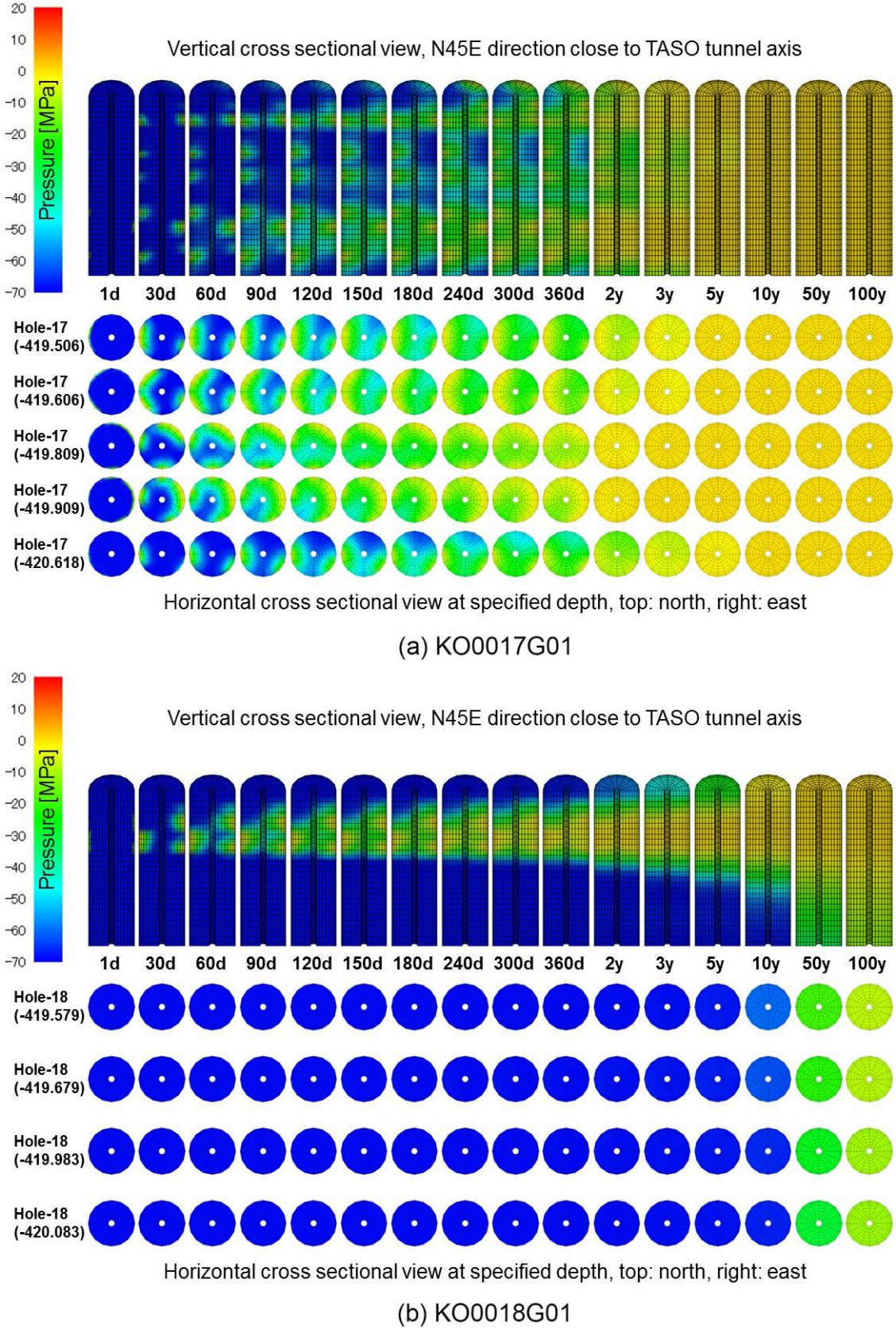

Figure 4-29. *Pressure distribution in bentonite column at KO0017G01 and KO0018G01, 1/50 transmissivity case model, realisation #04.*

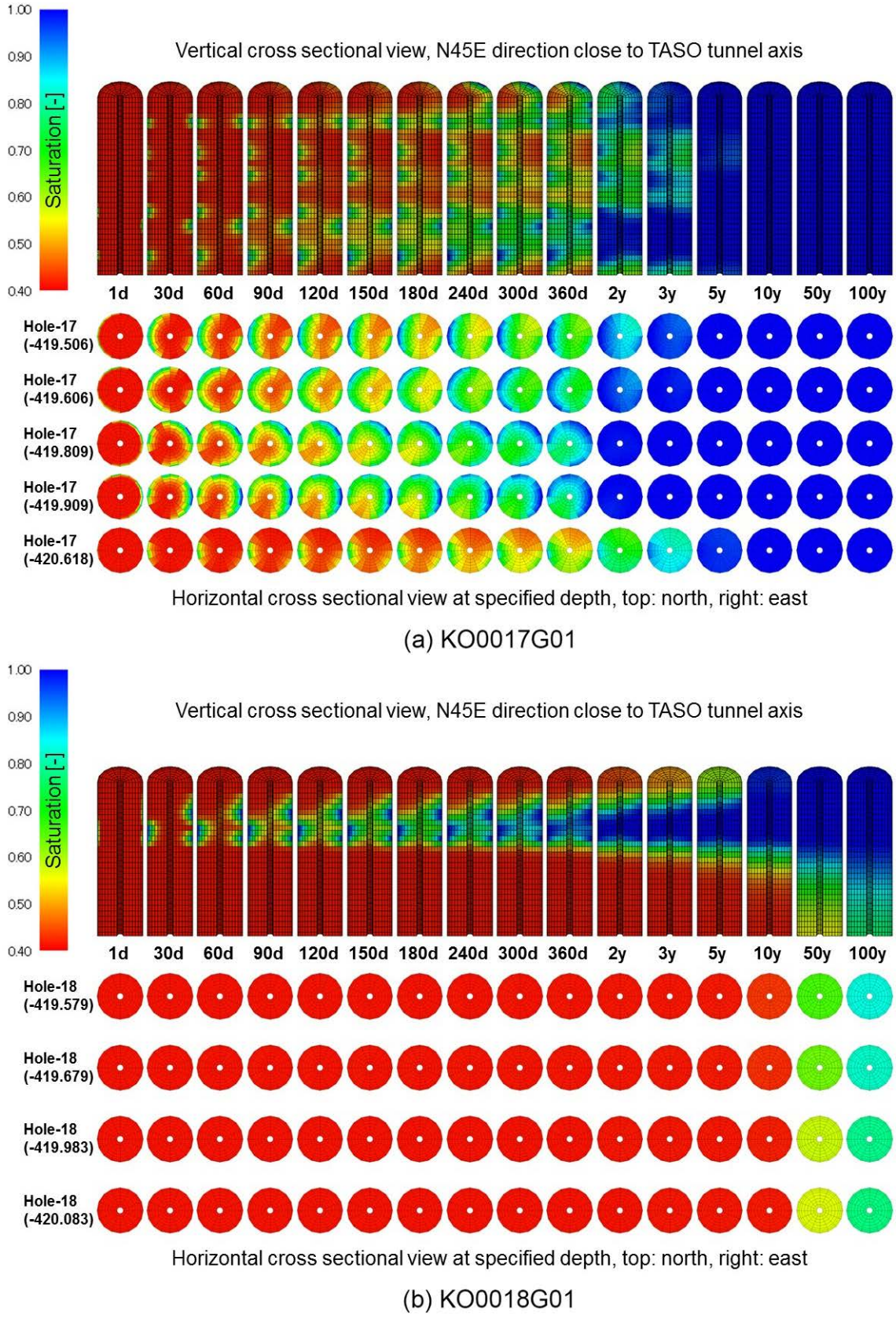

Figure 4-30. *Saturation distribution in bentonite column at KO0017G01 and KO0018G01, 1/50 transmissivity case model, realisation #04.*

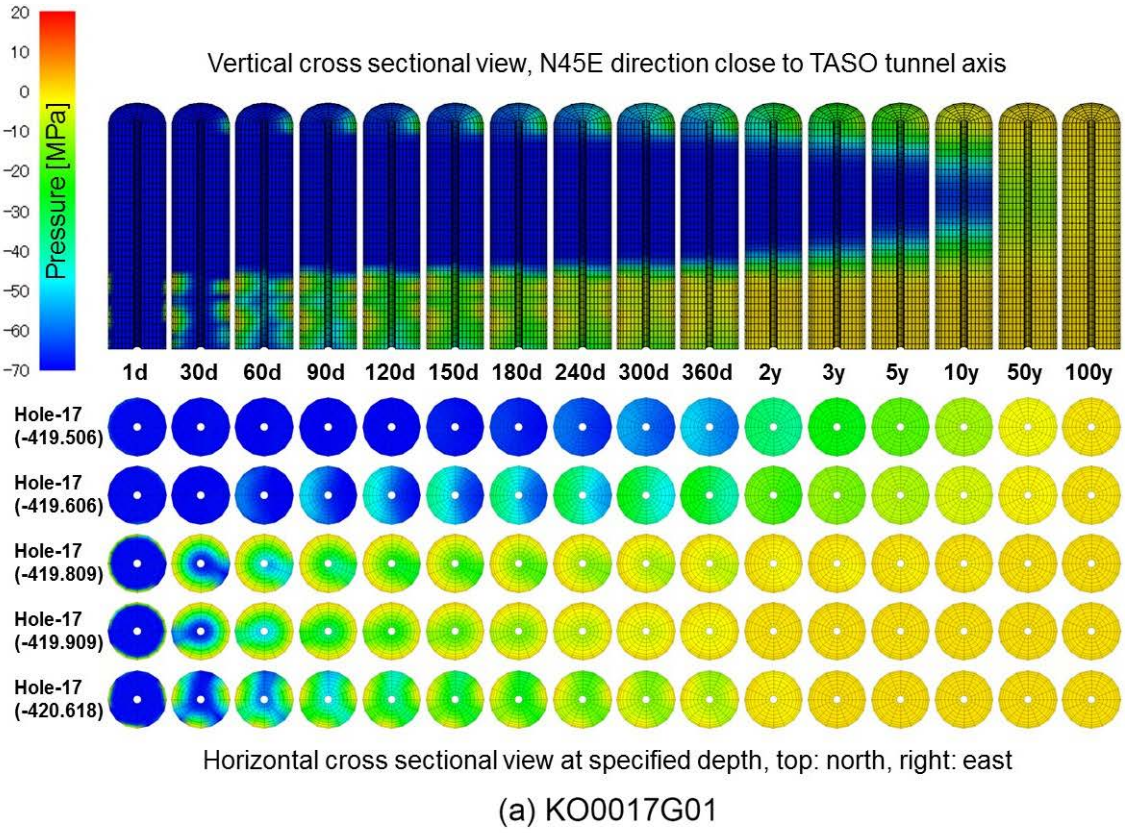

(a) KO0017G01

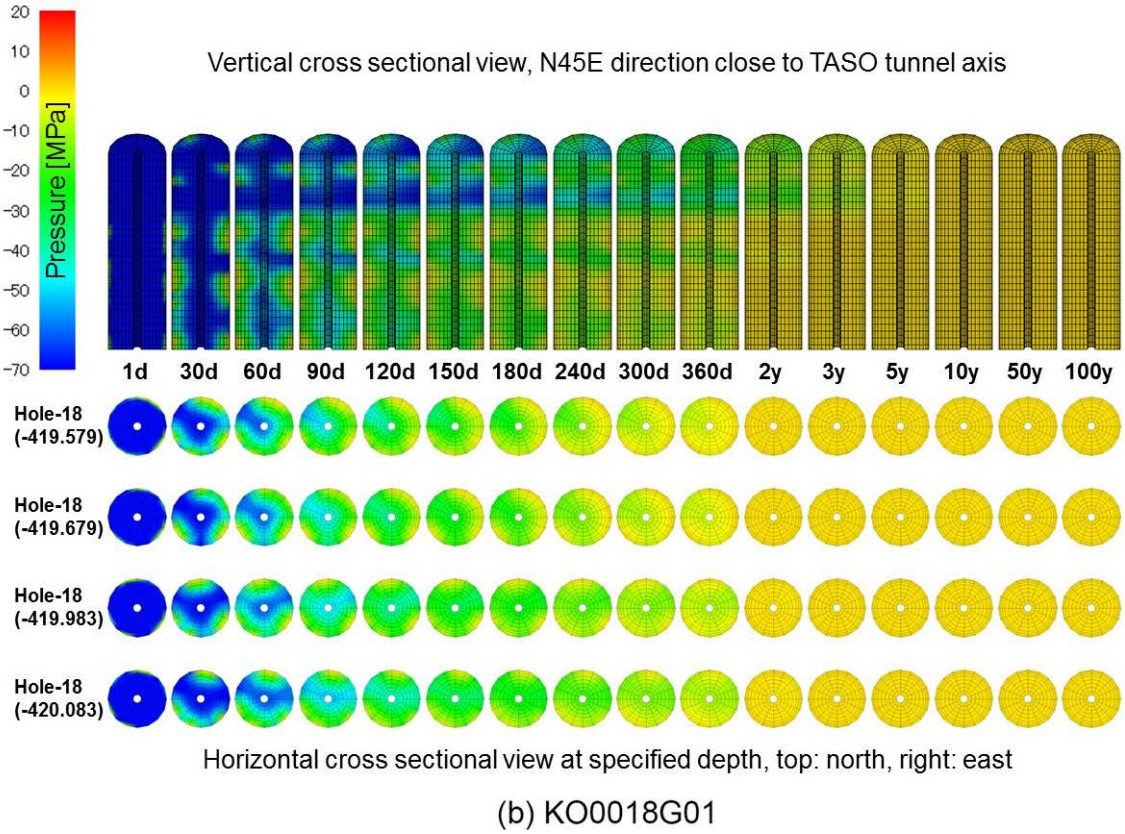

(b) KO0018G01

Figure 4-31. *Pressure distribution in bentonite column at KO0017G01 and KO0018G01, 1/50 transmissivity case model, realisation #05.*

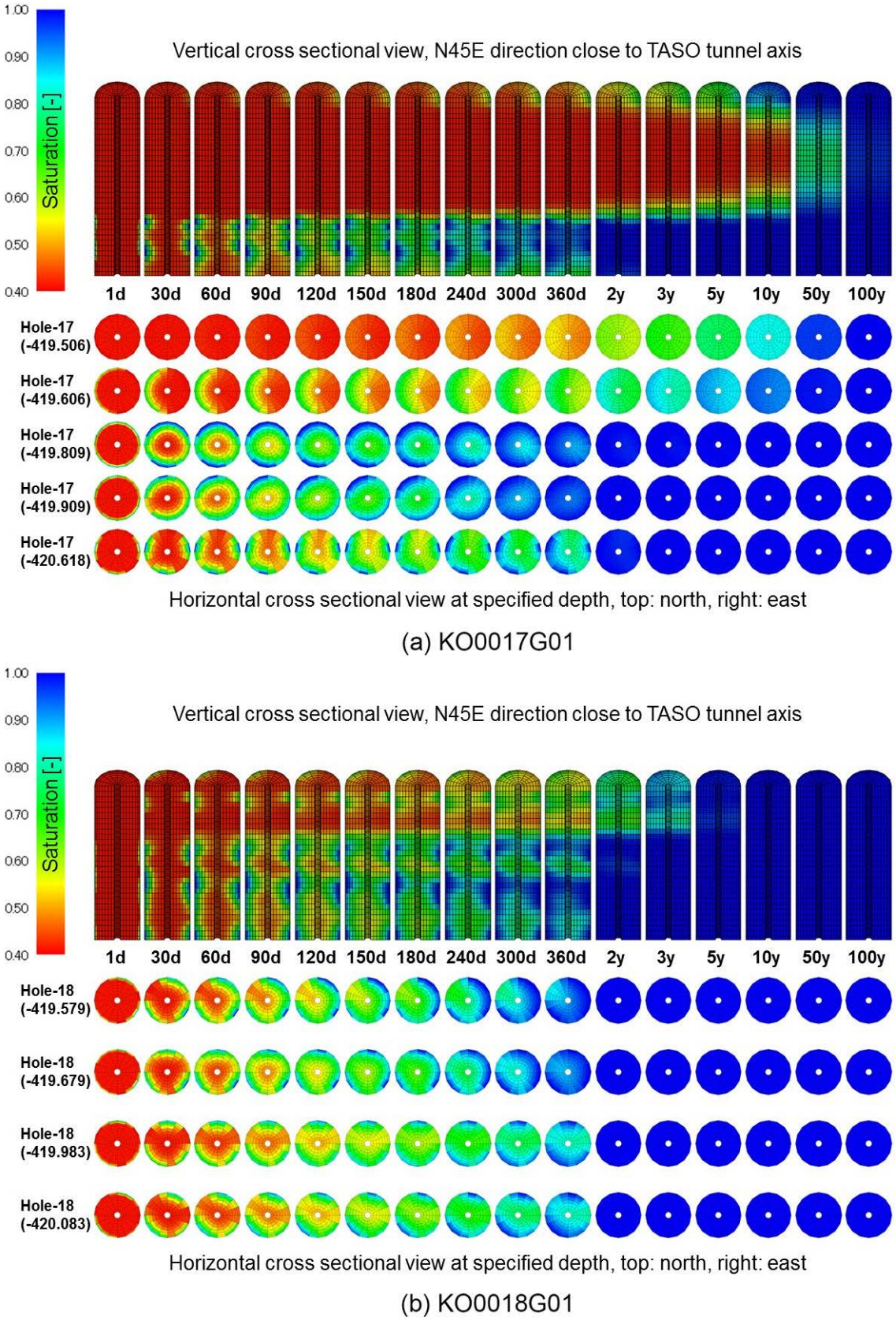

Figure 4-32. *Saturation distribution in bentonite column at KO0017G01 and KO0018G01, 1/50 transmissivity case model, realisation #05.*

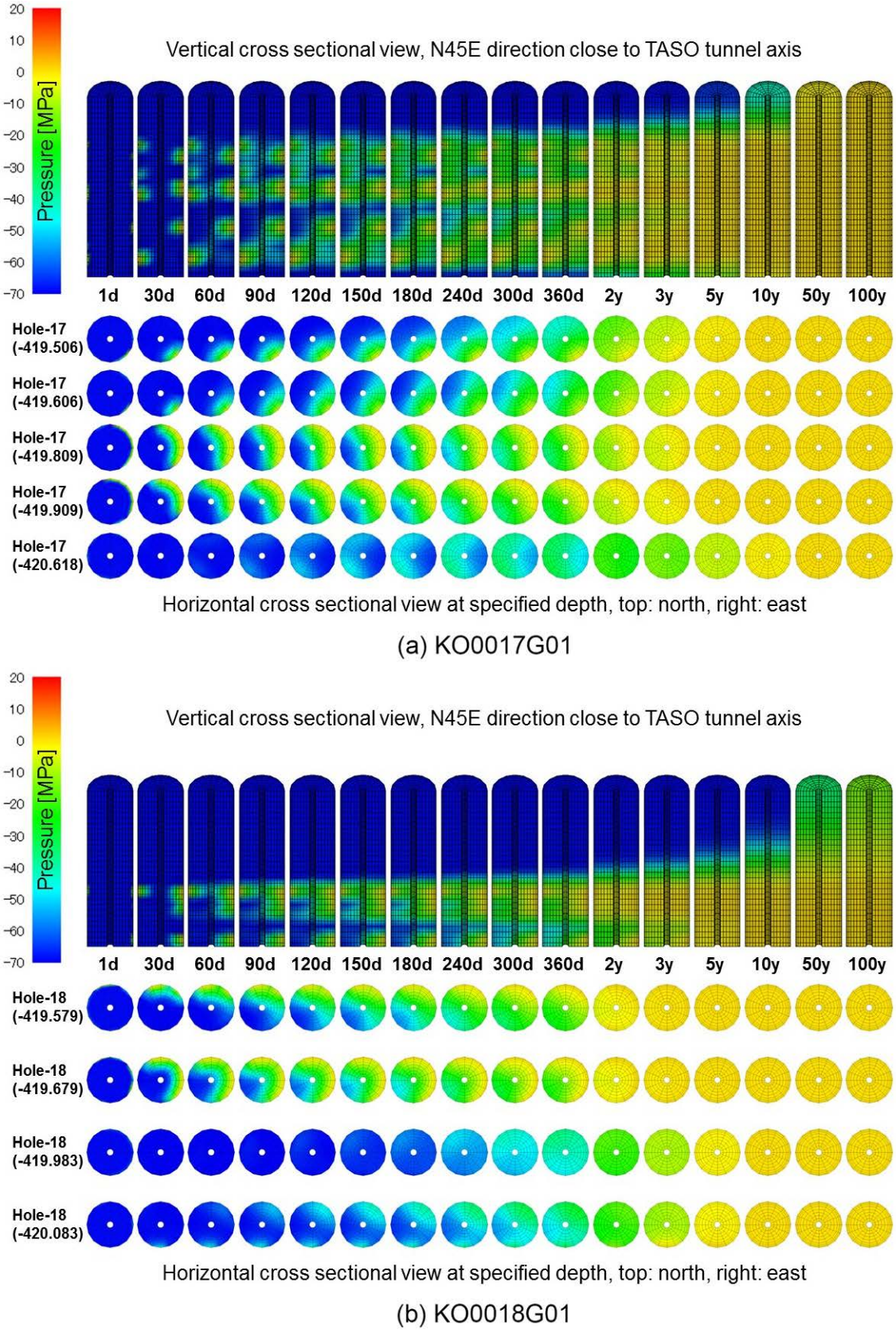

Figure 4-33. *Pressure distribution in bentonite column at KO0017G01 and KO0018G01, fracture conditioning case model, realisation #01.*

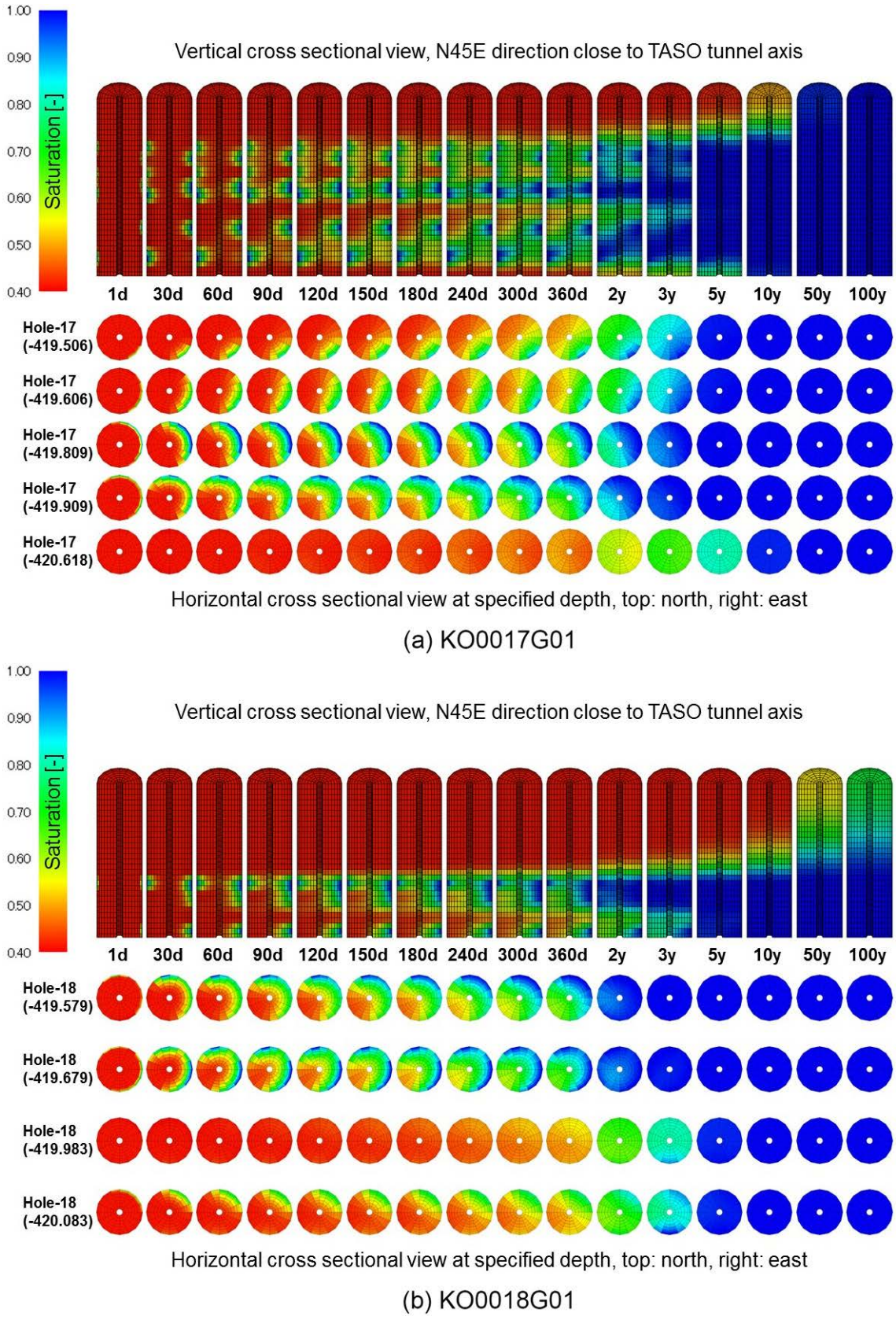

Figure 4-34. *Saturation distribution in bentonite column at KO0017G01 and KO0018G01, fracture conditioning case model, realisation #01.*

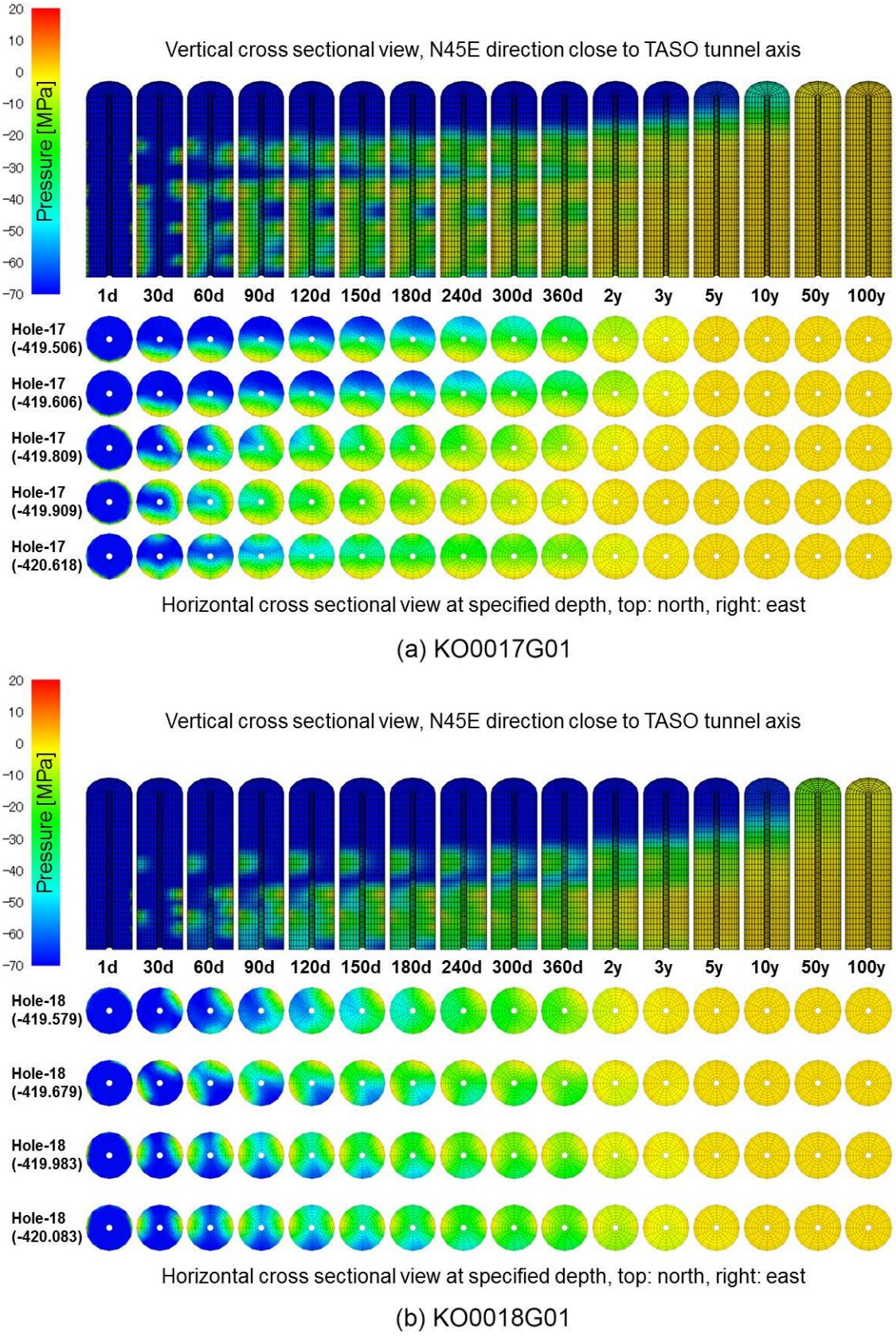

Figure 4-35. *Pressure distribution in bentonite column at KO0017G01 and KO0018G01, fracture conditioning case model, realisation #02.*

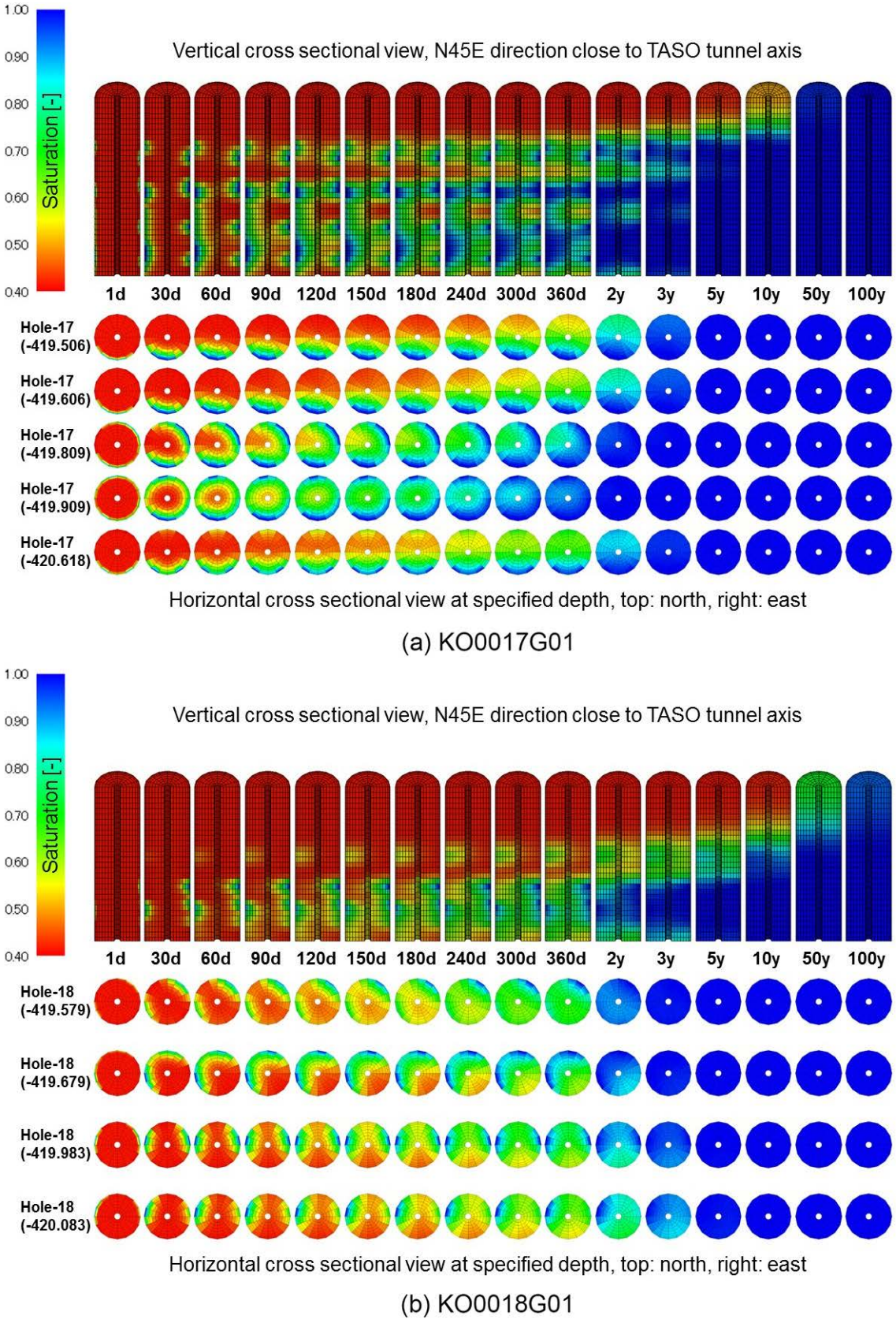

Figure 4-36. *Saturation distribution in bentonite column at KO0017G01 and KO0018G01, fracture conditioning case model, realisation #02.*

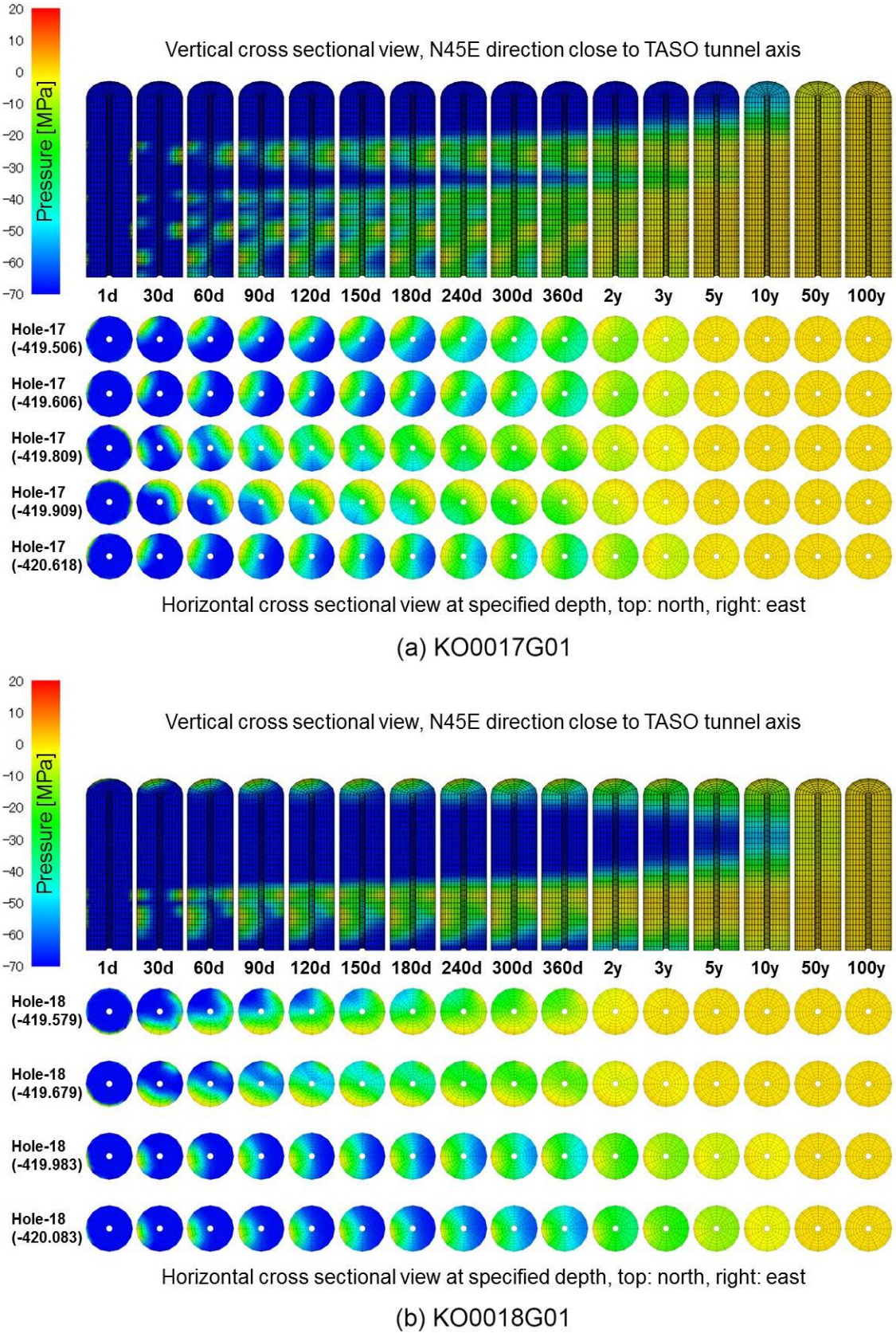

Figure 4-37. *Pressure distribution in bentonite column at KO0017G01 and KO0018G01, fracture conditioning case model, realisation #03.*

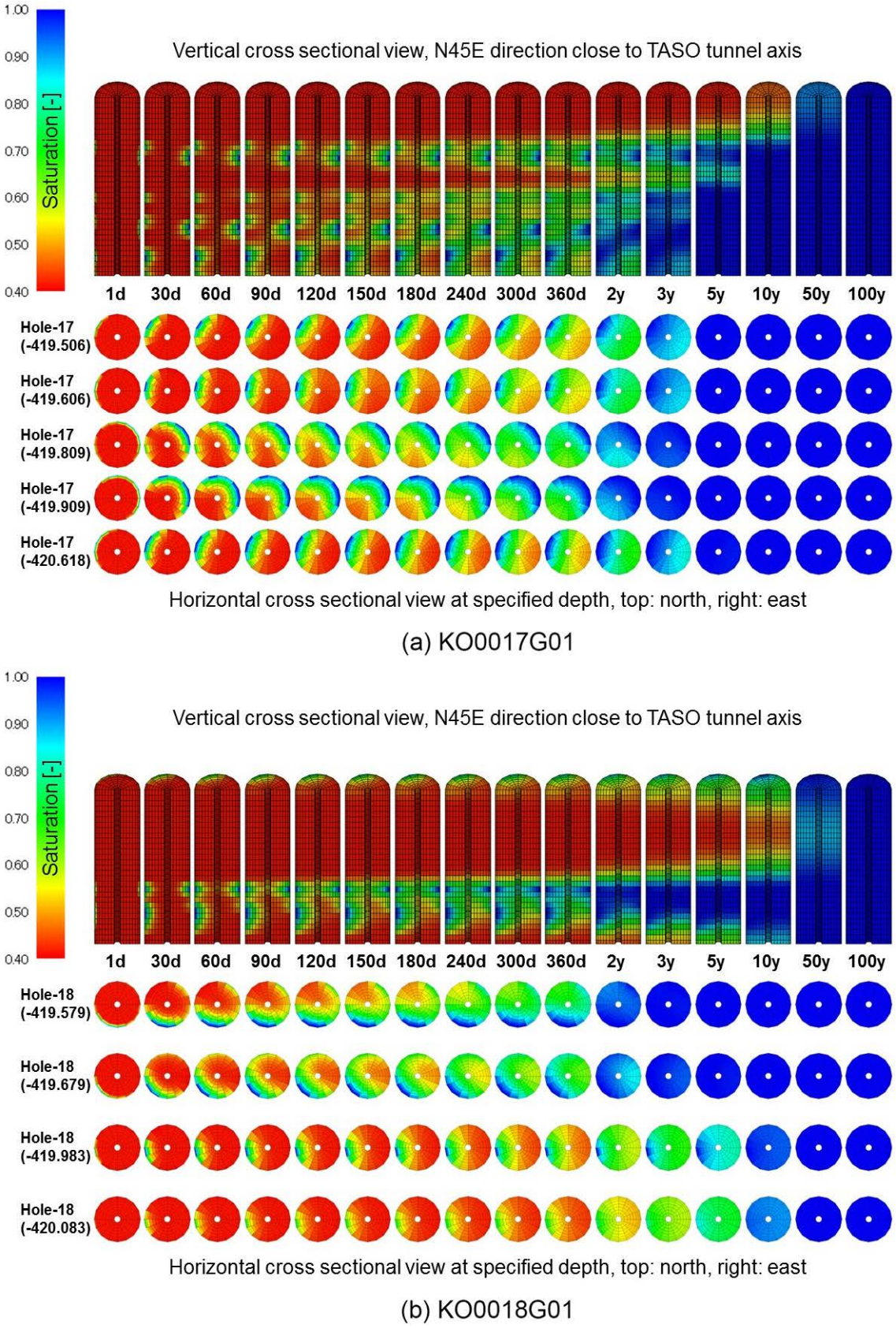

Figure 4-38. *Saturation distribution in bentonite column at KO0017G01 and KO0018G01, fracture conditioning case model, realisation #03.*

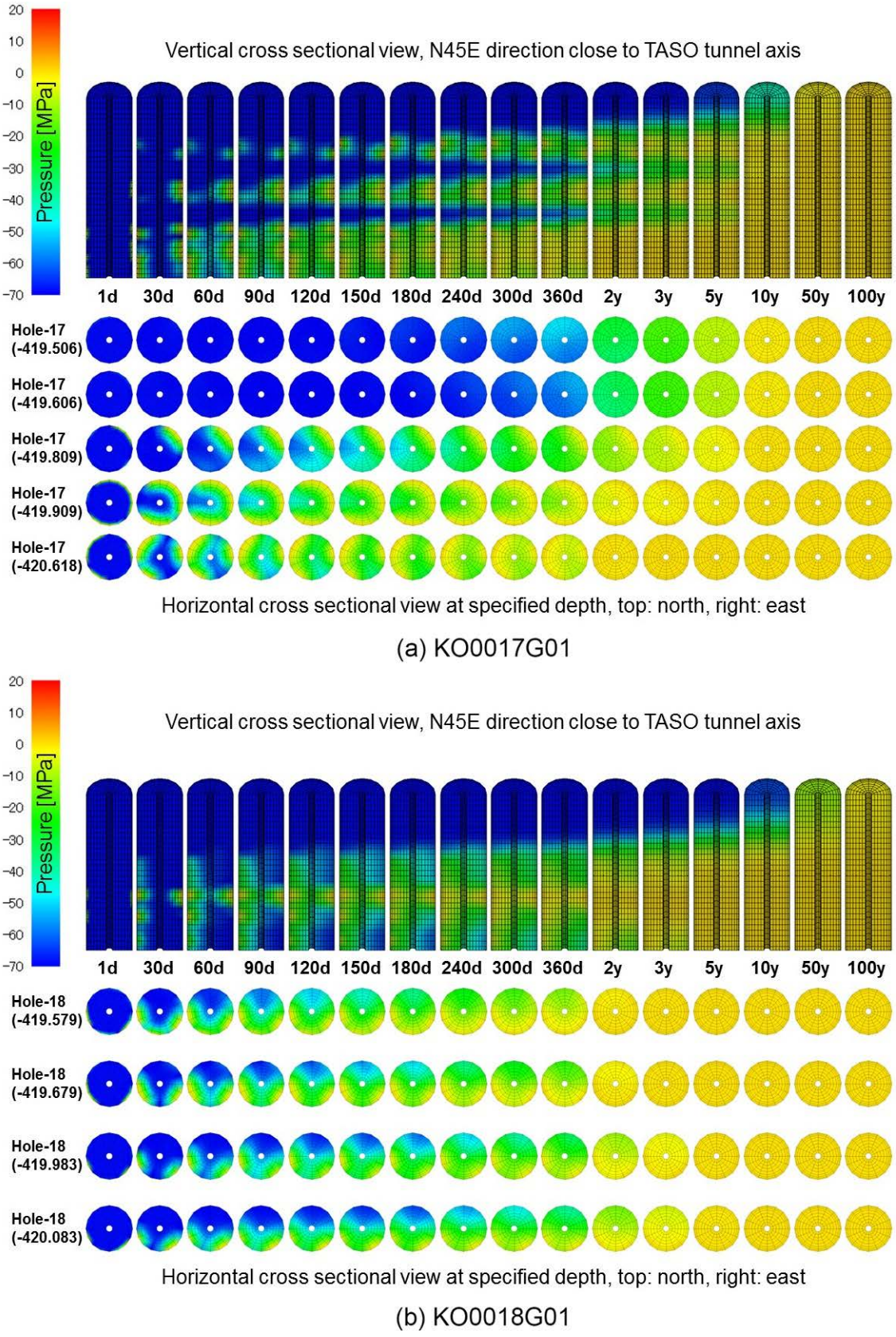

Figure 4-39. *Pressure distribution in bentonite column at KO0017G01 and KO0018G01, fracture conditioning case model, realisation #05.*

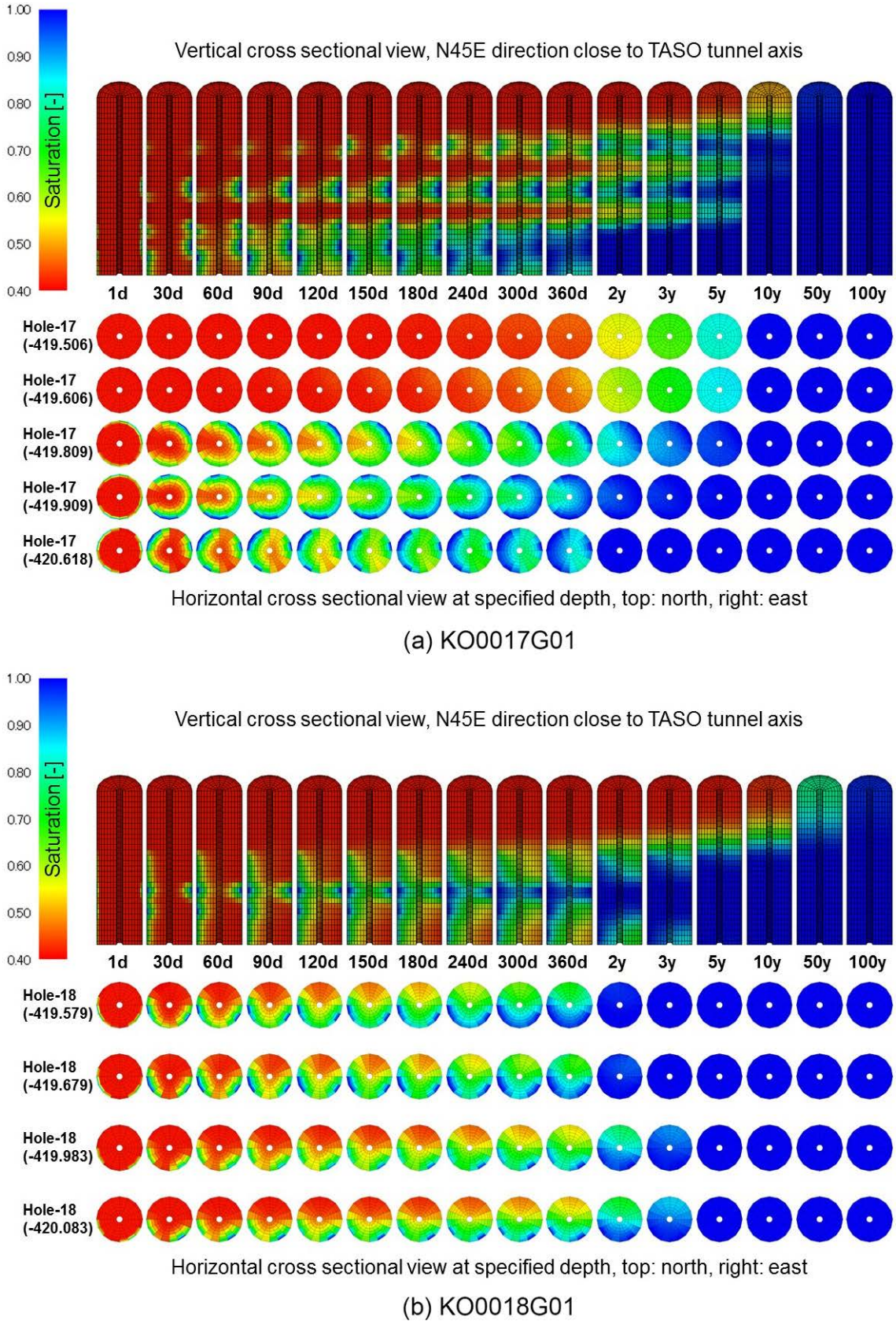

Figure 4-40. *Saturation distribution in bentonite column at KO0017G01 and KO0018G01, fracture conditioning case model, realisation #05.*

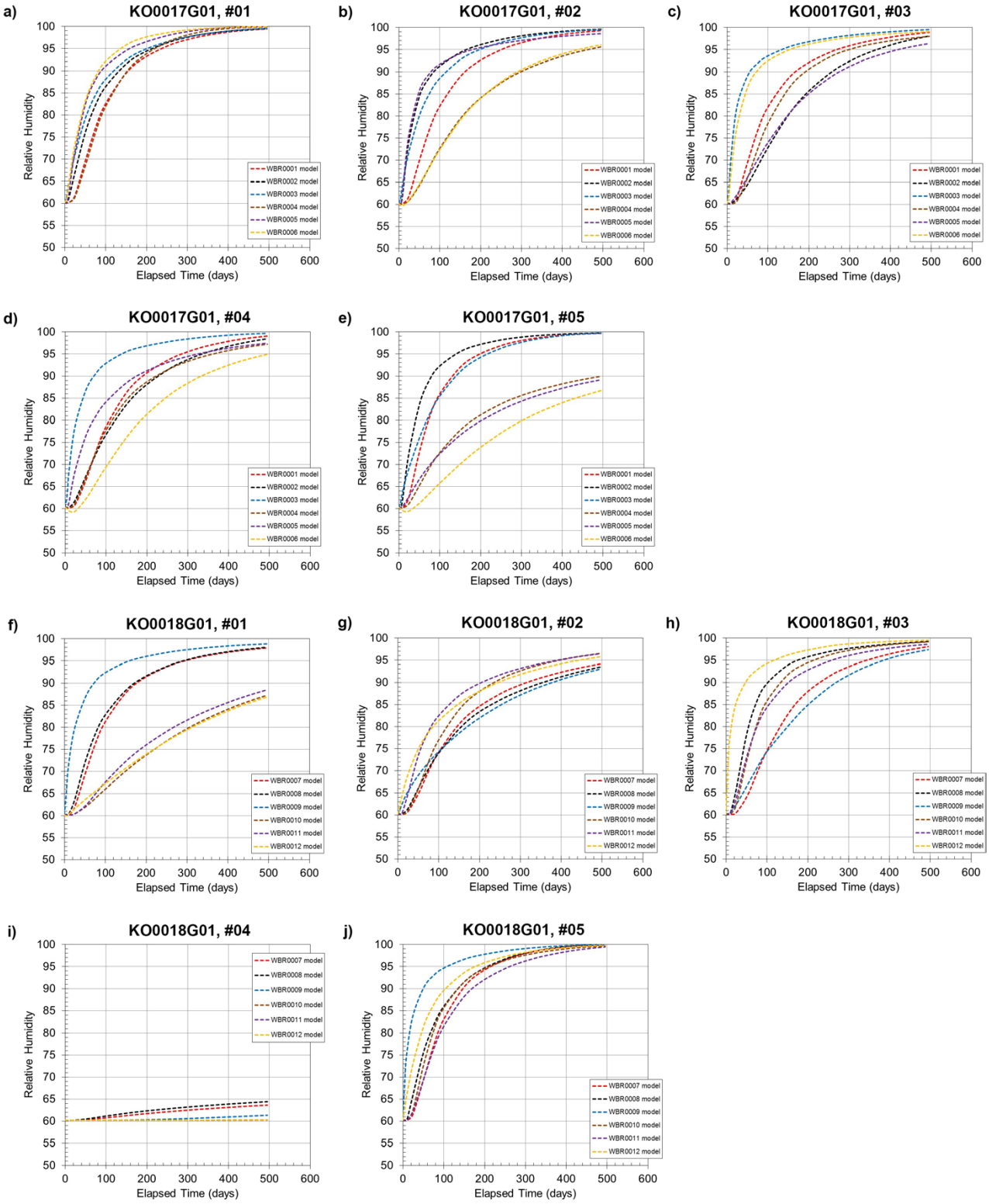

Figure 4-41. *Relative humidity at specified points, Base case model.*

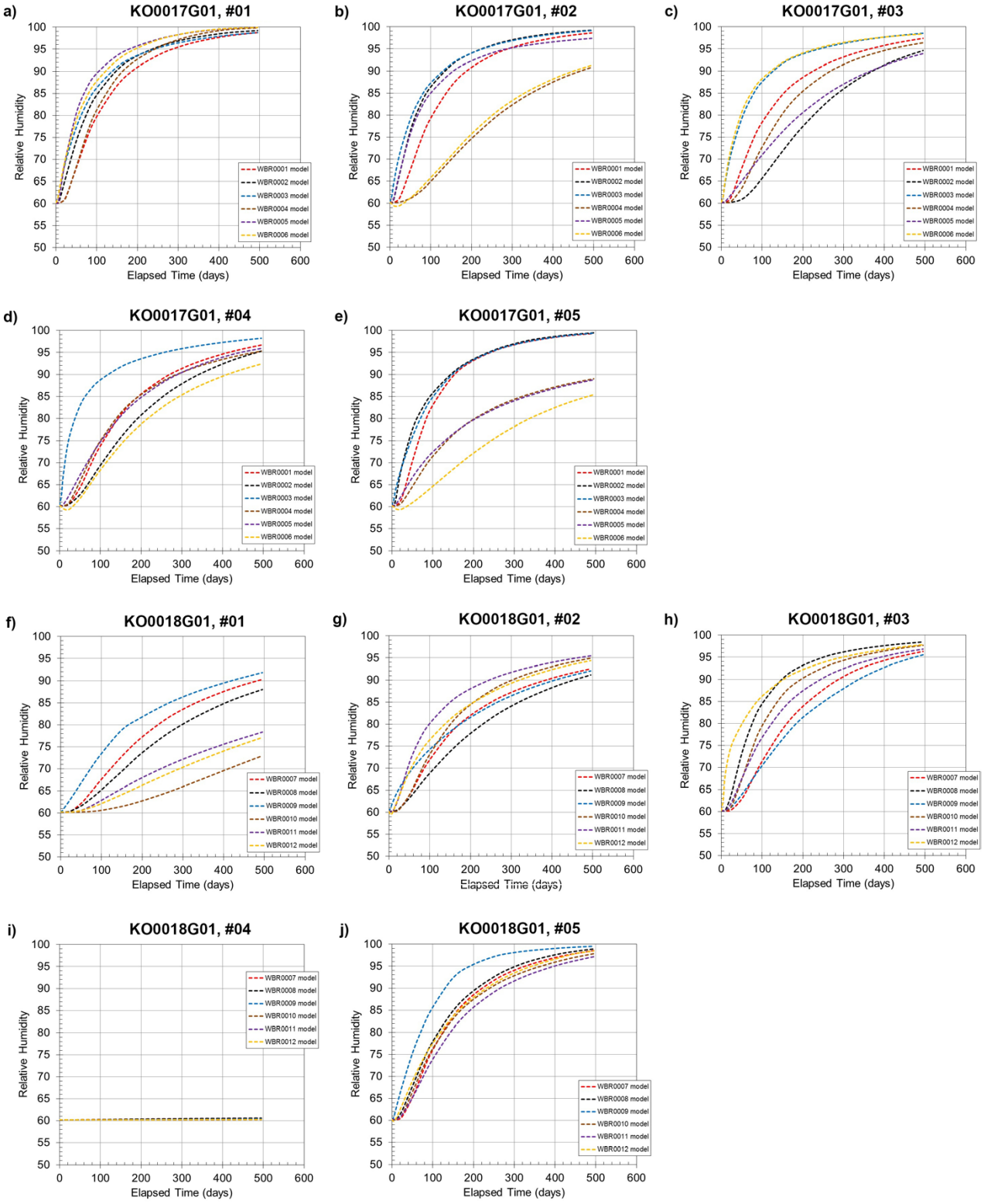

Figure 4-42. *Relative humidity at specified points, 1/50 transmissivity case model.*

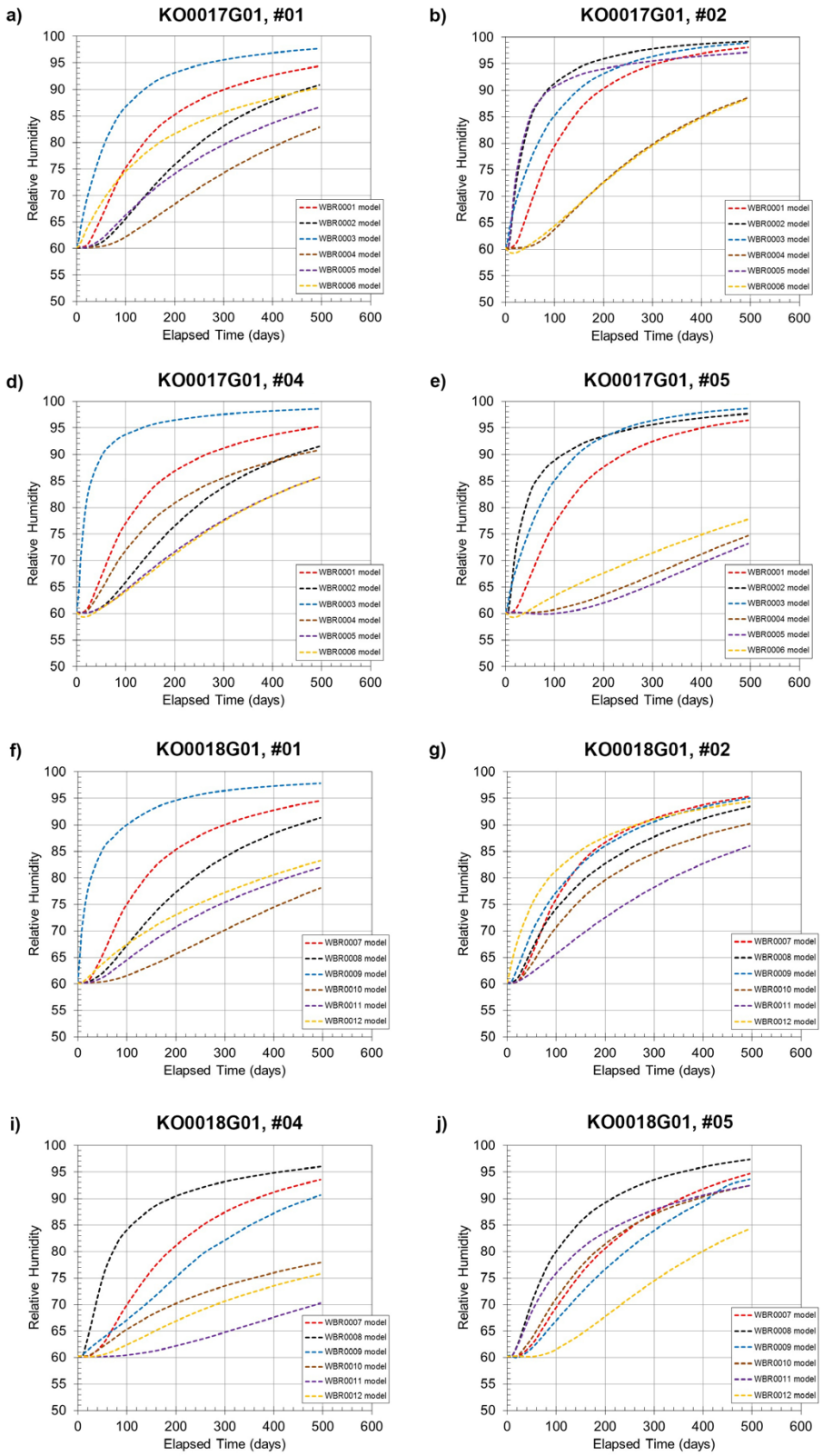

Figure 4-43. *Relative humidity at specified points, Fracture conditioning case model.*

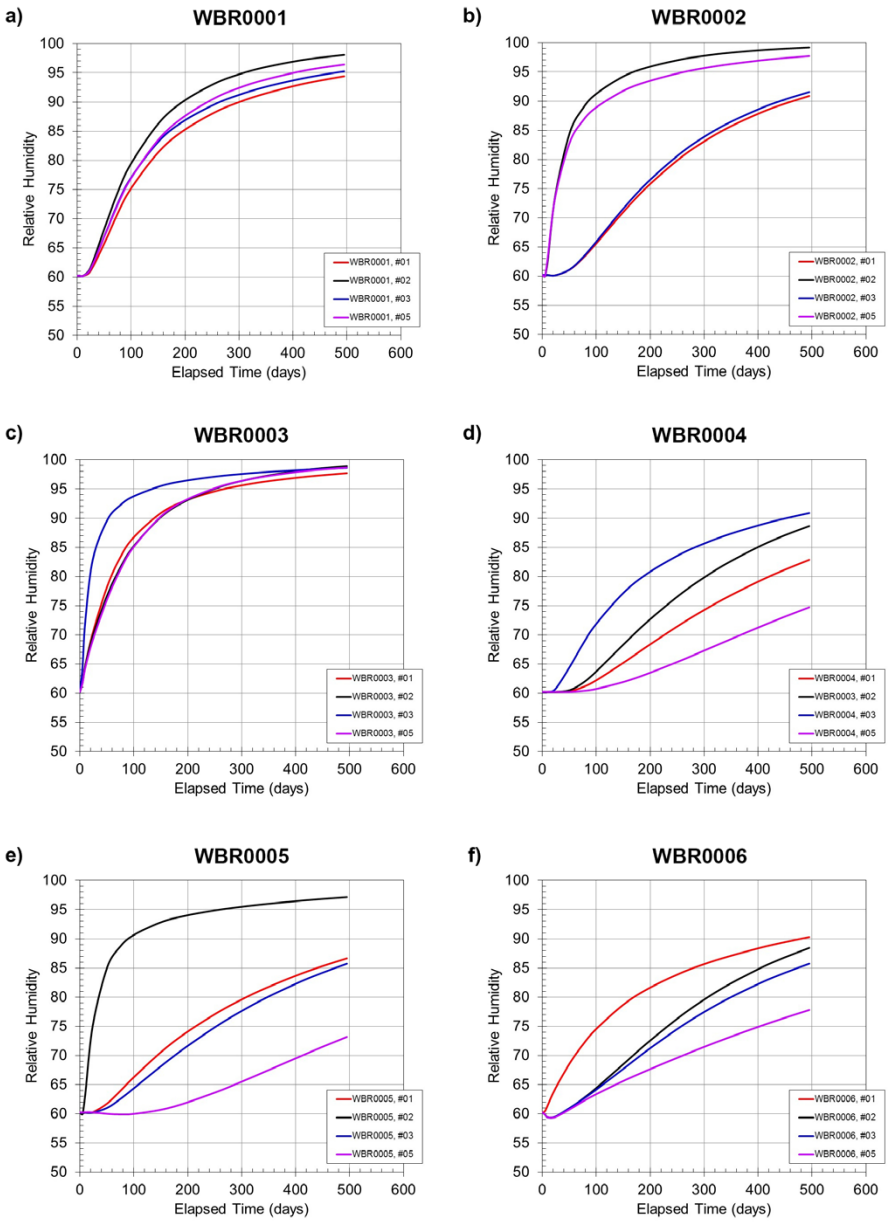

Figure 4-44. *Pore pressure and relative humidity at specified points, Fracture conditioning case model.*

4.5 Discussion

Alternative models

The alternative boundary conditions of DFN model for Task 8D1 were applied for examining the sensitivity of the alternative conditions to the flow rate and head values measured at the boreholes. The homogeneous head (−50 m) at the outer boundaries of the 40 m × 40 m × 40 m model region and the low permeable skin modelled by decreasing transmissivity by one order of magnitude within 1 m width from the outer surface of the model are considered. Three cases, a) low permeable skin, b) homogeneous constant head (−50 m) without low permeable skin, and c) homogeneous constant head (−50 m) with low permeable skin were made for the sensitivity calculations. A single realisation (01) of fracture conditioning case for Task 8D1 model was selected as reference case of this sensitivity analysis. The sensitivity of the alternative boundary conditions to the flow rate and head values at the boreholes are shown in Figure 4-45, which indicates a similar trend as Task 8C1 examination (Figure 3-13) and less significant sensitivity than stochastic variation shown in Figure 4-5 and Figure 4-7.

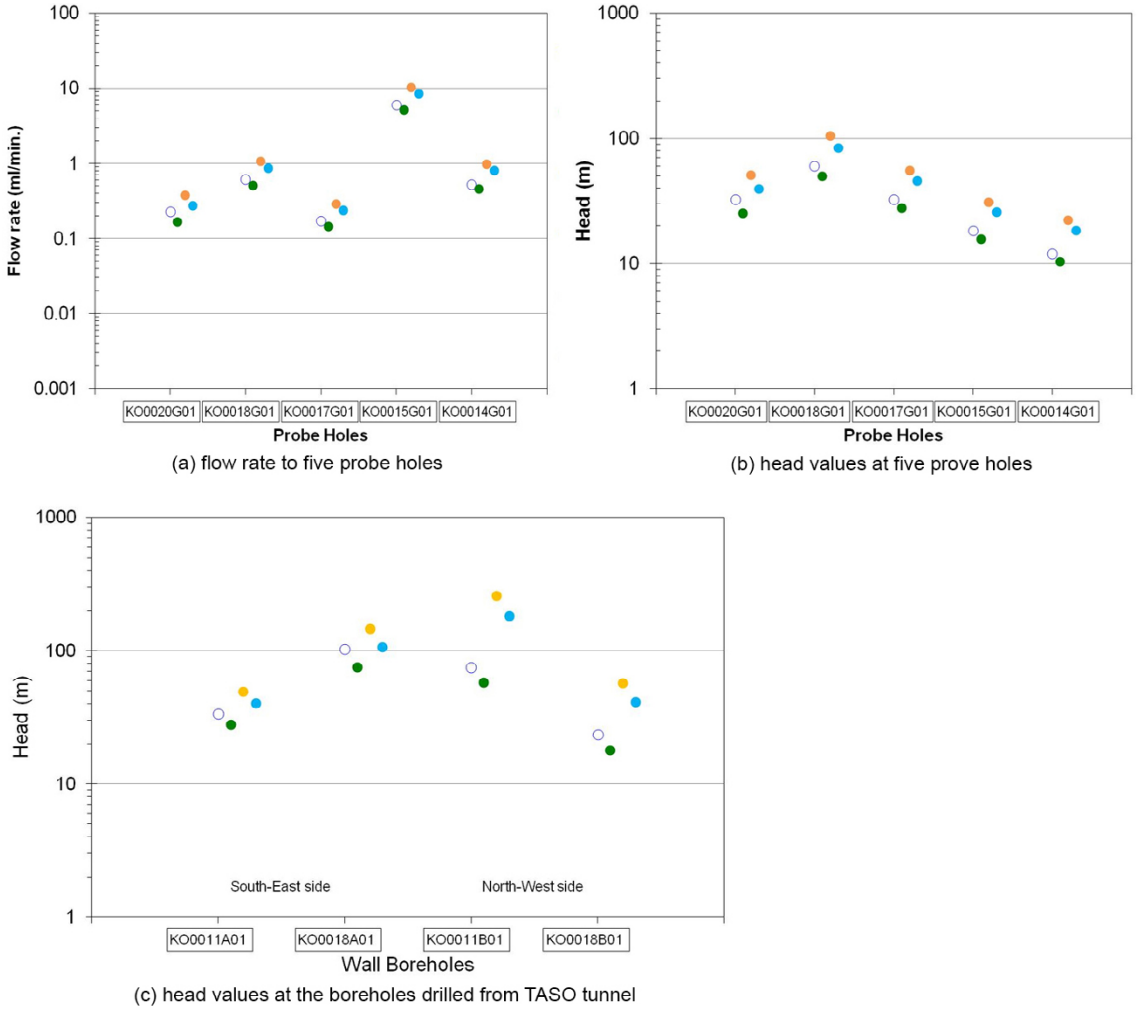

Figure 4-45. *Sensitivity analysis results for alternative boundary condition. Open circle (Blue): fracture conditioning case for Task 8D1 model (heterogeneous head). Solid circle (Green): a) with low permeable skin case. Solid circle (Yellow): b) homogeneous constant head (−50 m). Solid circle (Light blue): c) homogeneous constant head (−50 m) with low permeable skin.*

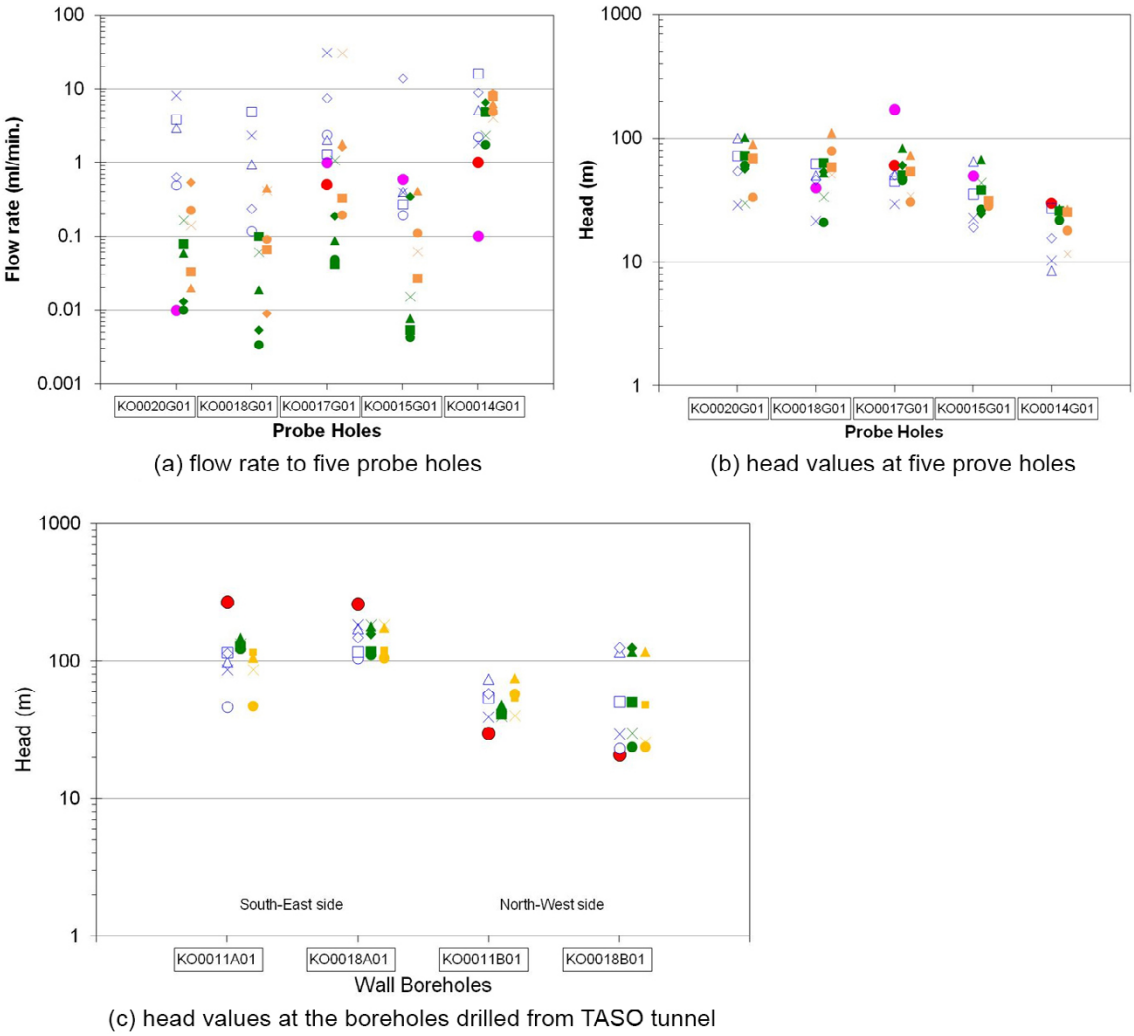

Figure 4-46. *Alternative analysis results without specific capacity condition in Tas8D1 model. Solid circle (Red): measured data provided in Task 8C. Solid circle (Pink): measured data provided in Task 8D. Open symbol (Blue): a) base case simulation results of five realisations. Solid symbol (Green): b) 1/50 transmissivity case simulation results of five realisations. Solid symbol (Yellow): c) fracture conditioning case simulation results of five realisations.*

In order to check the effectiveness of each modification, 1) adding deterministically defined fractures (Figure 4-2), and 2) conditioning specific capacity (Figure 4-3), conducted in Tas8D1 modelling, an additional alternative model case was added. A case of only adding deterministically defined fractures to a) base case, b) 1/50 transmissivity case and c) fracture conditioning case was compared with both Task 8C and Task 8D model results. Figure 4-46 shows the calculated flow rate and head values at the boreholes, which is comparable with Figure 3-18 (Task 8C1 model), and Figure 4-5 and Figure 4-7 (Task 8D1 model). By adding a small fracture at KO0017G01 and KO0018G01 for each, flow rate to these boreholes were significantly changed, and variability among the five stochastic realisations seems to become wider. Then, adding the specific capacity constraining, the variability seems to constrain to be narrower, but is not fully constrained to get a certain level of small variability (ex., smaller than one order of magnitude).

Evaluation of heterogeneity

One of the Task 8 objectives was to model and evaluate the heterogeneous distribution in space and time of water pressure and water content in bentonite. As discussed above, the model simulation could reproduce the heterogeneous distribution of pressure and saturation in space, as shown in Figures 4-13 through 4-40. In order to discuss the "heterogeneity" of pressure and/or saturation, a quantity measuring the heterogeneity should be defined from the view point of three-dimensional distribution (vertical section vs horizontal section) and spatial resolution. The quantity was also taken into account for the measurement methods of BRIE by in-situ sensors and sampling after dismantling the bentonite columns. The spatial and time resolution for the measurement should be considered to discuss the heterogeneity. The discussion based on the quantity measuring the heterogeneity might be useful for methodology development for the investigation and evaluation of the KBS-3 system.

Prediction of BRIE

The five stochastic realisations for the background DFN model were examined for three cases, base case, 1/50 transmissivity case, and fracture conditioning case, respectively. And, the wider variations for evaluating flow rate to the boreholes, among the five stochastic realisations were not fully constrained by fracture conditioning (Task 8C) and conditioning specific capacity around the BRIE area (Task 8D). The flow rates to specific points such as probe holes and 30 cm diameter enlarged boreholes were very sensitive to the balance between transmissivity of fractures and head distribution along the fractures beyond the borehole wall, and the head distribution around BRIE area. Although the locations of fractures intersecting the boreholes and the specific capacity at the boreholes was well conditioned, the gradient to the fractures feeding the boreholes where bentonite columns were installed was not as well constrained. The fact that multiple realisations produce similar results indicates that the head gradient in the rock might be less important than the details of the fracture pattern and properties that are constrained.

4.6 Conclusions and Recommendations

In this section, hydrogeological structure model in the 40 m × 40 m × 40 m block region around the TASO tunnel was modified as followed by the Task 8D1 specifications. The five stochastic realisations were examined to compare with the limited number of measurement data, and head and flow rate measured at the five probe boreholes and additional data obtained from four boreholes drilled from TASO tunnel horizontally. Two deterministically defined fractures observed at 30 cm diameter enlarged boreholes were added to the model. And, the specific capacity measured at five probe holes was used for calibrating the model to constrain hydraulic properties around the boreholes. All models, five realisations for each case (base case model, 1/50 transmissivity, and fracture conditioning) were applied for both Task 8D1 and Task 8D2 examinations.

From Task 8D examination, the following could be concluded:

- The simulated flow rate to the boreholes varies widely, more than one order of magnitude, among the stochastic realisations of the DFN model, even if constraining by the observed fracture locations and by the measured specific capacity. The prediction of flowing points and flow rate along the boreholes and/or tunnels was one of the challenges because the flow rate might be very sensitive to the balance among the hydraulic properties, head distribution, and other conditions at the borehole such as unsaturated behaviour.
- However, location and hydraulic properties of the intersecting fractures which could provide groundwater might be enough to predict the wetting bentonite, based on this simulation system (assuming only the fracture could provide groundwater to the bentonite), under the BRIE condition.
- An evaluation of the heterogeneous distribution of the groundwater in the bentonite requires a quantity measuring the heterogeneity. The quantity was also taken into account for the measurement methods of BRIE by in-situ sensors and sampling after dismantling the bentonite columns. The spatial and time resolution for the measurement should be considered to discuss the heterogeneity. The discussion based on the quantity measuring the heterogeneity might be useful for methodology development for the investigation and evaluation of the KBS-3 system.

5 Task 8F – Simulation of inflow and wetting of KO0017G01 and KO0018G01 based on results of BRIE

5.1 Objectives

Task 8F was a final subtask for Task 8 modelling studies. The main objective of Task 8F was to evaluate the resulting wetting of the bentonite installed in the two boreholes. Previous subtasks (Task 8C and Task 8D) had involved predictive modelling where results from bentonite wetting were not available. Task 8F allowed to use all of BRIE results documented in Fransson et al. (2017) to improve the knowledge of the bentonite rock interface with regard to groundwater flow. According to the Task 8 descriptions (Vidstrand et al. 2017), Task 8F only considered the bentonite wetting part. However, the scope of this calculation exercise was contained within the simulation of a sub-local and site-specific three-dimensional groundwater flow specifications similar to Task 8C and 8D, with all available data along with BRIE results. JAEA had developed an approach to Task 8 which considers the assumption that the discrete features dominate the delivery of groundwater to the bentonite, resulting in heterogeneous bentonite wetting behaviour. This assumption was implemented as FracMan Discrete Fracture Network (DFN) model for groundwater flow. The local hydraulic behaviour such as flow rate and head at the probe boreholes which were the performance measures to compare with BRIE results, might be fully influenced by the variability and uncertainty of this stochastic "HydroDFN" model. The uncertainty of the stochastic HydroDFN was quantified, in this subtask, based on the given a set of the stochastic input parameters. The probable range of the performance measures simulated by one thousand of stochastic HydroDFN models was presented. In addition, the influences of the uncertainty of the local hydraulic behaviour, in terms of the location and hydraulic properties of the fractures intersecting to the bentonite columns emplaced in the enlarged boreholes, onto the heterogeneous wetting process in bentonite was also examined.

5.2 Approach

The same system of the numerical codes as used for Task 8C and Task 8D were applied for this task. While, the HydroDFN was updated for Task 8F. One of the key assumptions in JAEA's Task 8 modelling is the assumed a functional relationship between transmissivity and fracture size. The correlation parameter values between transmissivity and fracture size were calibrated to the data measured at the boreholes around the prototype repository tunnel during JAEA's modelling for Task 8E (see Appendix A2). The variance of the lognormal distribution of transmissivity was also taken in account, in addition to a linear correlation between fracture radius and transmissivity.

Another key piece of data used to condition the Task 8F HydroDFN was the so called "Bentograph" picture, the pattern of shading observed at the surface of the dismantled bentonite column, which was assumed to directly map the locations where fractures deliver groundwater to the bentonite. The fracture locations and orientations indicated by the Bentograph are generally consistent with what was assumed based on borehole KO0018G data. This indicates that most of the geologically mapped fractures have the potential to provide groundwater to the bentonite even if their permeability is lower than the detection limit of the hydraulic investigation, such as groundwater inflow measurement, Posiva Flow Log, and nappy test as listed in Task 8 descriptions (Vidstrand et al. 2017). Unfortunately, the detection limit of each measurement is not clarified in Task 8 descriptions. Therefore, the data of location and orientation of geologically mapped fractures along five probe boreholes was applied for constraining the stochastic variability of the HydroDFN model. The transmissivity of fractures intersecting the probe boreholes was also constrained by specific capacity data measured along each of the five probe boreholes.

In this sub-task, 1 000 of the distinct realisations according to the stochastic parameter values for the fracture distributions were made to be applied to the groundwater flow simulations in rock, in order to evaluate the potential range of the prediction evaluated by the stochastic DFN model. The groundwater flow rate and head distribution along the five probe boreholes were compared with the measured values. Some of the realisations which could reproduce similar flow rate and head with the measured data were selected to simulated bentonite re-saturation behaviour by FracMan/MAFIC-Thames coupling simulation system.

5.3 Model Setup

Figure 5-1 shows (a) modelling region, (b) an example of HydroDFN model, and (c) the deterministically defined fractures used for the Task 8F studies. Three large fractures, NNW4, wfracture01 and wfracture02 were set as same as Task 8D specification (see Figure 3-2 and Table 3-1). Orientation of the water conducting fractures observed at the walls of 30 cm diameter holes along KO0017G01 and KO0018G01, were corrected as shown in Figure 5-2. The three stochastic background fracture sets were defined as listed in Table 3-2, which specifies a DFN model for geological fractures. In order to reduce computational size of the model, the fractures smaller transmissivity of 1×10^{-13} m^2/s were removed from the stochastic HydroDFN model. For Task 8F, the modified correlation factors between fracture radius and transmissivity examined in Task 8E was applied. The correlation factors between fracture size and transmissivity were calibrated to the data set which shows the heterogeneous transmissivity distribution measured around Prototype Repository tunnel in Task 8E studies, as described in the following equation:

$$T = \text{lognorm}(\mu, \sigma) \times r^{4.7}$$

where T is transmissivity, lognnorm(m, s) is lognormal distribution with average $m = 1 \times 10^{-13}$, and standard deviation $s = 3 \times 10^{-13}$, r is fracture radius. The random variables of the lognormal distribution were also taken in account, in addition to a liner correlation to fracture radius. An example of the modelled correlation between fracture radius and transmissivity is shown in Figure 5-3.

In order to evaluate the potential range of the prediction evaluated by the stochastic DFN model, 1 000 of the distinct realisations based on the stochastic parameter values for the fracture distributions were made to be applied to the groundwater flow simulations in rock, although only five realisations of DFN model were applied to groundwater flow and bentonite re-saturation calculation in Task 8C and 8D studies.

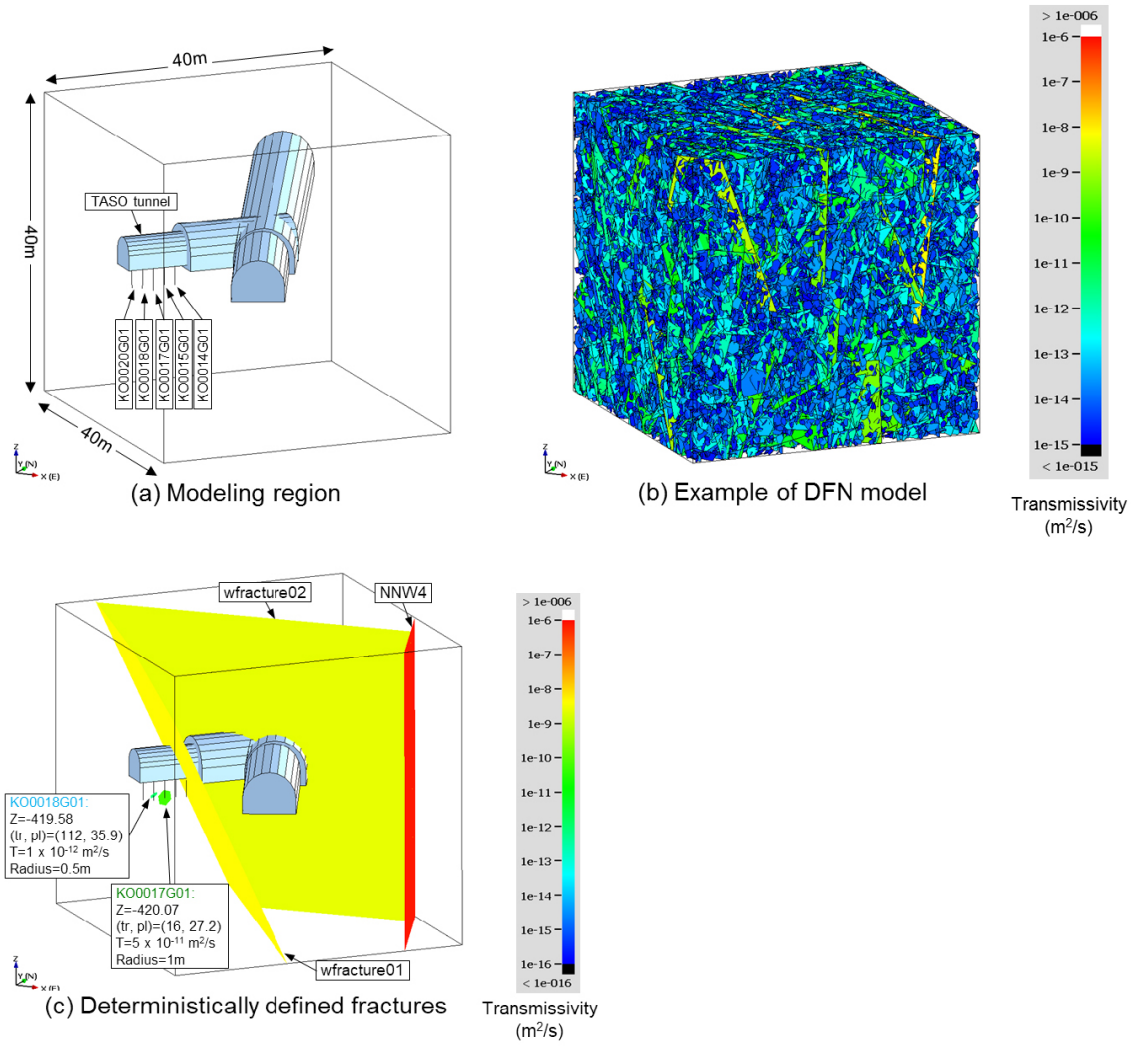

Figure 5-1. *DFN models used to be applied to the Task 8F studies.*

The defined flowing structures in KO0017G001 and KO0018G01 are given in the table below. The Adjusted z-elevation refers to the depth at which estimated fracture plane cross the center axis of the borehole. The extension of the fractures is largely unknown.

The fracture in KO0017G01 is not found in the tunnel floor mapping however it is clear from hydraulic responses that the fracture has a good connection with the deformation zone, denoted wfracture_01, however not likely a direct connection.

The fracture in KO0018G01 has not been found to have any good connection with any other observations. The fracture did not supply any water for the first couple of months.

Table 9-6 Fracture locations in boreholes KO0017G01 and KO0018G01.

Borehole	Diameter [mm]	Adjusted z-elevation [m]	Strike (deg) RT90	Dip (deg) RT90
KO0017G01	300	-420,07	139.5	62.8
KO0018G01	300	-419.58	214.7	54.1

Dip direction
17: 229.5, 18: 304.7

(a) Original values described in the Task specification

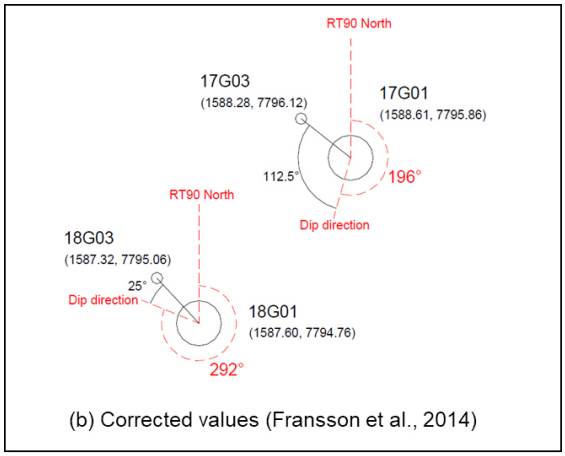

(b) Corrected values (Fransson et al., 2014)

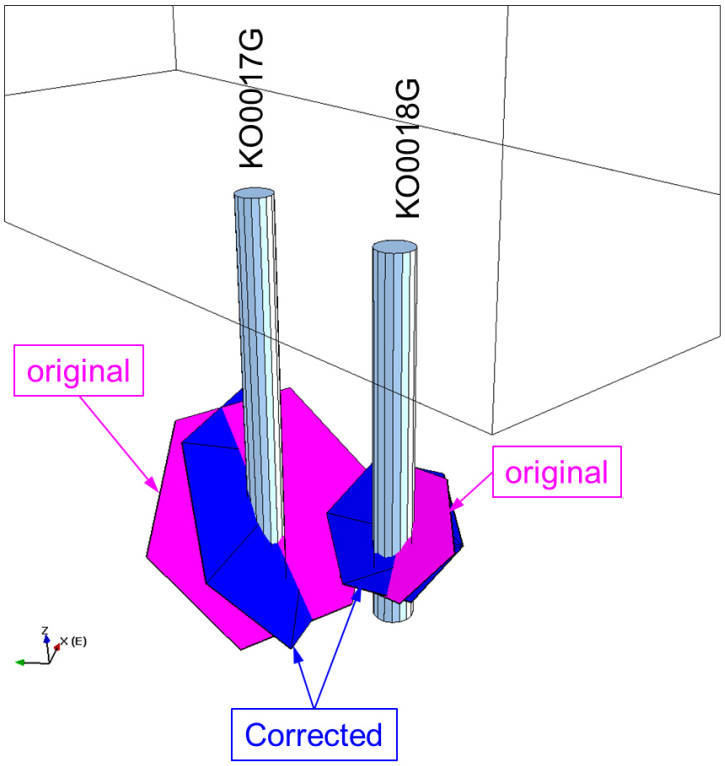

(c) Visual comparison of the fractures

Figure 5-2. *Orientation correction of the deterministically defined water conducting fractures.*

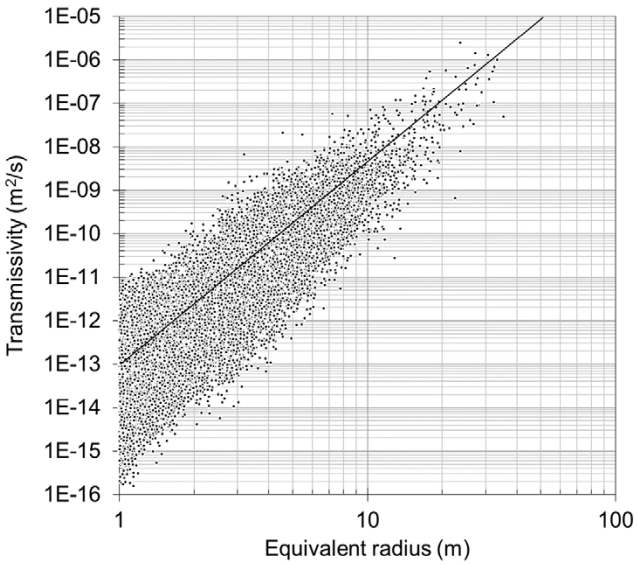

Figure 5-3. *An example of correlation between fracture radius and transmissivity.*

Bentograph features

Visual investigation of bentonite column surface dismantled from KO0018G hole indicates that the wetting area identified by relatively dark colour might be distributed along the traces of the fractures intersecting to the hole as shown in Figure 5-4(a), which is called “Bentograph features”. Figure 5-4(b) shows an example of the traces (red lines) to correspond to the “dark” points. The fractures corresponding to the sub-horizontal traces were compared with the fracture data set measured along the probe borehole. From the visual comparison of them (Figure 5-5), the location and the orientation of the fractures estimated from the Bentograph features are identical to the measured fractures compiled in the SKB’s database. This suggests that the fractures geologically observed along the boreholes might have a potential to behave a connecting void space to provide groundwater to the bentonite. The stochastically generated DFN models were compensated for the data observed along the five prove boreholes by the conditioning method used for Task 8C described in Figure 3-4. Although a few selected fractures were used as the conditioning data set in Task 8C, all fractures observed along the five probe boreholes compiled in SKB’s database (“p_fract_core_eshi.xls”) was applied in Task 8F studies. Figure 5-6 (a) shows the fracture traces of compiled in SKB’s database at the vertical cross section parallel to the five probe boreholes. Figure 5-6 (b) is an example of fracture traces along the vertical cross sectional plane of a stochastically generated DFN model. This stochastic DFN model was edited with the conditioning data set described in Figure 5-6 (a). Consequently, the constrained DFN model as shown in Figure 5-6 (c) was obtained. Transmissivity of the fractures which are intersecting to the probe boreholes were also adjusted. The borehole specific capacity measured at the five probe holes by the injection test was used to correct the fracture transmissivity around the probe boreholes in Task 8D. In this sub-task, with assuming that the specific capacity value might be approximated to equal to the transmissivity at measured packer section, the fracture transmissivity intersecting to each probe borehole was adjusted by multiplying the following value to each fracture.

$$\frac{C_j}{\sum_{i=1}^{n_j} T_i}$$

where T_i is transmissivity of i-th fracture intersecting to the probe borehole j , n_j is total number of fractures intersecting to the borehole j, and C_j is specific capacity of the borehole j. The specific capacity at each probe borehole are listed below (they are same as used for Task 8D).

- KO0014G01: 0.5–3.0 m, Q/dh 6.0×10^{-10} m^2/s
- KO0015G01: 0.75–3.03 m, Q/dh 1.7×10^{-7} m^2/s
- KO0017G01: 0.5–2.97 m, Q/dh 8.0×10^{-11} m^2/s including −420.07 m fracture (3.0×10^{-11} m^2/s excluding −420.07 m fracture)
- KO0018G01: 0.55–3.06 m, Q/dh 4.5×10^{-7} m^2/s, but 1×10^{-12} m^2/s at 2.1–3.1 m
- KO0020G01: 0.82–3.1 m, Q/dh 4.2×10^{-10} m^2/s

An example of transmissivity adjusted HydroDFN model is shown in Figure 5-6 (d).

The same boundary conditions as used for Task 8C and D were set. The heterogeneous head distribution estimated from the Äspö site scale model (Figure 2-5) was applied at the outer boundary. Atmospheric pressure was applied to the tunnel walls. For simulating head values at the packed off condition at the boreholes, the modelled packed off section was specified as a zero “group flux,” which assumes zero resistance to flow within a packer section of the borehole that heads are the same. While, for simulating flows to the probe boreholes, constant head equals to −417 m assuming average TASO tunnel floor is set to calculate overflow to the borehole collar which is drilled from TASO floor vertically.

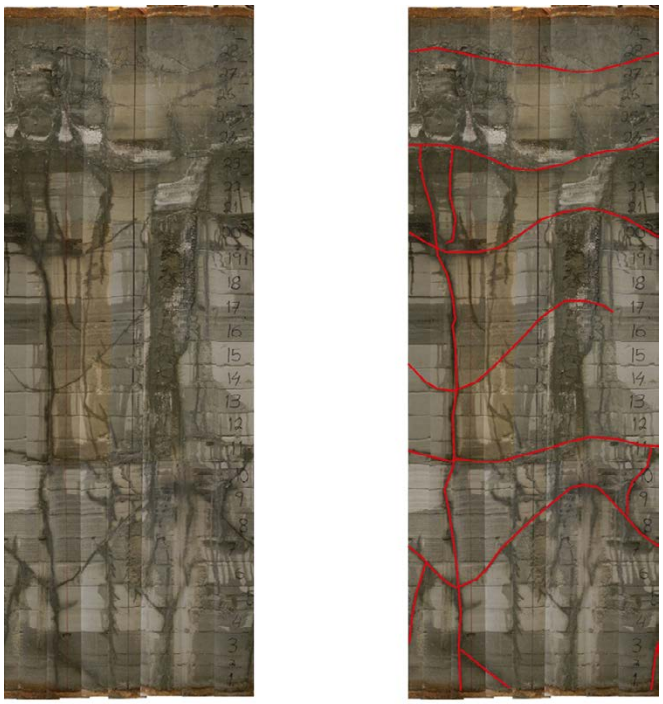

Figure 5-4. *Unfolding picture of bentonite surface of dismantled bentonite column from KO0018G bole.*

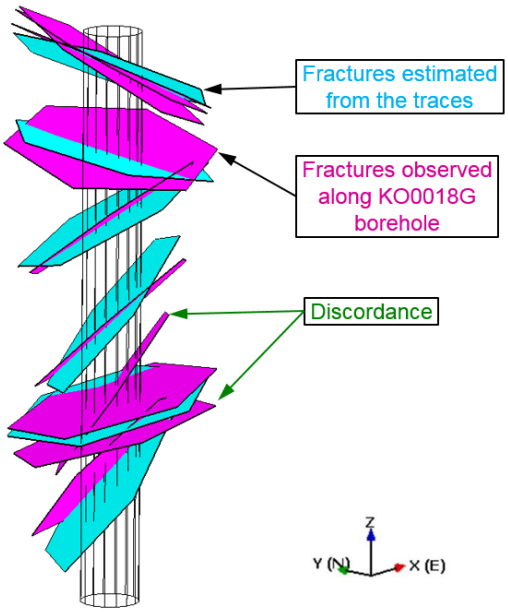

Figure 5-5. *Visual comparison between "Bentograph" fractures (light blue) and measured fractures along KO0018G (pink).*

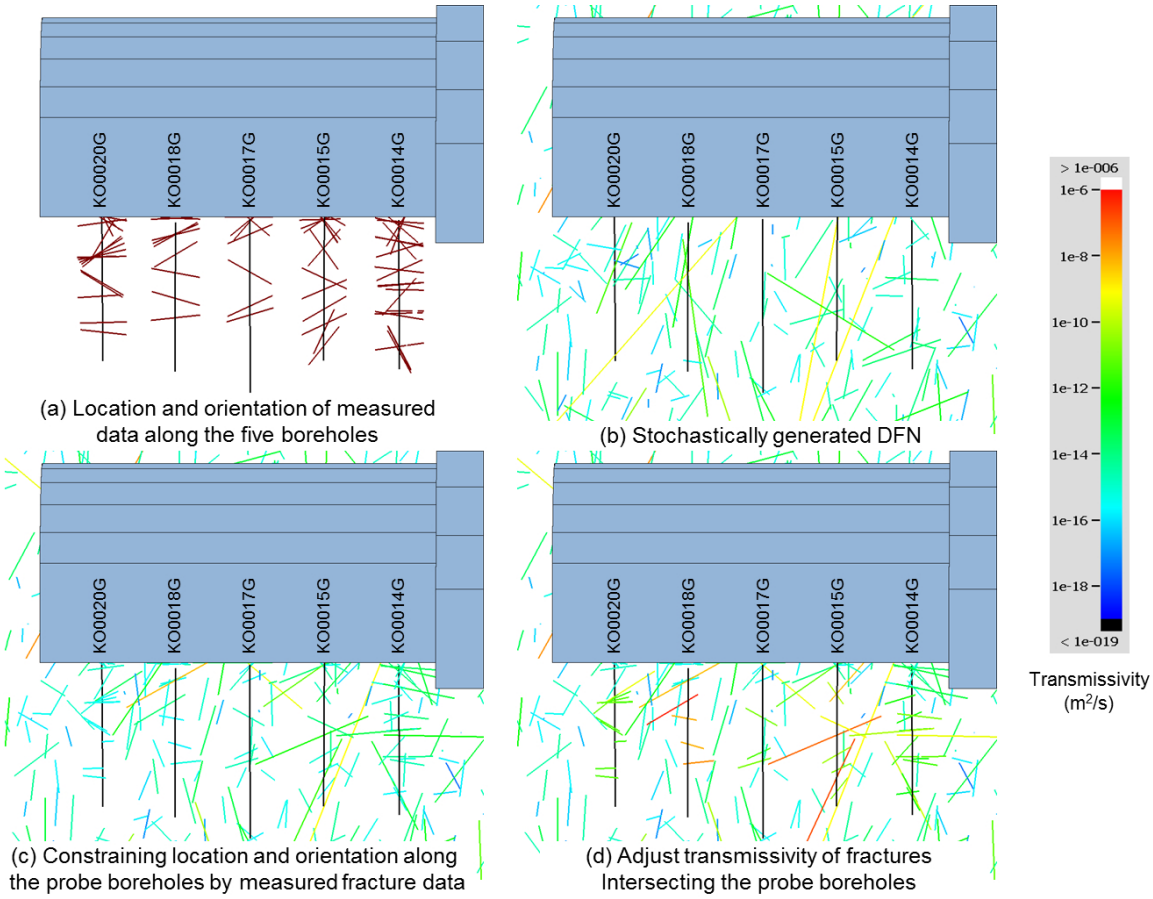

Figure 5-6. *Conceptual picture for constraining fracture location and orientation, and adjusting transmissivity intersecting to the probe boreholes; vertical cross sectional view along the holes.*

Groundwater flow simulations

The steady state groundwater flow simulations for both pressure and groundwater flow to the five probe boreholes were made for the 1 000 stochastic realisation of the HydroDFN models. Figure 5-7 shows the distribution of pressure (datum is TASO tunnel floor: −417 m) at and groundwater flow rate to the five probe holes, comparing with the measured data. The both measures distribute relatively wider range (several order of magnitude) among the stochastic realisations, although they cover the measured values. These results also range wider than the results of Task 8C and 8D, which were calculated by only five realisations. Because, the transmissivity distribution of the updated HydroDFN model calibrated by the data measured around the Prototype Repository tunnel (Task 8E) shows the distribution of relatively lower average value and large variance than Task 8C and 8D model as shown in Figure 5-8. Due to the wider transmissivity range, relatively high heterogeneous flow behaviour at local scale like the five probe boreholes might be modelled that might cause the unreasonable scattered distribution of pressure and flow rate to the boreholes.

The pressure and flow rate at KO0014G01 hole seem to converge to a certain range (about one order of magnitude). As shown in Figure 5-1, KO0014G01 penetrates the deterministic defined larger fracture, wfracture01, which might govern hydraulic behaviour of KO0014G01. On the other hand, the randomness of the stochastic HydroDFN model might affect on the hydraulic behaviour at the other probe holes, rather than the conditioned fractures which are intersecting to the probe holes. Because, head value and flow rate at the boreholes are controlled by not only a fracture intersecting the borehole, but also the network of fractures modelled by the stochastic background fracture. This indicates that further data might be required to be obtained for restricting this randomness of the stochastic HydroDFN model, such as the size and transmissivity of each intersected fracture at the borehole, and hydraulic connectivity around the boreholes. Although there might be no sophisticated investigation method, the transient pressure tomography and directional ground penetration radar might provide more data to constrain the flow field around the boreholes.

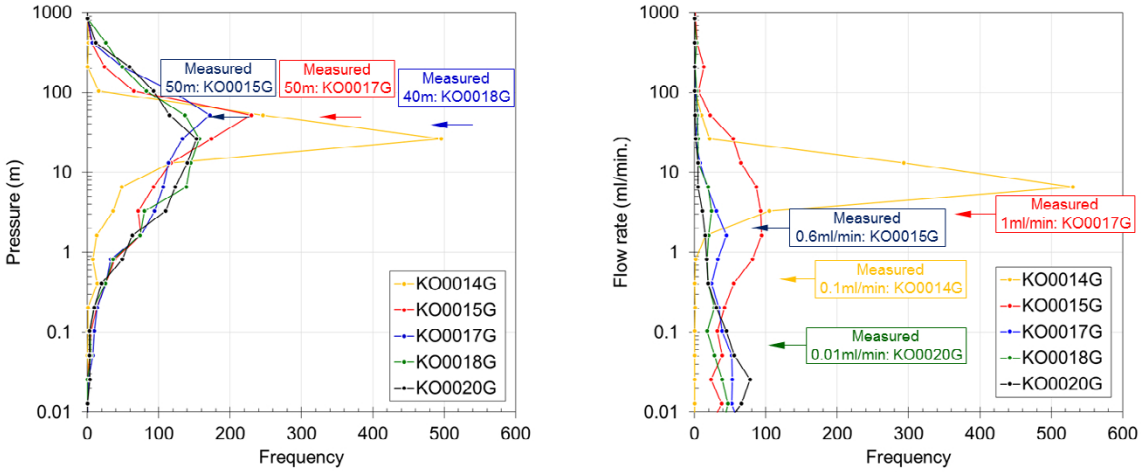

(a) Pressure distribution at the probe holes (b) Flow rate distribution to the probe holes

Figure 5-7. *Simulated pressure and flow rate distribution at the five prove holes.*

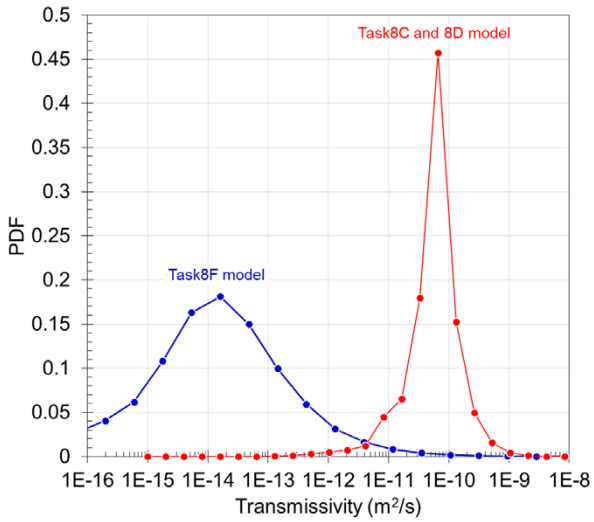

Figure 5-8. *Comparison of transmissivity distribution between Task 8C and 8D model and Task 8F model.*

Six realisations were screened out from one thousand realisations of the simulation results, by two criteria, RMSE (root mean square error between simulated and measured) of 1) pressure values and 2) flow rates at all measured sections of the five probe boreholes. All stochastic realisations should be applied to the bentonite wetting simulations by the coupling between FracMan and Thames, to analyse the effect of heterogenous flow field of the stochastically distributed DFN model on the bentonite wetting behaviour. However, due to the time consuming, the limited number of the realisations were selected for the coupling simulations, to demonstrate the effect of the heterogenous flow field in rock on the bentonite wetting behaviour. Figure 5-9 shows the comparison of the simulated pressure by the six selected realisations and flow rate with measured data. These models seem to reproduce similar pattern as measured pressure and flow rate. The RMSE of pressure and flow rate at measured probe boreholes are compared in Figure 5-10. The realisation number 217 is the least errors for both pressure and flow rate among the screened six realisations. The head distribution simulated by the realisation 217 is presented in Figure 5-11. Figure 5-12 shows the heterogeneous distribution of flow rate to the enlarged holes along KO0017G01 and KO0018G01 probe boreholes, with modelled fracture traces.

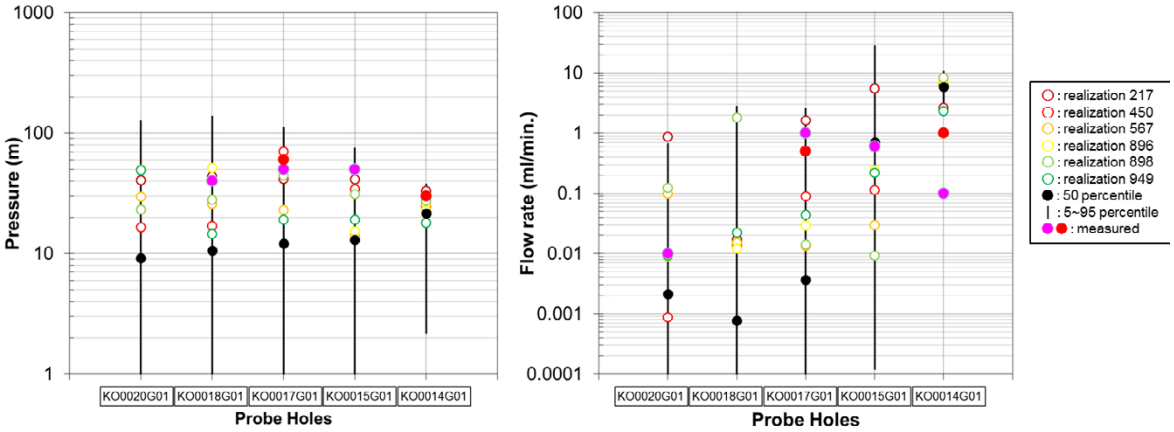

(a) Pressure distribution at the probe holes (datum is TASO tunnel floor: -417m)

(b) Flow rate distribution to the probe holes

Figure 5-9. *Comparison of simulated pressure and flow rate to five probe boreholes with measured data. The simulation results of screened six realisations were compared.*

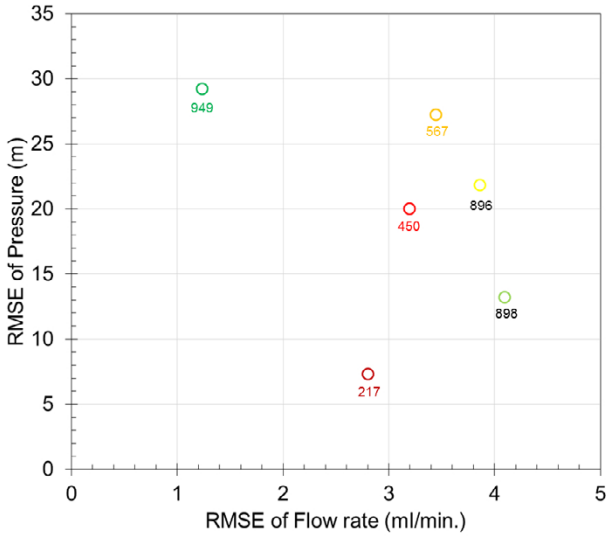

Figure 5-10. *RMSE of pressure and flow rate to the probe holes of screened six realisations. Numbers are the index of the realisation number.*

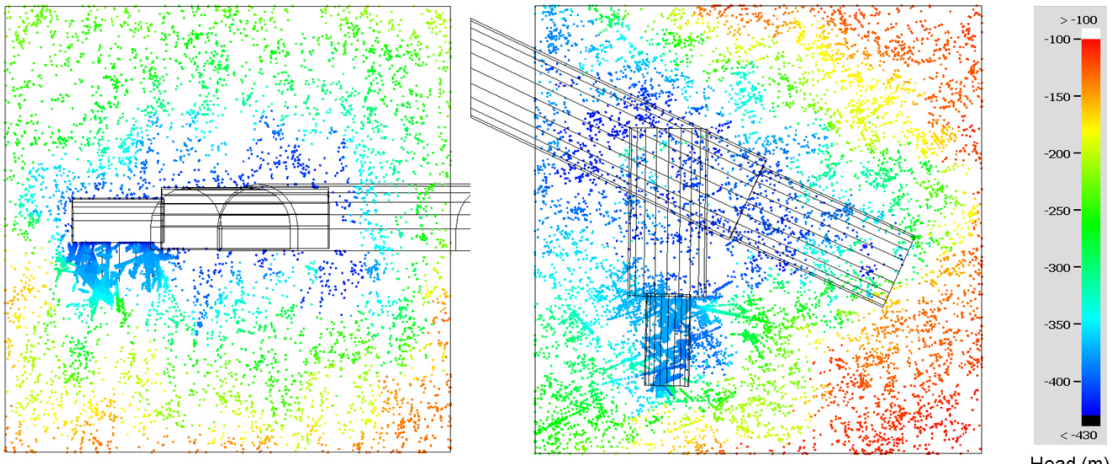

(a) Vertical section along the five probe holes

(b) Horizontal section 2m below of tunnel floor

Figure 5-11. *An example of simulated head distribution at vertical and horizontal cross section (realisation number: 217).*

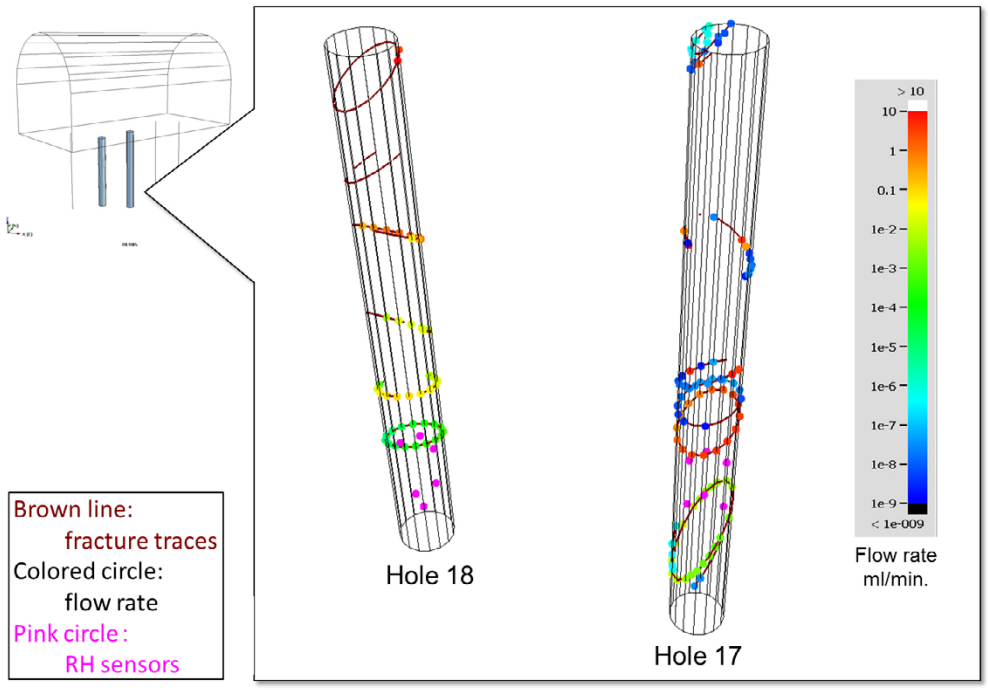

Figure 5-12. *An example of simulated flow rate to the enlarged hole along KO0017G01 and KO0018G01 probe boreholes (Hole 17, Hole 18, respectively) (realisation number: 217).*

5.4 Results

The localised groundwater flow of the selected six realisation models provide the heterogeneous wetting behaviour in bentonite columns installed in enlarged (30 cm) holes by the iterative simulation between FracMan and Thames codes. The same finite elements (Figure 4-4) and parameter values (Table 4-2) as used for Task 8D were applied. The calculation results for the selected six realisations are compared with the measured data as shown in Figure 5-13 ~ Figure 5-17.

Figure 5-13 shows the simulated saturation distribution at the surface of bentonite column after 510 days for the selected six realisations, comparing with the picture of dismantled bentonite column from Hole 18. These figures are illustrated by unfolding surface saturation of the bentonite column in counter clockwise rotation from the north, and white lines are modelled fracture traces intersecting to Hole 18. The most of fractures intersecting to Hole 18 might dominate saturation distribution at the bentonite surface. However, if the fractures have poor availability of providing water due to low permeability or the lack of hydraulic connectivity, the bentonite surface interconnected to the less water providing fractures seems to sustain unsaturated condition. For example, realisation 217 which has the least errors for head and flow rate to probe boreholes as shown in Figure 5-10, has wetting part along the fracture traces at top and middle part, but doesn't have wet part along the lowest fracture. They are not identical to the measured data.

Figure 5-14 and Figure 5-15 are the comparison of relative humidity evolutions at six sensor locations with measured data, at Hole 17 and Hole 18 respectively. Most of the measured data for both holes have rapid increase of relative humidity just after installing the bentonite column at Hole 17 and about 50 days after installing the bentonite at Hole 18. They might be caused by the flooding groundwater from the tunnel floor via the central tubes of the bentonite columns. In Hole 17, this occurred immediately after the installation and the filling of the outer slot. In Hole 18, this occurred around day 50. The effect of these artifacts were not taken into account for this modelling study. At Hole 17, the most cases could reproduce measured relative humidity. The lower section, WBR0001~WBR0003, might be governed by the deterministically defined fracture along KO0017G01 (Figure 5-1) and the upper section, WBR0004~WBR0006 might be a dry (or weakly wet) section. On the other hand, the simulation results vary among the model realisations. This might be caused by the variability of the heterogeneous hydraulic connectivity of the deterministically defined fracture along KO0018G01 (Figure 5-1).

Figure 5-16 and Figure 5-17 are the comparison of water content distribution at lower half of bentonite columns with measured data, at Hole 17 and Hole 18 respectively. At Hole 17, the simulation results seem to be identical to the measured water content distribution, except for the bottom of the hole. The bottom of the holes were filled by sand (thickness 5 cm at Hole 17 and 3 cm at Hole 18) that might introduce water to the bottom part of the bentonite columns. This effect was also not taken into account for the models. At Hole 18, the distribution of simulated water content also varies among the model realisations as well as the relative humidity. Although the distribution of measured water content might be weakly governed by the deterministically defined fracture along KO0018G01, the modelled deterministically defined fracture could not well control water supply to the bentonite column.

The evolutions of saturation distribution at the surface of columns and vertical cross section along TASO tunnel axis during BRIE period (30days, 90 days, 180 days 360 days and 410 days for Hole 17, 510 days for Hole 18) for six realisations are shown in Figure 5-18 ~ Figure 5-29. Form these figures, the heterogeneous wetting behaviour in bentonite columns in early period after emplacing the bentonite columns such as BRIE could be reproduced by heterogeneous groundwater supply by the network of fractures. The key factors might be location and orientation of the fractures interconnecting to the bentonite columns, and their hydraulic connectivity which controls available water supply to the bentonite columns.

The long-time bentonite wetting behaviour up to 100 years was also calculated for six realisations. Figure 5-30 ~ Figure 5-35 show the distribution of heterogeneous bentonite saturation at vertical cross section along TASO tunnel axis and horizontal sections at specified depths near the locations of relative humidity sensors. The most of the cases could attain saturated condition for whole bentonite columns by 100 years, although the bentonite columns took heterogeneous wetting behaviour at the beginning. However, some cases (realisation number 217, 896, 898 for Hole 17) could not reach to full saturation by 100 years as shown in Figure 5-36.

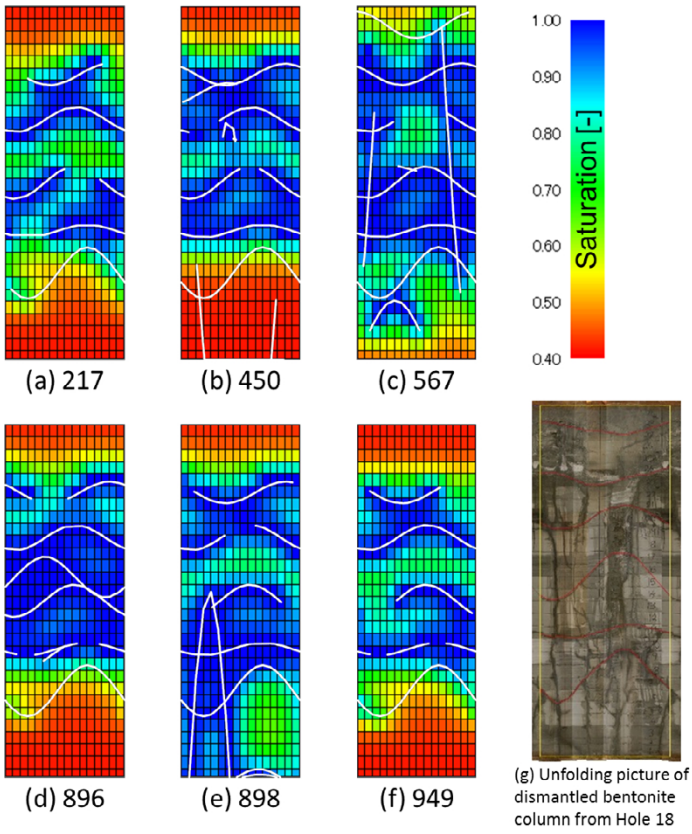

Figure 5-13. *Simulated saturation distribution at the surface of bentonite column after 510 days for (a) ~ (f) the six realisations comparing with (g) the picture of dismantled bentonite column from Hole 18. (Unfolding illustration of counter clockwise from north.)*

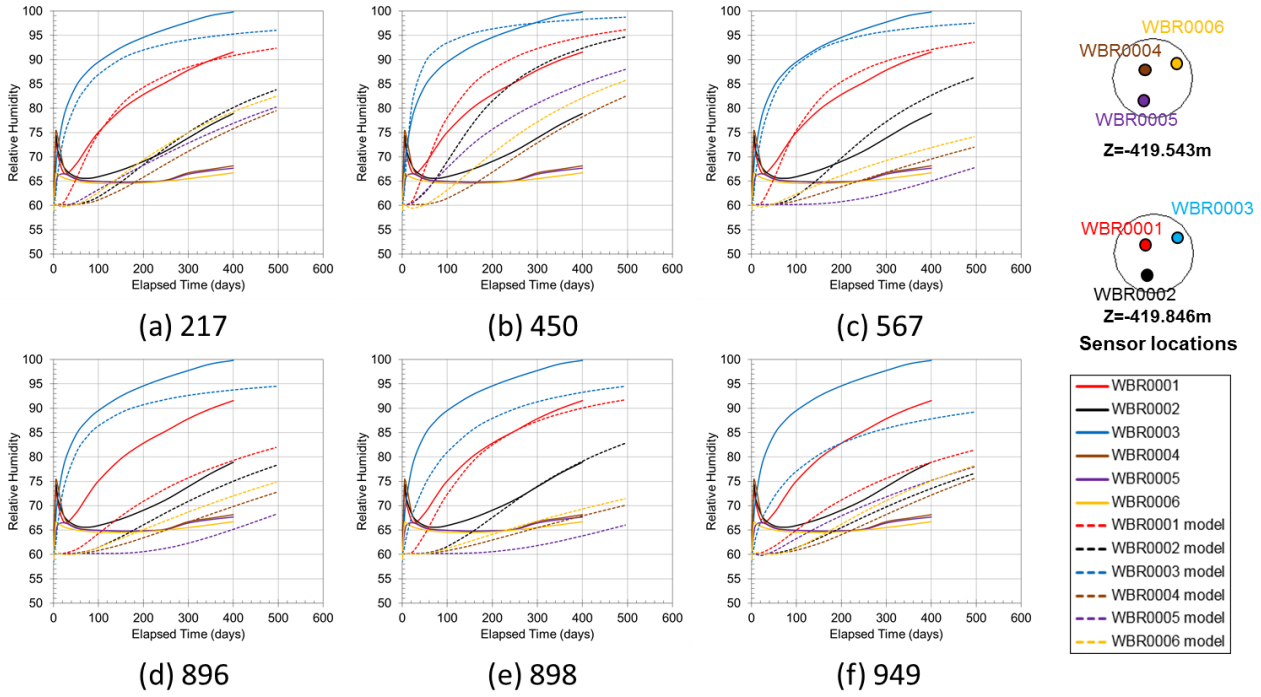

Figure 5-14. *Comparison of simulated relative humidity at six sensor locations with measured data at Hole 17 for (a) ~ (f) the six realisations.*

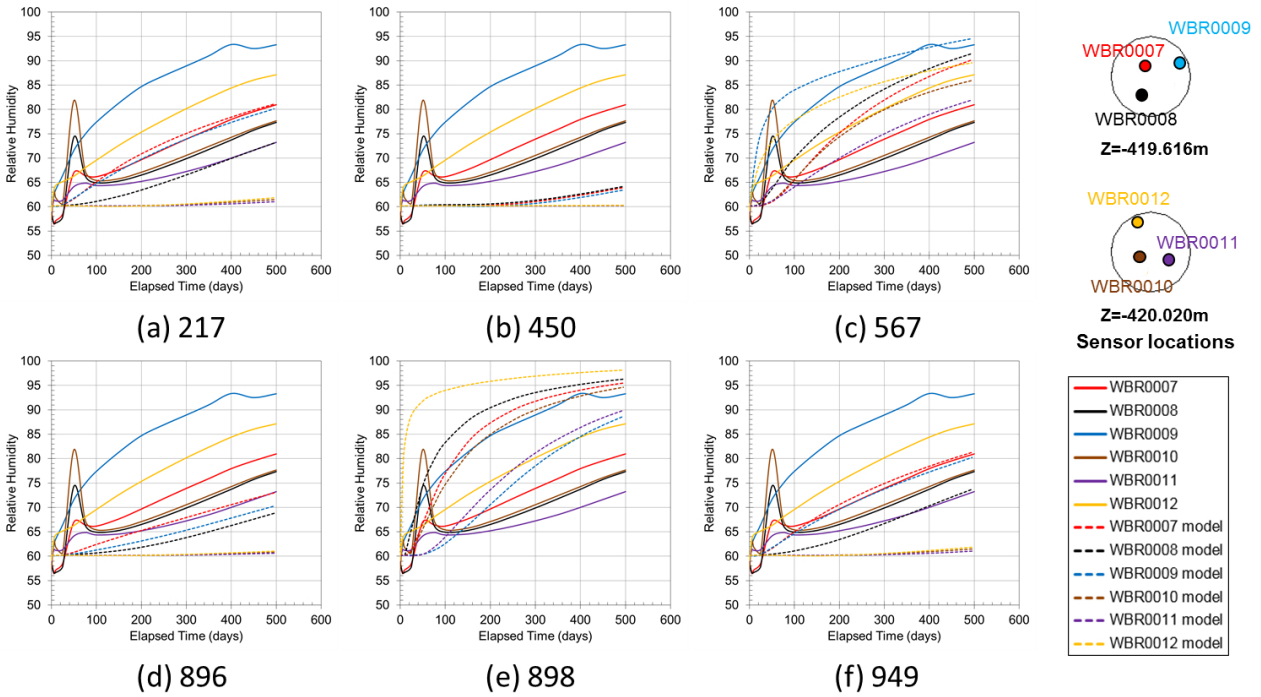

Figure 5-15. *Comparison of simulated relative humidity at six sensor locations with measured data at Hole 18 for (a) ~ (g) the six realisations.*

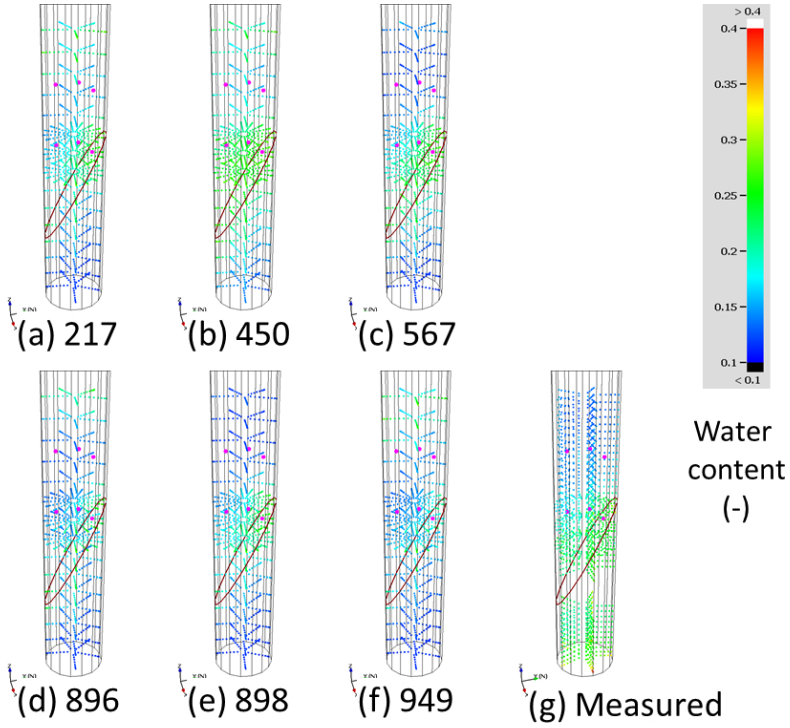

Figure 5-16. *Comparison of simulated water content at the lower part of bentonite column for (a) ~ (f) the six realisations with (g) measured data dismantled from Hole 17. Red line: fracture trace of deterministically defined fracture along KO0017G01. Pink dots: locations of relative humidity sensors.*

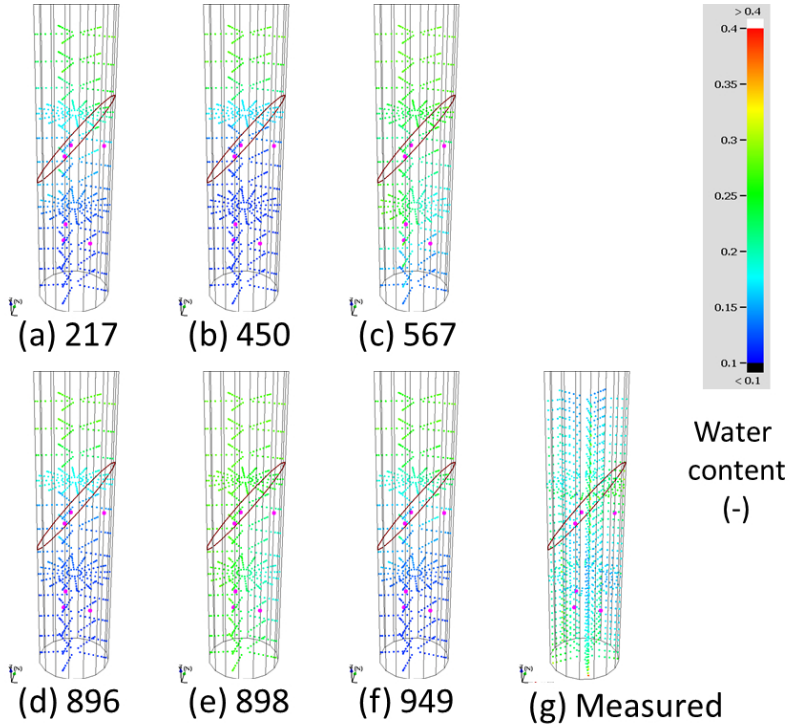

Figure 5-17. *Comparison of simulated water content at the lower part of bentonite column for (a) ~ (f) the six realisations with (g) measured data dismantled from Hole 18. Red line: fracture trace of deterministically defined fracture along KO0018G01. Pink dots: locations of relative humidity sensors.*

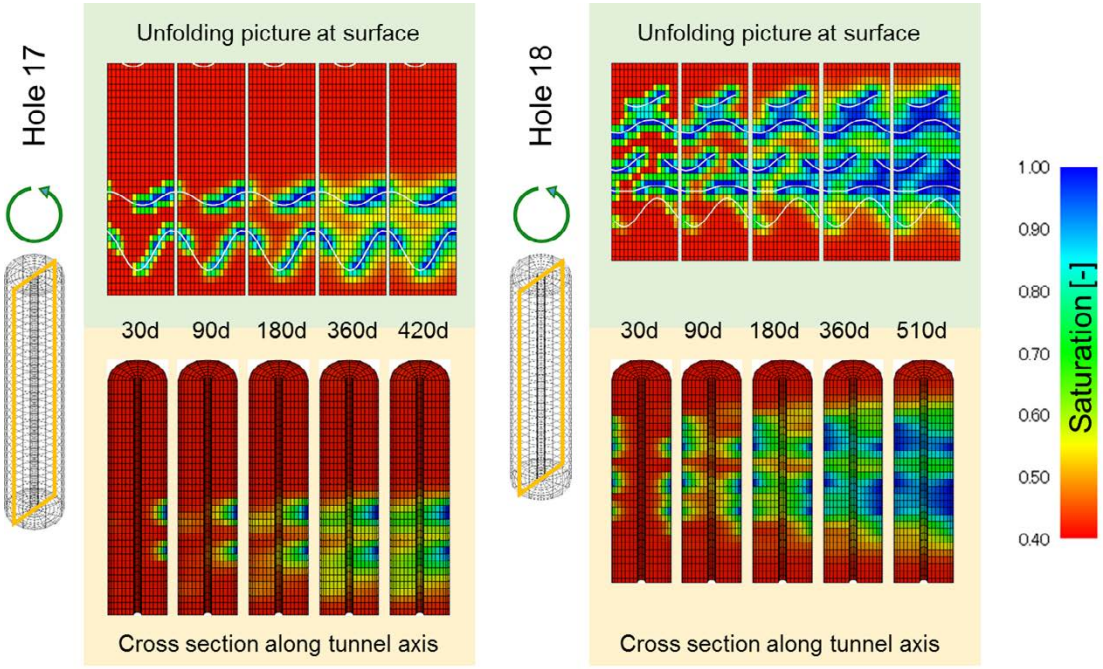

Figure 5-18. *Simulated bentonite saturation during BRIE period. Upper: unfolding picture at bentonite surface with fracture traces (white line). Lower: cross section along tunnel axis, Left: Hole 17, Right: Hole 18. (Realisation number: 217)*

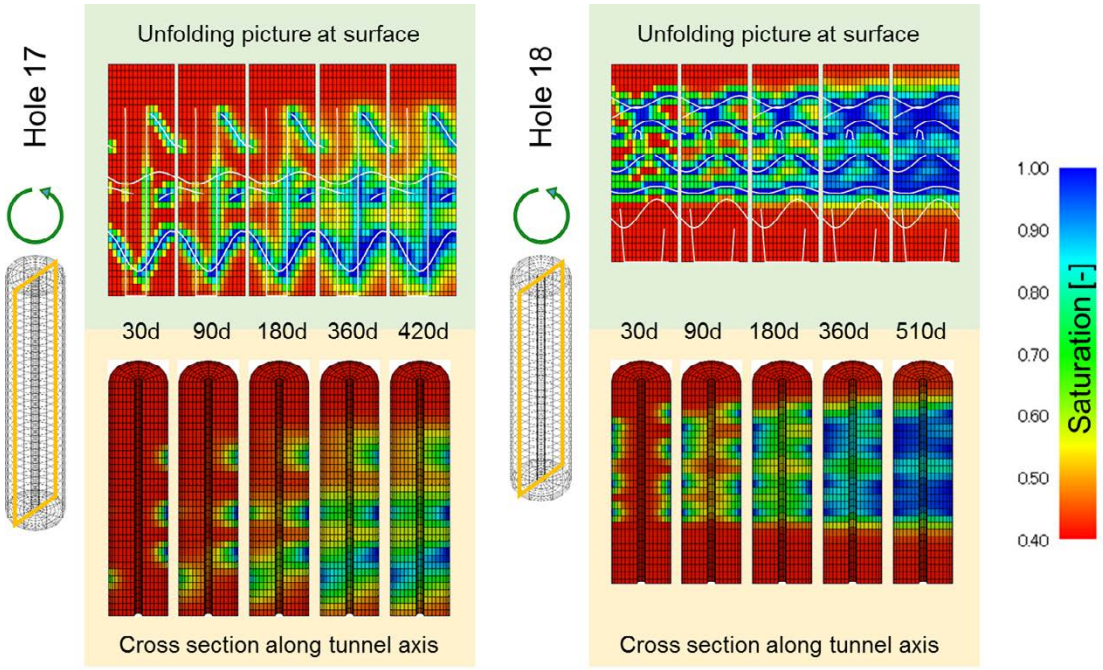

Figure 5-19. *Simulated bentonite saturation during BRIE period. Upper: unfolding picture at bentonite surface with fracture traces (white line). Lower: cross section along tunnel axis, Left: Hole 17, Right: Hole 18. (Realisation number: 450)*

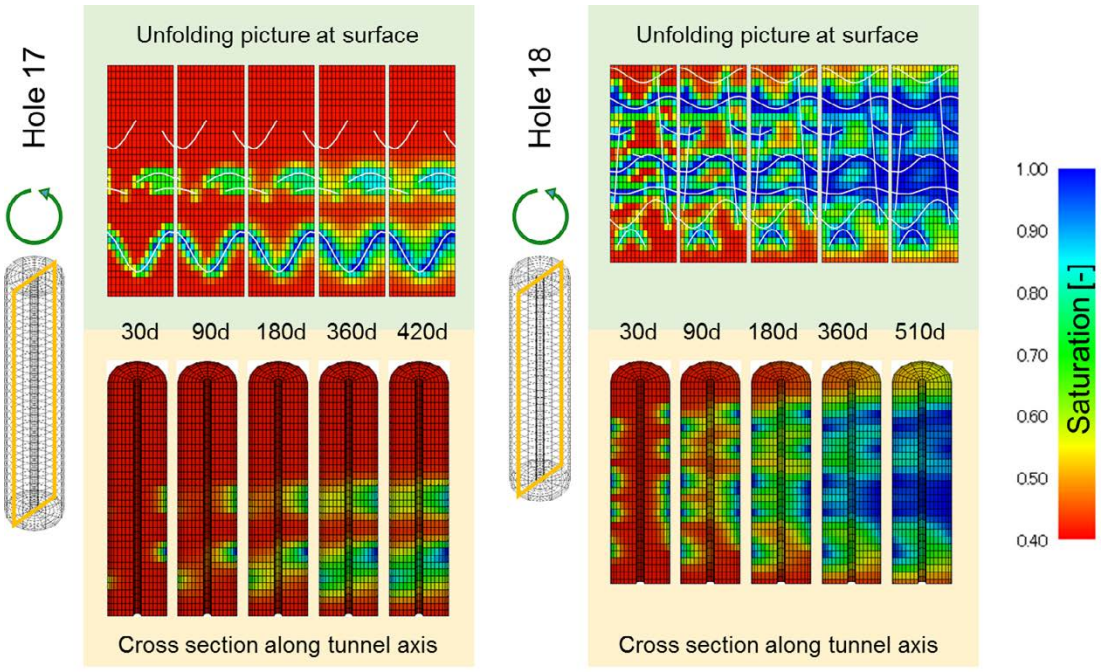

Figure 5-20. *Simulated bentonite saturation during BRIE period. Upper: unfolding picture at bentonite surface with fracture traces (white line). Lower: cross section along tunnel axis, Left: Hole 17, Right: Hole 18. (Realisation number: 567)*

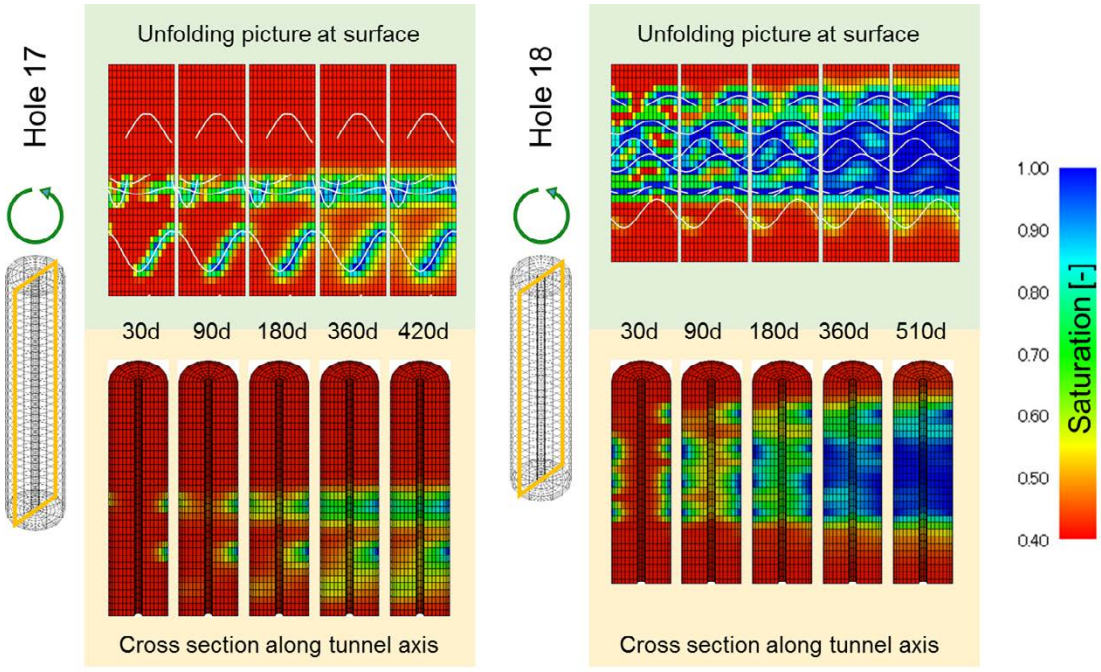

Figure 5-21. *Simulated bentonite saturation during BRIE period. Upper: unfolding picture at bentonite surface with fracture traces (white line). Lower: cross section along tunnel axis, Left: Hole 17, Right: Hole 18. (Realisation number: 896)*

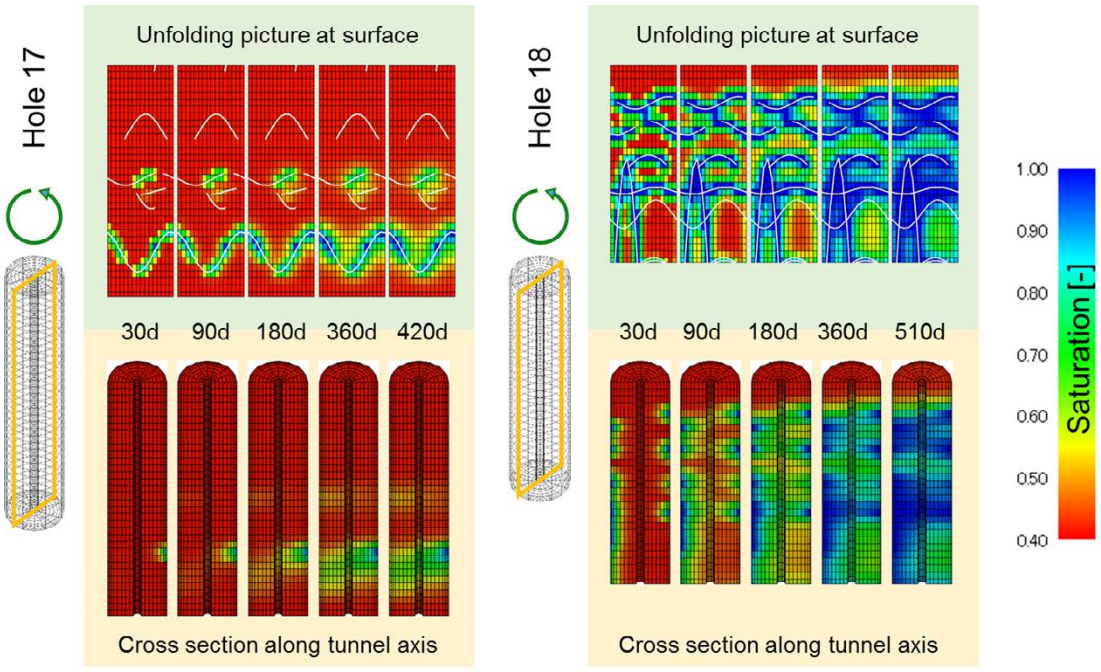

Figure 5-22. *Simulated bentonite saturation during BRIE period. Upper: unfolding picture at bentonite surface with fracture traces (white line). Lower: cross section along tunnel axis, Left: Hole 17, Right: Hole 18. (Realisation number: 898)*

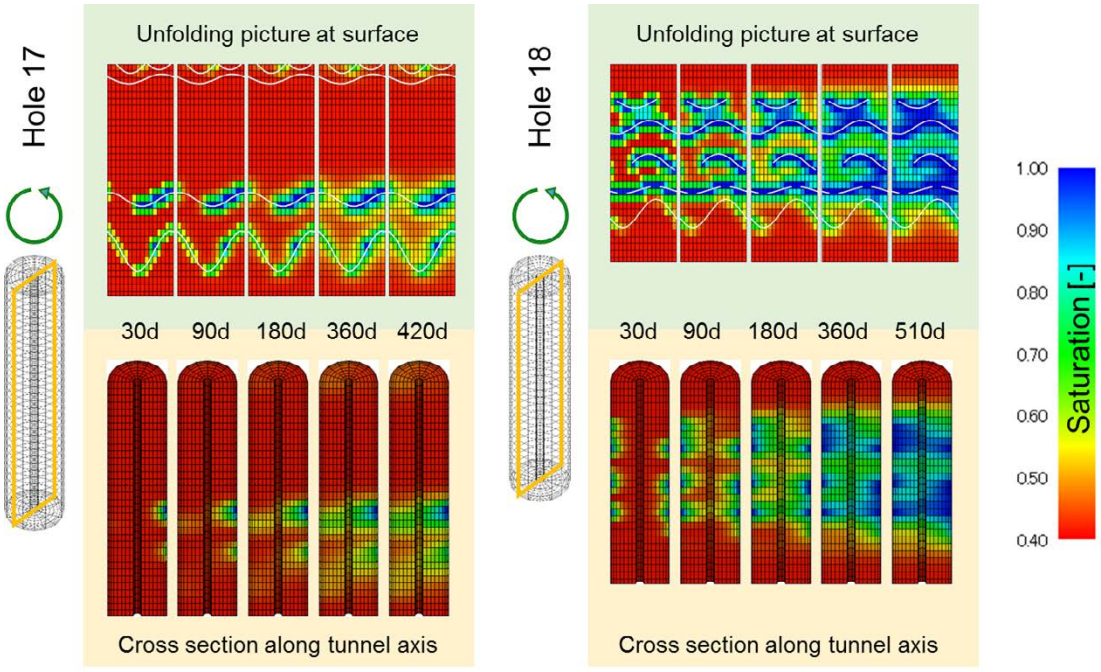

Figure 5-23. *Simulated bentonite saturation during BRIE period. Upper: unfolding picture at bentonite surface with fracture traces (white line). Lower: cross section along tunnel axis, Left: Hole 17, Right: Hole 18. (Realisation number: 949)*

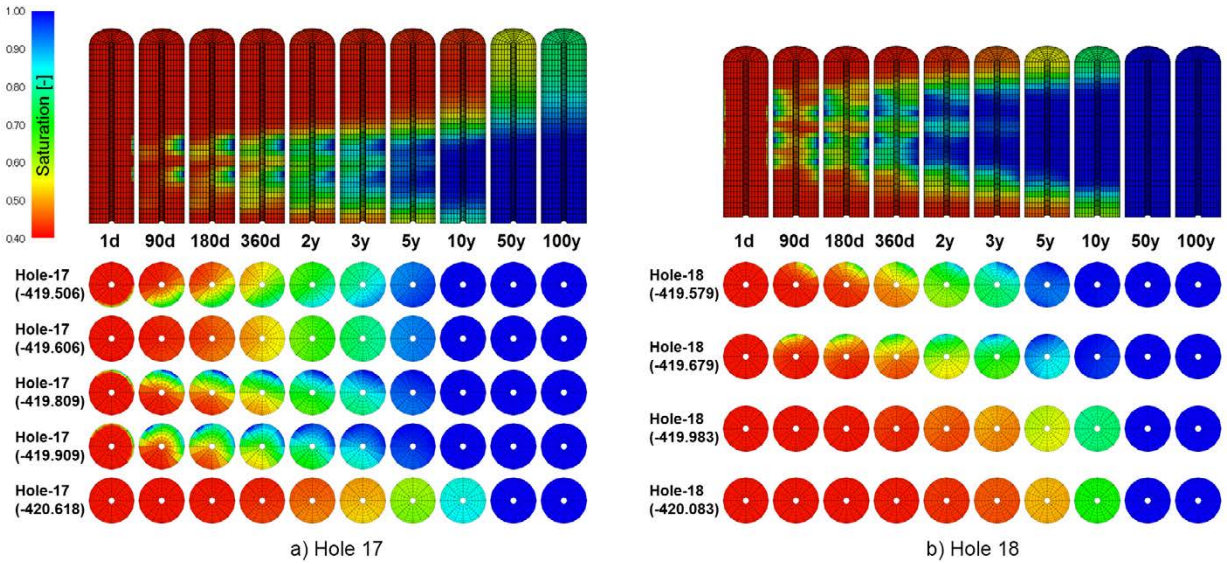

Figure 5-30. *Simulated bentonite saturation up to 100 years (Realisation number: 217). Upper: cross section along tunnel axis, Lower: horizontal section at specified depths.*

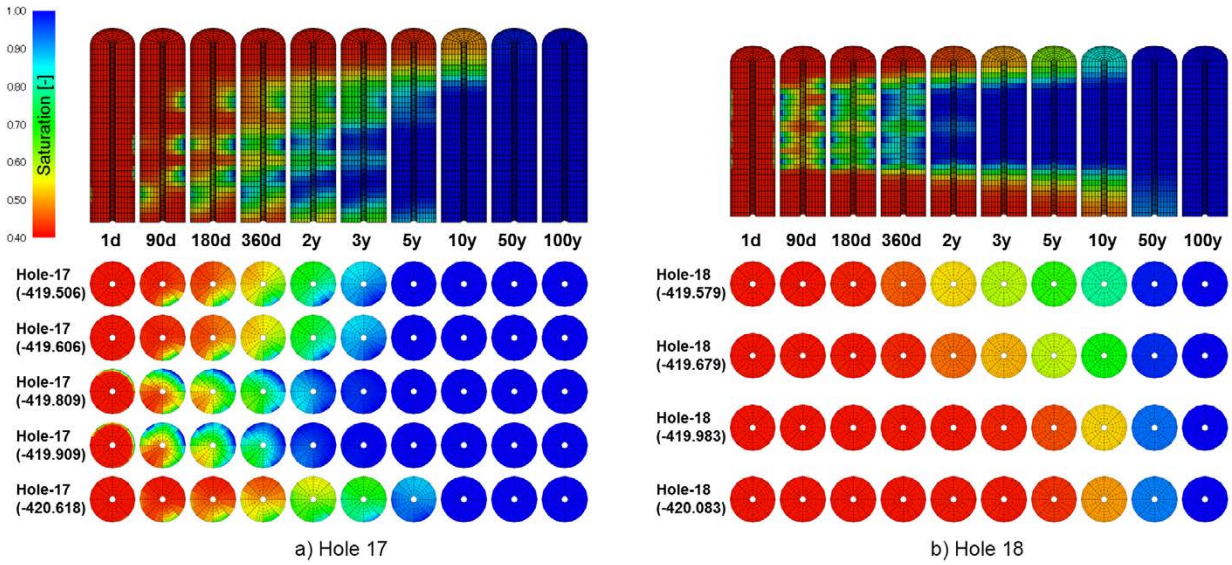

Figure 5-31. *Simulated bentonite saturation up to 100 years (Realisation number: 450). Upper: cross section along tunnel axis, Lower: horizontal section at specified depths.*

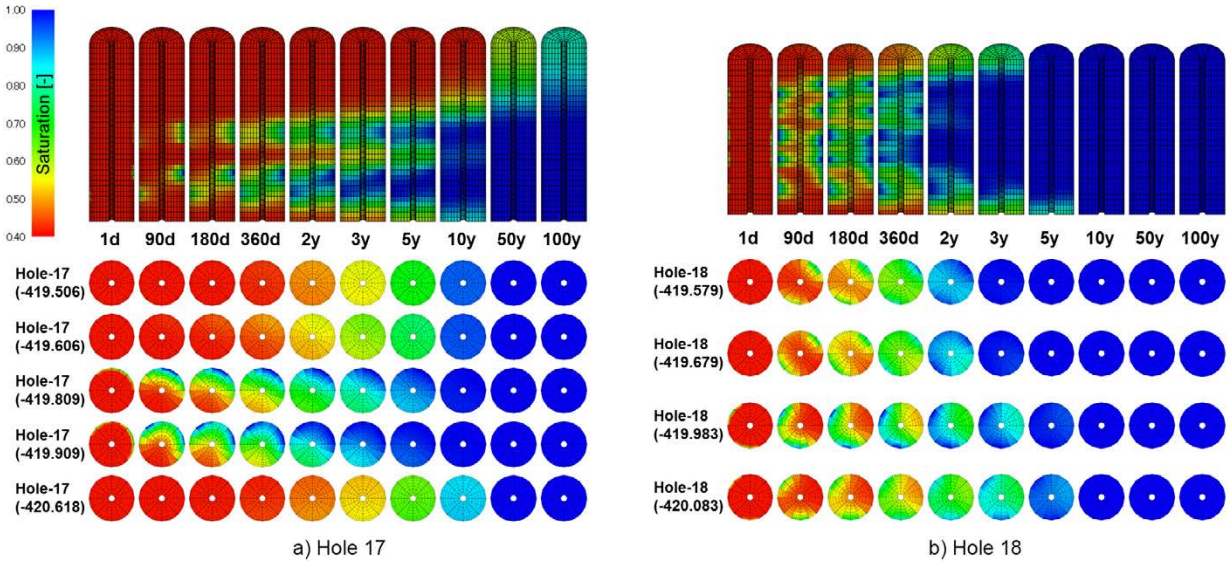

Figure 5-32. *Simulated bentonite saturation up to 100 years (Realisation number: 567). Upper: cross section along tunnel axis, Lower: horizontal section at specified depths*

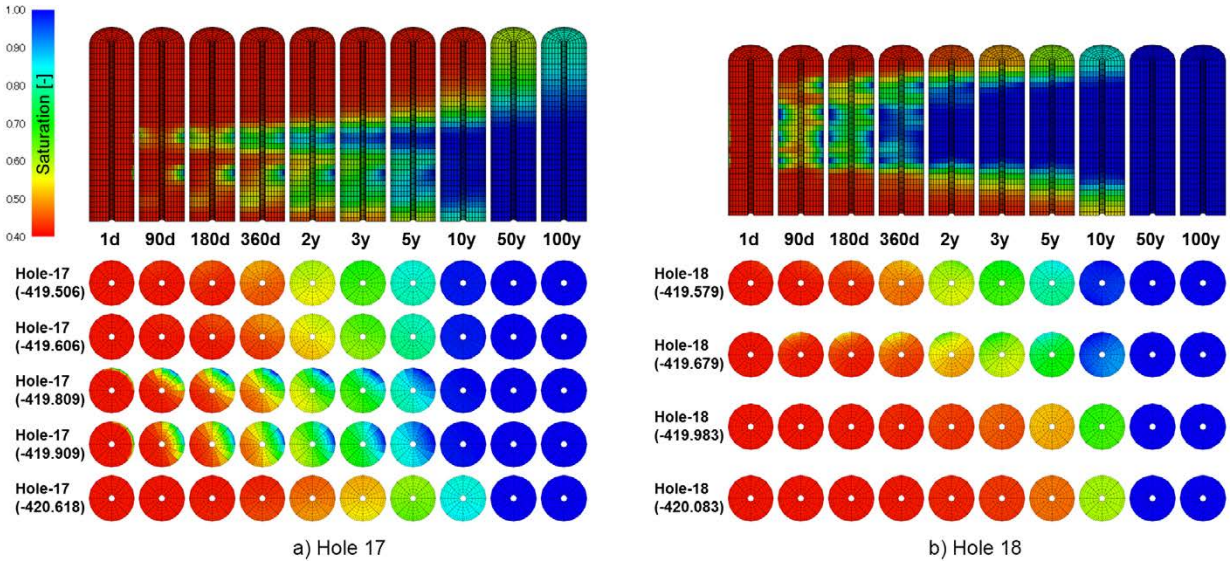

Figure 5-33. *Simulated bentonite saturation up to 100 years (Realisation number: 896). Upper: cross section along tunnel axis, Lower: horizontal section at specified depths.*

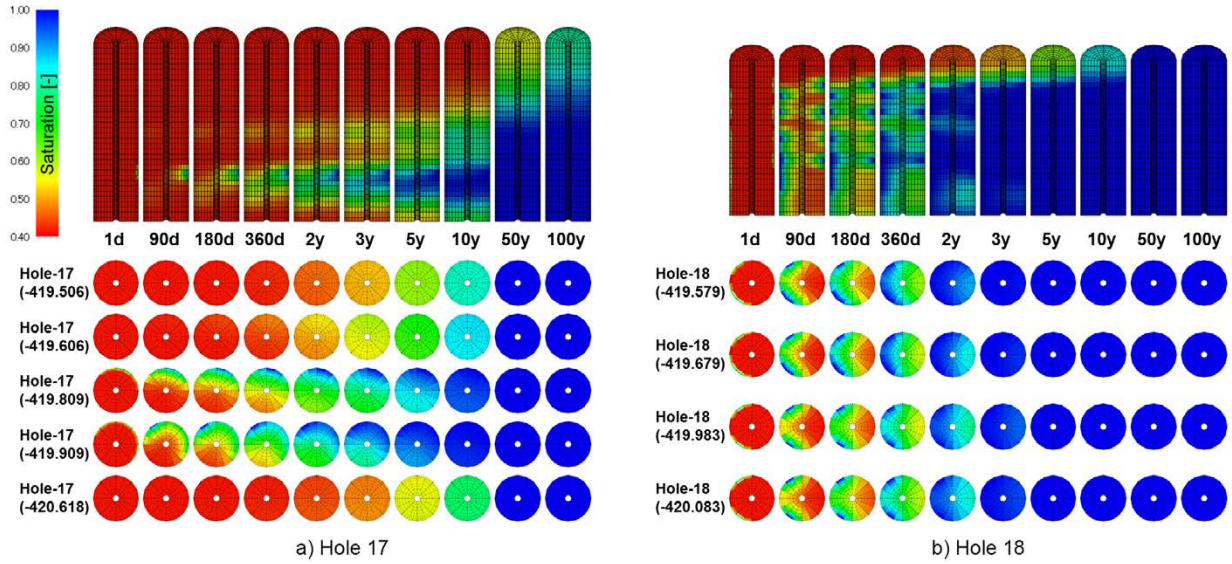

Figure 5-34. *Simulated bentonite saturation up to 100 years (Realisation number: 898). Upper: cross section along tunnel axis, Lower: horizontal section at specified depths.*

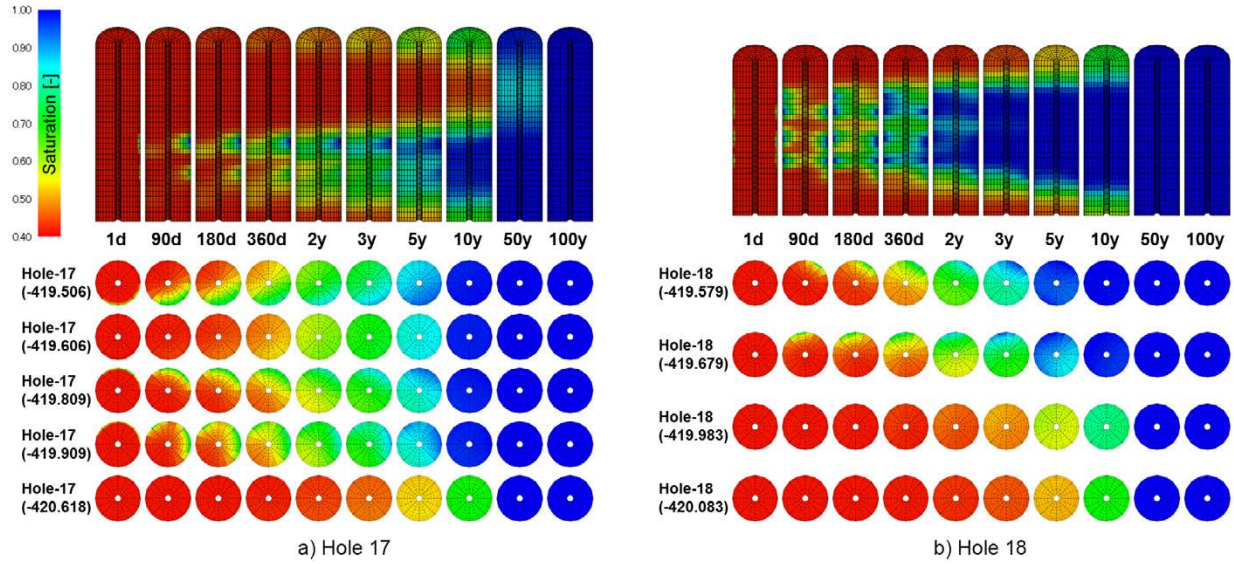

Figure 5-35. *Simulated bentonite saturation up to 100 years (Realisation number: 949) Upper: cross section along tunnel axis, Lower: horizontal section at specified depths.*

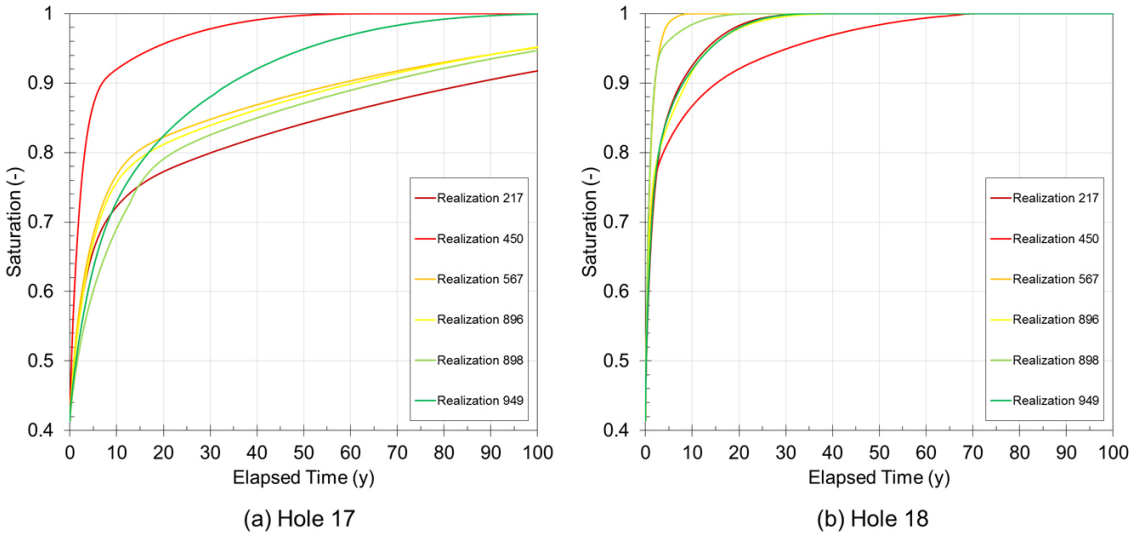

Figure 5-36. *Evolution of saturation of whole bentonite columns for six realisations.*

5.5 Discussion

The Thames simulation with heterogeneous groundwater flow calculation in rock provided a good match to BRIE observations of heterogeneous wetting behaviour in the bentonite column emplaced in Hole17 and Hole18 for these DFN realisations. As described in Section 5.4, the heterogeneous wetting behaviour in bentonite column might be fully affected by location and orientation of the fractures interconnecting to the bentonite columns, and their hydraulic connectivity which controls available water supply to the bentonite columns. Further conditioning was carried out to examine the sensitivity of HydroDFN parameters for bentonite wetting. The sensitivity of these factors was examined for Hole 18 by a single realisation of the model (realisation number 567) as a case study. Figure 5-37 shows the fractures intersecting to Hole 18, before and after the model modification. From Figure 5-13(c), the lowest fracture intersecting to Hole 18 should be removed to reproduce "Bentograph" features as shown in Figure 5-13(g). The model modification was made as shown in Figure 5-37 (b). The heterogeneous wetting behaviour at surface and vertical cross-sectional view of the bentonite column Hole 18 was compared between before and after the model modification of the model, as shown in Figure 5-38. Removing the fracture intersecting to the lower part of the bentonite column Hole 18 affected on the saturation behaviour of the bentonite column by vanishing the saturation part below the trace of deterministically defined fracture. It also influenced on the water supply to the bentonite through the deterministically defined fracture. Figure 5-39 shows the revolution of relative humidity at six sensor locations before and after the model modification of realisation number 567. Figure 5-40 shows the simulated water content distribution at the time of dismantling at the lower part of Hole 18, compared with the measured data. They indicate that the relative humidity and water content around the relative humidity sensor were significantly reduced by modifying the model. The further model modification was made as a case study. To improve reproducibility of measured relative humidity, the ability of the water supply through the deterministically defined fracture was changed by enlarging radius from 0.5 m to 1.0 m and moving 20 cm downward, without having any justifications. Figure 5-41 shows the simulation results of the further modified model. Relative humidity revolutions at six sensor locations were improved by enlarging fracture radius and adjusting location of the fracture.

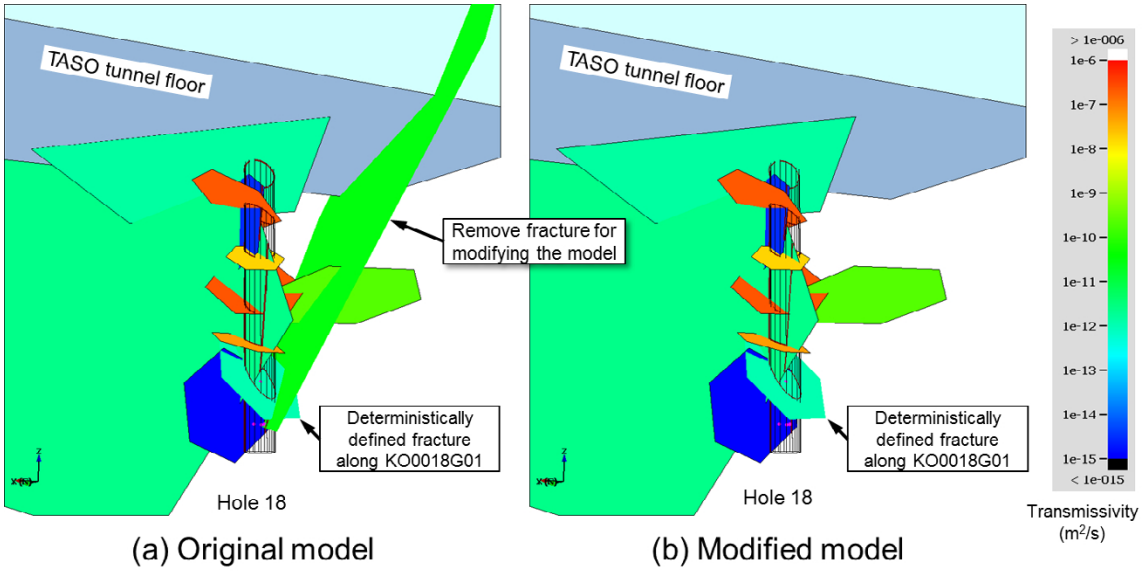

Figure 5-37. *Fractures intersecting to Hole 18 (realisation number 567). Pink dot: location of relative humidity sensors.*

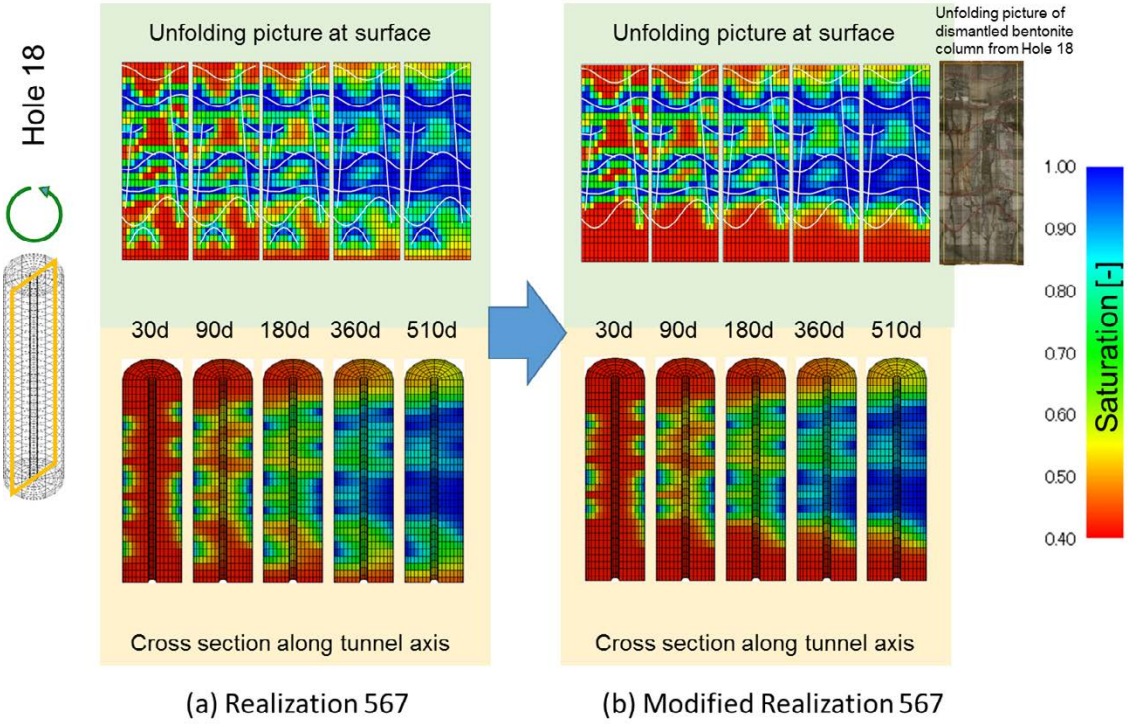

Figure 5-38. *Comparison of simulated saturation between before and after the modification of the model.*

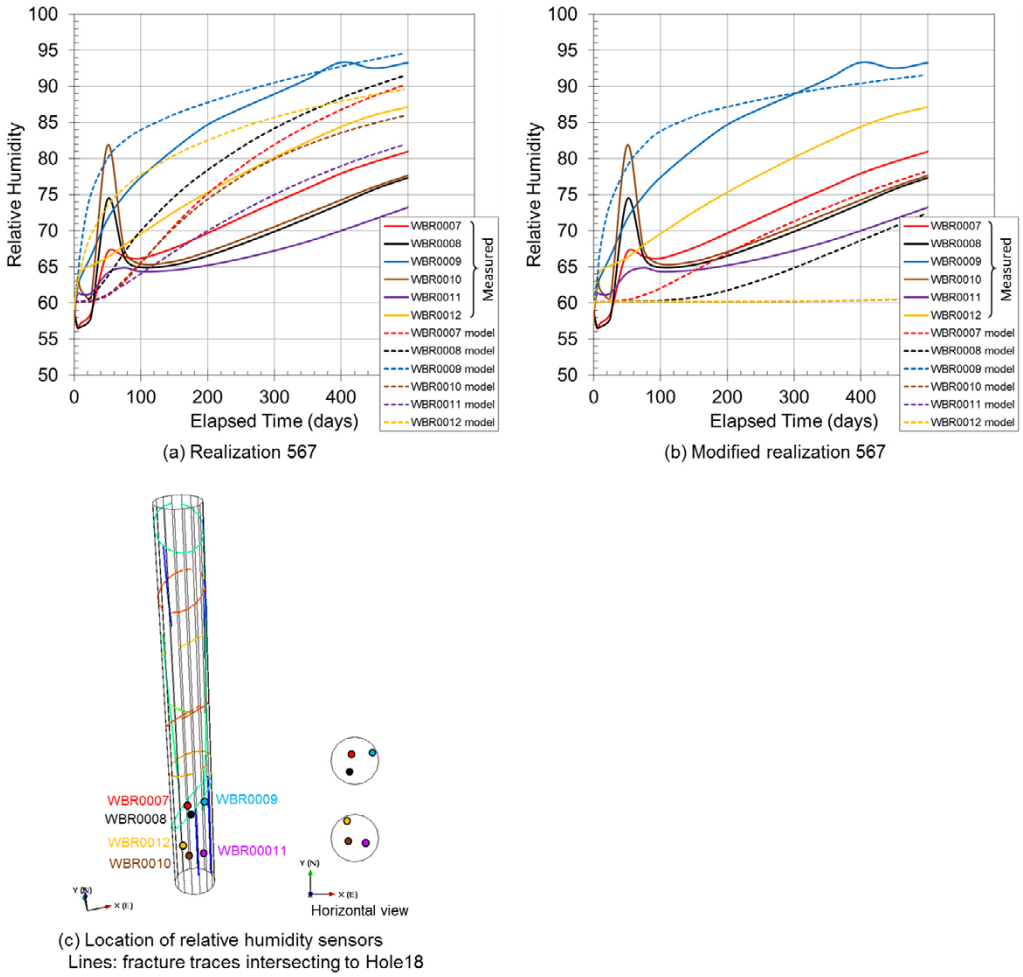

Figure 5-39. *Evolution of relative humidity at six sensor locations between before and after the modification of the model.*

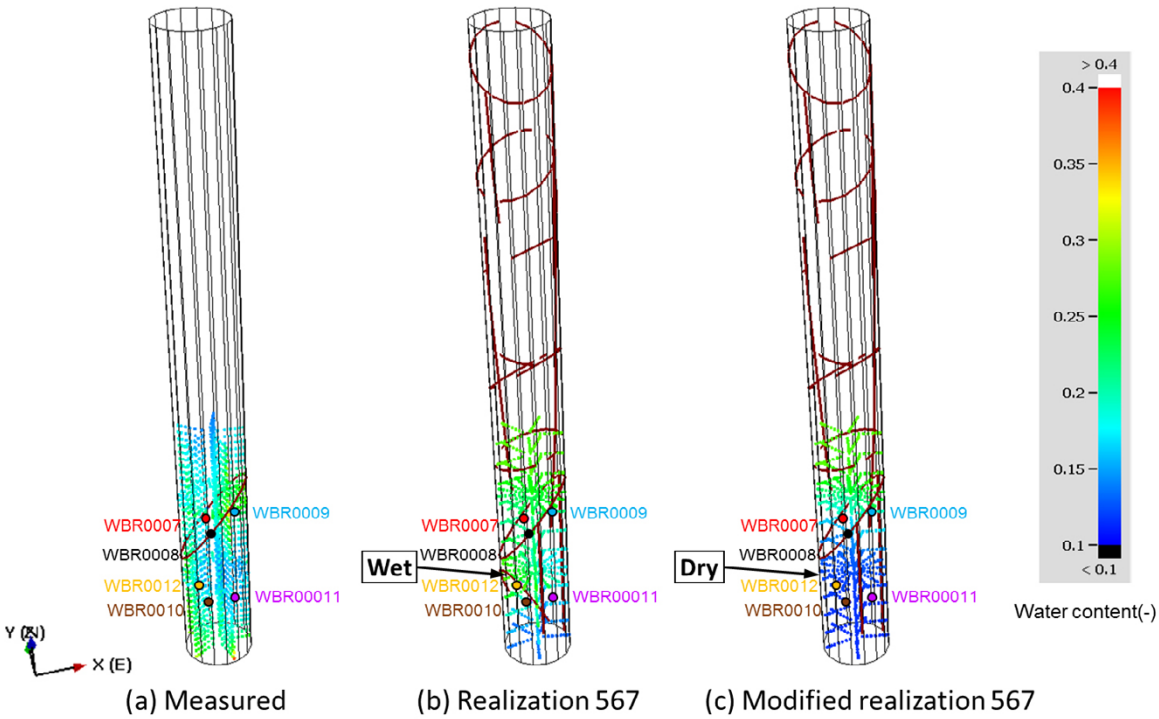

Figure 5-40. *Water content distribution at the bottom part of Hole18, comparison among measured, original model and modified model. Brown lines: fracture traces intersecting to Hole 18.*

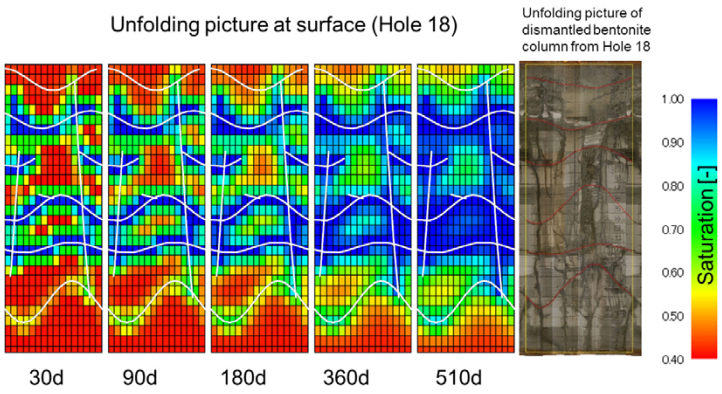

(a) Saturation distribution of bentonite surface

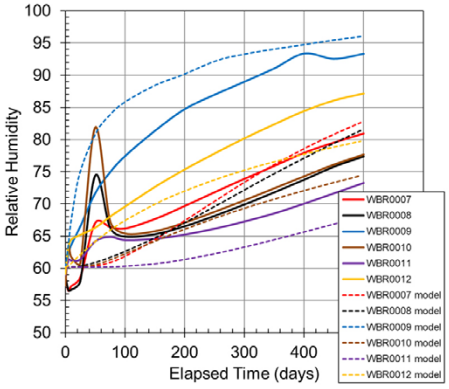

(b) Evolution of relative humidity

Figure 5-41. *Simulation results after the further model modification of realisation 567.*

Adjustment of the hydraulic connectivity and location of the intersecting fractures obtained an improved match to the measured heterogeneous bentonite wetting. This indicates that the hydraulic connectivity and location of the intersecting fractures can have a significant influence of the heterogeneous wetting distribution of the bentonite columns. In order to reproduce local scale heterogeneous wetting behaviour in bentonite as shown by the data of relative humidity sensor and water content, the location and the hydraulic connectivity of the fractures potentially supplying water to bentonite and smaller scale hydraulic heterogeneity such as flow channeling in a single fracture might be required. For example, the heterogenous inflow measurement data along the fracture traces, head distribution within a fracture plane, and spatial aperture distribution might be useful for modelling such a smaller scale of heterogeneous flow behaviour.

5.6 Conclusions and Recommendations

In this section, hydrogeological model in the 40 m × 40 m × 40 m block region around the TASO tunnel was updated. One of the key assumptions in this study for Task 8 modelling was the assumption of a functional relationship between transmissivity and fracture size. The correlation parameter values between transmissivity and fracture size were calibrated to the data measured at the boreholes around the prototype repository tunnel during modelling for Task 8E (see Appendix A2). The variance of the lognormal distribution of transmissivity was also taken in account, in addition to a linear correlation between fracture radius and transmissivity. Another key piece of data used to condition the Task 8F HydroDFN was “Bentograph” features, the pattern of shading observed at the surface of the dismantled bentonite column, which was assumed to directly map the locations where fractures deliver ground-water to the bentonite. The fracture locations and orientations indicated by the Bentograph features

might be generally consistent with what was assumed based on borehole KO0018G01 data. This indicates that most of the geologically mapped fractures have the potential to provide groundwater to the bentonite even if their permeability is lower than the detection limit of the hydraulic investigation. Therefore, the data of location and orientation of geologically mapped fractures along five probe boreholes was applied for constraining the stochastic variability of the HydroDFN model. The transmissivity of fractures intersecting the probe boreholes was also constrained by specific capacity data measured along each of the five probe boreholes.

To quantify the uncertainty of the stochastic HydroDFN, one thousand realisations of the stochastic HydroDFN model were examined by the Darcy flow simulations. The simulated groundwater flow rate and pressure at the five probe boreholes were compared with BRIE measurements. The simulated flow rate and pressure from the one thousand realisations does cover the measured values, but distributes over a wide range. However, the simulated pressure and flow rate at the KO0014G01 hole from the one thousand realisations matches the measurements with a relatively narrower range. This might be due to the effect of the deterministically defined larger fracture, called wfracture01, located close to the borehole.

Six realisations were screened out from one thousand realisations of the simulation results, by two criteria, RMSE (root mean square error between simulated and measured) of 1) pressure values and 2) flow rates at all measured sections of the five probe boreholes. The selected six realisations were used for applied to the bentonite wetting simulations with Thames code. The results of bentonite wetting calculation were compared with measured data, the "Bentograph" picture of surface of the dismantled bentonite column from Hole 18, the evolution of relative humidity data measured by six sensors installed in each bentonite column, and the spatial distribution of water content measured by sampling of dismantled bentonite columns. In general, Thames provided a good match to BRIE observations of heterogeneous wetting behaviour in the bentonite column emplaced in Hole17 and Hole18 for this DFN realisation. Further conditioning was carried out to identify the sensitivity of HydroDFN parameters for bentonite wetting. Adjustment of the hydraulic connectivity and transmissivity of the intersecting fractures obtained an improved match to the measured heterogeneous bentonite wetting. This indicates that the hydraulic connectivity and transmissivity of the intersecting fractures might have a significant influence on the heterogeneous wetting distribution in the bentonite columns.

In summary, if the rock matrix has limited ability of water supply to the bentonite (very low permeability), which is smaller than bentonite water uptake capability, JAEA's FracMan-Thames DFN/Bentonite wetting simulation approach and the assumption of fracture dominated bentonite wetting appears to be able to provide a reasonable approximation to the observed heterogeneous bentonite wetting behaviour of BRIE. The location, orientation, transmissivity (flow capacity), and hydraulic connectivity of fractures intersecting to the bentonite column were shown to be the key parameters to model the heterogeneous wetting behaviour in bentonite. The geologically mapped fracture data along the boreholes was shown to be useful to constrain the stochastic HydroDFN model to reproduce the locations of bentonite wetting. However, a lack of data for the hydraulic connectivity and permeability of these mapped fractures caused an uncertainty of the model evaluation results, and the data was not enough to reproduce the local scale heterogeneous bentonite wetting behaviour as shown by the data of relative humidity sensors and water content. Based on our findings as described above, we would suggest that a systematic investigation at pilot holes, including both geological mapping of the fractures and also testing of the hydraulic properties of the low permeable fractures and their extent, by conducting the transient pressure tomography and directional ground penetration radar investigation of each intersecting fracture, might be required to get more practical prediction of heterogeneous wetting behaviour in bentonite, as observed in BRIE.

6 Summary and Conclusions

6.1 Summary and conclusion

An aim of Task 8 was to improve the knowledge of the bedrock-bentonite interface with regard to groundwater flow, mainly based on a set of data obtained by Bentonite Rock Interaction Experiment (BRIE) at Äspö HRL. JAEA developed an approach to Task 8 which considers the assumption that the discrete features dominate the delivery of groundwater to the bentonite columns emplaced into the vertically drilled boreholes from TASO tunnel floor, resulting in heterogeneous bentonite wetting behaviour. In this study, geological fractures which are larger radius than 0.25 m were assumed to be modelled. This assumption was implemented as a FracMan Discrete Fracture Network (DFN) model for groundwater flow. Due to the assumption, no permeable rock matrix was implemented. In general, the model simulations should require any kind of assumptions due to the less understanding of processes and/or properties, or the less available data for the object modelling. The careful comparison of the assumptions with the realistic conceptual model as listed in Table 1-1 might be helpful for the modelling work. And, it is important to proceed modelling work with considering causal relationship between the key modelling factors affecting on the simulation results and the assumptions applying for the modelling.

From the examination using simplified Task 8B model specification, a capability of newly developed simulation system implicitly coupling two codes, groundwater flow simulation code through DFN model (FracMan/MAFIC) and a thermo-hydro-mechanical coupling code for continuous porous media (Thames), could be demonstrated for both of heterogeneous flow through the fractures and groundwater movement in bentonite without any significant numerical oscillations, although pulse type pressure increase might be generated at the time of saturation at the bentonite surface. It was also confirmed that the system could simulate two major fundamental processes: the saturation time at the bentonite surface is controlled by availability of groundwater flow of fractures connecting to the bentonite, and groundwater flow rate through the interface is controlled by the groundwater diffusion behaviour in bentonite after being saturated at the bentonite surface.

Task 8C and Task 8D were the prediction of hydraulic condition at the probe boreholes and bentonite wetting behaviour by the hydrogeological structural model in the 40 m × 40 m × 40 m block region around the TASO tunnel. The effect of uncertainty of the HydroDFN model was mainly evaluated. The variability for simulated flow rate to the boreholes seemed to be wider among the stochastic realisations of the DFN model, even if constraining by the observed fracture locations and by the measured specific capacity. The prediction of flowing points and flow rate along the boreholes and/or tunnels would be one of the challenges because the flow rate might be very sensitive to the balance among the hydraulic properties, head distribution, and other conditions at the borehole such as unsaturated behaviour. However, location and hydraulic properties of the intersecting fractures which could provide groundwater might be enough to predict the wetting bentonite, based on this simulation system (assuming only the fracture could provide groundwater to the bentonite), under the BRIE condition. By coupling these HydroDFN models with groundwater movement simulation in the bentonite columns, the heterogeneous propagation of groundwater from limited number of flow points (fractures) could be reproduced. An evaluation of the heterogeneous distribution of the groundwater in the bentonite requires a quantity measuring the heterogeneity. The quantity was also taken into account for the measurement methods of BRIE by in-situ sensors and sampling after dismantling the bentonite columns. The spatial and time resolution for the measurement should be considered to discuss the heterogeneity. The discussion based on the quantity measuring the heterogeneity might be useful for the methodology development for the investigation and evaluation of the KBS-3 system.

The HydroDFN was updated by data obtained BRIE in Task 8F studies. The correlation parameter values between transmissivity and fracture size were calibrated to the data measured at the boreholes around the prototype repository tunnel. The variance of the lognormal distribution of transmissivity was also taken in account, in addition to a linear correlation between fracture radius and transmissivity. Another key piece of data used to condition the Task 8F HydroDFN was Bentograph features, the pattern of shading observed at the surface of the dismantled bentonite column, which was assumed to directly map the locations where fractures deliver groundwater to the bentonite. The fracture

locations and orientations indicated by the Bentograph features might be generally consistent with what was assumed based on borehole KO0018G01 data. This indicates that most of the geologically mapped fractures have the potential to provide groundwater to the bentonite even if their permeability might be lower than the detection limit of the hydraulic investigation. Therefore, the data of location and orientation of geologically mapped fractures along five probe boreholes was applied for constraining the stochastic variability of the HydroDFN model. The transmissivity of fractures intersecting the probe boreholes was also constrained by specific capacity data measured along each of the five probe boreholes.

To quantify the uncertainty of the stochastic HydroDFN, one thousand realisations of the stochastic HydroDFN model were examined by the Darcy flow simulations. The simulated groundwater flow rate and pressure at the five probe boreholes were compared with BRIE measurements. The simulated flow rate and pressure from the one thousand realisations does cover the measured values, but distributes over a wide range. Because, the HydroDFN model was generated based on the stochastic sampling from probability density functions of the fracture parameters, such as orientation, radius and transmissivity. To reduce the uncertainty of the HydroDFN, further data to constrain the local flow field is required. All stochastic realisations should be applied to the bentonite wetting simulations by the coupling between FracMan and Thames, to analyse the effect of heterogenous flow field of the stochastically distributed DFN model on the bentonite wetting behaviour. However, due to the time consuming, the limited number of the realisations were selected for the coupling simulations, to demonstrate the effect of the heterogenous flow field in rock on the bentonite wetting behaviour. Six realisations which could reproduce reasonable results comparing with measured data, were screened out from one thousand realisations of the simulation results, and they were examined for the bentonite wetting simulations with Thames code. The results of bentonite wetting calculation were compared with measured data, the Bentograph picture of surface of the dismantled bentonite column from Hole 18, the evolution of relative humidity data measured by six sensors installed in each bentonite column, and the spatial distribution of water content measured by sampling of dismantled bentonite columns. In general, Thames provided a good match to BRIE observations of heterogeneous wetting behaviour in the bentonite column emplaced in Hole17 and Hole18 for these HydroDFN realisations. Further conditioning was carried out to identify the sensitivity of HydroDFN parameters for bentonite wetting. Adjustment of the hydraulic connectivity and transmissivity of the intersecting fractures obtained an improved match to the measured heterogeneous bentonite wetting. This indicates that the hydraulic connectivity and transmissivity of the intersecting fractures can have a significant influence of the heterogeneous wetting distribution of the bentonite columns.

6.2 Comments and Recommendations

In summary, JAEA's FracMan-Thames DFN/Bentonite wetting simulation approach and the assumption of fracture dominated wetting appears to be able to provide a reasonable approximation to the observed heterogeneous bentonite wetting behaviour of BRIE. Bentonite wetting model and parameter values were verified by the water uptake test data. The location, orientation, transmissivity (flow capacity), and hydraulic connectivity of fractures intersecting to the bentonite column are uncertain, and the key parameters to model the heterogeneous wetting behaviour in bentonite. The geologically mapped fracture data along the boreholes was shown to be useful to constrain the stochastic HydroDFN model to model the locations of bentonite wetting. However, a lack of data for the hydraulic connectivity and permeability of these mapped fractures caused an uncertainty of the model evaluation results, and the data was not enough to reproduce the local scale heterogeneous bentonite wetting behaviour as shown by the data of relative humidity sensors and water content. Based on our findings as described above, we would suggest that a systematic investigation at pilot holes, including both geological mapping of the fractures and testing of the hydraulic properties of the low permeable fractures and their extent, by conducting the transient pressure tomography and directional ground penetration radar investigation of each intersecting fracture, might be required to get more practical prediction of heterogeneous wetting behaviour in bentonite, as observed in BRIE.

References

SKB's (Svensk Kärnbränslehantering AB) publications can be found at www.skb.com/publications. SKBdoc documents will be submitted upon request to document@skb.se.

Bear J, 1972. Dynamics of Fluids in Porous Media. Mineola NY: Dover Publications.

Chijimatsu M, Fujita, T, Kobayashi A, Nakano, M, 2000. Experiment and validation of numerical simulation of coupled thermal, hydraulic and mechanical behaviour in the engineered buffer materials. International Journal for Numerical and Analytical Methods in Geomechanics, 24, 403–424.

Dershowitz W, Lee G, Josephson N, 2007. FracMan Interactive Discrete Feature Data Analysis, Geometric Modelling, and Exploration Simulation. User Documentation, Version 7. Seattle, WA: Golder Associates, Inc.

Fransson Å, Åkesson M, Andersson L, 2017. Bentonite Rock Interaction Experiment Characterization of rock and installation, hydration and dismantling of bentonite parcels. SKB R-14-11 Svensk Kärnbränslehantering AB.

Johannesson L-E, 2014. Prototype Repository. Measurements of water content and density of the retrieved buffer material from deposition hole 5 and 6 and the backfill in the outer section of the Prototype Repository. SKB P-13-14, Svensk Kärnbränslehantering AB.

Miller I, Lee G, Dershowitz W, 2001. MAFIC, Matrix / fracture interaction code with head and solute transport, User documentation, version 2.0. Redmond, WA: Golder Associates, Inc.

Philip J R, de Vries D A, 1957. Moisture movement in porous material under temperature gradients. Eos Transactions American Geophysical Union, 38, 222–232.

Remy N, Boucher A, Wu J, 2009. Applied Geostatistics with SGeMS: A User's Guide. Cambridge: Cambridge University Press.

Sawada A, Uchida M, Shimo M, Yamamoto H, Takahara H, Doe T W, 2000. Non-sorbing tracer migration experiments in fractured rock at the Kamaishi Mine, Northeast Japan. Engineering Geology, 56, 75–96.

SKB, 2011. Long-term safety for the final repository for spent nuclear fuel at Forsmark Main report of the SR-Site project. SKB TR-11-01, Svensk Kärnbränslehantering AB.

Stigsson M, Outters N, Hermanson J, 2001. Äspö Hard Rock Laboratory, Prototype Repository Hydraulic DFN Model no:2. SKB IPR 01-39, Svensk Kärnbränslehantering AB.

Vidstrand P, Stigsson M, Åkesson M, Fransson Å, 2017. SKB Task Forces EBS and GWFTS, Modelling the interaction between engineered and natural barriers, A compilation of Task 8 descriptions. SKB P-16-05, Svensk Kärnbränslehantering AB.

Appendix

A1 Verification by Water Uptake Experiment

The water-uptake test was a laboratory test, which was performed on bentonite blocks with the same MX-80 bentonite and the same radial dimensions and density as in the field experiment, BRIE. The objective of the test was to provide experimental data of hydration behaviour in the bentonite blocks under the well-controlled condition in the laboratory (Vidstrand et al. 2017).

The bentonite blocks were installed in steel cylinders as shown in Figure A-1. A plastic filter was mounted on the inside of the cylinder which facilitated a free access of water along the circumference of the block. The cylinder and the top lid were equipped with sensors for measurement of total pressure and relative humidity. Three tests were performed:

i) with free access of water during ~ 203 days,

ii) with free access of water during ~ 107 days, and

iii) with the access of water limited to an initial filling of the outer slot and left to equilibrate during ~ 100 days.

Three sets of experimental results were obtained:

i) evolutions of the cumulative water uptake,

ii) evolutions of the relative humidity at two points, and

iii) profiles of degree of saturation along radial direction.

These data were used for verifying the numerical simulation code, Thames, applying to calculate bentonite wetting process for BRIE.

The water uptake test was modelled with Thames as a hydraulic problem. The axis symmetrical model was made for representing the 1/16 of circular bentonite block as shown in Figure A-2. A trapezoidal shape of the numerical model was discretised into the finite elements. Same spatial resolution along the cylindrical axis of the bentonite as the model for the BRIE (see Figure 3-6), except for the size of first layer from the outer side which was changed from 7 mm to 5 mm for adjusting to the initial water balance as described below, was applied. Same thickness as the bentonite block, 100 mm was set to the thickness of each element. The width of each element was changed according to the distance from centre of the bentonite block. The homogeneous single constant porosity (44 %) was set for all elements. The initial condition of saturation (42 %) corresponding to an initial suction value of 89.9 MPa based on the retention curves was applied for the bentonite block except for the outer 5 mm of the model. The initial water filling of the outer slot (1 mm of clearance between bentonite block and test cylinder) was considered by applying water saturated conditions from the start in the outer 5 mm of the model (corresponding to an additional water volume of 0.12 litres for a thickness of 10 cm) as specified. The liquid pressure at the outer boundary was kept constant at an atmospheric level (0.1 MPa). The other faces of the model, inner, top, bottom and sides were specified as no flow boundary. The calculation was made under the isothermal condition at 20 °C. Parameter values used for Thames calculation of water uptake experiment are summarised in Table A-1.

The calculation results were compared with the experimental data, as shown in Figure A-3. In general, the model results are in good agreement with the measured data. The detail comparison is discussed below.

The water uptake was evaluated as the flow rate for the entire circumference by multiplying 16 to correct value calculated by 1/16 axis symmetrical model of circular bentonite block. Moreover, an initial inflow 0.2 litres was added to the calculated water uptake value (0.08 litres representing the filter volume, and 0.12 litres volume of the outer slot). As shown in Figure A-3 (a), the calculated water uptake is identical with the experimental result.

The relative humidity at the radii 40, 80 and 120 mm from the centre of the circular bentonite block are shown in Figure A-3 (b). The model could reproduce the similar distribution of the relative humidity as measured. At outer point (0.12 m) was very identical to measured. However, at middle point (0.08 m) and inner point (0.04 m), model seems to slightly overestimate than measured.

The degree of saturation profiles at 107 and 203 days are compared in Figure A-3 (c). The model calculation results in the range of measured saturation except for an outer part at 107 day, where model calculation result is slightly larger than measured data.

(a) Test cylinder

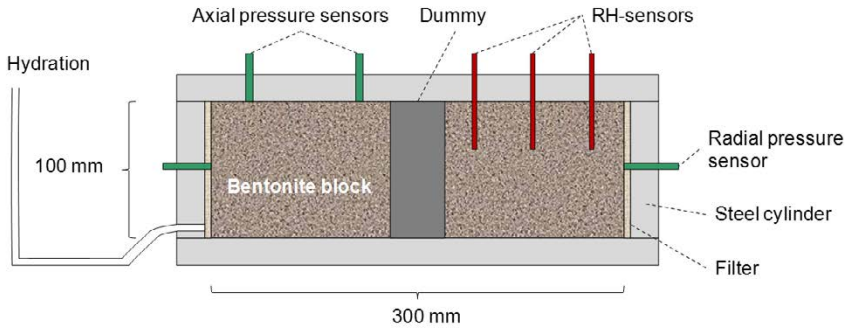

(b) Conceptual illustration of water uptake experiment

Figure A-1. *Setup of water uptake experiments.*

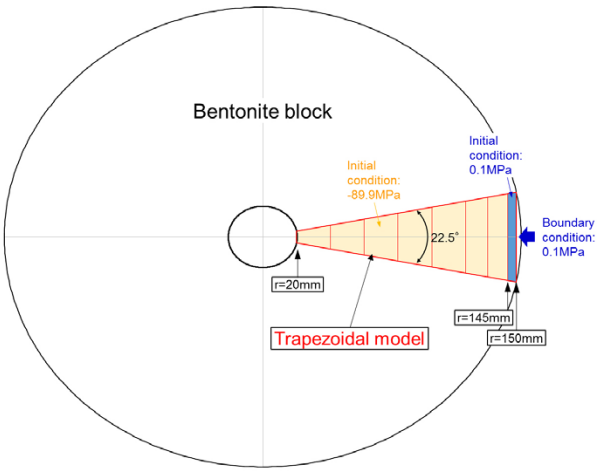

(a) Horizontal sectional view of bentonite

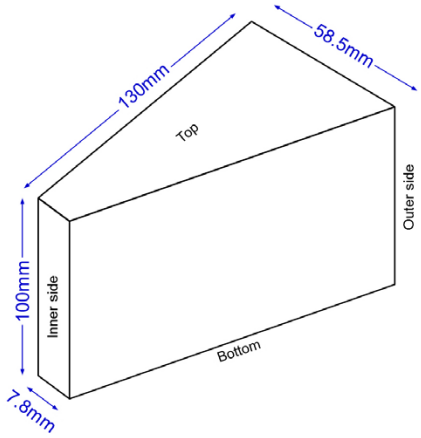

(b) Bird's-eye view of trapezoidal block and cylindrical model region shape of the numerical model

Figure A-2. *Conceptual illustration of the model.*

Table A-1. Parameter values used for Thames calculation of water uptake experiment.

Parameter	Unit	Value
Porosity	-	0.44
Intrinsic permeability	m^2	6.4×10^{-21}
Relative permeability, k_r	-	$k_r = S_l^3$ S_l: water saturation
Water retention curve		van Genuchten's equation $S_l(P_l) = \left\{1 + \left(\frac{P_g - P_l}{P_0}\right)^{\frac{1}{1-\lambda}}\right\}^{-\lambda}$ P_l: water pressure P_g: Gas pressure: 0.1MPa P_0: empirical constant: 10MPa λ: empirical constant: 0.28
Water density	kg/m^3	1 000
Water viscosity	Pa s	0.001
Initial Saturation	%	42
Temperature	°C	20

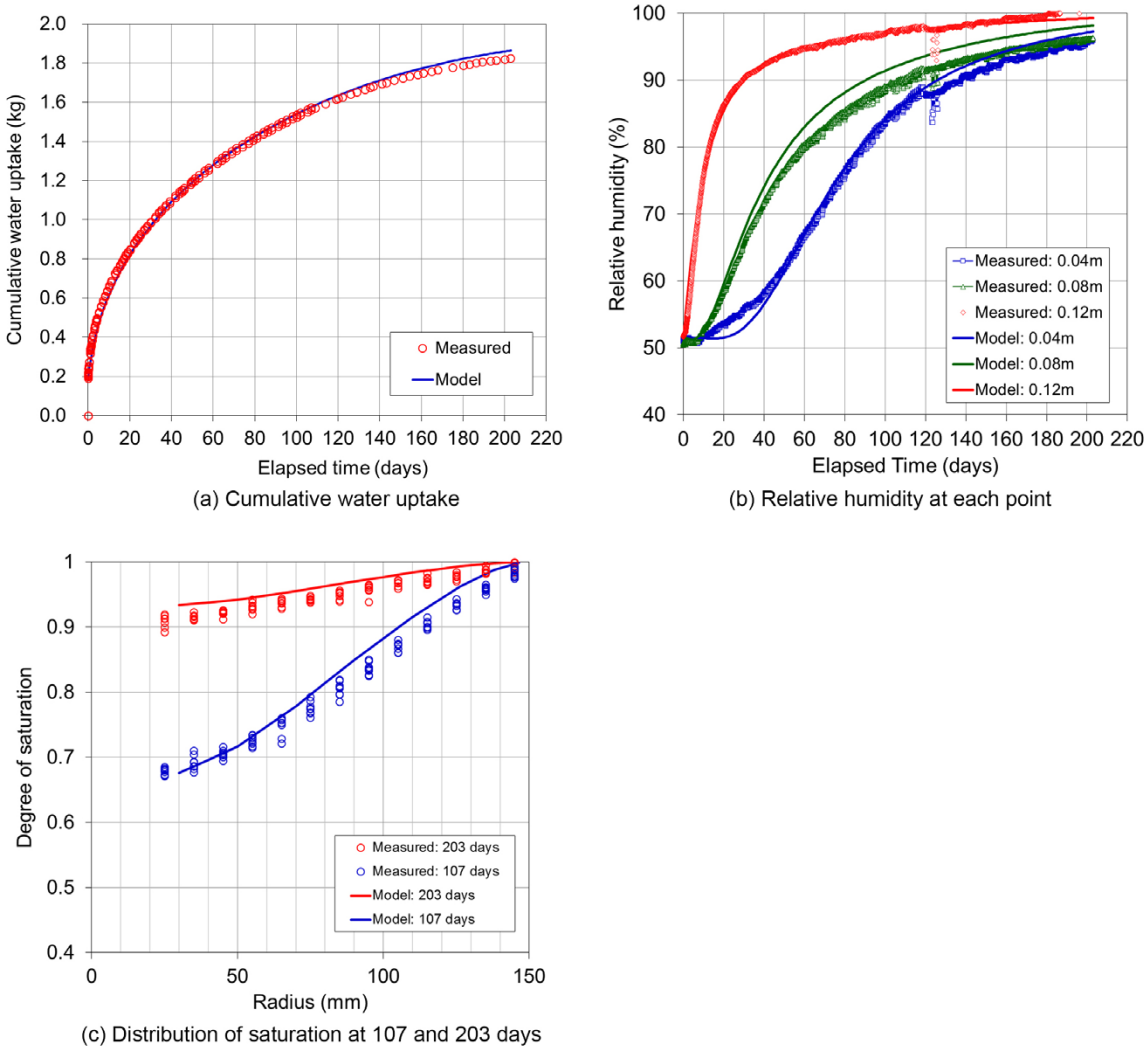

(a) Cumulative water uptake

(b) Relative humidity at each point

(c) Distribution of saturation at 107 and 203 days

Figure A-3. *Comparison between numerical model calculations and experimental results.*

A2 Simulation of Prototype Repository Project

A2.1 Introduction

This sub-task was defined as an extend sub-task of Task 8, called “Task 8E”, concerning predictions of deposition hole interactions as part of modelling the Prototype Repository Project (Vidstrand et al. 2017). The Prototype Repository was located at 450 m depth in the Äspö HRL (Figure A-4), and simulated a part of a KBS-3 nuclear waste repository. The aim of the Prototype Repository was to demonstrate the integrated function of the repository components and to provide a full-scale reference for comparison with models and assumptions. The Prototype Repository was designed, constructed and tested, to the extent possible, to simulate the real deep repository system regarding preparations, machinery for installation and deposition, geometry, materials, and rock environment.

The Prototype Repository Tunnel (TADSA), 65 m long and 5 m in diameter, was excavated using a Tunnel Boring Machine (TBM). Six full-scale vertical deposition holes, 8.37 m deep and 1.75 m in diameter, were bored in the TADSA tunnel. The Prototype Repository consisted of two sections (Figure A-5). The installation of section 1 of the Prototype Repository was made during summer and autumn 2001 and section 2 was installed in spring and summer 2003.

Task 8E was primarily intended to be a hydrogeological model with coupled heat transport along with the calculation of saturation behaviour of bentonite in the deposition holes and backfill in the tunnel. The major differences from BIRE are 1) actual scale of the deposition holes, and 2) thermal road by the heated overpack. The calculation system developed for the simulation of BRIE should be up-scaled to the actual scale of the multiple deposition holes with a tunnel above the holes filled by the backfill materials, and be modified to take account of the thermal effect coupling with hydration process in the bentonite.

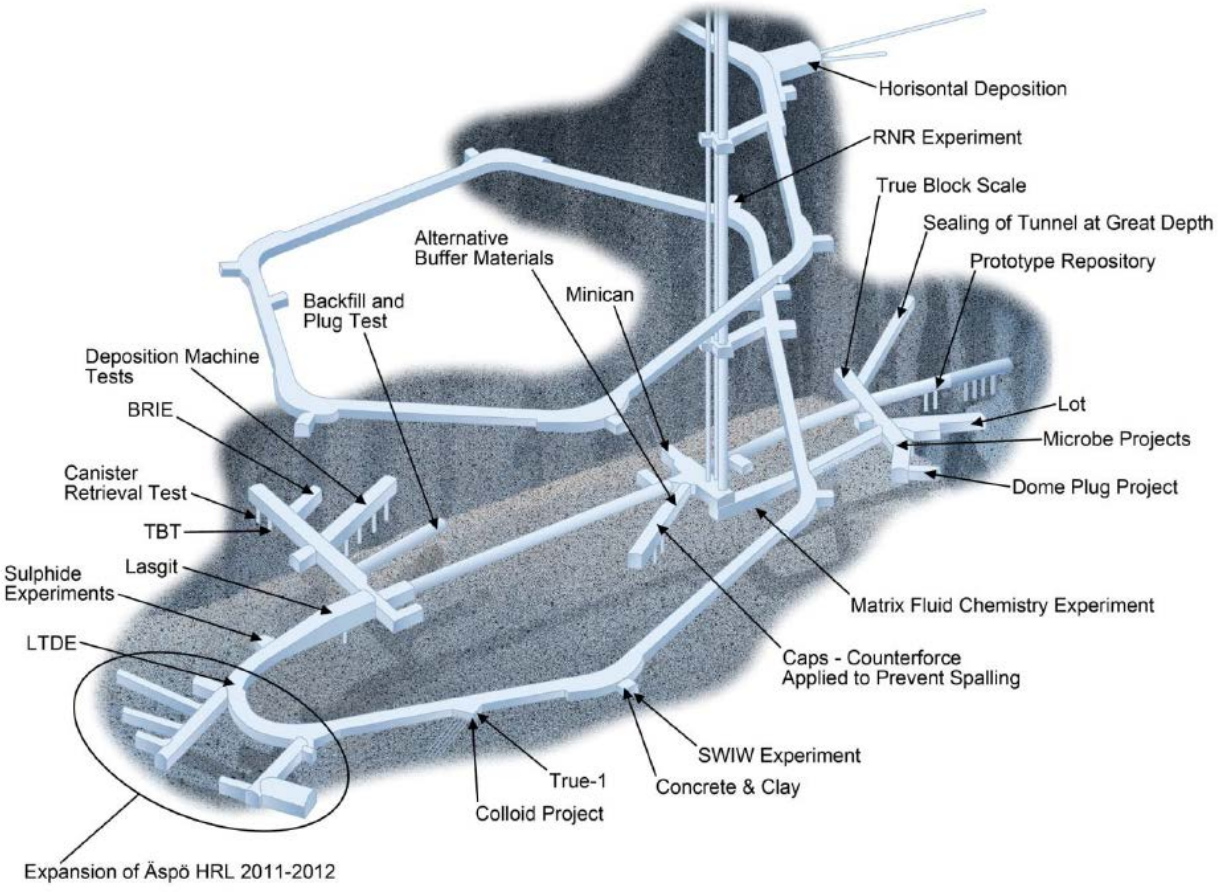

Figure A-4. *Illustration of the Äspö HRL and location of Prototype Repository Project.*

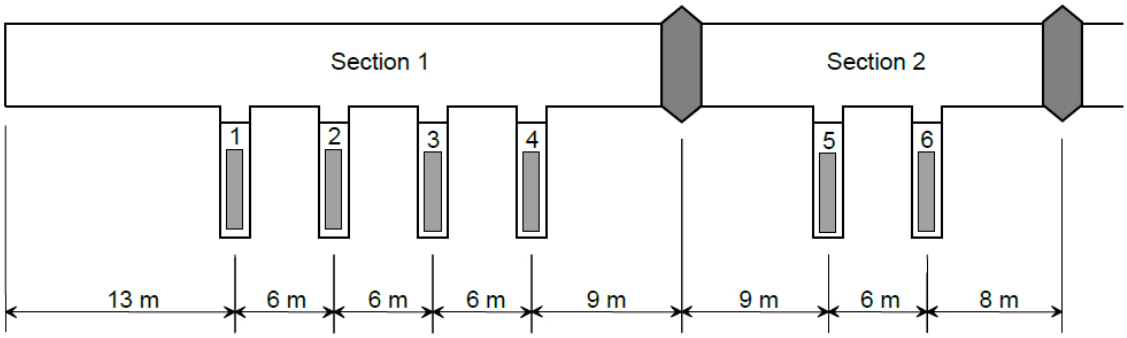

Figure A-5. *Schematic view of the Prototype Repository.*

Hydraulic boundary conditions were provided from a regional scale hydrogeological model which in part uses the same large-scale geometrical framework as supplied in Task 8C and 8D. Geometrical specifications, along with a site-specific geological structure model were given as CAD data. The same stochastic fracture statistics given as intensity, size and orientation were intended to be applied.

Hydrogeological Model in Rock

The modelling region was specified as 150 m × 150 m × 100 m block as shown Figure A-6. The Prototype Repository Tunnel was located at the centre of the modelling region.

The same stochastic fracture sets (three sets) defined as listed in Table 3-2 were applied to represent the back ground geological DFN model. The hydraulic properties of the geological DFN model were calibrated by the heterogeneous transmissivity distribution measured around Prototype Repository Tunnel as shown Figure A-7 and Figure A-8. The measured transmissivity shows a relatively wide distribution ($10^{-11} \sim 10^{-6}$ m^2/s). The calibration was made by simulating the virtual hydraulic tests at four boreholes (Figure A-9) which were oriented parallel to those in which packer tests conducted. The virtual hydraulic tests were conducted under the simplified condition: constant head boundary condition at outer boundary (0 m) and at each water injecting borehole (1 m), and no flow boundary condition at the tunnel walls. The steady state flow simulations were made for each injecting borehole, respectively. From the calculated flow rate injecting to the borehole, Q (m^3/s) the transmissivity, T (m^2/s), at each injecting borehole was evaluated by the Thiem's equation.

$$T = \frac{Q}{\Delta h}\frac{\ln(R_{outer}/r_{hole})}{2\pi}$$

where R_{outer} is the radius of the outer boundary (m), r_{hole} is the borehole radius (m) and Dh is the hydraulic head difference (1 m). Assuming a radius of outer boundary R_{outer} = 30 m, and the borehole radius r_{hole} = 0.038 m, ln(R/r)/2p is close to 1. Then, T is approximately equivalent to the specific capacity (Q/Dh) (Sawada et al. 2000). A set of 100 realisations of the stochastic DFN model was used to obtain a simulated transmissivity distribution, and the calibration was made by adjusting the correlation parameters to improve the match between simulated and measured hydraulic tests (Figure A-10). The calibrated correlation between fracture size and transmissivity is described in the following equation:

$$T = \text{lognorm}(\mu, \sigma^2) \times r^{4.7}$$

where T is transmissivity, lognnorm(m, s^2) is lognormal distribution with average m = 1×10^{-13}, and standard deviation s^2 = 3×10^{-13}, r is fracture radius. The random variables of the lognormal distribution were also taken in account, in addition to a liner correlation to fracture radius. An example of the calibrated correlation between fracture radius and transmissivity is shown in Figure A-11. The resulting conditioned HydroDFN model as shown in Figure A-12 has a relatively wider distribution of the fracture transmissivity, when compared to the reference HydroDFN model used to Task 8C and 8D (Figure 3-4).

The HydroDFN was also updated by implementing deterministically defined fractures (DDFs) to constrain the stochastic DFN model to measured fracture trace maps. The fracture traces implemented deterministically were those with a FPI (Full Perimeter Intersection: which means fracture that intersects the full tunnel perimeter), which is one of the indicators of the relatively larger fracture (SKB 2011). Figure A-13 (a) shows the fracture trace map observed at the Prototype Repository Tunnel and the deposition holes. Figure A-13 (b) shows the selected FPI traces at each tunnel and deposition hole.

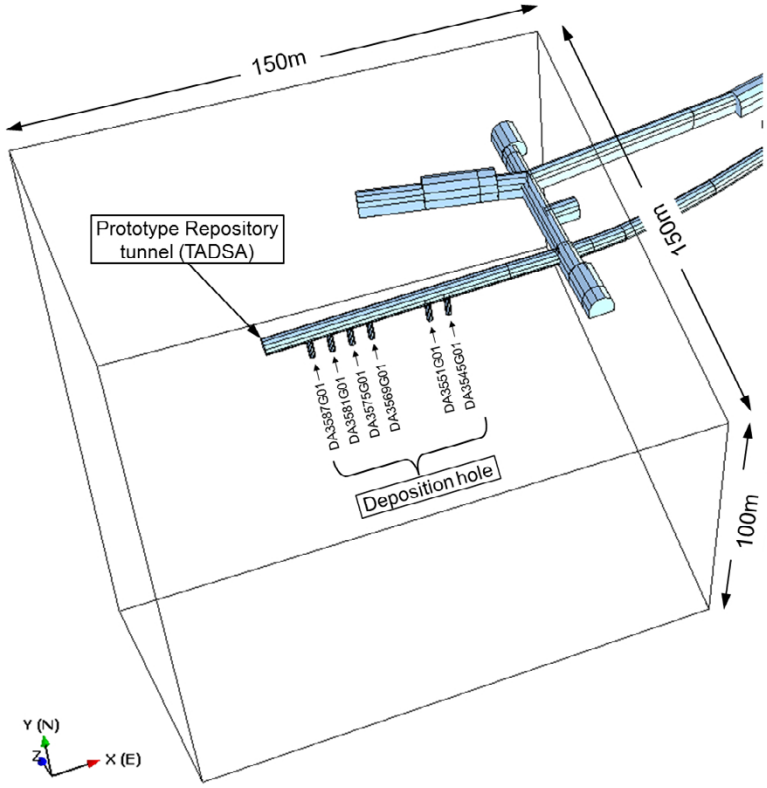

Figure A-6. *Task 8E modelling region and tunnels.*

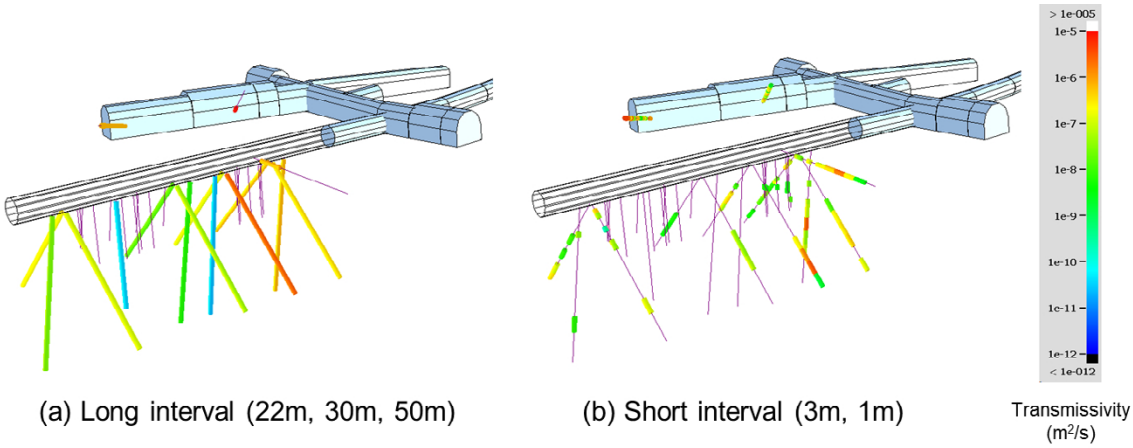

Figure A-7. *Spatial distribution of transmissivity measured by packer test around Prototype Repository Tunnel.*

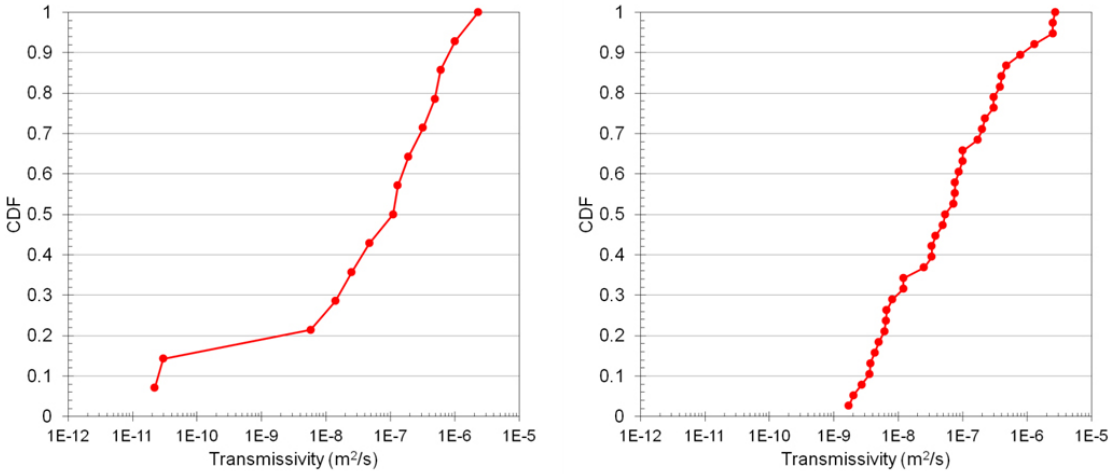

Figure A-8. *Cumulative transmissivity distribution measured around Prototype Repository Tunnel.*

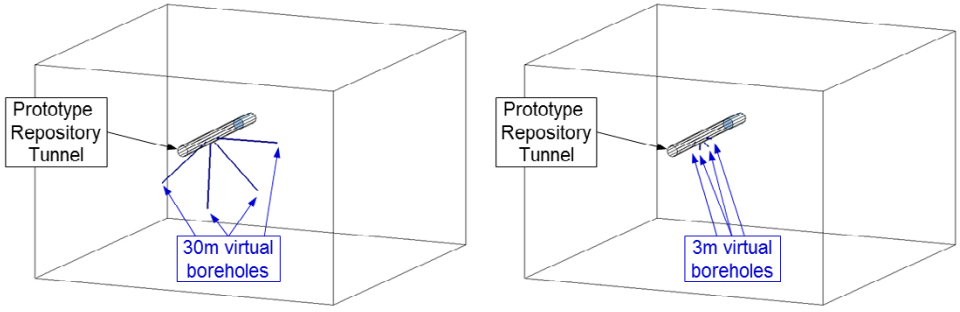

Figure A-9. *Four different direction of virtual boreholes for both 30 m and 3 m intervals of packer section.*

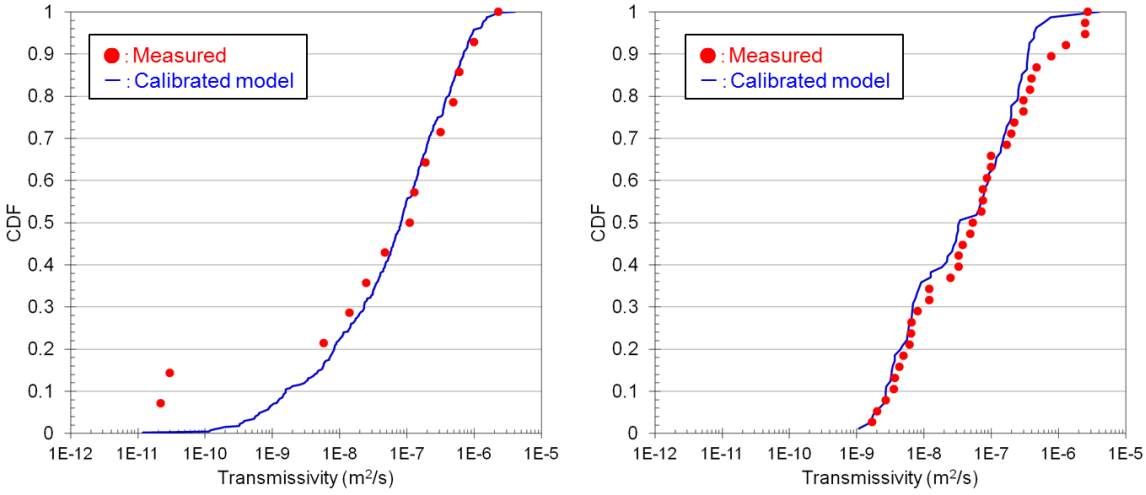

Figure A-10. *Comparison between the calibrated model results and measured transmissivity (Cumulative distribution).*

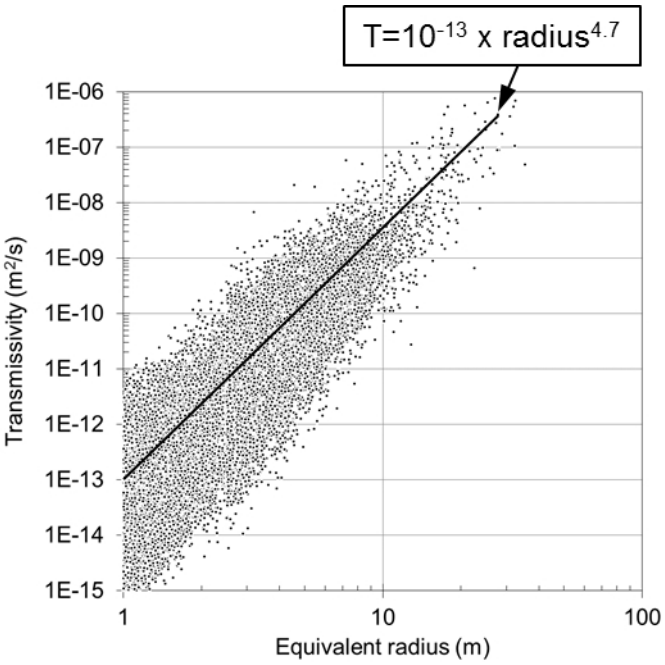

Figure A-11. *An example of correlation between fracture radius and transmissivity calibrated for Task 8E.*

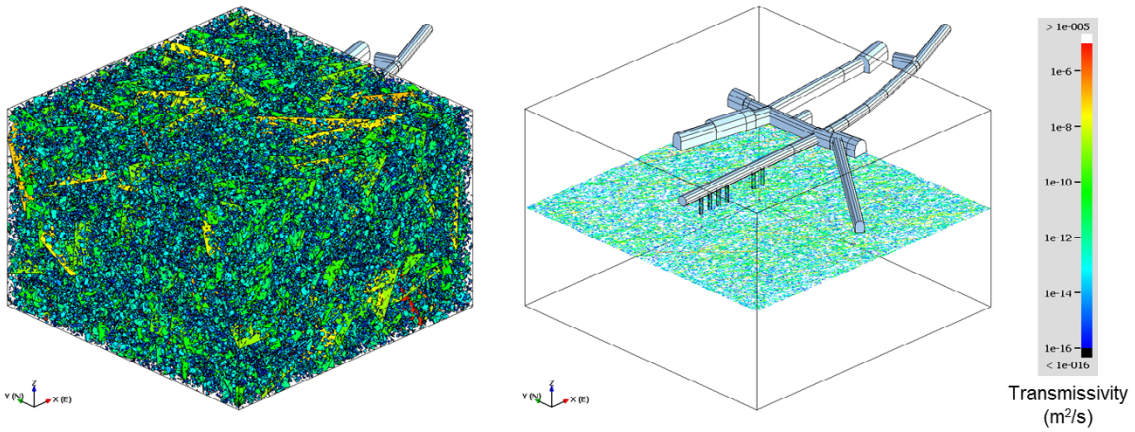

Figure A-12. *An example of HydroDFN model calibrated for Task 8E.*

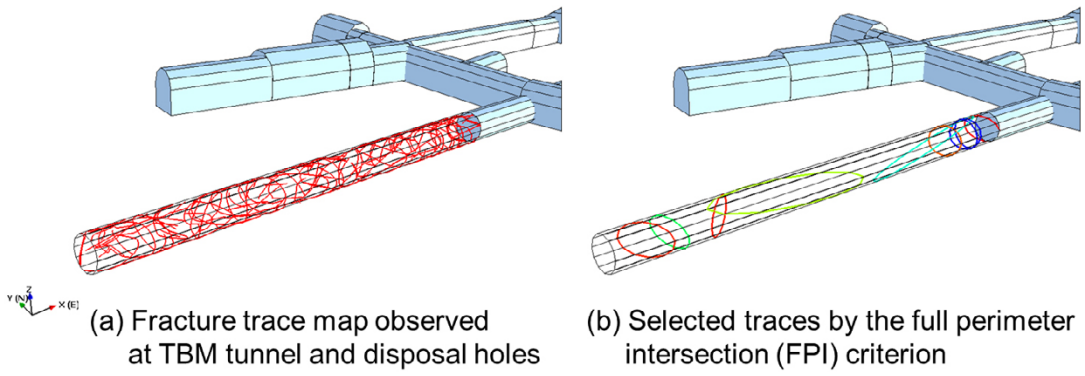

Figure A-13. *Fracture trace map observed at Prototype Repository Tunnel and deposition holes.*

The FPI fractures observed at Prototype Repository Tunnel wall were assumed to be large enough to be extended to model boundary as shown in Figure A-14 (a). Nine deterministically defined large fractures (No.1~9) identified by the FPI at Prototype Repository Tunnel were modelled. Total number of FPI fractures observed at the deposition holes was 25, and the radius of them was assumed to be 3.5 m in order to avoid direct connection of these fractures to the adjacent holes. The transmissivity of the nine deterministically defined large fractures were estimated from the packer test data observe along the boreholes which intersect to the around the Prototype Repository Tunnel as shown in Figure A-15 through Figure A-23. No short interval hydraulic test was performed along the deposition holes (including the pilot boreholes before excavating the deposition holes) to estimate transmissivity of each deterministically defined fractures at the deposition holes, although the detailed scale of hydraulic investigation should be required for evaluating the heterogeneous groundwater flow behaviour in fractured rock vicinity of the deposition hole. The transmissivity measured along the pilot boreholes before excavating the deposition holes were divided equally among the deterministically defined fractures intersecting the deposition holes, as listed in Table A-2.

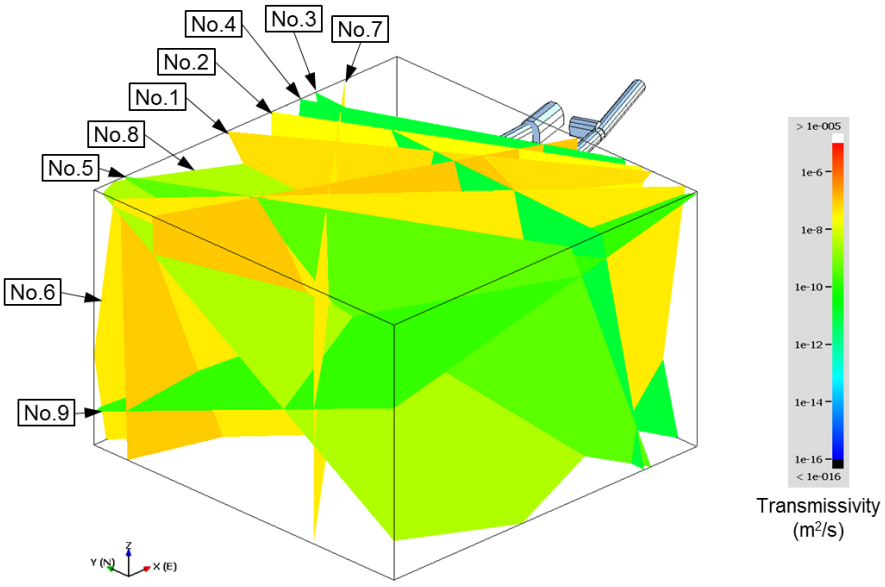

Figure A-14. *Deterministically defined fractures (DDFs) estimated from FPI criterion of fracture trace map at Prototype Repository.*

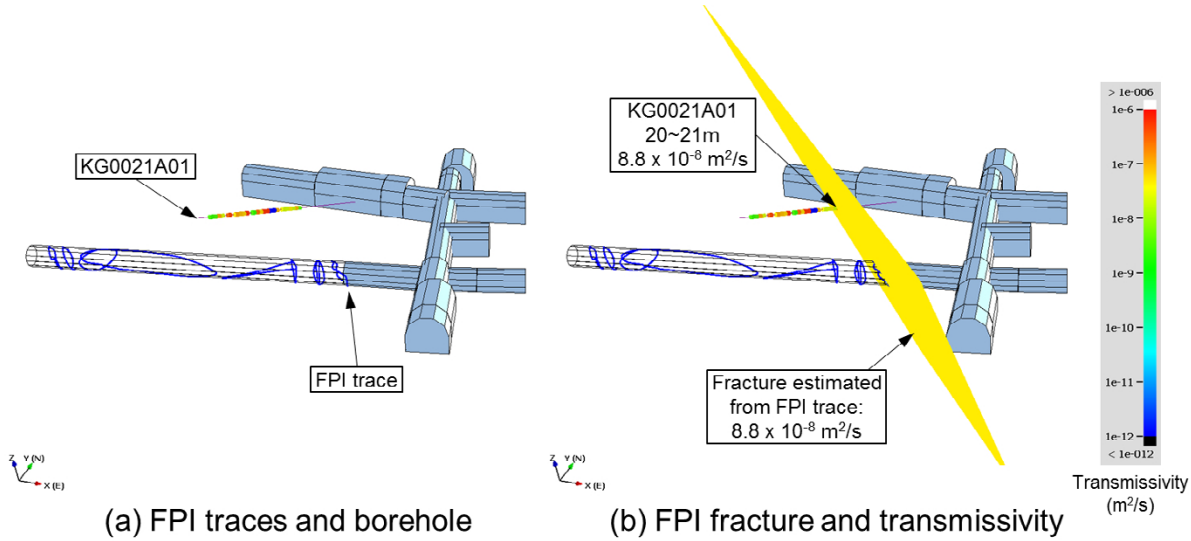

Figure A-15. *Transmissivity estimation of deterministically defined fracture (No. 1).*

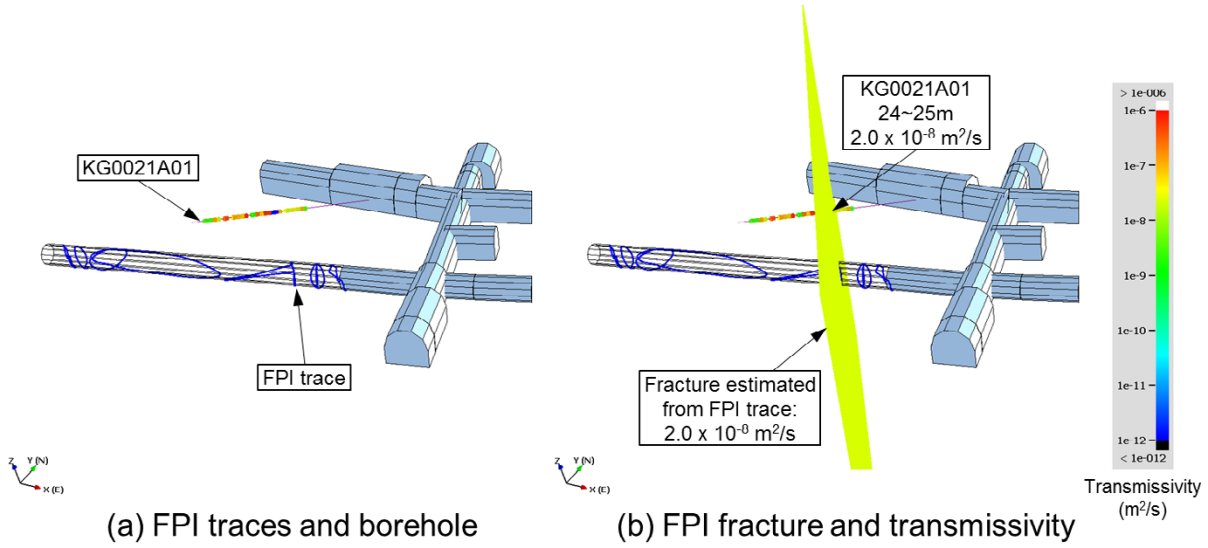

Figure A-16. *Transmissivity estimation of deterministically defined fracture (No. 2).*

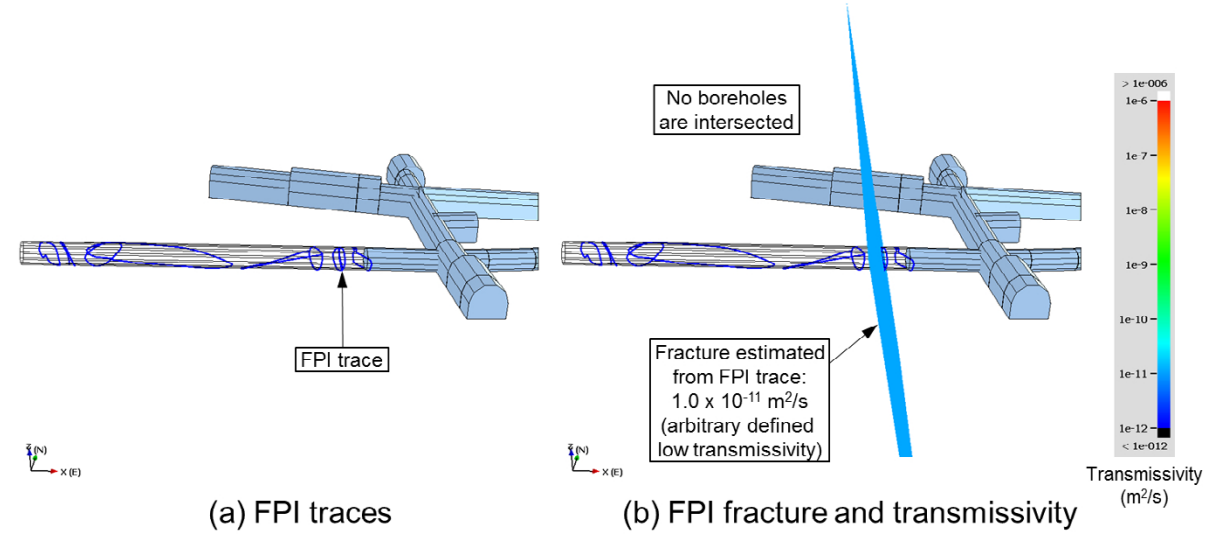

Figure A-17. *Transmissivity estimation of deterministically defined fracture (No. 3).*

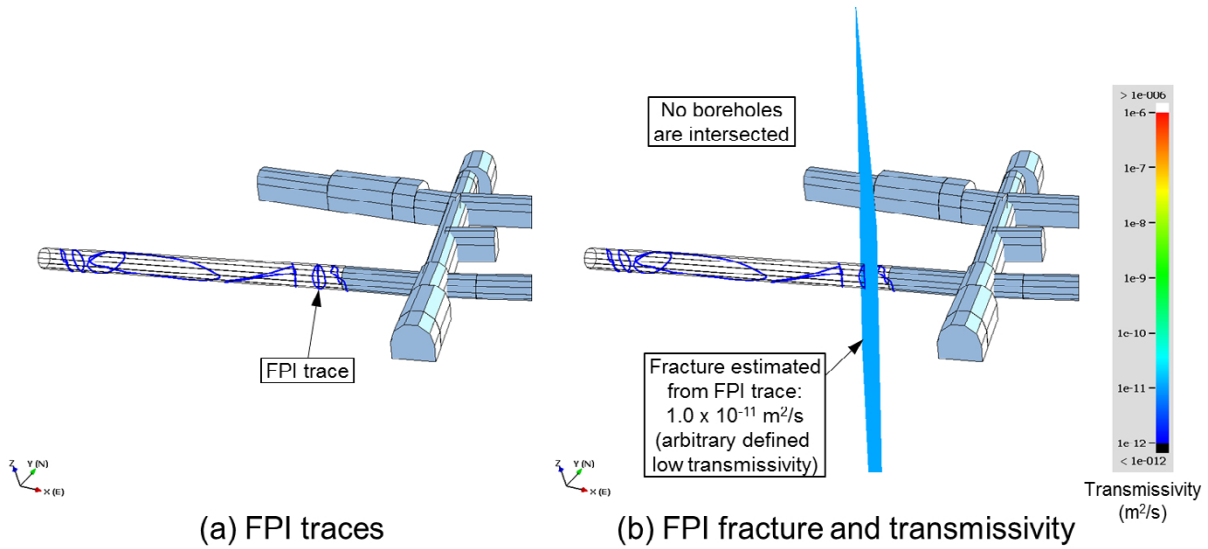

Figure A-18. *Transmissivity estimation of deterministically defined fracture (No. 4).*

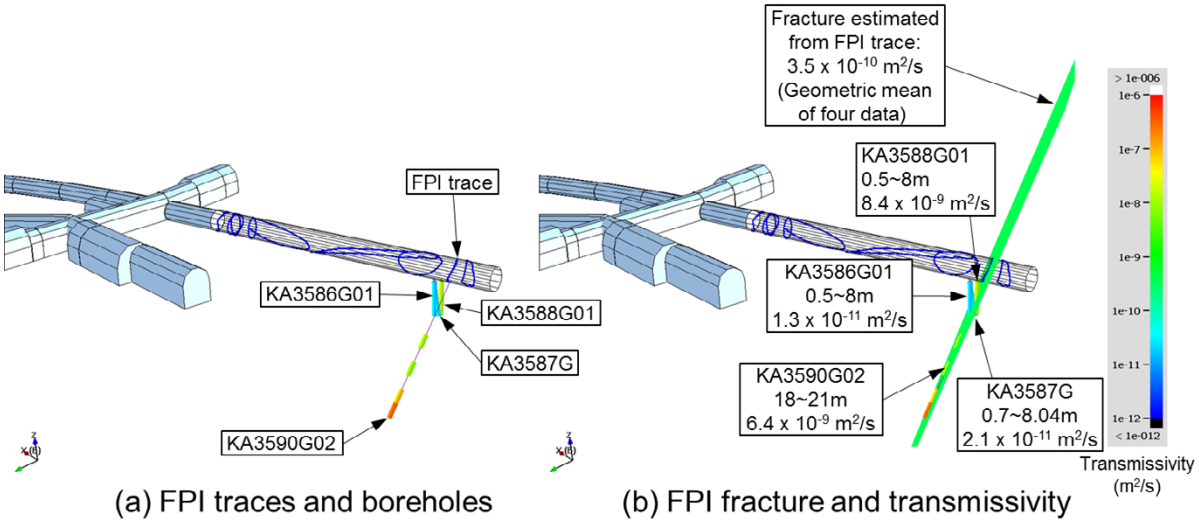

Figure A-19. *Transmissivity estimation of deterministically defined fracture (No. 5).*

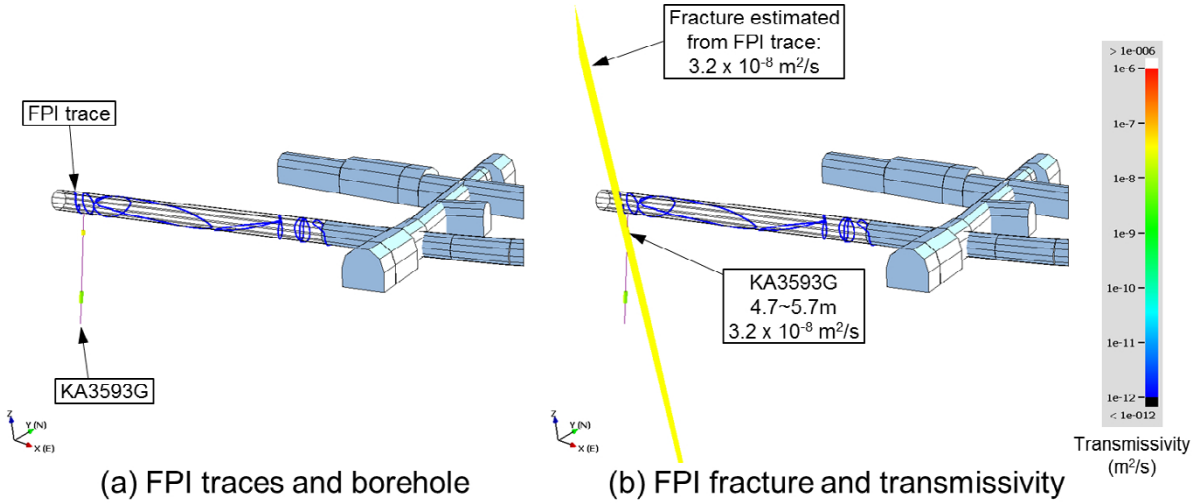

Figure A-20. *Transmissivity estimation of deterministically defined fracture (No. 6).*

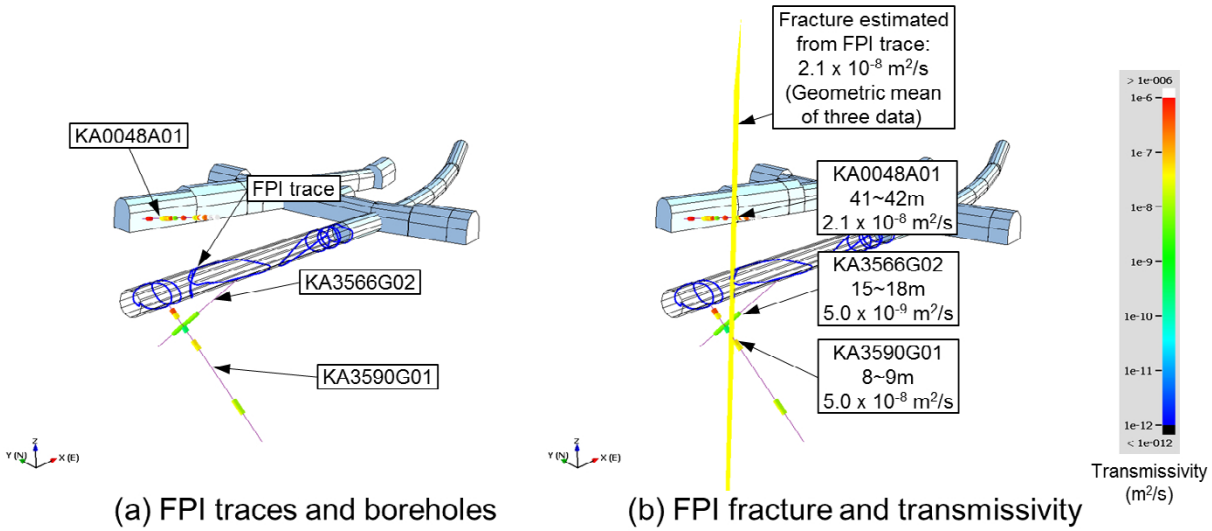

Figure A-21. *Transmissivity estimation of deterministically defined fracture (No. 7).*

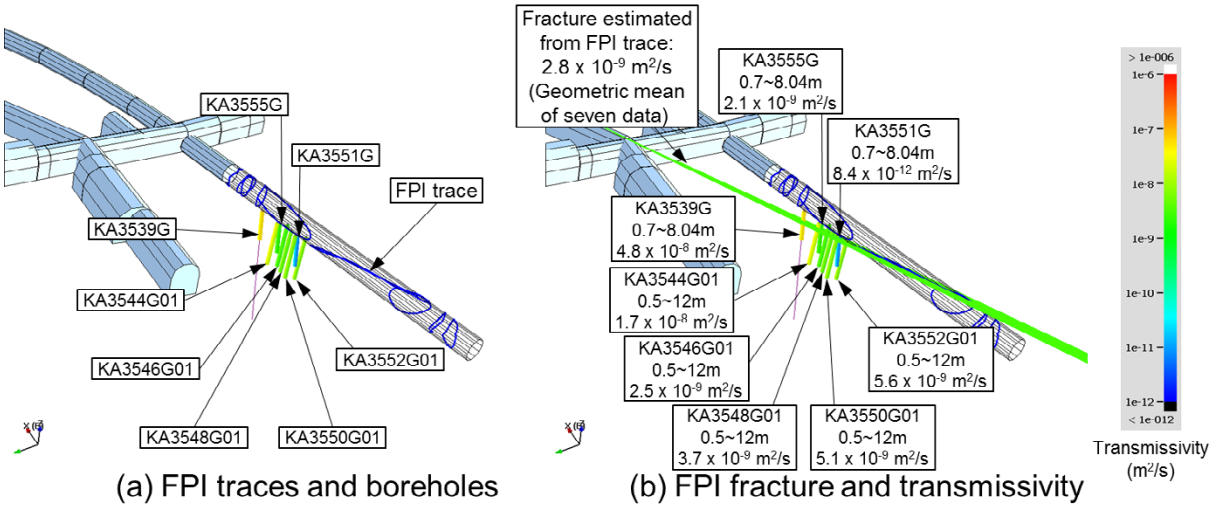

Figure A-22. *Transmissivity estimation of deterministically defined fracture (No. 8).*

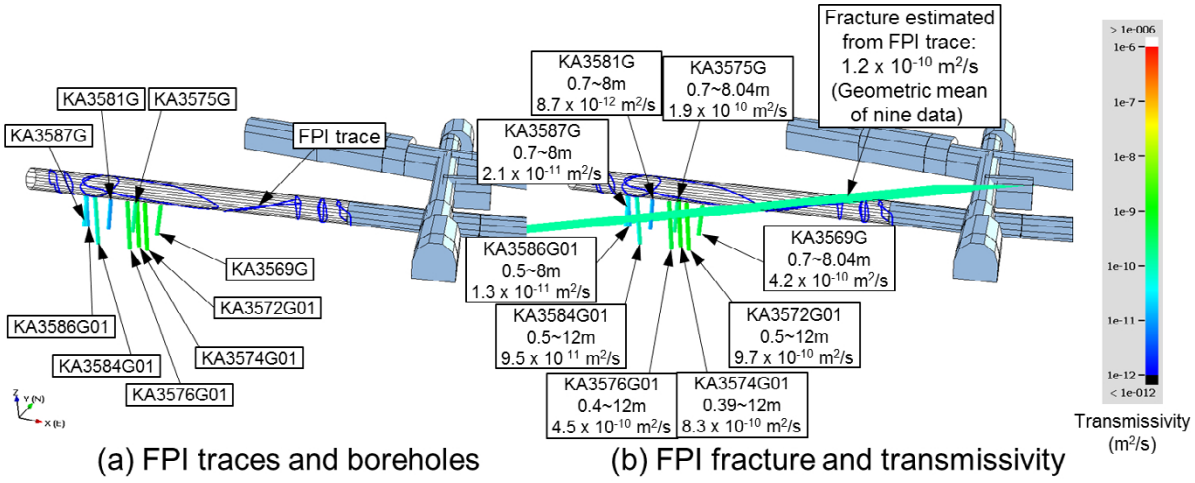

Figure A-23. *Transmissivity estimation of deterministically defined fracture (No. 9).*

Stigsson et al. (2001) also defined two larger fractures, “Fracture1” and “Fracture2” around the Prototype Repository Tunnel, as shown in Figure A-24 (a). In this modelling study, these fractures were also extended to the model boundary to introduce the high head to the vicinity of the tunnel, but were terminated by DDF No.8 to avoid intersecting to the tunnel.

The modelled trace length distribution intersecting at Prototype Repository Tunnel was compared with the measured data as shown in Figure A-13(a). Figure A-25 shows complementary cumulative distribution of the fracture traces observed at the Prototype Repository Tunnel. The fracture size distribution specified in Task 8C and 8D was power low model with power, $b = k_r + 1 = 3.6$ (see Table 3-2) which might underestimate the number of the larger fractures (black line) than measured data (red open circle). However, it became to closer to the measured (blue line), if the nine DDFs were added to the model specified in Task 8C and 8D.

Location and orientation of fractures observed at prove boreholes, KA3587G, KA3581G, KA3575G, KA3569G and KA3545G along each DH were conditioned as same as Task 8C examination. Figure A-26 shows the conceptual illustrations for constraining location and orientation of fractures, and adjusting fracture transmissivity intersecting to the probe boreholes.

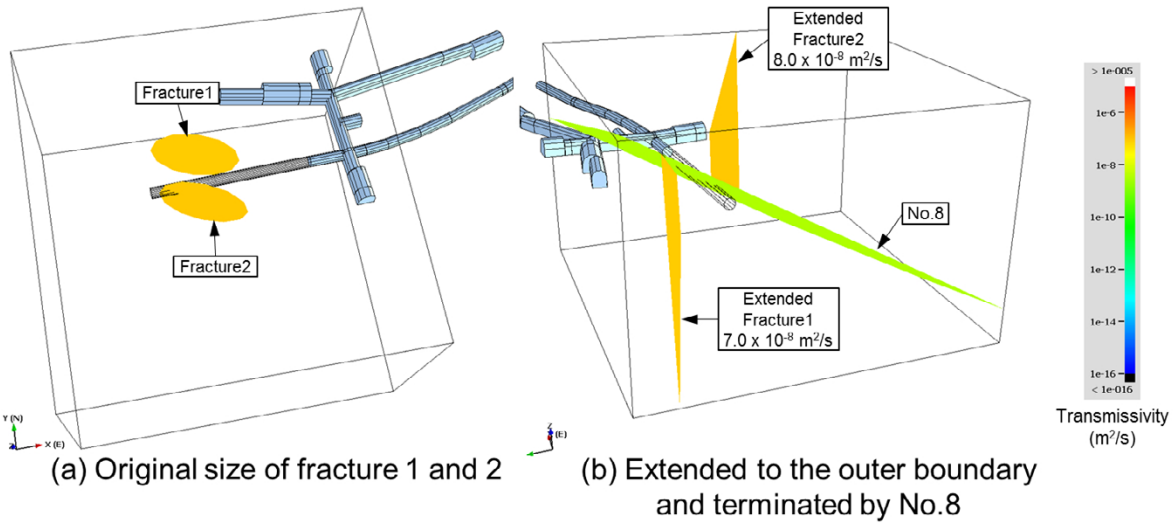

Figure A-24. *Modification of the Fracture 1 and Fracture 2 specified by Stigsson et al. (2001).*

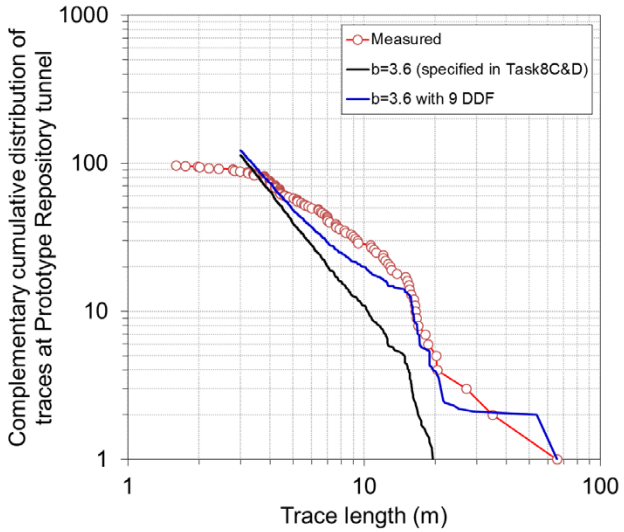

Figure A-25. *Comparison modelled trace length distribution with measured data at Prototype Repository Tunnel.*

Table A-2. Transmissivity estimation of the deterministically defined fracture at each deposition hole.

Deposition hole	Borehole	Measured Transmissivity (m^2/s)	Number of deterministically defined fracture	Equally divided transmissivity (m^2/s)
DA3587G01	KA3587G	2.1×10^{-11}	2	1×10^{-11}
DA3581G01	KA3581G	8.7×10^{-12}	5	1×10^{-12}
DA3575G01	KA3575G	1.9×10^{-10}	2	1×10^{-10}
DA3569G01	KA3569G	4.2×10^{-10}	3	1×10^{-10}
DA3551G01	KA3551G	8.4×10^{-12}	8	1×10^{-12}
DA3545G01	KA3545G	2.1×10^{-9}	5	5×10^{-10}

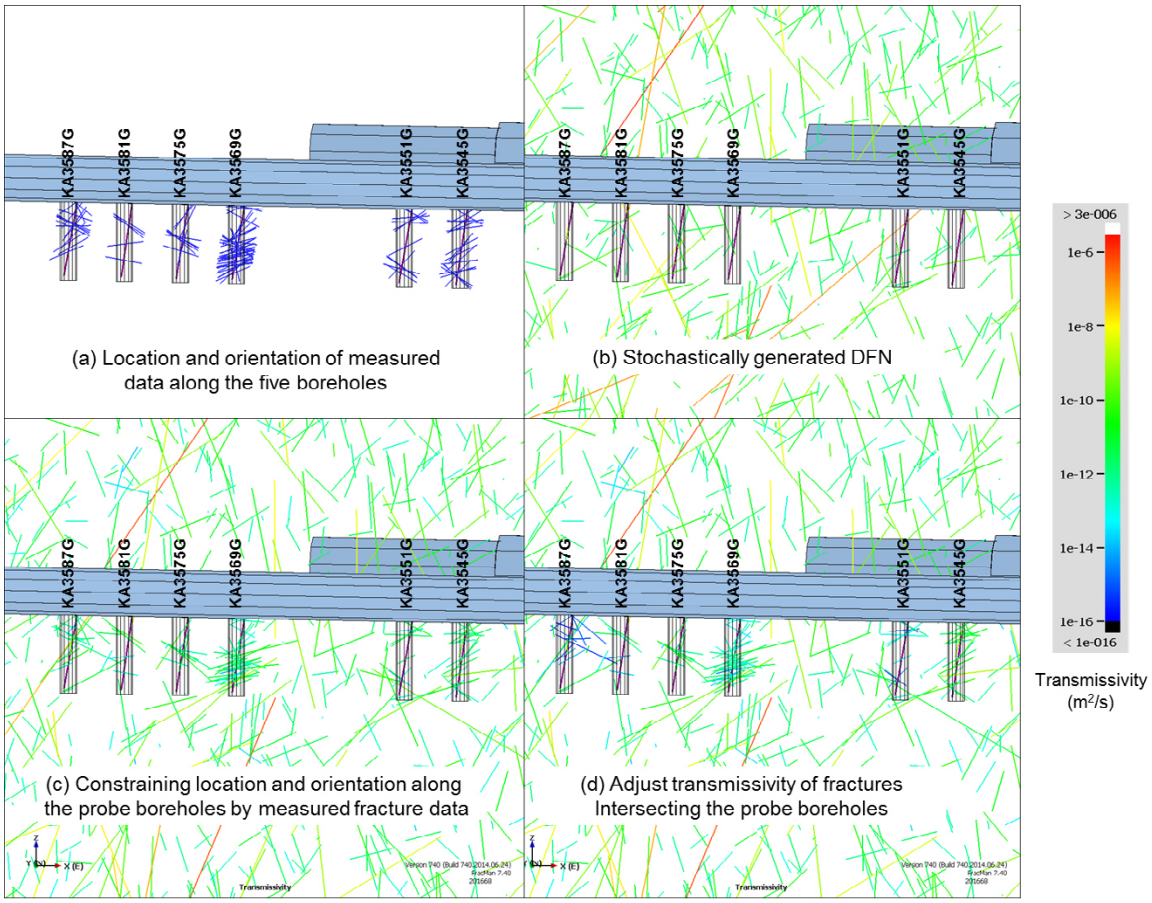

Figure A-26. *Conceptual illustrations for constraining location and orientation of fractures, and adjusting fracture transmissivity intersecting to the probe boreholes; vertical cross sectional view along the deposition holes.*

The fracture transmissivity intersecting to each probe borehole was adjusted by multiplying the following factor to each fracture.

$$\frac{C_j}{\sum_{i=1}^{n_j} T_i}$$

where T_i is transmissivity of i-th fracture intersecting to the probe borehole j , n_j is total number of fractures intersecting to the borehole j, and C_j is measured transmissivity of the borehole j, as listed below;

- KA3545G: $C = 2.1 \times 10^{-9}$ m²/s
- KA3551G: $C = 8.4 \times 10^{-12}$ m²/s
- KA3569G: $C = 4.2 \times 10^{-10}$ m²/s
- KA3575G: $C = 1.9 \times 10^{-10}$ m²/s
- KA3581G: $C = 8.7 \times 10^{-12}$ m²/s
- KA3587G: $C = 2.1 \times 10^{-11}$ m²/s

Simulation of groundwater flow to the tunnel and deposition holes

The steady state groundwater flow simulations were carried out, to study the probabilistic range of the stochastic DFN model with deterministically defined fractures by the FPI fractures and conditioning fractures observed at the probe boreholes. 1 000 stochastic realisations of the HydroDFN model were examined. These simulations assumed an atmospheric pressure condition on tunnel and disposal holes walls, and the Task 8 description's heterogeneous fixed head boundary condition at the outer boundaries of the model as shown in Figure A-27. An alternative case of homogeneous head, −47 m that equals to about 400 m above the Prototype Repository Tunnel was also applied as outer boundary conditions, to archive relatively higher pressure distribution around the tunnel.

Figure A-28 shows the steady state flow simulation results with the heterogeneous head at outer boundary condition case. The simulations were able to reproduce a base range of flow rate distribution to the tunnel, and could cover the range of the flow rate distribution to the disposal holes. The simulated pressure distribution around Prototype Repository Tunnel was compared with measured data (Figure A-29). The pressure was measured at the Prototype Repository Tunnel as datum. The simulated pressure underestimated the measured data. One of the potential reasons is that outer boundary head (specified by the Task 8 descriptions) is relatively lower than the high pressure measured around the Prototype Repository Tunnel. Figure A-30 shows the comparison simulated pressure (an example of a single realisation of 1 000 realisations) and measured data along the boreholes. This result suggests that it might be required to apply higher pressure boundary to introduce high pressure within the model, especially at south side and a part of bottom of Prototype Repository Tunnel.

An alternative boundary condition for outer boundary was applied to archive relatively higher pressure distribution around Prototype Repository Tunnel. A homogeneous head, −47 m that equals to about 400 m above the prototype tunnel, was chosen. Figure A-31 shows the steady state flow simulation results with the homogeneous head at outer boundary condition case. The simulated flow rate to the tunnel and deposition holes of homogeneous head boundary case are relatively higher than those of heterogenous head boundary case, especially at section 2 area of Prototype Repository Tunnel due to high pressure outer boundary at east side of the modelling block. The simulated pressure seems to be closer to measured data, as shown in Figure A-32 and Figure A-33.

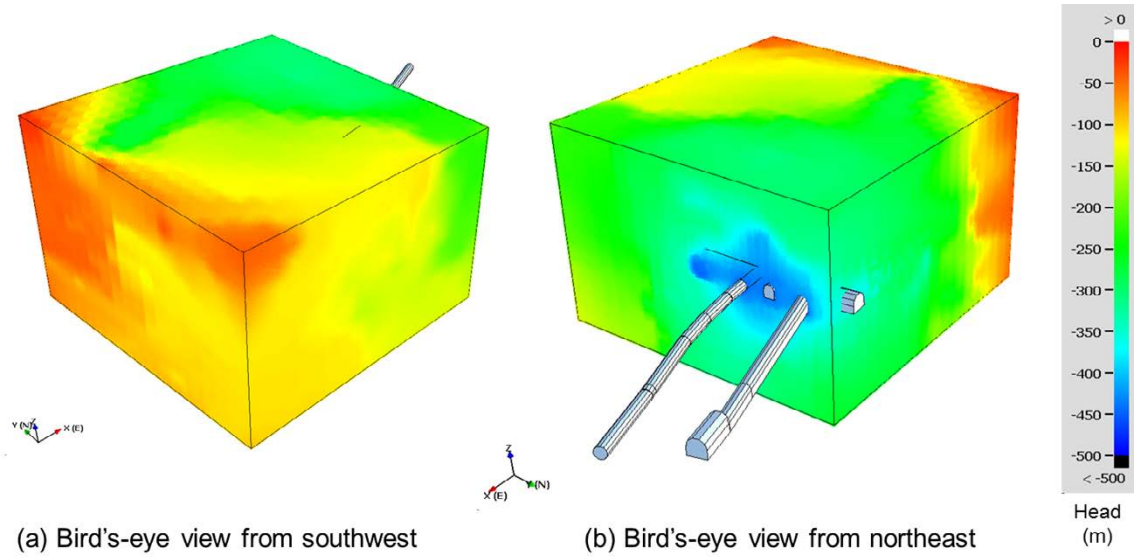

Figure A-27. *Heterogeneous head distribution estimated from Äspö site model by DarcyTool for specifying constant head outer boundary condition.*

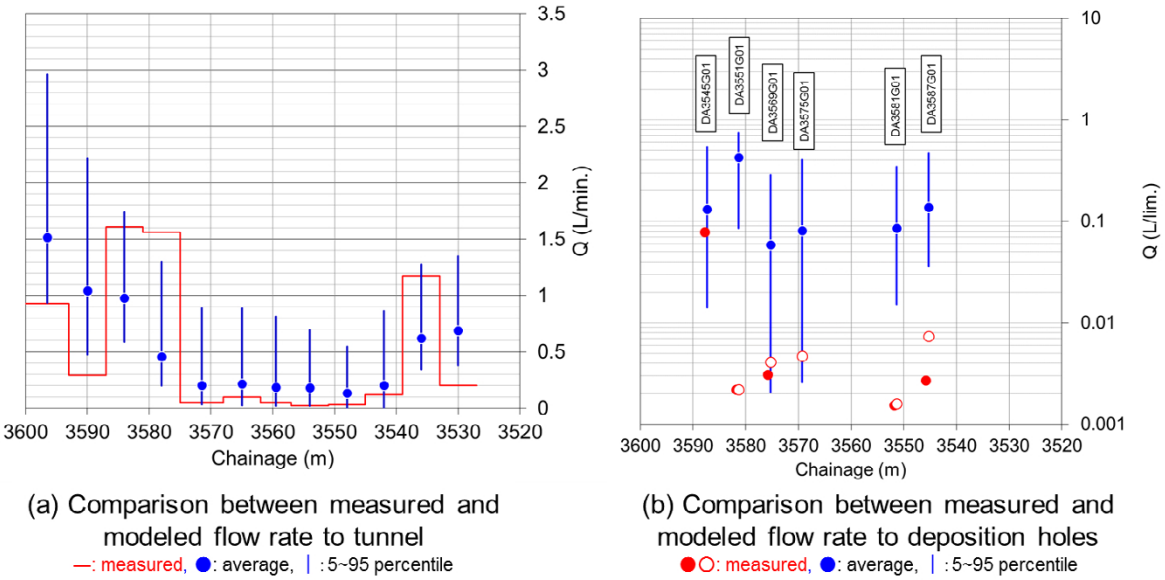

Figure A-28. *The simulated flow rate to tunnel and deposition holes comparing with the measured data (Heterogeneous head boundary case).*

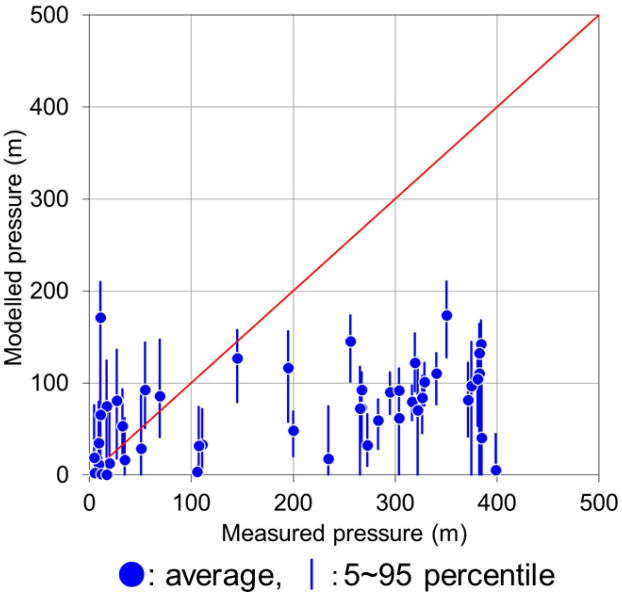

Figure A-29. *Comparison between measured and modelled pressure around TBM tunnel (Heterogeneous head boundary case).*

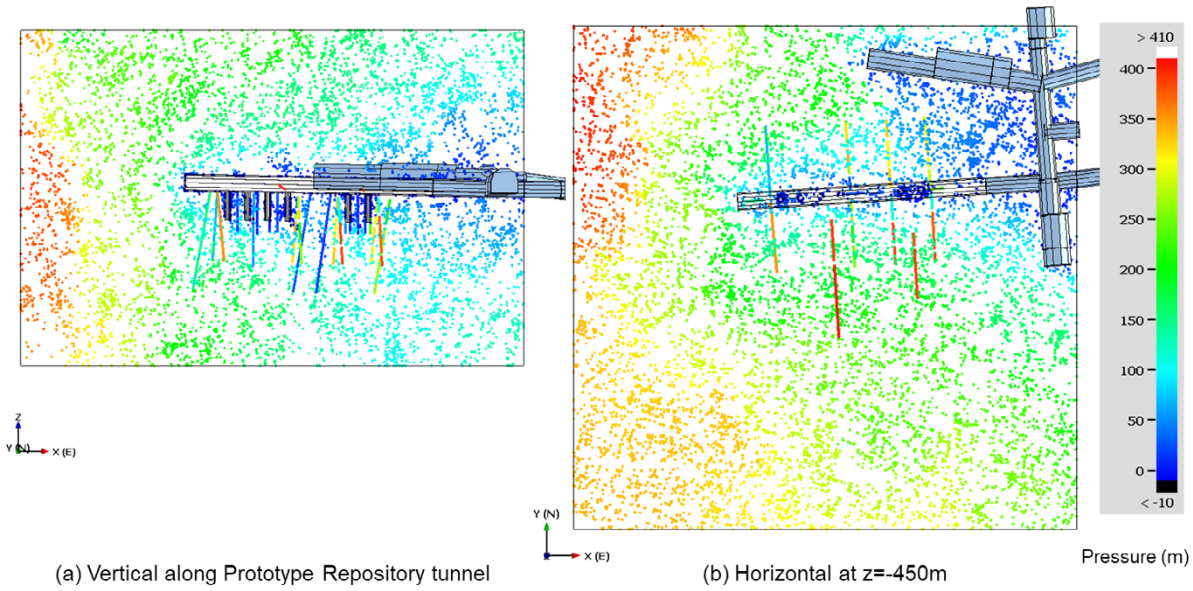

Figure A-30. *The simulated pressure distribution compared with measured data along the boreholes, the case of realisation number 782 (Heterogeneous head boundary case).*

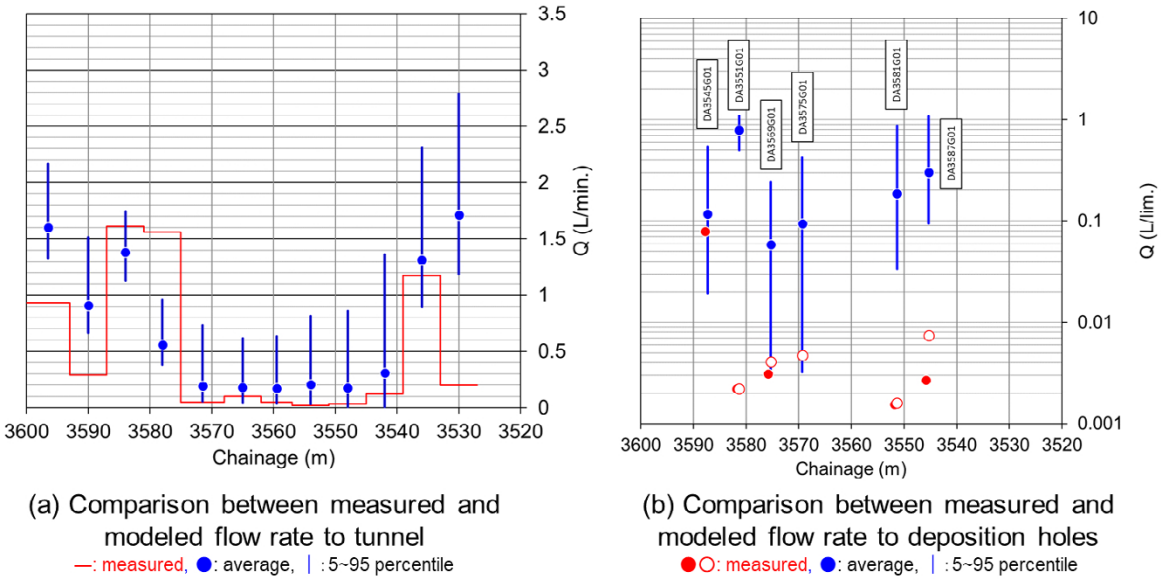

Figure A-31. *The simulated flow rate to tunnel and deposition holes comparing with the measured data (Homogeneous head boundary case).*

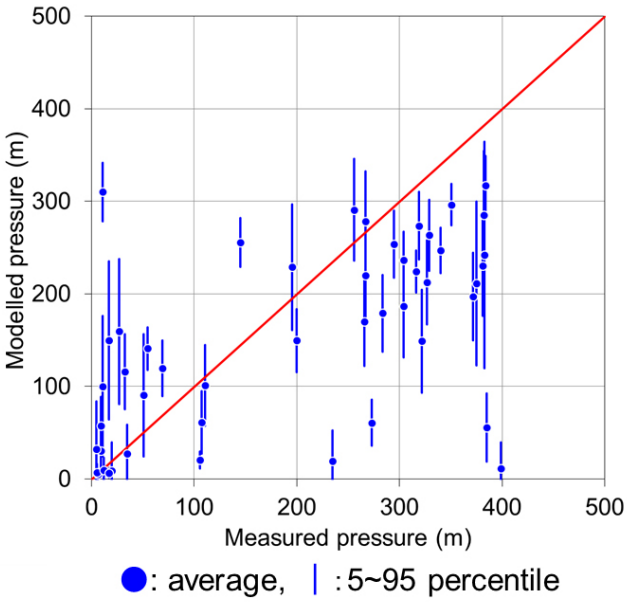

Figure A-32. *Comparison between measured and modelled pressure around TBM tunnel (Homogeneous head boundary case).*

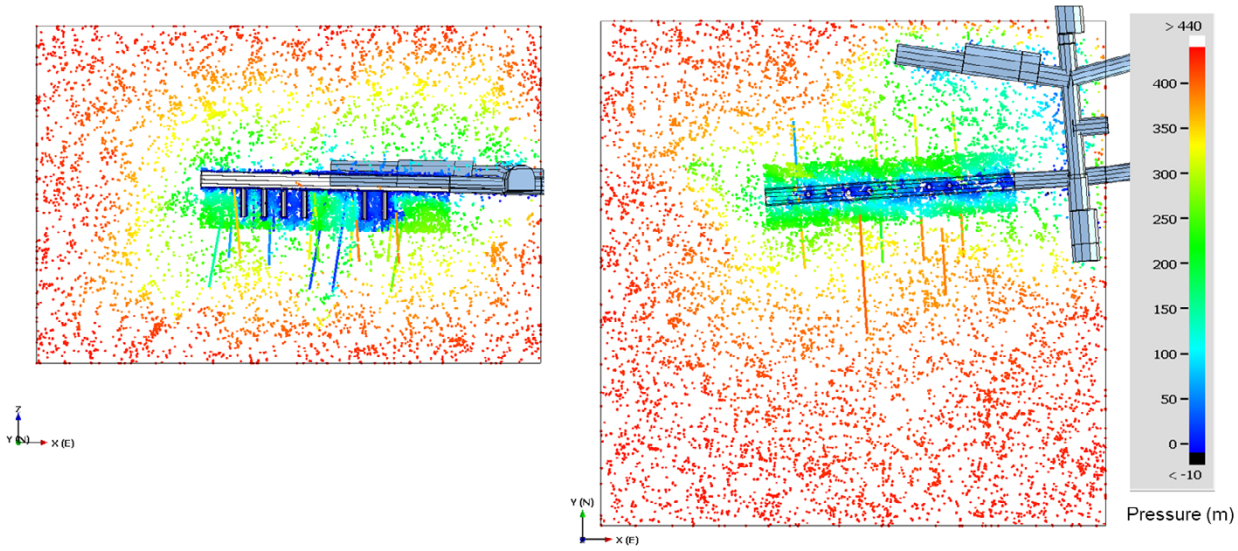

(a) Vertical along Prototype Repository tunnel (b) Horizontal at z=-450m

Figure A-33. *The simulated pressure distribution compared with measured data along the boreholes, the case of realisation number 837 (Homogeneous head boundary case).*

A single realisation of the HydroDFN model was selected for use in coupled FracMan/MAFIC and Thames code simulations of bentonite saturation behaviour under the thermal load condition, to demonstrate capability of the coupling simulation. To identify the case of a realisation, the 1 000 stochastic realisations were sorted using RMSE (root mean square error between simulated and measured flow rate to tunnel sections and deposition holes) as an index (Figure A-34). Then, realisation number 837, showing the lowest RMSE for the flow rate to deposition hole and relatively low RMSE to Prototype Repository Tunnel, was picked up. Figure A-35 shows the simulated flow rate to tunnel and deposition holes comparing with the measured data, of realisation number 837 case.

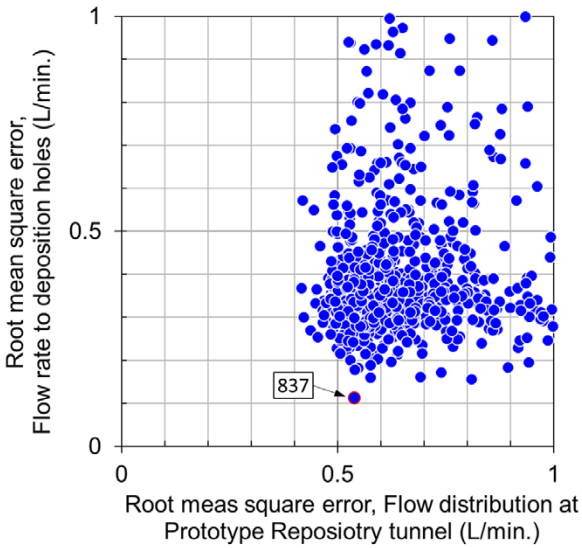

Figure A-34. *Root mean square error distribution of 1 000 realisations between simulated and measured flow rate to tunnel sections and deposition holes. The case of realisation number 837 was selected (Homogeneous head boundary case).*

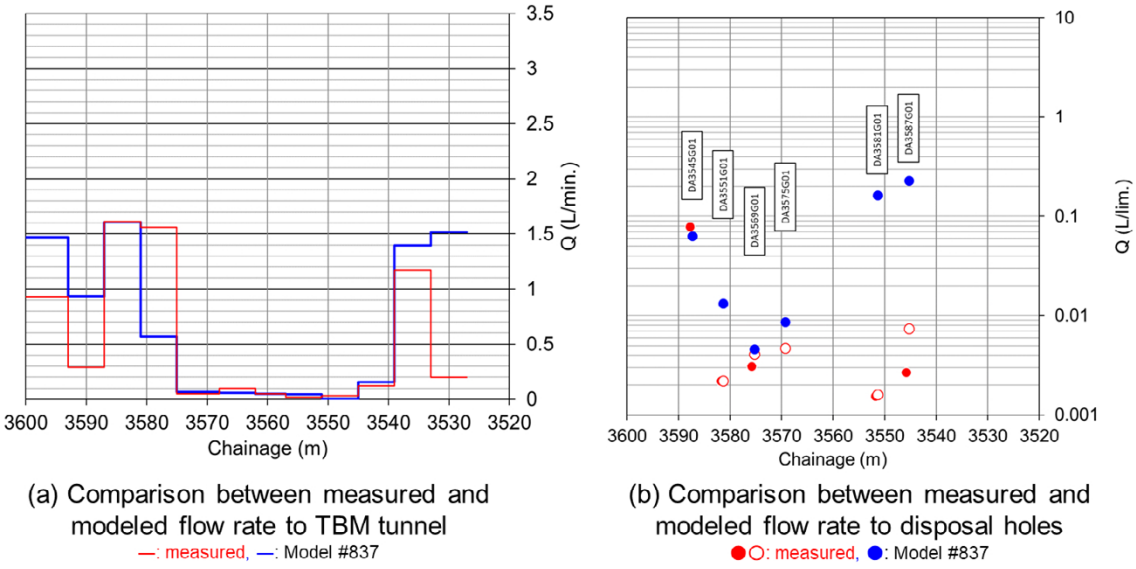

Figure A-35. *The simulated flow rate to tunnel and deposition holes comparing with the measured data, the case of realisation number 837 (Homogeneous head boundary case).*

Coupling simulation of groundwater flow and bentonite wetting at the deposition holes

Bentonite wetting simulations were conducted after updating coupling simulation method with considering the heat transport from heater simulating canister package (overpack). Figure A-36 illustrates conceptual model of the updated coupling method between FracMan/MAFIC and Thames. The hydration behaviour both of bentonite in six deposition holes (DH1~6) and backfill in tunnel above each hole was calculated by Thames, coupling with groundwater flow through HydroDFN in rock as shown in Figure A-36. Same interface programs, MTOT and TTOM as the simulation for BRIE (see Figure 2-1) were applied, for coupling between FracMan/MAFIC and Thames. Thermal load from heater simulating canister package (overpack) was also coupled with the hydration simulation in Thames code. Rock model was added to Thames calculation, to simulate heat transport dissipating to outer boundary in rock. However, thermal-hydraulic (T-H) coupling was ignored in rock, and the T-H coupling behaviour was considered only in bentonite and backfill. Because, we focused on the thermal effect on the heterogeneous hydration behaviour in bentonite and backfill, in order to simplify this demonstration study.

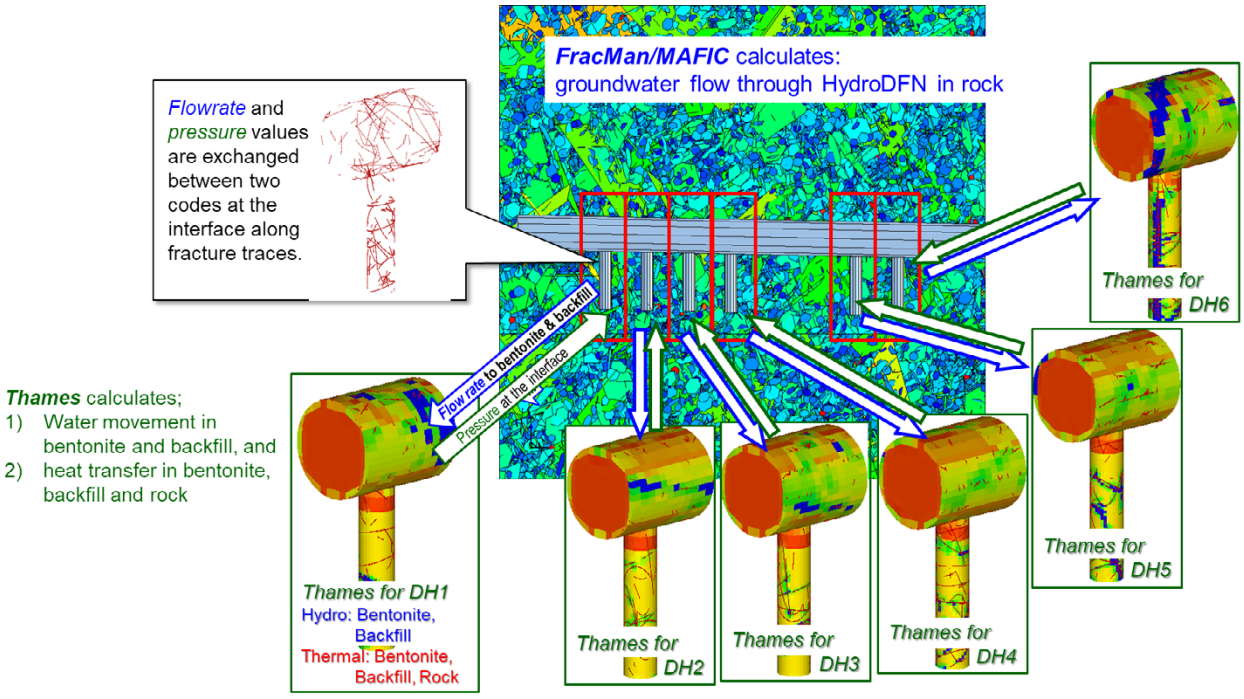

Figure A-36. *Conceptual illustration of updated coupling method between FracMan/MAFIC and Thames.*

It was also assumed that temperature increase might not significantly affect on hydraulic behaviour in HydroDFN in rock. Figure A-37 shows the finite element mesh for Thames calculations at/around each deposition hole (DH1~6). Outer boundary condition of rock and backfill was fixed temperature (15 °C), and no flow boundary, respectively. This no flow boundary could induce artificial discontinuity of hydraulic behaviour along Prototype Repository Tunnel. The fixed temperature (80 °C) was applied to the overpack at each deposition hole. The parameter values for Thames calculation is listed in Table A-3.

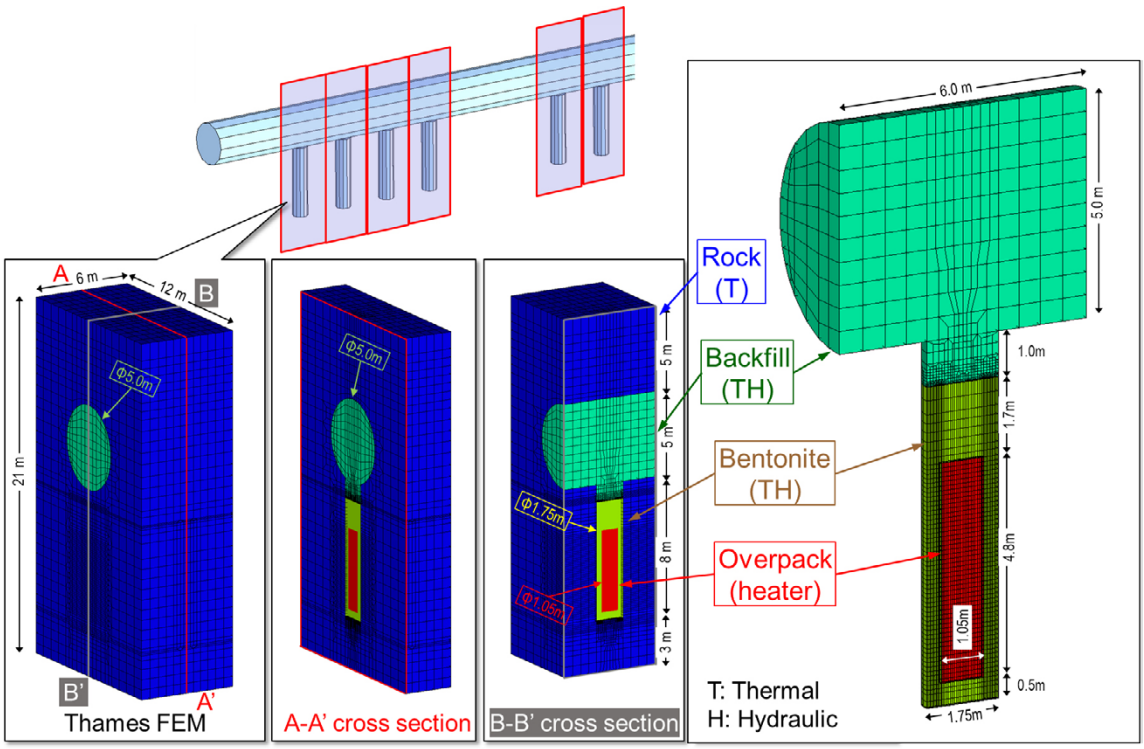

Figure A-37. *Overview of finite element mesh for Thames calculations.*

Table A-3. Major Material properties and initial conditions, used for T-H coupling simulation of Thames.

Parameters	unit	Rock	Backfill	Bentonite	remark
Porosity	-	0.01	0.355	0.355	
Dry density	Mg/m^3	2.438	1.734	1.734	
Intrinsic permeability	m^2	-	5.0×10^{-19}	2.0×10^{-21}	
Relative permeability, k_r	-	-	$k_r = S_l^3$ S_l: water saturation	$k_r = S_l^3$ S_l: water saturation	
Water retention curve (van Genuchten model)	m	-	$\theta_s = 0.4$, $\theta_r = 0$ $\alpha = 1.2 \times 10^{-3}$ (1/m), $n = 1.25$	$\theta_s = 0.355$, $\theta_r = 0$ $\alpha = 3.32 \times 10^{-4}$ (1/m), $n = 1.18$	θ_s: Saturated water content θ_r: residual water content
Thermal water diffusivity	$m^2/s/K$	-	Dependent on saturation and temperature	Dependent on saturation and temperature	Figure A-38
Heat conductivity	W/m/K	0.74	Dependent on saturation	Dependent on saturation	Figure A-39
Specific heat	kJ/kg/K	1.66	Dependent on saturation	Dependent on saturation	Figure A-40
Initial saturation	%	100	67	86.4	
Initial temperature	°C	15	15	15	

Thermal gradient caused by heater (overpack) controls moisture movement. In Thames, moisture movement under temperature gradient is modelled by "thermal water diffusivity" (Philip and Vries, 1957), which is dependent on saturation and temperature (Figure A-38). Heat conductivity and specific heat capacity were specified by a function of water content (gravimetric), shown in Figure A-39 and Figure A-40, respectively.

A single realisation of HydroDFN model selected in previous section was applied to demonstrate the capability of coupling simulation method. The results, pressure, saturation, temperature distribution at each section (DH1~6) are shown in Figure A-41 (30 days), A-42 (180 days), A-43 (360 days), A-44 (720 days), A-45 (1 080 days) and A-46 (1 800 days). The heterogeneous hydration behaviour in bentonite and backfill caused by the discrete groundwater supply from rock (HydroDFN) under the homogeneous heat transport from the overpack (heater) could be demonstrated by using the coupling simulation method of FracMan/MAFIC and Thames. In order to obtain more reasonable results, which are comparable with in-situ data (e.g., Johannesson, 2014), further examinations such as reviewing and optimising the HydroDFN model and the parameter values of T-H coupling model in Thames should be required.

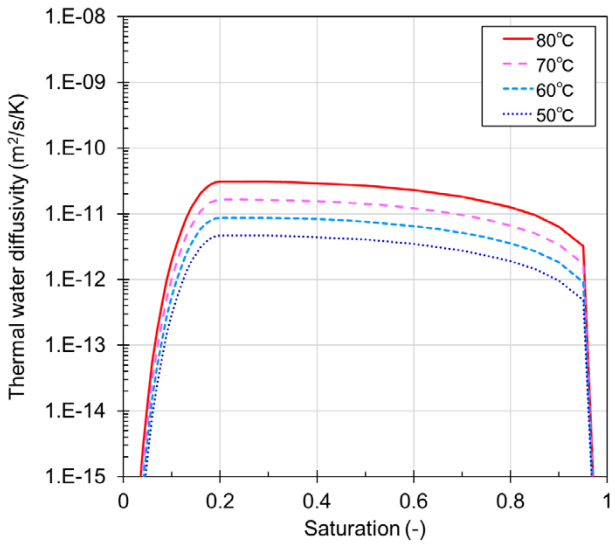

Figure A-38. *Thermal water diffusivity at bentonite and backfill.*

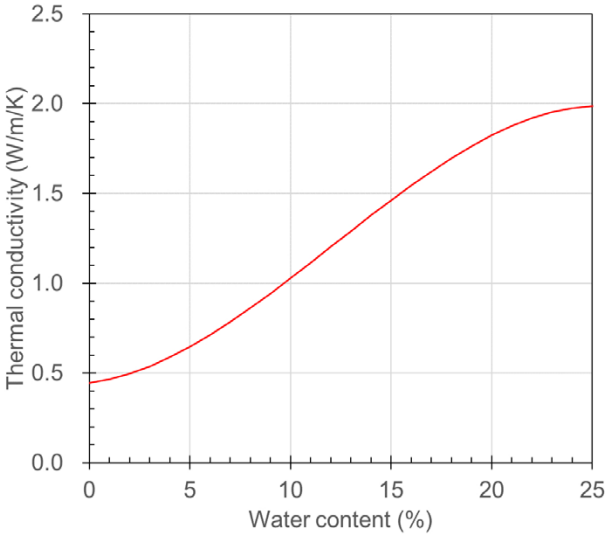

Figure A-39. *Thermal conductivity at bentonite and backfill.*

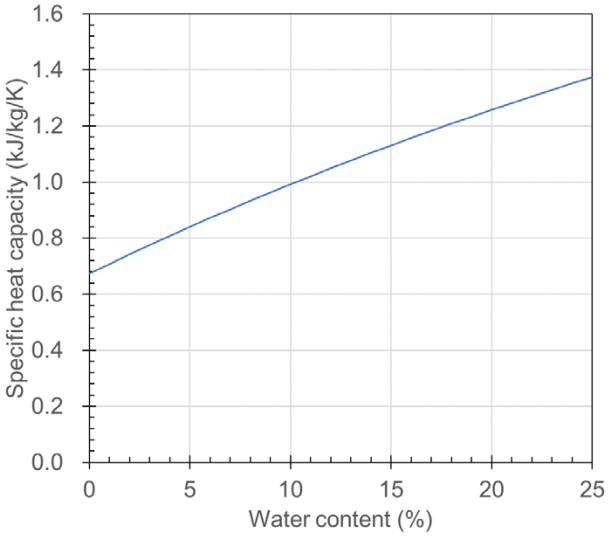

Figure A-40. *Specific heat capacity at bentonite and backfill.*

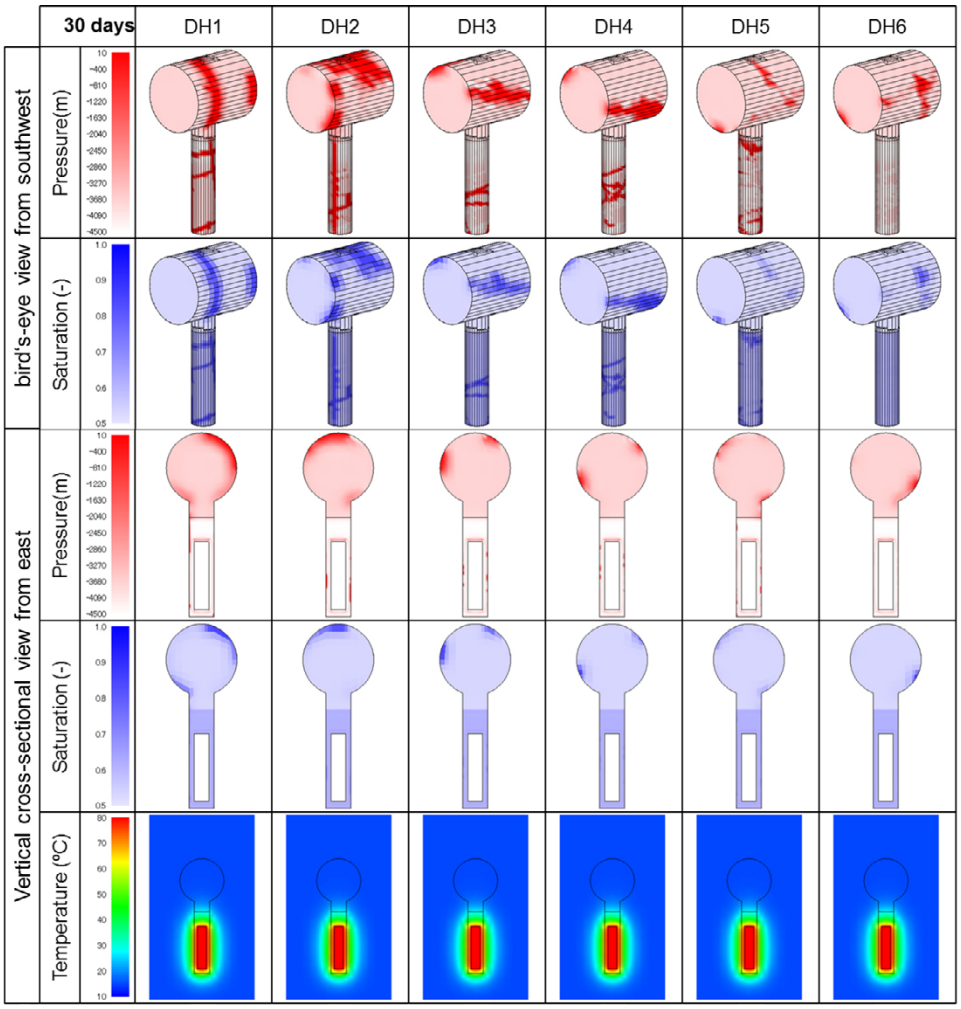

Figure A-41. *Coupling simulation results for each deposition hole after 30 days.*

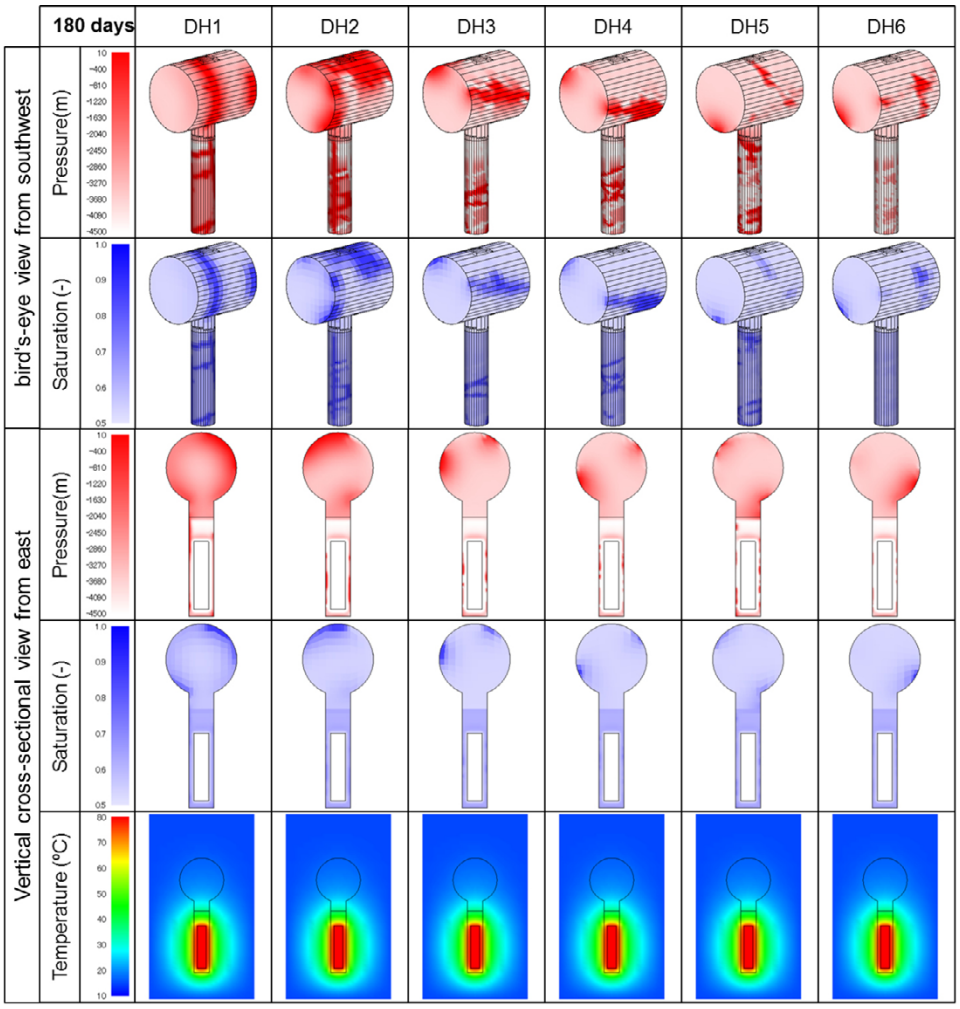

Figure A-42. *Coupling simulation results for each deposition hole after 180 days.*

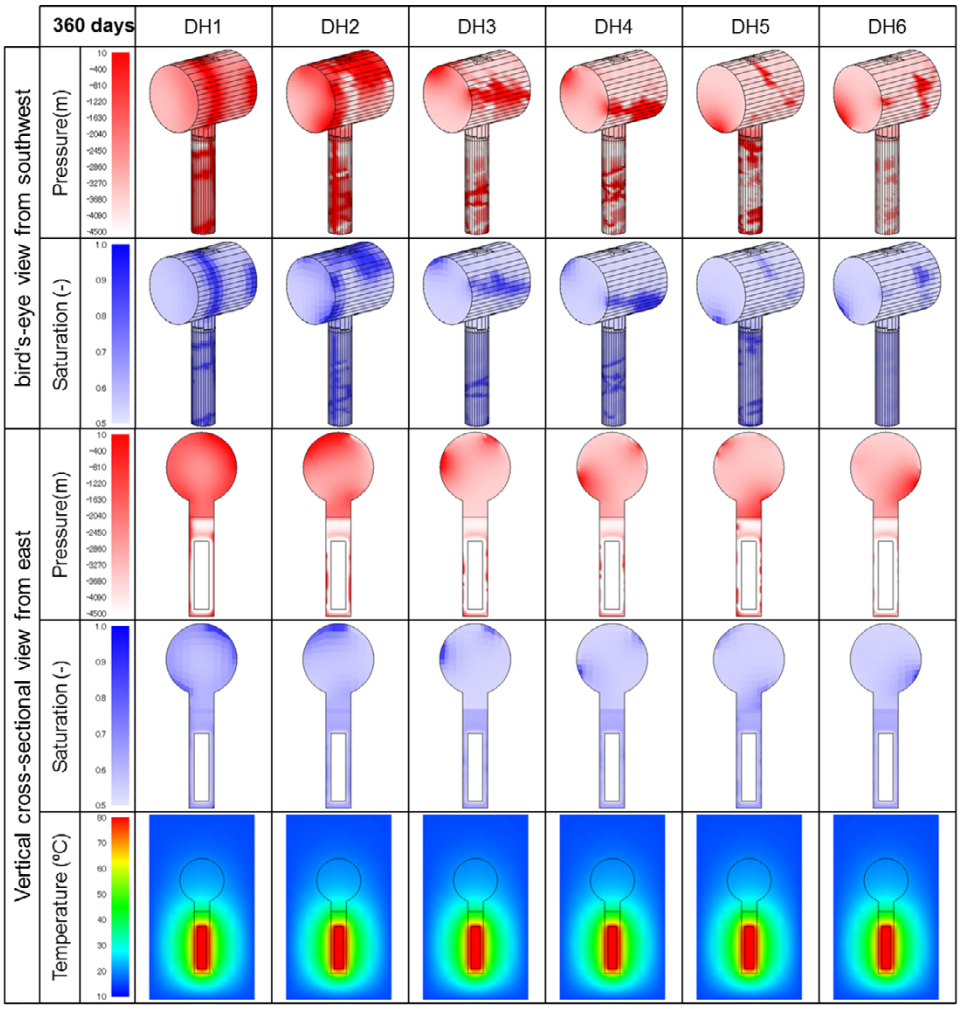

Figure A-43. *Coupling simulation results for each deposition hole after 360 days.*

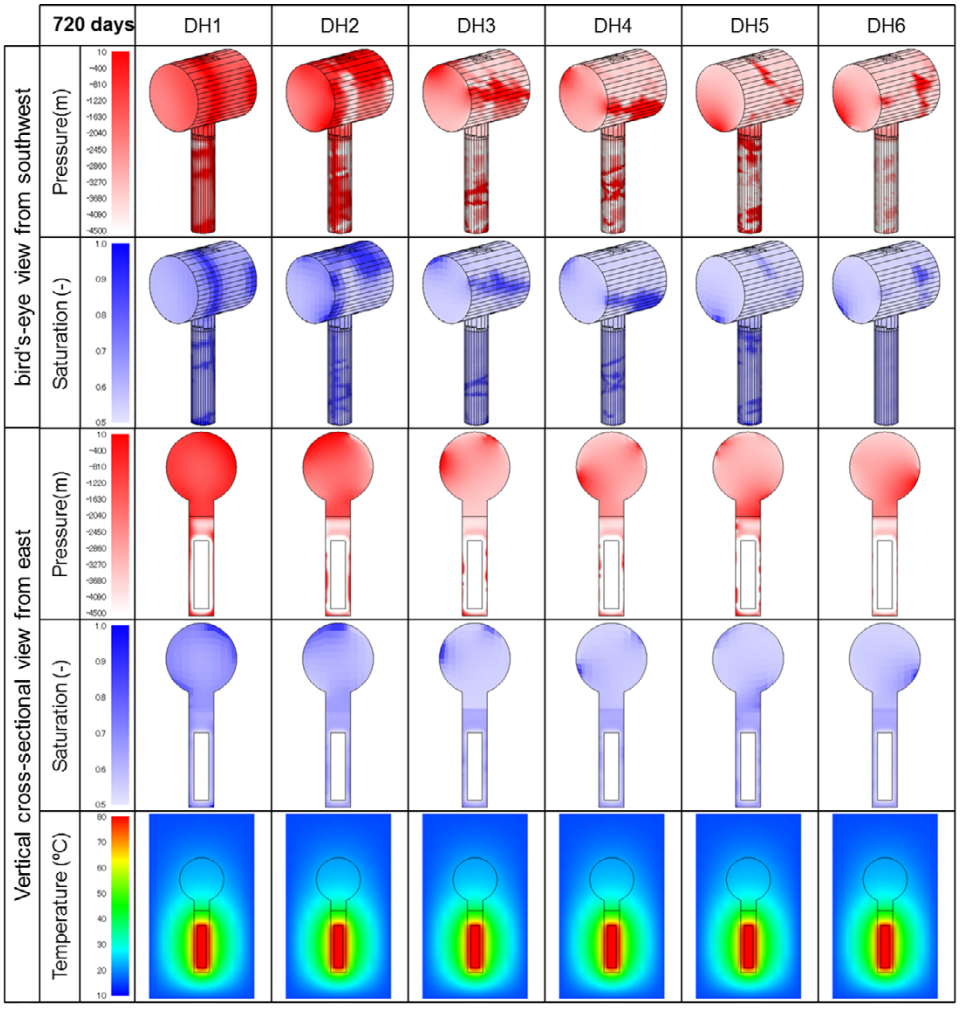

Figure A-44. *Coupling simulation results for each deposition hole after 720 days.*

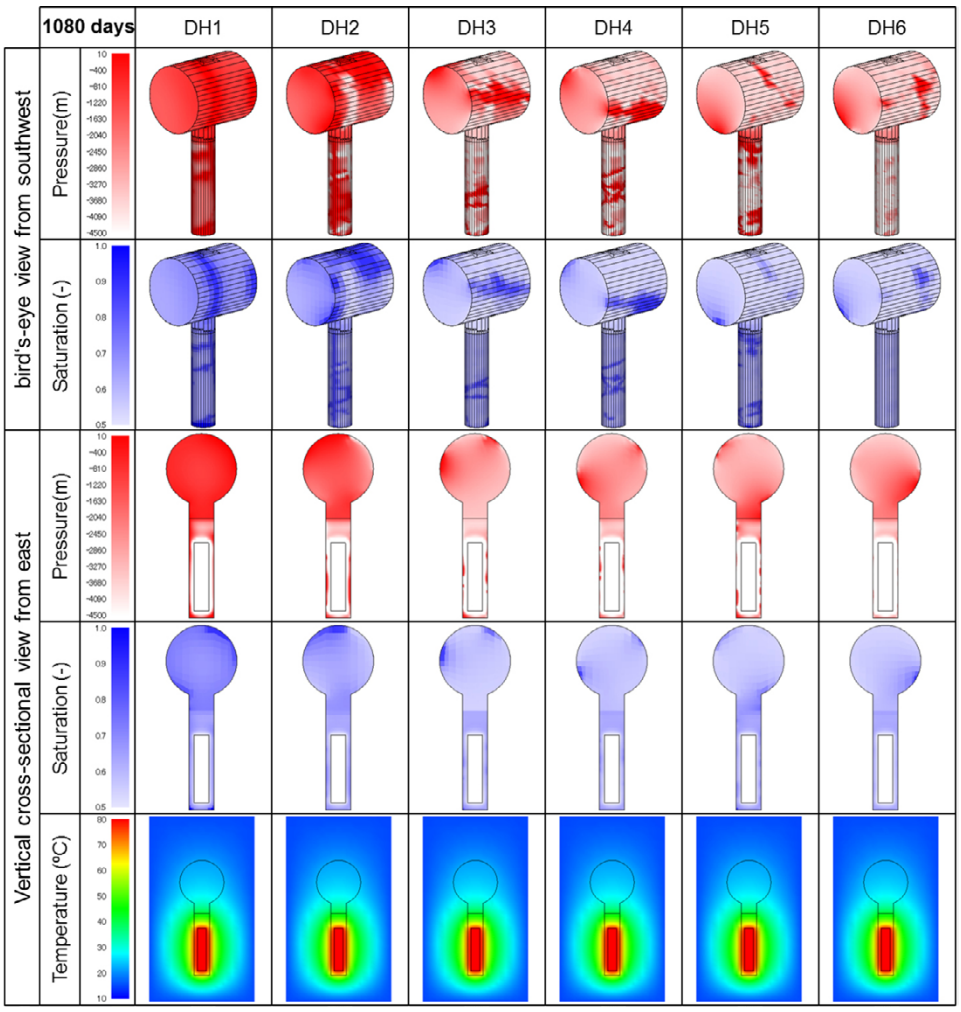

Figure A-45. *Coupling simulation results for each deposition hole after 1 080 days.*

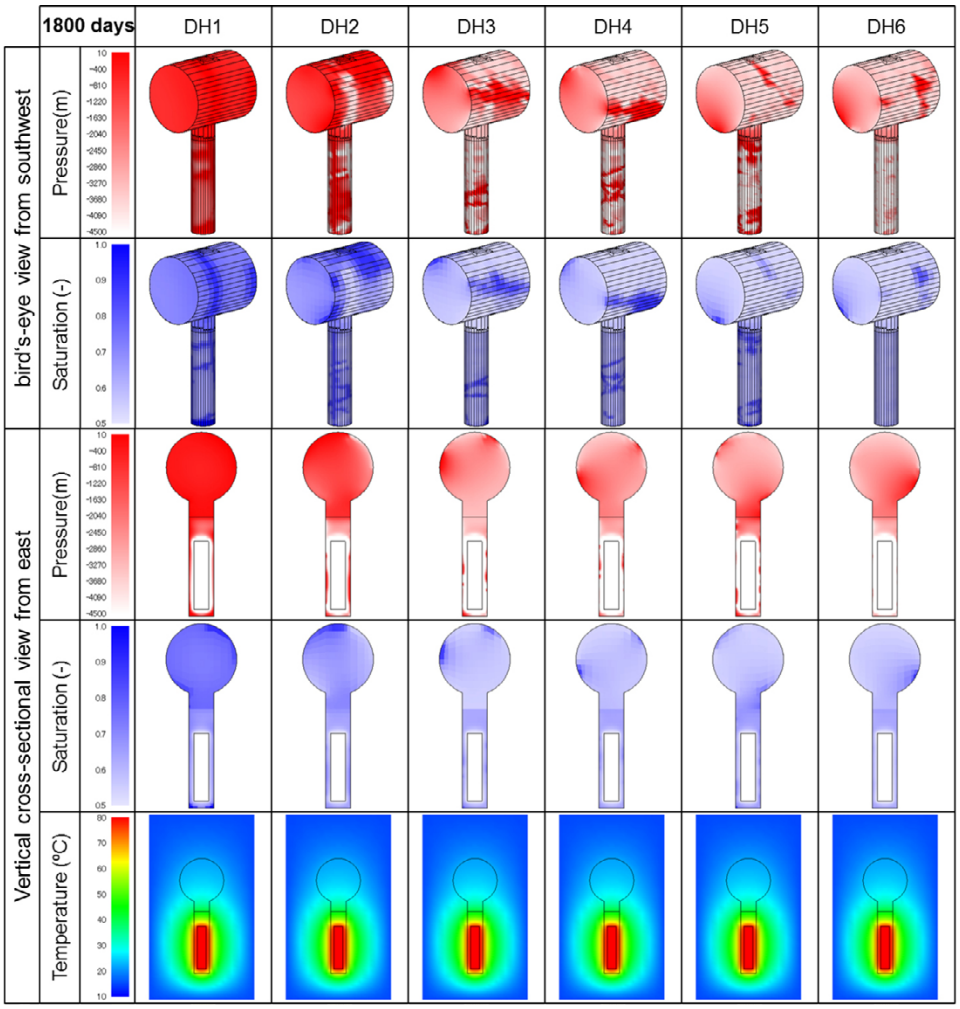

Figure A-46. *Coupling simulation results for each deposition hole after 1 800 days.*

Arkitektkopia AB, Bromma, 2023

SKB is responsible for managing spent nuclear fuel and radioactive waste produced by the Swedish nuclear power plants such that man and the environment are protected in the near and distant future.

skb.se